Universität Zürich
Medizinische Fakultät

Zentrum für Klinische Forschung (ZKF) / Center for Clinical Research (CCR)
Clinical Trials Center (CTC)

Program

- 13th Day of Clinical Research
- Georg-Friedrich-Götz-Preisverleihung 2014
- 16. Hartmann Müller Gedächtnisvorlesung

Zurich, June 12, 2014

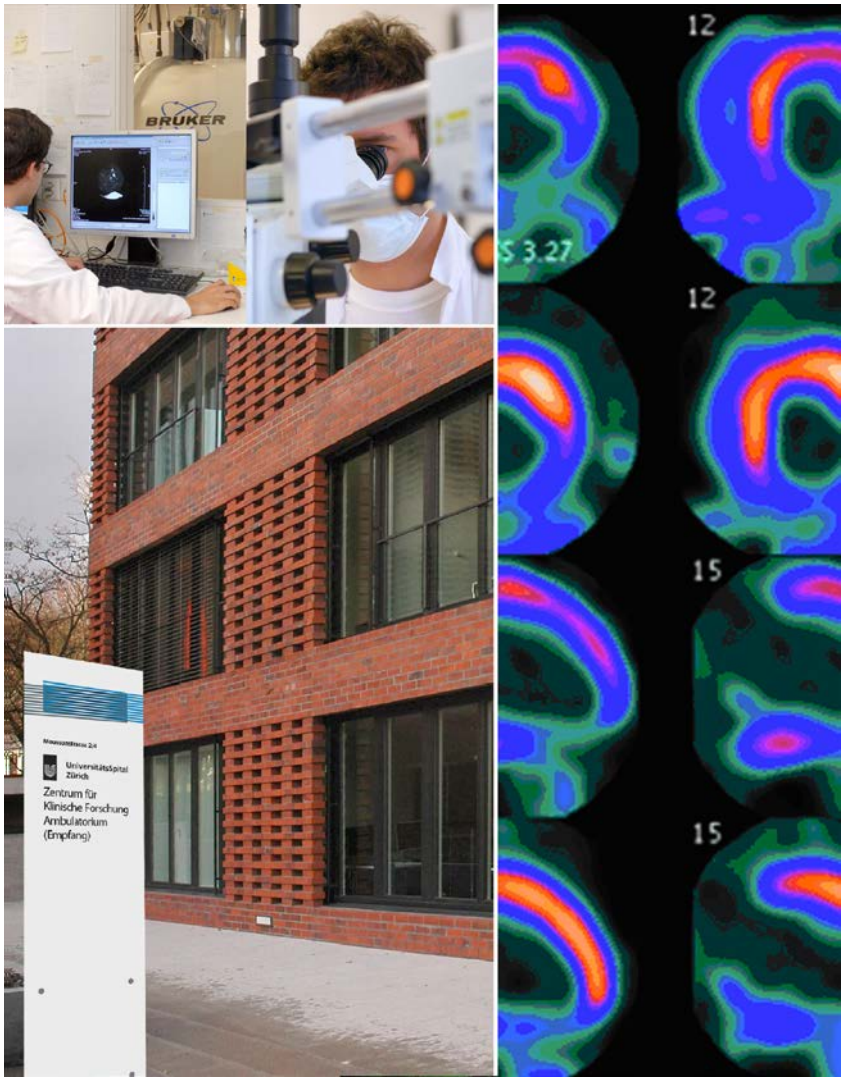

UniversitätsSpital Zürich

Universität Zürich[UZH]

Assoziierte Kliniken
Kinderspital Zürich
Universitätsklinik Balgrist
Kinder- und Jugendpsychiatrischer Dienst des Kantons Zürich
Psychiatrische Universitätsklinik

Structure of the Center for Clinical Research/ Clinical Trials Center

Kuratorium
Prof. Dr. K. W. Grätz (Dekan, ex officio)
Prof. Dr. D. Wyler (Prorektor, ex officio)
Prof. Dr. E. Seifritz
Prof. Dr. J. Hodler
Prof. Dr. T. Lüscher
Prof. Dr. P.-A. Clavien
Prof. Dr. M. Pruschy
Prof. Dr. S. Gay
Prof. Dr. R. Nitsch
lic. oec. HSG R. Ziegler
Prof. Dr. B. Stieger
Prof. Dr. G. Zünd (Managing Director)

Direktorium
Prof. Dr. M. Weller
Prof. Dr. B. Beck Schimmer
Prof. Dr. A. von Eckardstein (Co-Direktor)
Prof. Dr. R. Graf
Prof. Dr. A. Aguzzi (Co-Direktor)
Prof. Dr. G. A. Kullak-Ublick
Prof. Dr. H. Moch
Prof. Dr. G. Spinas
Prof. Dr. G. Zünd (Managing Director)

Geschäftsstelle ZKF
Robin Schneider, MBA
Geschäftsführer

Clinical Trials Center
PD Dr. G. Senti
Leitende Ärztin Clinical Trials Center

Biologisches Zentrallabor
Dr. Hugo Battaglia
Leiter Biologisches Zentrallabor

Zentrum für Regenerative Medizin
Prof. Dr. Dr. Simon P. Hoerstrup
Leiter Zentrum für Regenerative Medizin

Forschungsgruppenleiterkonferenz
Leitung: Prof. Dr. B. Beck-Schimmer
Prof. Dr. R. Graf
Scientific Research Group Leaders of the University Hospitals of Zurich (University Hospital, Children's Hospital, Balgrist University Clinic, Psychiatric University Hospital) and related institutions of the Faculty of Medicine

Table of contents

Bild Vorderseite: Verification of potential ischemia or scar tissue by PET in stress/rest test

Program

Thursday, June 12, 2014

Grosser Hörsaal Ost

08.15 **Eröffnung**
Prof. Dr. Gregor Zünd
Managing Director ZKF, Direktor Forschung und Lehre UniversitätsSpital Zürich

08.20 **Begrüssung**
Prof. Dr. Jürg Hodler MBA
Ärztlicher Direktor, UniversitätsSpital Zürich

08.25 **Begrüssung**
Prof. Dr. Dr. Klaus W. Grätz
Dekan der Medizinischen Fakultät der Universität Zürich

08.35 **16. Hartmann Müller Gedächtnisvorlesung**
Einführung und Preisverleihung durch Prof. Dr. Gerhard Rogler

08.40 **Vorlesung der Preisträgerin**
Prof. Dr. Fiona Powrie

09.35 Coffee Break

Session 1: Cardiovascular/Metabolics/Endocrinology

Chairpersons: Prof. Dr. Christian Matter, Prof. Dr. Oliver Kretschmar

09.50 **Wissenschaftliches Hauptreferat**
"Discontinued randomized controlled trials: reason, characteristics and associated problems"
Prof. Dr. Jan Krützfeldt, Oberarzt, Klinik für Endokrinologie, Diabetologie und Klinische Ernährung, UniversitätsSpital Zürich

10.10 **The tumor suppressor CDKN1A (p21) is targeted by the microRNA family miR-130 in hypoxia-induced pulmonary hypertension (Abstract No. 2214)**
M. Brock, TJ. Haider, J. Vogel, M. Gassmann, M. Kohler, S. Ulrich, LC. Huber

10.20 **Glycolytic inhibition with 2-deoxyglucose retards disease progression in Han:SPRD rats with polycystic kidney disease (PKD) (Abstract No. 2251)**
M. Riwanto, S. Kapoor, D. Rodriguez, I. Edenhofer, S. Segerer, R.P. Wüthrich

10.30 **Functional Characterization and Categorization of Missense Mutations that Cause Methylmalonyl-CoA Mutase Deficiency (Abstract No. 2115)**
P. Forny, DS. Froese, T. Suormala, WW. Yue, MR. Baumgartner

10.40 **Sugar-sweetened beverages with moderate amounts of fructose, but not sucrose induce fatty acid synthesis in healthy young men – a randomized cross over study (Abstract No. 2123)**
M. Hochuli, I. Aeberli, A. Weiss, M. Hersberger, H. Troxler, P. Gerber, GA. Spinas, K. Berneis

Session 2: Cancer

Chairpersons: Prof. Dr. Isabelle Schmitt-Opitz, Prof. Dr. Roger Stupp

10.55 **Wissenschaftliches Hauptreferat**
„Current and Future Research Concepts in Radiation Oncology"
Prof. Dr. Matthias Guckenberger, Klinikdirektor, Klinik für Radio-Onkologie, UniversitätsSpital Zürich

11.15 **Identification of Novel Targets for Radiosensitization of Non–Small Cell Lung Cancer by Secretome Analysis (Abstract No. 2139)**
A. Sharma, S. Bender, A. Broggini-Tenzer, O. Riesterer, M. Pruschy

11.25 **Boger, H. Schulze-Bergkamen, T. Lüdde, H. Moch, M. Heikenwalder, A. Weber**
An apoptosis-driven pathway to hepatocarcinogenesis in mice and men (Abstract No. 2257)
Y. Boege, M. Malehmir, F. Böhm, L. Frick, J. Friemel, J. Mertens, R. Maire, M. Vucur, B. Müllhaupt,

11.35 **hSIRP α-tg-hTPO-Expressing RAG2-/-, IL2Ry-/- immunodeficient mice - a xenograft model for human polycythemia vera (Abstract No. 2191)**
R. Müller, A. Theocharides, M.G. Manz

11.45 **Intracavitary Cisplatin-Fibrin Chemotherapy after Resection for Malignant Pleural Mesothelioma Patients (INFLuenCe-Meso) – preliminary results (Abstract No. 2248)**
I. Opitz, O. Lauk, M. Meerang, M. Friess, G. Wuilleret, C. Bommeli, A. Jetter, D. Günther, R. Stahel, W. Weder

11.55 Lunch/Posterviewing

Session 3: Stem Cell Research, Regenerative Medicine and Advanced Technologies

Chairpersons: Prof. Dr. Martin Wolf, Prof. Dr. Daniel Eberli

13.30 **Wissenschaftliches Hauptreferat**
"Discontinued randomized controlled trials: reasons, characteristics and associated problems"
Prof. Dr. Dirk Bassler, Klinikdirektor, Klinik für Neonatologie, UniversitätsSpital Zürich

13.50 **Marrow stromal cell based transcatheter aortic valve implantation – experiences in a preclinical animal model (Abstract No 2258)**
M. Emmert, B. Weber, P. Wolint, PE. Dijkman, V. Falk, SP. Hoerstrup

14.00 **Aging-associated intrinsic and extrinsic factors control hematopoietic stem cell behavior (Abstract No. 2200)**
L V. Kovtonyuk, R. Radpour, H. Takizawa, M G. Manz

14.10 **Maintenance of human hematopoiesis and hematopoietic stem cells in in vivo engineered bone organs (Abstract No. 2226)**
K. Fritsch, P. Bourgine, E. Piccinini, M G. Manz, I. Martin, H. Takizawa

14.20 **Dental pulp stem cells enhance the vascularization of 3D silk scaffold constructs for tissue engineering purposes (Abstract No. 2266)**
A. Woloszyk, J. Buschmann, T. Mitsiadis

Session 4: Infection/Immunity/Inflammation

Chairpersons: PD Dr. Thomas Kündig, Prof. Dr. Karin J. Metzner

14.35 **Wissenschaftliches Hauptreferat**
"Heterosubtypic antibodies to influenza viruses"
Prof. Dr. Lars Hangartner, Institut für Medizinische Virologie, Universität Zürich

14.55 **Long Term Sedation with Volatile Anesthetics Compared To Propofol Improves outcome in a Rodent Model of Sepsis (Abstract No. 2085)**
M. Schläpfer, T. Piegeler, RO. Dull, DE. Schwartz, RD. Minshall, B. Beck Schimmer[1]

15.05 **Wnt5A is a crucial factor for the pro-inflammatory response of human vascular endothelial cells to IL-4 (Abstract No. 2174)**
T. Skaria, G. Schoedon-Geiser

15.15 **Silibinin Prior to Triple Therapy Leads to End of Treatment Success in Most Difficult to Treat HIV/Hepatitis C Co-Infected Individuals (Abstract No. 2102)**
DL. Braun, A. Rauch, N. Durisch, N. Eberhard, QA. Anagnostopoulos, B. Ledergerber, R. Weber, J. Fehr

15.25 **Comparative effectiveness of immune-cell depletion and a targeted therapy against LTbR-signaling in the treatment of autoimmune pancreatitis (Abstract No. 2233)**
GM. Seleznik, Th. Reding, J. Browning, S. Segerer, S. Sonda, M. Heikenwalder, R. Graf

15.35 Coffee Break

Session 5: Neurosciences/Pharmacology

Chairpersons: Prof. Dr. Christian Baumann, Prof. Dr. Adriano Aguzzi

15.50 **Wissenschaftliches Hauptreferat**
„Methylphenidat (Ritalin): zwischen Pharmakologie und Gesellschaftsdiskussion“
Prof. Dr. Susanne Walitza, Direktorin, Kinder- und Jugendpsychiatrischer Dienst Kanton Zürich, Kinder- und Jugendpsychiatrie Universität Zürich

16.10 **Impaired Executive Functions in Complex Tasks in Children and Adolescents Born Very Preterm (Abstract No. 2199)**
F. Wehrle, B. Latal, R. Huber, R. O'Gorman, L. Kaufmann, A. Hüsser, C. Verrey, C. Hagmann

16.20 **The flexible tail of the prion protein mediates the toxicity of anti-prion antibodies (Abstract No. 2175)**
T. Sonati, J. Falsig Pedersen, R. Reimann, S. Hornemann, P. Baral, B. Wieland, M. Swayampakula, M. James, A. Aguzzi

16.30 **An Ongoing Cluster Randomized Trial to Assess the Effect of Specific Alerts in Potassium-Increasing Drug-Drug Interactions (Abstract No. 2169)**
E. Eschmann, PE. Beeler, J. Blaser

16.40 **A novel fluorescence-based live-imaging assay for sensitive detection of neuronal cell loss in hippocampal organotypic slice cultures (Abstract No. 2212)**
K. Frontzek, P. Georgiadis, T. Sonati, S. Sorce, P. Schwarz, A. Aguzzi

16.50 Posterpreis

17.05 Verleihung Georg Friedrich Götzpreis 2014

18.20 Apéro

Cardiovascular/Metabolics/Endocrinology

Basic Research

2081
PP. Becker, J. Schmitt, B. Niesler, O. Tschopp, F. Berr, A. Canbay, T. Dandekar, B. Müllhaupt, A. Geier
MicroRNAs as Mediators in the Pathogenesis of Non-Alcoholic Fatty Liver Disease and Steatohepatitis

2096
E. Unterleutner, F. Barchiesi, B. Imthurn, RK. Dubey
G-protein Coupled Estrogen Receptor mediates Capillary formation and Induces Vasculogenic pathway ALK1/pSMAD1/5/8

2131
T. Gorski, J. Krützfeldt[1]
Do myoblasts from different mouse strains differentiate into brown adipocytes?

2134
A. Galimov, J. Krützfeldt
An FGF-microRNA pathway provides a link between mitochondrial activity and muscle differentiation

2142
B. Gjoksi, C. Ghayor, F. Weber
The potential of N-methylpyrrolidone (NMP) to prevent osteoporosis and enhance bone regeneration in vivo

2154
Y. Plutino, F. Barchiesi, B. Imthurn, R. Dubey
Activation of Intracellular Calcium Triggers DHT-induced phopshoSmad1/5/8 Signaling in EPCs

2158
Z. Gai, C. Hiller, S.H. Chin, D. Konrad, A.. Kullak-Ublick
Uninephrectomy augments the effects of high fat diet induced obesity on gene expression in mouse kidney

2165
L. Rigassi, Y. Plutino, F. Barchiesi, N. Simigdala, B. Imthurn, R. Dubey
Regulation of microRNAs in Endothelial Progenitor Cells (EPCs) by Sex Steroids

2177
K. Drägert, I. Bhattacharya, E. Haas, P. Seebeck, U. Held, A. Azzi, S. Brown, M. Hall, R. Humar, E. Battegay
Adipocyte-specific knockout of rictor impairs anti-contractile properties of PVAT and increases mean arterial pressure in mice

2194
JW. Deuel, F. Vallelian, DJ. Schaer
Lipid degradation catalyzed by free heme is a hallmark of endothelial hemoglobin toxicity.

2210
M.G. Dietrich, R.A. Zuellig, B.A. Hemmings, G.A. Spinas, R. Lehmann, O. Tschopp, M. Niessen
PKBα regulates pancreatic β-cell mass

2214
M. Brock, TJ. Haider, J. Vogel, M. Gassmann, M. Kohler, S. Ulrich, LC. Huber
The tumor suppressor CDKN1A (p21) is targeted by the microRNA family miR-130 in hypoxia-induced pulmonary hypertension

2230
GA. Kullak-Ublick, WE. Thasler, J. Mwinyi
Bile acid induced changes in the expression of miRNAs and genes involved in drug metabolism and disposition

2231
T. Claro da Silva, J. Mwinyi, GA. Kullak-Ublick, C. Hiller
Vitamin D3 Alters Expression of Intestinal Drug Transporters, Metabolizing Enzymes and miRNAs in Caco-2 Cells

2237
I. Bhattacharya, A. Perez Dominguez, K. Drägert, R. Humar, E. Battegay, E. Haas
Hypoxia enhances the effect of tumor necrosis factor in adipocytes by elevating the expression of inducible nitric oxide synthase and cyclooxygenase-2

2249
A. Zhakupova, M. Krols, S. Janssens, A. Von Eckardstein, T. Hornemann
REGULATION OF THE MAMMALIAN SERINE PALMITOYLTRANSFERASE

Translational Research

Abstract-ID: 2079
D. Rodriguez, M. Riwanto, I. Edenhofer, S. Segerer, RP. Wüthrich, S. Kapoor
EFFECT OF THE SGLT2 INHIBITOR DAPAGLIFLOZIN ON CYSTIC DISEASE PROGRESSION IN PCK RATS WITH AUTOSOMAL RECESSIVE POLYCYSTIC KIDNEY DISEASE

2105
FM. Morsbach, SG. Gordic, RG. Göttii, CG. Gruner, HA. Alkadhi, RM. Manka
Quantitative Comparison of 2D and 3D Late Gadolinium Enhancement MR Imaging for Cardiomyopathies

2106
FM. Morsbach, WM. Wurnig, HA. Alkadhi
Feasibility and Value of Iterative Reconstructions for Urinary Stone Characterization on Single-Source Dual-Energy CT

2115
P. Forny, DS. Froese, T. Suormala, WW. Yue, MR. Baumgartner
Functional Characterization and Categorization of Missense Mutations that Cause Methylmalonyl-CoA Mutase Deficiency

2162
M. Linecker, E. Kachaylo, P. Limani, AC. Piguet, C. Tschuor, DA. Raptis, M. Foti, R. Graf, JF. Dufour, A. Vuck, P. Kambakamba, P. Kron, B. Humar, PA. Clavien
The impact of exercise and ω3- fatty acids on ischemia reperfusion injury and regeneration of fatty liver

2196
KC. Brunner, CHF. Hämmerle, MÖ. Özcan[1]
Fatigue Strength and Weibull Characteristics of Inlay-retained Resin-bonded Fixed Dental Prosthesis

2228
H. Giral, M. Keel, A. Kratzer, C. Tournaire, T F. Lüscher, A. Aguzzi, U. Landmesser
Identification of miRNAs regulating inflammatory leukocyte recruitment: functional high-throughput screening (HTS)

2234
A. Kratzer, N. Kraenkel, MF. Mueller, H. Giral, J. Manz, G. Treichel, P. Jakob, TF. Luescher, U. Landmesser
miR-223 and miR-181a as potential role players in monocyte subpopulations from patients with acute and stable coronary syndrome

2250
N. Samartzis, I. Ihnenfeld, A. Noske, EP. Samartzis, D. Fink, P. Imesch
Tissue microarray analysis of steroid receptors including GPER in adenomyosis

2251
M. Riwanto, S. Kapoor, D. Rodriguez, I. Edenhofer, S. Segerer, R.P. Wüthrich
Glycolytic inhibition with 2-deoxyglucose retards disease progression in Han:SPRD rats with polycystic kidney disease (PKD)

2261
I. Alecu, TW. Mühlbradt, C. Arenz, A. Penno, C. Thiele, A. Von Eckardstein, T. Hornemann
Trafficking and Metabolism of 1-Deoxysphingolipids and Their Implications in Pathophysiological Changes

2265
R. Meletta, A. Müller, L. Mu, A. Chiotellis, N. Borel, Z. Rancic, P.A. Kaufmann, S.M. Ametamey, R. Schibli, S.D. Krämer
Evaluation of radiolabeled inhibitors of the immune co-stimulatory molecule CD80 for vulnerable atherosclerotic plaque imaging

Clinical Trials

2123
M. Hochuli, I. Aeberli, A. Weiss, M. Hersberger, H. Troxler, P. Gerber, GA. Spinas, K. Berneis
Sugar-sweetened beverages with moderate amounts of fructose, but not sucrose induce fatty acid synthesis in healthy young men – a randomized cross over study

2184
B. Ammann, R. Knols, P. Baschung Pfister, RA. De Bie, ED. De Bruin
Application of principles of exercise training in sub-acute and chronic stroke survivors: a systematic review

2185
VJ. Jacomella, GP. Gerber, MK. Mosimann, MH. Husmann, CT. Thalhammer, IW. Wilkinson, KB. Berneis, BA. Amann-Vesti
Small dense low density lipoprotein particles are associated with poor early outcome after angioplasty in peripheral artery disease

2244
M. Frick, V. Jacomella, S. Roth, B. Amann -Vesti, N. Ulmer, M. Husmann
Pulse wave velocities in peripheral arterial disease derived from carotid-femoral and brachial assessments

2252
RK. Clemens, TK. Kreindel, AI. Alomari
Imaging Characterization of Central Conducting Lymphatic Anomalies

2253
RK. Clemens, C. Stamoulis, BR. Amann - Vesti, AI. Alomari
Sclerotherapy in Venous malformations: Risk of Intraprocedural Complications

2254
RK. Clemens, C. Stamoulis, BR. Amann - Vesti, AI. Alomari
Ethiodol in Sclerotherapy of Venous Malformations

Cancer

Basic Research

2103
A. Theocharides, S. Dobson, E. Laurenti, F. Notta, V. Voisin, PY. Cheng, M. Minden, C. Mullighan, E. Torlakovic, J. Dick
The Ikaros 6 isoform cooperates with BCR-ABL1 to induce human acute myeloid leukemia in xenografts

2107
St. Georgiopoulou, F. Aimi, I. Kalus, F. Lehner, I. Bhattacharya, K. Drägert, P. Limani, M. Rüegg, MN. Hall, N. Lindenblatt, E. Haas, EJ. Battegay, R. Humar
Endothelial mTORC2 is essential for capillary remodeling and de novo angiogenesis in response to FGF2

2109
A. Mortezavi, S. Salemi, N. Rupp, PJ. Wild, D. Eberli
Reduced autophagy levels are associated with a higher Gleason score, tumor stage and an increased rate of prostate cancer specific death

2113
K. Wronska, J. Reber, S. Haller, S. Schaefer, R. Schibli, C. Mueller
Targeted Tumor Therapy Using 177Lu-Folate in Combination with 5-Fluorouracil as a Radiosensitizing Agent

2114
A. Theocharides, R. Müller, Y. Saito, M. Manz
Development of a xenograft model for myelofibrosis

2127
P. Limani, Ch. Tschuor, A. Schlegel, E. Kachaylo, M. Linecker, JH. Jang, S. Georgiopoulou, JM. Lehn, R. Graf, B. Humar, PA. Clavien
Inositol trispyrophosphate (ITPP) and its anti-hypoxic potential in colorectal metastases of the liver

2130
M. Nuvolone, S. Sorce, P. Pelczar, E. Rushing, F. Lavatelli, G. Palladini, G. Merlini, A. Aguzzi
Generation of a conditional transgenic mouse model of immunoglobulin light chain (AL) amyloidosis.

2135
T. Piegeler, M. Schläpfer, RO. Dull, B. Beck-Schimmer, RD. Minshall
Mechanistic insight regarding a possible inhibition of malignant cell metastatic potential by amide-linked local anesthetics

2145
G. Iotzova-Weiss, SN. Freiberger, I. Kleiber-Schaaf, P. Johansen, L. French, GFL. Hofbauer
TLR4 is a negative regulator of keratinocyte proliferation

2149
M. Meerang, A. Boss, E. Felley-Bosco, O. Lauk, S. Arni, B. Bitanihirwe, R. Stahel, W. Weder, I. Opitz
Evaluation of Tumor Imaging Techniques for Malignant Pleural Mesothelioma orthotopic Rat Model

2163
K. Grabliauskaite, S. Sonda, E. Saponara, T. Reding Graf, R. Gra
Loss of p21WAF1/Cip1 accelerates senescence and acinar-to-ductal metaplasia formation during pancreatitis

2164
K. Grabliauskaite, S. Sonda, E. Saponara, T. Reding Graf, R. Graf
Acinar-specific TGF-b signalling regulates acinar cell regeneration

2180
JF. Glaus Garzon, K. Léger, K. Bartnicka, I. Jurisica, M. Hottiger, R. Wenger, L. Borsig
The Role of Hypoxia and Inflammation in the Tumor Microenvironment of Colon Carcinoma

2183
JH. Jang, Y. Yamada, I. De Meester, S. Arni, P. Limani, W. Weder, W. Jungraithmayr
Inhibition of CD26/DPP4 decreased lung tumor growth

2188
IT. Tritschler, JS. Schroeder, MW. Weller
The TGF-beta superfamily coreceptor TbRIII modulates both Smad1/5/8 and Smad2 signaling pathways in gliomas

2191
R. Müller, A. Theocharides, M.G. Manz
hSIRPα-tg-hTPO-Expressing RAG2-/-, IL2Ry-/- immunodeficient mice - a xenograft model for human polycythemia vera

2195
C. Corrò, M. Rechsteiner, H. Moch
Non-invasive identification of VHL mutations in plasma by deep-sequencing with subsequent assessment of mutant pVHL functionality in FFPE by FRET in ccRCC patients

2203
C. Eberhardt, M. Wurnig, A. Wirsching, M. Lesurtel, A. Boss
Assessment of tissue diffusion and pseudo-diffusion of abdominal organs by intravoxel incoherent motion MRI in a cohort of C57Bl/6 mice

2208
GM. Seleznik , Th. Reding, S. Sonda, M. Souter, M. Heikenwalder, R. Graf
Lymphotoxin promotes acinar cell reprogramming and accelerates pre-neoplastic conversion in Kras induced pancreatic tumorigenesis

2215 :
HC. Wong, HE. Kohrt, JA. Shizuru, AMS. Müller
Maximizing Graft-Versus-Leukemia effects by WT1-vaccination of donors and stringent selection of allograft components

2227
E. Saponara, S. Sonda, G. Seleznik, K. Grabliauskaite, T. Reding, R. Graf
Serotonin regulates cytoskeletal remodeling during the formation of pancreatic acinar-to-ductal metaplasia

2247
J. Kresoja-Rakic, G. Ziltener, R. Stahel, E. Felley-Bosco
Characterization of the mechanisms regulating calretinin expression in malignant pleural mesothelioma

2260
R. Schweizer, P. Kamat, HJ. Klein, P. Kaenel, S. Salemi, M. Calcagni, P. Giovanoli, D. Eberli, A. Andres, JA. Plock
Adipose-derived mesenchymal stem cells may promote breast cancer growth and metastatic spread

2262
H. Sievert, N. Pällmann, K. Miller, I. Hermans-Borgmeyer, S. Venz, A. Sendoel, M. Preukschas, M. Schweizer, S. Böttcher, T. Streicher, M. Manz, M. Balabanov, J. Hauber, K. Duncan, N. Parrinello, S. Balabanov
A novel mouse model for inhibition of DOHH mediated hypusine modification reveals crucial function for embryonic development, proliferation and oncogenic transformation

2264
M. Balabanov, N. Pällmann, M. Preukschas, D. Steinemann, W. Hofmann, A.. Gompf, T. Streichert, T. Braunschweig, M. Copland, K. Rudolph, C. Bokemeyer, S. Koschmieder, A. Schuppert, S. Balabanov, T. Brümmendorf
A “telomere-associated secretory phenotype” (TASP) cooperates with BCR-ABL to drive malignant proliferation of leukemic cells

Translational Research

2086
T. Mehra, G. Grözinger, S. Mann, S. Mann, A. Naumann, R. Moos, W. Omlor, M. Röcken, CD. Claussen, S. Clasen, C. Garbe
Primary Localization and Tumor Thickness as Prognostic Factors of Survival in Patients with Mucosal Melanoma

2139
A. Sharma, S. Bender, A. Broggini-Tenzer, O. Riesterer, M. Pruschy
Identification of Novel Targets for Radiosensitization of Non–Small Cell Lung Cancer by Secretome Analysis

2150
M. Meerang, B. Bitanihirwe, M. Friess, K. Bérard, A. Soltermann, E. Felley-Bosco, B. Seifert, R. Stahel, W. Weder, I. Opitz
NF2/Hippo Pathway Dysregulation as Predictors of Survival for Mesothelioma Patients Treated with Multimodal therapy

2159
SN. Freiberger, G. Iotzova-Weiss, PF. Cheng, MP. Levesque, R. Dummer, K. Skak, GFL. Hofbauer
Investigating the Mechanism of Action of Ingenol Mebutate in Squamous Cell Carcinoma

2167
A. Kashyap, E. Delamarche, P. Schraml, G V. Kaigala, A. Soltermann
Local DNA extraction from tissue sections using the Microfluidic Probe for mutation profiling of tumors

2172
K J. Nytko, K J. Pruschy
Dynamic Changes of Tumor Hypoxia under Treatment with Ionizing Radiation

2189
S. Bengs, A. Weber, S. Lang, S. Vavricka, P. Frei, M. Halama, M. Fried, G. Rogler, M. Scharl
PTPN2 (TC-PTP), PTPN9 (PTP-MEG2) and PTPN23 (HD-PTP) are involved in the regulation of the JAK-STAT and MAPK/ERK pathway in colorectal cancer (CRC)

2209
CF. Waschkies, T. Reding Graf, GM. Seleznik, U. Ungethüm, R. Graf
Magnetic Resonance Imaging of the Pancreas in a Transgenic Mouse Model of Pancreatic Carcinogenesis

2219
J. Mwinyi, K. Vokinger, A. Jetter, U. Breitenstein, C. Hiller, GA. Kullak-Ublick, A. Trojan
Impact of variable CYP Genotypes on Breast Cancer Relapse in Patients undergoing adjuvant Tamoxifen Therapy

2220
LD. Frick, Y. Böge, F. Böhm, J. Friemel, L. Quagliata, LM. Terracciano, M. Heikenwälder, A. Weber
Biliary/progenitor-cell markers and liver-specific Wnt target genes define distinct subgroups of hepatocellular carcinoma

2221
EX. Keller, C. Acevedo, A. Mortezavi, P. Kardas, J. Samaridis, T. Sulser, HH. Hirsch, M. Provenzano
Antibody response against BK virus large tumor antigen as an independent predictor of biochemical recurrence after radical prostatectomy
with PCa at first diagnosis.

2222
S. Sanchez, J. Mata Pavia, S. Lindner, E. Charbon, M. Wolf
Last generation near infrared imaging system

2235
A. Renganathan, J. Kresoja-Rakic, N. Echeverry, G. Ziltener, B. Vrugt, I. Opitz, R. Stahel, E. Felley-Bosco
GAS5 long non coding RNA in malignant pleural mesothelioma

2242
D. Vital, M. Roessle, RD. Laske, GF. Huber
Prognostic markers of salivary gland carcinomas

2243
N. Echeverry, G. Ziltener, R. Stahel, E. Felley-Bosco
Characterizing sensitivity to dual PI3K/mTOR inhibitors in Mesothelioma

2245
J. Mata Pavia, S. Sanchez Majos, E. Charbon, M. Wolf
Measurement and modeling of microlenses for sensitivity enhancement of novel near-infrared imager.

2246
RD. Laske, I. Scholz, C. Meerwein, D. Vital, M. Rössle, GF. Huber
Is perineural invasion really a predictive factor?

2257
Y. Boege, M. Malehmir, F. Böhm, L. Frick, J. Friemel, J. Mertens, R. Maire, M. Vucur, B. Müllhaupt, R. Boger, H. Schulze-Bergkamen, T. Lüdde, H. Moch, M. Heikenwalder, A. Weber
An apoptosis-driven pathway to hepatocarcinogenesis in mice and men

Clinical Trials

2108
A. Mortezavi, E. Keller, C. Fankhauser, PJ. Wild, M. Provenzano, T. Sulser, D. Eberli
Needle biopsy performed in a tertiary care center results in significantly less clinically relevant undergrading of prostate cancer

2117
A. Kostron, M. Friess, P. Kestenholz, D. Schneiter, I. Inci, S. Hillinger, W. Weder, I. Opitz
Perioperative outcome for meothelioma patients undergoing induction chemotherapy followed by extrapleural pneumonectomy compared to pleurectomy / decortication

2118
I. Opitz, M. Friess, P. Kestenholz, D. Schneiter, T. Frauenfelder, DL. Nguyen-Kim, B. Seifert, RA. Stahel, W. Weder
The Zurich Score: Improved patient selection for mesothelioma patients undergoing surgery after induction chemotherapy. A review of 12 years' experience

2151
PK. Kambakamba, CT. Tschuor, PK. Kron, KS. Slankamenac, PAC. Pierre Alain, ML. Lesurtel
Impact of Epidural Analgesia on Perioperative Kidney Function in Hepatic Surgery.

2248
I. Opitz, O. Lauk, M. Meerang, M. Friess, G. Wuilleret, C. Bommeli, A. Jetter, D. Günther, R. Stahel, W. Weder
Intracavitary Cisplatin-Fibrin Chemotherapy after Resection for Malignant Pleural Mesothelioma Patients (INFLuenCe-Meso) – preliminary results

Stem Cell Research, Regenerative Medicine and Advanced Technologies

Basic Research

2084
S. Stübinger, K. Nuss, K. Klein, P. Kronen, B. Von Rechenberg
Osseointegration of dental implants: Are sheep a suitable model?

2091
D. Li, E. Schlaepfer, C. Knowlton, B. Kim, A. Audigé, R. Speck
Vpx mediated Degradation of SAMHD1 Does Not Render HSCs more Permissive to Lentiviral Gene Transfer

2104
CNA. Nombela-Arrieta, MGM. Manz
Quantitative Imaging of Hematopoietic Bone Marrow Microenvironment in Health and Disease

2110

RF. Speck, R. Myburgh, KH. Krause, P. Salmon, MS. Pepper
Evidence of a functioanl cure for HIV by gene engineering HIV-resistant CD4+ T cells in humanized mice

2121
O. Evrova, J. Houska, M. Calcagni, E. Bonavoglia, P. Giovanoli, V. Vogel, J. Buschmann
Bioactive DegraPol electrospun scaffold produced by emulsion electrospinning for tendon repair application – scaffold characterization and release kinetics of biomolecules

2122
G. Meier Bürgisser, M. Calcagni, A. Müller, E. Bonavoglia, G. Fessel, JG. Snedeker, P. Giovanoli, J. Buschmann
Prevention of Peritendinous Adhesions Using an Electrospun DegraPol Polymer Tube: a Histological, Ultrasonographic and Biomechanical Study in Rabbits

2124
S. Salemi, A. Mortezavi, T. Sulser, D. Eberli
The Role of Autophagy in the Differentiation of Adipose Derived Stem Cells to Functional Smooth Muscle Cells for Urologic Tissue Engineering

2125
S. Salemi, A. Mortezavi, M. Horst, R. Gobet, T. Sulser, D. Eberli
The role of authophagy in neuropathic bladder remodeling

2132
A. Mizbani, J. Krützfeldt
Identification of microRNAs involved in the activation of adult skeletal muscle stem cells

2133
K. Turcekova, J. Krützfeldt
Regulation of skeletal muscle differentiation by a distinct subset of microRNAs

2138
A. Wirsching, E. Melloul, R. Graf, PA. Clavien, M. Lesurtel
Temporary Portal Vein Occlusion does not compromise Liver Regeneration of the occluded lobes

2140
DE. Haralampieva, SO. Salemi, TH. Betzel, IV. Dinulovich, ST. Kraemer, TU. Sulser, CH. Handschin, SI. Ametamey, DA. Eberli
Non-Invasive Tracking Of Muscle Precursor Cells For Muscle Tissue Engineering

2141
C D. Schuh, E. Craigie, D. Hänni, A. Hall
Multiphoton imaging of intracellular structure and function in the renal proximal tubule

2144
M. Rottmar, M. Wurnig, A. Boss, D. Eberli
Magnetization transfer (MT)-MRI characterizes in vivo fiber formation of muscle precursor cells

2181
A. Hegglin, S. Mikkat, M. Russ, M. Kreutzer, B. Vollmar, P. Giovanoli, MO. Glocker, N. Lindenblatt
Rho-GDI 2-connected signalling during skin graft revascularization – a proteomic study

2200
L V. Kovtonyuk, R. Radpour, H. Takizawa, M G. Manz
Aging-associated intrinsic and extrinsic factors control hematopoietic stem cell behavior

2226
K. Fritsch, P. Bourgine, E. Piccinini, M G. Manz, I. Martin, H. Takizawa
Maintenance of human hematopoiesis and hematopoietic stem cells in in vivo engineered bone organs

2232
D. Natsiou, T. Mitsiadis, L. Jimenez-Rojo
3D in vitro culture for the expansion of dental epithelial stem cells

2238
E. Kachaylo, Ch. Tschuor, P. Limani, P. Ramadori, M. Foti, B. Humar, R. Graf, PA. Clavien
DEFICIENT MICRORNA-21 INDUCTION PROMOTES SMALL-FOR-SIZE SYNDROME FOLLOWING EXTENDED HEPATECTOMY IN MICE

2239
P. Pagella, A. Woloszyk, E. Neto, M. Lamghari, T. Mitsiadis
Cross-talk between sensory innervation and mesenchymal stem cells for orofacial regeneration in a microfluidics co-culture system.

2241
H. Takizawa, Y. Saito, L. Kovtonyuk, K. Fritsch, M. Manz
Lipopolysaccharide impairs hematopoietic stem cell function via direct activation of Toll-like receptor 4 pathway

2263
JA. Plock, J. Schnider, HJ. Klein, W. Zhang, W. Tsuji, K. Marra, P. Giovanoli, V. Gorantla
Immunomodulation with Adipose and Bone Marrow Derived Mesenchymal Stem Cells in Vascularized Composite Allotransplantation

2266
A. Woloszyk, J. Buschmann, T. Mitsiadis
Dental pulp stem cells enhance the vascularization of 3D silk scaffold constructs for tissue engineering purposes

2267
L. Jaatinen, S. Salemi, S. Miettinen, J. Hyttinen[2], D. Eberli
Neuronal differentiation of adipose-derived stem cells by electric current and copper for bladder engineering

2269
YC. Yakkala, KD. Kingston, SY. Saito, ST. Sparwasser, TH. Takizawa, MM. Manz
Flt3 expression in Hematopoietic Stem Cells

Translational Research

2097
N. Ruangsawasdi, M. Zehnder, F. Weber
Fibrin Gel Improved Tissue Ingrowth and Cell Differentiation in Human Immature Premolar Implanted in Rats

2157
A. Aguzzi, A. Ahlm, K. Arroyo, M. Bieri, B. Li, G. Manco, B. Piccapietra, L. Takacs, C. Tournaire, A. Varol, S. Yakushev
High-throughput automated genotyping of transgenic laboratory animals

2176
PE. Dijkman, L. Frese, B. Weber, A. Driessen-Mol, MY. Emmert, J. Sherman, J. Gruenenfelder, N. Cesarovic, B. Sanders, P. Zilla, V. Falk, FPT. Baaijens, SP. Hoerstrup
Off-the-shelf Decellularized Tissue-Engineered Heart Valves Repopulate and Remodel rapidly in pre-clinical animal models

2213
A. König, D. Cadosch, M. Werner[1], HP. Simmen, A. Wanner, C. Cinelli
Prospective isolation of perivascular stem cells for the treatment of critical size bone injuries

2255
MY. Emmert, P. Wolint, S. Winklhofer, H. Alkadhi, V. Falk, SP. Hoerstrup
Intramyocardial transplantation and in vivo tracking of human stem cell based three dimensional microtissues in the porcine heart

2256
MY. Emmert, P. Wolint, J. Pavicevic, E. Caliskan, V. Falk, SP. Hoerstrup
Image guided evaluation of cellular retention and survival after intramyocardial transcatheter based mesenchymal stem cell transplantation into the infarcted pig heart

2258
M. Emmert, B. Weber, P. Wolint, PE. Dijkman, V. Falk, SP. Hoerstrup
Marrow stromal cell based transcatheter aortic valve implantation – experiences in a preclinical animal model

2270
F. Wolpert, I. Tritschler, A. Steinle, M. Weller, G. Eisele
A disintegrin and metalloproteinases (ADAM) 10 and 17 modulate the immunogenicity of glioblastoma stem cells

Clinical Trials

2148
D. Scheiner, D. Fink, D. Perucchini, C. Betschart
Urogynaecologic operations in Switzerland between 1998 and 2013

2156
M. Weisskopf, G. Bucklar, J. Blaser
Tools in a Clinical Information System Supporting Clinical Trials at a Swiss University Hospital

Infection/Immunity/Inflammation

Basic Research

2078
MR. Spalinger, C. Chassard, S. Kasper, L. Biedermann, S. Vavricka, I. Frey-Wagner, K. Attrot, C. Lacroix, M. Fried, G. Rogler, M. Scharl
T cell specific loss of PTPN2 leads to miss-balanced T helper cell differentiation resulting in aggravated intestinal inflammation

2082
M-A. Rochat, E. Schläpfer, R.F. Speck
Promising Role of Toll-Like Receptor (TLR) Agonist in Concert with Prostratin for Eradication of Latently HIV-Infected cells

2083
VV. Vongrad, J. Imig, P. Mohammadi, S. Kishore, L. Jaskiewicz, M. Zavolan, J. Hall, N. Beerenwinkel, HF. Günthard, KJ. Metzner
The Role of RNA Interference in HIV-1 Infected Primary Human Monocyte-Derived Macrophages

2085
M. Schläpfer, T. Piegeler, RO. Dull, DE. Schwartz, RD. Minshall, B. Beck Schimmer[1]
LONG TERM SEDATION WITH VOLATILE ANESTHETICS COMPARED TO PROPOFOL IMPROVES OUTCOME IN A RODENT MODEL OF SEPSIS

2111
C. Lutz, M. Caj, M. Fried, G. Rogler, M. Hausmann
MyD88 signaling is not essential in intestinal fibrosis in mice

2126
IL. Leonardi, FN. Nicholls, BT. Tewes, RG. Greinwald, GR. Rogler, IFW. Frey-Wagner
Oral administration of DSS induces a cecum localized colitis in rabbits

2128
C. Zhu, N J. Kräutler, B. Li, I. Abakumova, P. Schwarz, C. Tiberi, P. Pelczar, E J. Rushing, M. Heikenwälder, G. Rogler, A. Aguzzi
Inappropriate enteric lymphotoxin β receptor signaling causes iron-deficient anemia

2136
RD. Kouyos, A. Rauch, DL. Braun, S. Yerly, J. Böni, T. Klimkait, V. Aubert, B. Ledergerber, HF. Günthard
Higher risk of sexually acquired HCV-coinfection in MSM with wide HIV transmission bottleneck

2146
Ms. Bombardo Ayats, Ms. Sonda, Mr. Graf
Epigenetic acetylation mechanisms are activated during progenitor cell-based regeneration in the adult pancreas.

2147
Ms. Bombardo Ayats, Mr. Graf, Ms. Sonda
Epigenetic acetylation mechanisms are activated during progenitor cell-based regeneration in the adult pancreas.

2152
E. Becker, C. Stanzel, K. Atrott, G. Rogler, I. Frey-Wagner
Effects of isotretinoin treatment on epigenetic programming in T cells

2153
E. Becker, C. Stanzel, S. Schmidt, K. Atrott, L. Biedermann, A. Rehman, D. Jonas, C. Von Mering, G. Rogler, I. Frey-Wagner
Effects of isotretinoin treatment on murine gut microbiota composition

2166
A. Cee, K. Atrott, M. Fried, G. Rogler, I. Frey-Wagner
Tissue specific overexpression of Nrf2 worsens acute but not chronic intestinal inflammation.

2170
RC. Gerosa, S. Boettcher, MG. Manz
The regulatory role of non-hematopoietic bone marrow cells in steady-state and during hematopoietic stress

2174
T. Skaria, G. Schoedon-Geiser
Wnt5A is a crucial factor for the pro-inflammatory response of human vascular endothelial cells to IL-4

2178
D. Kenkel, A. Boss, M. Wurnig, D. Nanz, C. Rossi
Whole-body diffusion tensor imaging (DTI)

2179
YL. Kok, C. Oberle, NK. Campbell, F. Di Giallonardo, C. Leemann, H. Kuster, B. Joos, D. Braun, HF. Günthard, KJ. Metzner
Replication Capacity of Primary HIV-1 Isolates From Acutely Infected Patients in Macrophages

2182
Y. Saito, L. Kovtonyuk, H. Takizawa, MG. Manz
Impact of commensal microbiota on hematopoietic stem and progenitor cell homeostasis

2201
P. Kellner, M. Müller, P. Eugster, M. Schläpfer, B. Beck-Schimmer
Long-term sedation with sevoflurane offers protective effects in a rat model of acute lung injury

2204
Y. Yamada, J. Jang, I. Inci, W. Weder, W. Jungraithmayr
The CD26-costimulatory pathway is critical for Th17-mediated lung allograft acceptance

2205
L. Peter, Th. Reding, G.M. Seleznik, S. Sonda, R. Graf
Effects of p21 deficiency in murine autoimmune pancreatitis

2206
A. Wyss, T. Raselli, K. Atrott, I. Frey-Wagner, AW. Sailer, G. Rogler, B. Misselwitz
The role of EBI2 and oxysterols in the pathogenesis of inflammatory bowel diseases (IBD) and the generation of lymphoid structures in mouse intestine

2207
K. Schilcher, F. Andreoni, S. Uchiyama, T. Ogawa, RA. Schuepbach, AS. Zinkernagel
Increased NET-mediated Staphylococcus aureus clearance through inhibition of nuclease activity by clindamycin and immunoglobulin

2211
K. Schlesinger, S. Sonda, R. Graf
3,3',5-Triiodothyronine Improves Pancreatic Regeneration in Murine Acute Pancreatitis

2223
DM. Heuberger, M. Ender, RA. Schuepbach
Co-receptor Dependent Activation of Protease Activated Receptors by Clotting Proteases.

2233
GM. Seleznik, Th. Reding, J. Browning, S. Segerer, S. Sonda, M. Heikenwalder, R. Graf
Comparative effectiveness of immune-cell depletion and a targeted therapy against LTbR-signaling in the treatment of autoimmune pancreatitis

2268
SN. Schweizer, TC. Tiberi, RE. Rushing, WH. Welzl, WM. Wojtal, ST. Suter
The absence of TNF exacerbates spontaneous neuroinflammation in MOG-specific TCR-transgenic (2D2) mice

Translational Research

2077
NK. Campbell, F. Di Giallonardo, Y. Duport, C. Leemann, S. Schmutz, HF. Günthard, KJ. Metzner
Generation of Individual Specific HIV-1 Full Length Reference Genomes via Illumina Sequencing

2087
N. Leimer, A. Furrer, M. Schwarz, AS. Bahlmann, F. Andreoni, U. Matt, K. Seidl, RA. Schüpbach, AS. Zinkernagel
Staphylococcus aureus Small Colony Variants are induced by low pH

2089
A. Tarnutzer, C.M. Zürcher, F. Andreoni, K. Schilcher, R.A. Schuepbach, A.S. Zinkernagel
Clindamycin and Intravenous immunoglobulin influence Group A Streptococcus virulence factor activity

2098
I. Inci, M. Schuurmans, S. Hillinger, P. Kestenholz, C. Benden, W. Weder
Lung transplantation for emphysema: Impact of age on short and long-term survival

2099
K. Seidl, M. Leemann, Y. Achermann, AS. Zinkernagel
Role of SCCmec in Staphylococcus aureus induced endothelial cell cytotoxicity

2143
SM. Frei, MR. Spalinger, A. Fürst, E. Jehle, M. Fried, G. Rogler, MM. Scharl
Pathogen-Associated Molecular Pattern Contribute to Fistula-Associated Epithelial-Mesenchymal

Clinical Trials

2090
S. Jordan, B. Maurer, M. Toniolo, BA. Mihel, O. Distler
Comparison of performance of new ACR/EULAR and old ACR classification criteria for systemic sclerosis

2093
B. Maurer, N. Graf, B. Michel, C. Metzig, V. Lanius, D. Khanna, O. Distler
Prediction of worsening of skin fibrosis in patients with diffuse systemic sclerosis using the EULAR Scleroderma Trials and Research (EUSTAR) registry

2100
DL. Braun, RD. Kouyos, B. Balmer, C. Grube, R. Weber, HF. Günthard
Atypical Clinical Presentations Occur in One Third of 293 Patients with a Primary HIV-1 Infection

2101
DL. Braun, RD. Kouyos, R. Ghenzi, C. Grube, R. Weber, HF. Günthard
Increasing rates of STI are Linked to Reduced Condom Use in Patients with Primary HIV-infection

2102
DL. Braun, A. Rauch, N. Durisch, N. Eberhard, QA. Anagnostopoulos, B. Ledergerber, R. Weber, J. Fehr
Silibinin Prior to Triple Therapy Leads to End of Treatment Success in Most Difficult to Treat HIV/Hepatitis C Co-Infected Individuals

Neurosciences/Pharmacology

Basic Research

2080
P. Mayank L. Hofstetter, B. Stieger
Proteomic and transcriptomic approach to explore novel ATPases in rat canalicular membrane

2092
N. Cesarovic, M. Arras, P. Jirkof
Impact of inhalation anaesthesia, surgery and analgesia on home cage behaviour in mice

2094
R. Gerig, S. Ihrle, JH. Sim, C. Röösli, A. Eiber, A. Huber
Mechanical properties of the incudo-malleolar joint in the middle ear

2095
G. Bertolini, AA. Tarnutzer, KP. Weber, D. Straumann, S. Marti
Mechanism of rebound nystagmus

2116
C. Feuerstacke, C. Stieger
Role of Skeletal Muscle Transport Systems in Statin-Induced Myotoxicity

2137
A. Lau, D. Goniotaki, P. Pelczar, S. Hornemann, A. Aguzzi
Examining the Communication between Domains of the Prion Protein

2160
M. Einsiedler, V. Chandrasekar, T. O'Connor, S. Yaganoglu, A. Lau, A. Aguzzi
Glia-Dependent Non-Cell Autonomous Toxicity in Prion Disease

2161
M. Einsiedler, V. Chandrasekar, T. O'Connor, S. Yaganoglu, A. Lau, A. Aguzzi
Glia-Dependent Non-Cell Autonomous Toxicity in Prion Disease

2171
AKK. Lakkaraju, H. Budka, P. Liberski, A. Aguzzi
Molecular mechanisms involved in the development of spongiform phenotype and neurotoxicity in prion infections.

2186
B. Li, S. Hornemann, C. Zhu, G. Meisl, T. P.J.Knowles, A. Aguzzi
Sensitive prion infectivity titration with an automated homogeneous-phase bioassay: Digital Prion Infectivity Assay (dPIA)

2187
P. Dametto, C. Bridel, A. Lakkaraju, L. Villiger, T. O'Connor, U. Herrmann, P. Pelczar, T. Rülicke, D. McHugh, A. Adili, A. Aguzzi
MEMBRANE TETHERING OF THE FLEXIBLE TAIL OF THE PRION PROTEIN TRIGGERS UNFOLDED PROTEIN RESPONSE AND NEURODEGENERATION
2192
R. Reimann, T. Sonati, S. Hornemann, A. Aguzzi
Safety assessment of potentially therapeutic anti-prion antibodies

2193
A. Senatore, M. Hermann, P. Pelczar, A. Aguzzi
MODELING GENETIC PRION DISEASES LINKED TO EXTRA OCTAPEPTIDE REPEATS: PATHOGENIC MECHANISMS AND OCTAPEPTIDE LIGAND BASED THERAPY

2197
DG. Goniotaki, AL. Lakkaraju, SS. Sorce, AG. Aguzzi
Inhibition of metabotropic glutamate receptor 5 (mGluR5) is protective against prion-induced toxicity

2198
S. Sorce, M. Nuvolone, A. Keller, J. Falsig, A. Varol, P. Schwarz, H. Budka, A. Aguzzi
The NADPH oxidase enzyme NOX2 contributes to the pathology of prion diseases

2212
K. Frontzek, P. Georgiadis, T. Sonati, S. Sorce, P. Schwarz, A. Aguzzi
A novel fluorescence-based live-imaging assay for sensitive detection of neuronal cell loss in hippocampal organotypic slice cultures

2216
F. Scholkmann, S. Kleiser, M. Pastewski, T. Hapuarachchi, C. Hagmann, JC. Auchère, M. Wolf
Using nonlinear data analysis and data mining to assess physiological changes in preterm infants measured with near-infrared spectroscopy, pulse oximetry and electrocardiography

2240
L. Horvath, D. Bodmer, V. Radojevic, A. Monge Naldi
Activin signaling disruption in the cochlea does not influence hearing in adult mice

Translational Research

2088
E. Eschmann, S. Karlen, M. Schneemann, J. Blaser
Should ePrescribing Systems Prevent Incorrect Intravenous Bolus Orders?

2168
US. Herrmann, A. Schütz, D. Saban, M. Nuvolone, H. Shirani, D. Huang, B. Li, B. Ballmer, A. Aslund, J. Mason, EJ. Rushing, H. Budka, P. Hammarstrom, A. Böckmann, KP. Nilsson, A. Caflisch, B. Meier[3], S. Hornemann, A. Aguzzi
The antiprion activity of polythiophenes is specified by regioregular ionic bonds to amyloid

2175
T. Sonati, J. Falsig Pedersen, R. Reimann, S. Hornemann, P. Baral, B. Wieland, M. Swayampakula, M. James, A. Aguzzi
The flexible tail of the prion protein mediates the toxicity of anti-prion antibodies

2199
F. Wehrle, B. Latal, R. Huber, R. O'Gorman, L. Kaufmann, A. Hüsser, C. Verrey, C. Hagmann
Impaired Executive Functions in Complex Tasks in Children and Adolescents Born Very Preterm

2202
F. Wehrle, A. Hüsser, A. Buchmann, B. Bea, R. Huber, R. O'Gorman, K. Kaufmann, H. Speckbacher, C. Verrey, C. Hagmann
Volume of Cerebellum and Thalamus Is Associated with Working Memory Performance in Children and Adolescents Born Very Preterm

Clinical Trials

2119
N. Peter, T. Kleinjung, L. Horath, M. Wichser, St. Buechi, St. Weidt

PRISM (PICTORIAL REPRESENTATION OF ILLNESS AND SELF MEASURE) AS A NEW ASSESSMENT TOOL FOR SUFFERING IN TINNITUS PATIENTS

2120
A. Ioannidis, GO. Galluci, S. Borzangy, RE. Jung, CHF. Hämmerle, HP. Weber, GI. Benic
Evaluation of titanium-zirconium narrow diameter dental implants: 3 year of a multicenter randomized controlled clinical trial

2129
N. Aellig, GA. Kullak-Ublick, N. Corti
Rifampicin and Phenprocoumon – A Challenging Combination

2169
E. Eschmann, PE. Beeler, J. Blaser
An Ongoing Cluster Randomized Trial to Assess the Effect of Specific Alerts in Potassium-Increasing Drug-Drug Interactions

2173
YV. Valko, EW. Werth, CB. Bockisch, PV. Valko, KW. Weber
Polysomnography detects benign paroxysmal positional vertigo

2217
An. Kegel, Wk. Lai, Sa. Reidt, No. Dillier
Measuring the real-life localization performance of hearing impaired persons in the laboratory

2224
NC. Corti, SW. Weiler, MH. Hofer, TH. Hess, SW. Wehrli
Colistimethate sodium and Colistin Pharmacokinetics in Ambulatory Hemodialysis – A Case Report

2236
SJ. Schreiner, T. Kirchner, A. Gietl, SC. Steininger, M. Wyss, E. Gruber, A. Buck, S. Leh, R. Nitsch, K. Prüssmann, C. Hock, A. Henning, PG. Unschuld
INVESTIGATING REGIONAL RELATIONSHIPS BETWEEN AMYLOID-BETA AND BRAIN METABOLISM IN HEALTHY ELDERLY CONTROLS

2259
RM. Fakin, HJ. Klein, P. Giovanoli, M. Calcagni
To suture or not to suture? Outcome assessment after epineural coaptation of digital nerves with different testing modalities

2077

NK. Campbell[1], F. Di Giallonardo[1], Y. Duport[1], C. Leemann[1], S. Schmutz[1], HF. Günthard[1], KJ. Metzner[1]

Generation of Individual Specific HIV-1 Full Length Reference Genomes via Illumina Sequencing

Universitätsspital Zürich[1]

Introduction:
Current methods in the evolutionary analysis of viral next-generation sequencing (NGS) data employ the usage of aligning sequence reads to a reference genome. Although practical this convention carries the risk of losing data due to the genetic distance between these sequences and the reference, and subsequently leading to an underestimation of diversity. *De novo* assembly as an alternative approach also has short comings. It is especially problematic when investigating the diversity of very heterogeneous viruses such as the human Immunodeficiency virus type 1 (HIV-1). Despite the varied assortment of alignment algorithms currently available, the development of a sophisticated work-flow to overcome all these obstacles is of paramount importance for minimising the loss of reads, so as to obtain an overview of the dominant variants present in the viral population of interest.

Methods:
HIV-1 RNA was isolated from patients' samples, whole genome amplification was performed using 5 overlapping amplicons followed by fragmentation and sequencing via the Illumina shotgun approach (2x150bp or 2x250bp paired-end read length). To establish the work flow we analysed 8 HIV-1 acutely infected (more homogeneous population) and 8 HIV-1 chronically infected patients (more diverse population). Quality filters such as removing terminal ambiguous nucleotides, a minimum central Phred score >35 in addition to trimming 8 nucleotides from the 5' and 3' terminus of the reads, and a length >230 nucleotides were used to reduce the frequency of instrument derived sequencing errors. These pre-processed read files were then subjected to three rounds of alignment: first, to a HIV-1 HXB2 clonal reference, then, to the consensus generated by the HXB2 alignment, and again to the consensus generated by the second alignment.

Results:
Implementing this work-flow we were able to recover on average over 4.45% of the reads lost when aligned to HXB2 (4.19% for acute and 4.7% for chronic) corresponding to an average increase of 78,868 reads in the alignments from 93.5% to 97.9%. Resulting in an average increase of 1.3% in observed diversity over the entire genome: 1.1% acute and 1.5% chronic.

Conclusion:
Herein we've illustrated the advantages of applying sophisticated alignment work-flows for the generation of sample specific reference sequences, which is essential for high confidence evolutionary analysis. Using HIV-1 as an example, we were able to recover on average 4.45% of the reads that were initially lost when aligned to an HXB2 reference and thus artificially reduce the diversity observed within the samples. In regards to HIV-1 evolutionary studies a sample specific reference is an ideal starting point for future longitudinal and cross sectional analyses.

2078

MR. Spalinger[1], C. Chassard[2], S. Kasper[1], L. Biedermann[1], S. Vavricka[3], I. Frey-Wagner[1], K. Attrot[1], C. Lacroix[2], M. Fried[1], G. Rogler[1], M. Scharl[1]

T cell specific loss of PTPN2 leads to miss-balanced T helper cell differentiation resulting in aggravated intestinal inflammation

Gastroenterolgy, University Hospital Zürich, Zürich[1], Institute of Food, Nutrition and Health, Swiss Federal Institute of Technology Zürich, Zürich[2], Gastroenterology and Hepatology, City Hospital Triemli, Zürich[3]

Introduction:
Presence of a loss-of-function variant within the gene locus encoding protein-tyrosine phosphatase non-receptor type 2 (PTPN2) results in increased risk for Crohn's disease (CD). In the intestine, regulation of T helper (Th) cell responses are important to maintain tolerance towards self-antigens and harmless non-self antigens derived from commensals as well as food particles. In CD, deregulated immune responses with enhanced levels of Th1 and Th17 cells are observed. Here we addressed the role of PTPN2 in Th cell differentiation during intestinal inflammation.

Methods:
Mice lacking PTPN2 in T cells ($PTPN2^{deltaT}$ mice) and control littermates were treated with DSS to induce acute or chronic colitis. Th cell subsets and cytokine expression/secretion were analyzed by FACS, RT-PCR and ELISA; intestinal microbiota was analyzed by pyrosequencing. Intestinal biopsies from CD patients were analyzed for Th associated transcription factors (TF) and cytokines by RT-PCR and serum was analyzed by ELISA.

Results:
Upon 10 d DSS treatment, $PTPN2^{deltaT}$ mice (n=9 per group) suffered from aggravated colitis, as characterized by enhanced weight loss ($p< 0.01$), increased endoscopic and microscopic colitis scores ($p<0.05$ each), pronounced shortening of the colon and enhanced MPO levels ($p<0.05$ each) when compared to DSS-treated wild-type (WT) mice. In $PTPN2^{deltaT}$ mice, DSS-induced increase of Th1 and Th17 cells and associated TF/cytokines (TBX21/IFN-g and RORC/IL-17, respectively) was significantly enhanced ($p<0.001$ and $p<0.05$, respectively) while DSS-mediated induction of Th2 and regulatory T (Treg) cells was reduced. Similar results were observed in chronic DSS induced colitis (n=7 per group). Further, DSS treatment resulted in intestinal dysbiosis with increased levels of bacteroidetes and proteobacteria and a concomitant reduction in firmicutes. These effects were drastically enhanced in DSS treated $PTPN2^{deltaT}$ mice. In aged $PTPN2^{deltaT}$ mice (>6 month), inflammatory infiltrates into liver, kidney and skin could be observed, indicative for a systemic loss of tolerance. In CD patients featuring the IBD associated loss-of function variant in PTPN2, we observed enhanced expression/secretion of T-bet/IFNg and RORC/IL-17 in intestinal biopsies and serum samples (n=9, $p<0.05$, each), but reduced IL-10/IL-13 levels when compared to samples from PTPN2 WT CD patients.

Conclusion:
Our data demonstrate that T cell specific loss of PTPN2 results in profound changes in Th cell compartments with an increase in pro-inflammatory Th1 and Th17 cells/cytokines and a reduction in regulatory mechanisms. This promotes intestinal inflammation and results in a generalized loss of tolerance. Taken together our results explain how the CD associated PTPN2 variant and Th cell deregulation are functionally linked.

2079

D. Rodriguez1, M. Riwanto1, I. Edenhofer1, S. Segerer2, RP. Wüthrich2, S. Kapoor1

EFFECT OF THE SGLT2 INHIBITOR DAPAGLIFLOZIN ON CYSTIC DISEASE PROGRESSION IN PCK RATS WITH AUTOSOMAL R ECESSIVE POLYCYSTIC KIDNEY DISEASE

Nephrology and Physiology, University of Zurich, Zurich, Switzerland1, Division of Nephrology, University Hospital Zurich, Zurich, Switzerland2

Introduction:
Autosomal recessive polycystic kidney disease (ARPKD) is an inherited disease in which clusters of fluid-filled sacs (cysts) form in the kidneys, often leading to kidney failure by the age of 10 and a reduced lifespan. Dapagliflozin is a selective inhibitor of the sodium-glucose cotransporter 2 (SGLT2) which induces renal glycosuria. The role of SGLT2 and the therapeutic effect of dapagliflozin in progressing stages of ARPKD have not been studied. Therefore we examined the effect of dapagliflozin in PCK rat, an orthologous animal model of ARPKD.

Methods:
Dapagliflozin (DAPA) (10 mg/kg/day) or vehicle (CON) were administered orally via gavage to 6 week-old male PCK rats (n=8 per group) for a total of 6 weeks. Blood and urine were collected at baseline and after 3 and 6 weeks of treatment to assess parameters of renal function. At the end of the treatment, rats were sacrificed and kidneys were harvested for histological analysis.

Results:
Throughout 6 weeks of treatment, DAPA significantly increased urine output (DAPA 57.3±19.2, CON 19.3±2.3 ml/day at week 6) and resulted in higher osmolar excretion (DAPA 62.5±15.8, CON 23.9±2.8 mosm/day) and higher glucose excretion (DAPA 23.4±12.0, CON 0.3±0.3 mmol/day) in PCK rats. After 3 weeks of treatment, DAPA-treated rats displayed a higher clearance for creatinine (DAPA 3.06±0.40, CON 2.56±0.54 ml/min), BUN (DAPA 1.71±0.34, CON 1.23±0.31ml/min) and uric acid (DAPA 0.55±0.13, CON 0.41±0.17 ml/min), whereas after 6 weeks there was no difference between DAPA and CON. Furthermore, DAPA treated PCK rats displayed a 4.3-fold and 3.5-fold increase in albumin excretion at 3 and 6 weeks of treatment, respectively. Surprisingly, in vivo ultrasound imaging showed an increase in the cyst growth after 6 weeks of treatment with DAPA. DAPA-treated rats also had 23% higher total kidney weights after 6 weeks of treatment (p=0.005). In addition, histological analysis by PAS staining revealed a higher medullary cyst expansion in DAPA treated rats.

Conclusion:
Inhibition of glucose reabsorption with the SGLT2-specific inhibitor dapagliflozin caused significant glycuresis, hyperfiltration and albuminuria in PCK rats. Unexpectedly, the cyst growth was enhanced, suggesting that the factors which regulate cyst growth in this model act independently from the factors which control GFR. The mechanisms which link glycosuria and hyperfiltration to distal cyst growth remain to be elucidated.

2080

P. Mayank[1], L. Hofstetter[1], B. Stieger[1]

Proteomic and transcriptomic approach to explore novel ATPases in rat canalicular membrane

Institute of Pharmacology & Toxicology, University of Zurich, Zurich[1]

Introduction:
One important function of the liver is bile formation, which includes bile salt and lipid secretion and xenobiotic elimination. Various transport systems located in the basolateral (sinusoidal) and apical (canalicular) surfaces of the hepatocytes are necessary to produce bile. The rate limiting step for bile salt transport across hepatocytes is located at the canalicular membrane. In the canalicular membrane, several members of ATP-binding cassette family and of P4 ATPases are expressed and functionally characterized. However, the detailed molecular mechanisms of lipid secretion and the protection of the canalicular membrane against the detergent action of bile salts are still to be explored.

Methods:
Canalicular membranes were isolated with a standard method and extracted with alkaline bicarbonate. The proteomics study was performed at Functional Genomics Center Zurich (FGCZ) and the expression of novel P4 ATPase were confirmed using RT-PCR and western blot using standard protocols.

Results:
We identified 1745 unique proteins and 18000 unique peptides from rat canalicular membranes. Gene ontology study on identified proteins revealed over representation of transmembrane transporter activity when compared to previously published rat liver proteomic studies. Novel P4 ATPase (ATP8A1, ATP11A, ATP11C & ATP13A1) are identified in proteomics data. Additionally, RT-PCR and Western blot analysis shows high expression of ATP11C compared to other P4 ATPase, found in our study.

Conclusion:
The current analysis of the proteome data suggests the expression of additional P4-ATPases in liver, which will expand our knowledge on canalicular lipid secretion.

2081

PP. Becker[1], J. Schmitt[2], B. Niesler[3], O. Tschopp[4], F. Berr[7], A. Canbay[6], T. Dandekar[5], B. Müllhaupt[1], A. Geier[1]

MicroRNAs as Mediators in the Pathogenesis of Non-Alcoholic Fatty Liver Disease and Steatohepatitis

University Hospital Zürich (USZ), Department of Gastroenterology and Hepatology, Zürich, Switzerland[1], University Hospital Würzburg (UKW), Division of Hepatology, Würzburg, Germany[2], Institute of Human Genetics, University Hospital Heidelberg, Heidelberg, Germany[3], University Hospital Zürich (USZ), Department of Endocrinology, Diabetes and Clinical Nutrition, Zürich, Switzerland[4], University of Würzburg, Bioinformatik, Biozentrum, Würzburg, Germany[5], University Hospital, University Duisburg-Essen, Department for Gastroenterology and Hepatology, Essen, Germany[6], Paracelsus Medical University/ Salzburger Landeskliniken (SALK), Department of Medicine I, Salzburg, Austria[7]

Introduction:
The biological mechanisms of non-alcoholic fatty liver disease (NALFD) and non-alcoholic steatohepatitis (NASH) are not entirely understood particularly in human liver. Since microRNAs (miRNAs) have been discovered, scientists proofed a regulative function in various gene expression pathways. **Aim** of this project is to study miRNAs expression and related target gene mRNA expression patterns in different stages of human fatty liver disease.

Methods:
In an initial miRNA expression assay total RNA from liver tissue of 19 patients with NAFLD/NASH from the local biobank and five healthy controls was analyzed. A detailed metabolic and histological characterization was performed to obtain homogeneous groups for comparison of NAFLD vs. NASH. The NanoString® assay contains the measurement of 800 miRNAs in a multiplexed assay without previous amplification. Normalized data was analyzed. Newly described miRNA candidates as well as those already associated with fatty liver disease were replicated by quantitative rtPCR. Further replication of potential miRNA candidates was performed in a second cohort consisting of 35 NAFLD/NASH patients. At the same time a human gene expression array (Affymetrix PrimeView) was performed to investigate mRNA expression changes in miRNA target genes and involved signaling cascades in the initial cohort. Finally, expression changes and molecular interactions between miRNA and target genes were analyzed by mathematical network modeling.

Results:
Primary analysis showed significant p-values ($p<0.05$) after correction for almost 250 miRNAs in all calculations. A significant difference of the mean compared to control (log2 expression (±0.8 to ±3.264)) was defined to select potential candidates. Comparing the two different stages respective to signs of hepatic inflammation (NAFLD vs. NASH), a total number of 71 miRNAs with a significant difference were ($0.0001<=p>=0.042$) found.
13 miRNAs showed a significant deregulation in fatty liver disease compared to controls (e.g. miR 223-3p and mir21-5p). These results could be reproduced via rtPCR; selected findings could although be strengthened in a second cohort.
For newly assigned miRNAs with a distinct expression between NAFLD and NASH which have been connected with inflammatoric pathways in other studies, as well as established reference miRNAs (e.g. miR-33b, 34a-5p) quantification could be also replicated and give promising perspectives for comparing analysis of microRNA and mRNA results. Pathophysiological consequences on central metabolic and inflammatory signaling pathways are obtained by mathematical network modeling

Conclusion:
Our study identifies new functionally relevant miRNAs in liver tissue as mediators of central signaling pathways and clinically relevant pathophysiological events in fatty liver disease. These data from liver tissue imply a role of certain miRNAs as potential future prognostic biomarkers in serum to monitor the progression of fatty liver disease from bland steatosis to steatohepatitis.

2082

M-A. Rochat[1], E. Schläpfer[1], R.F. Speck[1]

Promising Role of Toll-Like Receptor (TLR) Agonist in Concert with Prostratin for Eradication of Latently HIV-Infected cells

Infectious Diseases and Hospital Epidemiology, University Hospital Zurich, Zurich[1]

Introduction:
Persistence of cryptic, replication competent but silent HIV provirus under anti-retroviral treatment still remains the major hurdle for HIV eradication. Reactivation of HIV transcription alone might not guarantee an efficient elimination of the latently infected cells in vivo. Thus, we hypothesize that triggering the innate immune system in concert with transcriptional enhancers will result in a Th1 supportive micro-environment, crucial to clear the latent reservoir.

Methods:
Cooperative compounds were screened on a co-culture of monocytes derived dendritic cells (MDDC) with J-lat cells clone 9.2, at a ratio 1:10. The model was subsequently characterized using flow-cytometry, neutralizing antibodies, transwell as well as a library of kinase inhibitors

Results:
Triggering of the NF-κB pathway by Prostratin, supported by TLR8agonist, resulted in an enhanced reactivation of HIV production (3 fold) compared to the compounds alone.
This combinatorial approach led to a drastic maturation of the MDDC, outlined by an increase in the activation markers, HLA-DR, CD80, CD83, CD86 as well as a secretion of TNF and MIP-1α. Moreover, Prostratin significantly down regulated Dc-Sign expression without inducing a pro-apoptotic phenotype.
The model consisted of two-step inducer, where Prostratin generate HIV reactivation through transcription factor availability, as well as a maturation of MDDC, which is fully achieved by addition of TLR8agonist. In the second step, TNF and co-stimulatory molecules accomplished a second signaling event, re-enforcing the effect of Prostratin in the latently infected cells.

Conclusion:
These findings provide evidence for an enhanced combinatorial reactivation approach, which might be able to target different mechanisms of latency through the involvement of concomitant signaling pathway events. Moreover, an HIV-specific CTL response could be subsequently mounted to constraint the residual infected cells.
Studies are on-going to assess the concept in vivo in HIV- infected humanized mice.

2083

VV. Vongrad[1], J. Imig[3], P. Mohammadi[4], S. Kishore[2], L. Jaskiewicz[2], M. Zavolan[2], J. Hall[3], N. Beerenwinkel[4], HF. Günthard[1], KJ. Metzner[1]

The Role of RNA Interference in HIV-1 Infected Primary Human Monocyte-Derived Macrophages

Division of Infectious Diseases and Hospital Epidemiology[1], Computational and Systems Biology, University of Basel[2], Institute of Pharmaceutical Sciences, ETH Zurich[3], Department of Biosystems Science and Engineering, ETH Zurich Basel[4]

Introduction:
Micro RNAs (miRNAs) and other small noncoding RNAs (sncRNAs) are key players in post-transcriptional gene regulation. We and other groups have described the presence of HIV-1 derived sncRNAs in different experimental setups; however, so far their biological function remained to a large extent unknown. Here we used a global, comprehensive approach to investigate whether viral small RNAs may play a role in the RNA interference (RNAi) pathway in primary human monocyte-derived macrophages (MDMs). Specifically, we aimed to characterize the profiles of host and HIV-1 derived small RNAs and the possible impact of these RNAs on the viral life cycle.

Methods:
We applied Argonaute 2 (Ago2) photoactivatable ribonucleoside-enhanced crosslinking and immunoprecipitation (PAR-CLIP) to MDMs infected with HIV-1_{JRFL} for 14 days from two different donors. It has been previously demonstrated that this approach enables identification of Ago2-bound miRNAs as well as of the miRNA-targeted mRNAs. Illumina sequencing was performed on PAR-CLIP and small RNA (18 to 30 nt) samples from the same donors, and small RNA sequencing was performed on HIV-1 infected MDMs from two additional donors.

Results:
The analysis of PAR-CLIP data demonstrated the absence of viral RNAs in Ago2-RISC, suggesting that viral sncRNAs do not enter the canonical RNAi pathway in MDMs. However, small RNA sequencing on samples from the same MDM cultures confirmed the presence of HIV-1 sncRNAs, although expressed at low levels (< 0.5 % of total small RNA fraction). Most host miRNAs revealed no significant change in expression levels between infected and non-infected MDMs.

Conclusion:
Our data indicate that it is unlikely that viral sncRNAs are incorporated as functional miRNAs or resemble targets for host miRNAs in Ago2-RISC. The presence of HIV-1 sncRNA as detected by small RNA sequencing implies alternative functional roles or biogenesis pathways. Future efforts are needed to uncover potential functions of HIV-1 derived sncRNAs in MDMs or other HIV-1 host cell typesormed on HIV-1 infected MDMs from two additional donors.

2084

S. Stübinger[2], K. Nuss[1], K. Klein[1], P. Kronen[1], B. Von Rechenberg[1]

Osseointegration of dental implants: Are sheep a suitable model?

Musculoskeletal Research Unit, Vetsuisse Faculty, University of Zurich, Zurich[1], Competence Center for Applied Biotechnology and Molecular Medicine [2]

Introduction:
The use of experimental animals to study the success and survival of implants is designed to answer questions that relate to the process of peri-implant bone regeneration. Evaluation of bone remodelling and osseointegration after different time points and treatment options are a standard procedure. However, to choose a reliable and comprehensive pre-clinical model for analyzing the biological and biomechanical performance of novel implant designs and surface modifications still remains to be a challenge in implant dentistry. For this reason it was the aim to evaluate basic suitability of the pelvic sheep model for analyzing osseointegration of implants.

Methods:
The results and outcomes of more than n=1000 implants in the pelvic sheep model were evaluated. In all animal studies included, implants were randomly placed in the cranial part of the left (n=9) and right (n=9) pelvis of each animal, alternating on either side of the linea glutea of the iliac wing (n= 18). Advantages and disadvantages of the pelvic sheep model for pre-clinical surgical research were scrutinized. A special focus was set on a critical assessment of the pelvic sheep model to closely resemble the anatomical characteristics of the human alveolar ridge. In this context especially the different morphology and healing processes of bony structures were investigated. The possibilities and limitations of the model for the examination of the bone-to-implant-contact as well as biomechanical testing were evaluated.

Results:
For the combined histological and biomechanical analysis the pelvic model in sheep proved to be a reliable experimental setup for testing bone remodelling and osseointegration of different implant designs and surface modifications. Especially the high number of implant test sites in one animal (n=18) as well as the possibility to place implants of a length of up to 10 mm under aseptic conditions rendered this model ideal for translational implant research. Implant placement in the pelvis allowed a differentiation and comparison between cortical and trabecular bone structures. Generally, a superficial cortical layer of about 1-3 mm and a underlying trabecular bone structure of about 7-9 mm around the linea glutea made it possible to achieve a good primary stability and fit of the implants. Due to the similar bone remodelling process in humans osseointegration could analysed after 2 and 8 weeks to resemble a “delayed immediate” and “delayed”surgical protocol.

Conclusion:
Due to commensurate bone metabolism rates as well as adequate biomechanics the iliac shaft of sheep provide a sound basis for the analysis of periimplant endosseous healing respecting the different healing patterns in cortical and trabecular bone. However, a limiting factor is that intraoral soft tissue structures and microbiological aspects cannot be evaluated. Therefore, further studies have to evaluate the influence of surface modifications on intraoral soft tissue integration.

2085

M. Schläpfer[1], T. Piegeler[1], RO. Dull[2], DE. Schwartz[2], RD. Minshall[2], B. Beck Schimmer[1]

LONG TERM SEDATION WITH VOLATILE ANESTHETICS COMPARED TO PROPOFOL IMPROVES OUTCOME IN A RODENT MODEL OF SEPSIS

Anesthesiology, USZ, Zurich[1], Anesthesiology, University of Illinois at Chicago[2]

Introduction:
Sepsis and septic shock are associated with a mortality of approximately 50% and tremendous healthcare costs [1]. Septic patients often require mechanical ventilation and long-term sedation. Due to the known immunomodulatory effects of volatile anesthetics [2] we hypothesized that sedation with these agents would be associated with better outcome compared to sedation with propofol in a rodent model of severe sepsis.

Methods:
Sepsis was induced by cecal ligation and puncture (CLP) in adult male Wistar rats. All animals were mechanically ventilated via a tracheotomy and were instrumented with an arterial and venous line. Sedation was maintained for 24 hours with propofol (5-10mg/kg/h), sevoflurane, desflurane or isoflurane (0.7 MAC). Two sham operated groups received isoflurane or propofol. Arterial blood gases were analyzed every 6h. 0.5ml/kg/h NaCl 0.9% was administered to all rats and doubled in septic animals if mean arterial pressure dropped <55mmHg.
Survival was analyzed using a Log-Rank test; biochemical data was assessed with Student's t-test or ANOVA.

Results:
1. Survival time decreased to 12h (mean) for animals in the CLP-propofol group, whereas survival was >56% after 24h in all other groups ($p<0.001$).
2. After 18h, base excess was significantly lower ($p<0.01$) in the propofol group comparet to the volatile groups (-20.6 for propofol vs. -11.7, -11.8 and -14.2mEq/l for isoflurane, sevoflurane and desflurane).
3. Sham operated animals sedated with propofol showed a 2.7-fold increase in endotoxin levels after 24 hours compared to isoflurane ($p<0.0001$). At 12h endotoxin levels in septic CLP-animals were twice as high in the propofol compared to the isoflurane group ($p<0.0001$).
4. Propofol led to a more pronounced inflammatory reaction when compared to the volatile groups: TNFa levels at 12h were 133 vs. 549pg/ml ($p<0.001$) in septic isoflurane animals compared to propofol and 23 vs. 89pg/ml in sham animals after 24h ($p<0.05$).

Conclusion:
1. Survival of septic rats sedated with the 3 most commonly used volatile anesthetics was significantly higher compared to sedation with propofol.
2. Acidosis developed faster in animals sedated with propofol.
3. The inflammatory response was attenuated in the volatile groups compared to the corresponding propofol groups.
4. Translated into a clinical scenario septic patients might benefit from sedation with volatile anesthetics.

References

1. *Int Care Med* 2002, **28**(10):1440-1446.
2. *Clin Exp Immunol* 2009, **155**(2):224-230.

2086

T. Mehra[1], G. Grözinger[2], S. Mann[2], S. Mann[2], A. Naumann[3], R. Moos[1], W. Omlor[4], M. Röcken[5], CD. Claussen[2], S. Clasen[2], C. Garbe[5]

Primary Localization and Tumor Thickness as Prognostic Factors of Survival in Patients with Mucosal Melanoma

Medical Directorate, UniversitätsSpital Zürich, Zürich [1], Department of Diagnostic and Interventional Radiology, Eberhard-Karls-University Tübingen, Tübingen [2], Institute for Clinical Epidemiology and applied Biometry, Eberhard-Karls-University Tübingen, Tübingen[3], Brain Research Institute, UZH, Zürich, [4], Department of Dermatology, Eberhard-Karls-University Tübingen, Tübingen[5]

Introduction:
Primary mucosal melanoma is a rare neoplastic entity with albeit a high mortality. Nonetheless, data on survival and prognostic factors is scarce. Moreover, it is still unclear if the disease course allows for mucosal melanoma to be treated as primary cutaneous melanoma or if different therapeutic approaches need to be developed. Furthermore, this investigation is the first to present 10-year survival rates for mucosal melanomas of different anatomical localizations.

Methods:
116 cases of primary mucosal melanoma retrieved from the databases of the Comprehensive Cancer Center and of the Central Register of the German Dermatologic Society in Tübingen diagnosed between 10.09.1984 and 15.02.2011 were included. The parameters recorded included location, tumor thickness and overall survival. Overall survival was calculated with the Kaplan-Meier method. The duration of follow-up regime was usually 10 years, with an average interval of 47± 52 months, ranging from 1 month to 297 months. Assuming a general significance level of $\alpha = 0.05$, we considered results to be significant if $p < 0.017$ after Bonferroni-correction, as to maintain the error rate due to multiple testing ($n = 3$). Where applicable, findings were classified according to AICC 7th Edition, 2009.

Results:
We found a mean overall survival of 80.9 months, with an overall 2-year survival of 71.7 %, 5-year survival of 55.8 % and 10-year survival of 38.3 %. The 10-year survival rates for T1 ($n = 10$), T2 ($n = 18$), T3 ($n = 24$) and T4 ($n = 27$) stage tumors were 100.0 %, 77.9 %, 66.3 % and 10.6 % respectively. 10-year survival of melanomas of the vulva ($n = 41$) was 64.5 % in comparison to non-vulva mucosal melanomas ($n = 75$) with a survival rate of 22.3%.

Conclusion:
We found significant differences in survival of T-stage groups and between vulval and non-vulva localization of the primary significantly affected survival ($p < 0.0001$ and $p = 0.0006$ respectively). We could confirm the lower survival rates of mucosal melanoma in comparison to published survival rates of primary cutaneous melanoma. Survival rates in this analysis were higher than those previously reported for mucosal melanoma.

2087

N. Leimer[1], A. Furrer[1], M. Schwarz[1], AS. Bahlmann[1], F. Andreoni[1], U. Matt[1], K. Seidl[1], RA. Schüpbach[2], AS. Zinkernagel[1]

Staphylococcus aureus Small Colony Variants are induced by low pH

Division of Infectious Disease and Hospital Epidemiology, University Hospital of Zurich[1], Division of Surgical Intensive Care Medicine, University Hospital Zurich[2]

Introduction:
Staphylococcus aureus (SA) is a major human pathogen causing mild to life-threatening infections. SA has been shown to be able to invade and persist within a broad range of host cells. The ability of SA to survive intracellularly has been associated with the small colony variant (SCV) phenotype. SCVs represent a small growing subpopulation of SA and are characterized by reduced metabolism, down-regulated virulence factor expression and increased resistance to antibiotics. Thus, SCVs possess a well-adapted phenotype for intracellular persistence without causing cell damage. Moreover, the intracellular location protects the bacteria from extracellular immune responses and from antibiotics not penetrating eukaryotic cells. As a consequence, SA infections may relapse due to reemerging bacteria from intracellular reservoirs. SA clinical isolates rapidly alter their phenotype and revert from the slow growing SCV form back to the fast growing, highly virulent form. As phenotype switching is most likely an indispensable feature for causing chronic infections, we studied SCVs that evolve by cultivation of SA in growth conditions reflecting the environment in the human host. We used these conditions to screen for therapeutic strategies that help to eradicate the intracellular persisting bacteria.

Methods:
To determine the effect of prolonged intracellular persistence on the emergence of SCVs, host cells were infected with SA and the phenotype of recovered bacteria determined over seven days. To identify the intracellular SA location, host cells were infected with fluorescent labeled SA. Co-localization with the lysosomal marker LAMP-2 was visualized. Growth conditions mimicking the acidic milieu of phagolysosomes were then used to investigate the effect of low pH on SA phenotype. To investigate the potential of lysomotropic alkalizing agents in SCV eradication, the number and phenotype of persisting bacteria from treated and untreated cells were compared.

Results:
During the course of host cell infection, the number of intracellular surviving bacteria was reduced over time, but the percentage of SCVs increased, reaching up to 10 % after one week. Cell imaging experiments indicated that the majority of persisting bacteria accumulated within lysosomal compartments where the pH is low. Interestingly, SA survived in growth medium with similar acidity (pH 4.0-6.5) for up to four days. The percentage of bacteria manifesting the SCV phenotype increased greatly with increasing acidity, reaching up to 50 % SCVs at pH 4.0 buffered growth medium after four days. Host cells treated with agents raising intralysosomal pH showed a significant lower frequency of SCVs compared to non-treated cells.

Conclusion:
SA persisted within host cell lysosomes and survives in low pH. The emergence of SCVs in low pH medium suggests that this phenotype is better adapted to withstand this otherwise bactericidal environment. These results indicate that alkalizing agents might help to develop therapeutic strategies that ensure complete SCV reservoir eradication.

2088

E. Eschmann[1], S. Karlen[1], M. Schneemann[2], J. Blaser[1]

Should ePrescribing Systems Prevent Incorrect Intravenous Bolus Orders?

Medical Informatics Research Centre, Directorate of Research and Education, University Hospital, Zurich[1], Division of Internal Medicine, University Hospital, Zurich[2]

Introduction:
Computerized physician order entry (CPOE) has been reported to improve patient safety. However, unintended effects can occur. CPOE may shift responsibilities from nurses to physicians, e.g. when an order entry requires comprehensive information on drug dilution and administration. The purpose of this quality assessment was to determine potential hazards of the medication process not assisted by decision support. Orders of 40 drugs never to be administered as intravenous (iv) bolus were analysed.

Methods:
All e-prescriptions for inpatients at the University Hospital Zurich were included over a 25 months period following the introduction of CPOE except for treatments in intensive care units, emergency and operating rooms, and for oncological therapies.

Results:
We analysed 258,902 iv orders and 797,692 iv administrations in 76,467 inpatients. Drugs never to be administered as iv bolus were ordered 27,247 times, resulting in 78,516 administrations. 35 of these orders (0.13%) were incorrectly ordered as bolus for a total of 112 administrations (0.14%).

Conclusion:
The rates of incorrectly ordered iv bolus injections were low. In addition, nurses review orders before drug administration to reduce the risk of incidents. Nevertheless technical interventions could further minimise safety hazards by providing drug-specific default values for minimum infusion periods, or by restricting input options for the duration of iv administrations, e.g. for drugs never to be administered as a bolus. Introduction of CPOE may modify the collaboration of physicians and nurses and should therefore be monitored and managed as an iterative process of business improvements.

2089

A.. Tarnutzer[1], C.M. Zürcher[1], F.. Andreoni[1], K.. Schilcher[1], R.A. Schuepbach[1], A.S. Zinkernagel[1]

Clindamycin and Intravenous immunoglobulin influence Group A Streptococcus virulence factor activity

Infectious Diseases and Hospital Epidemiology, University Hospital Zurich, Zurich[1]

Introduction:
Through the production of a vast array of virulence factors (VFs), Group A *Streptococcus* (GAS) can cause life-threatening invasive infections such as necrotizing fasciitis. In addition to surgical debridement, the current treatment envisages a combination of the antibiotics penicillin and clindamycin, acting on the inhibition of bacterial cell wall formation and protein synthesis respectively. However, lethality remains high and alternative or complementary treatment strategies are therefore required. Addition of intravenous immunoglobulin (IVIG) is one option although its efficiency has not yet been fully established. This work aimed to investigate the effect of IVIG and sub-inhibitory concentrations of clindamycin, as found in necrotic tissues, on the activity and expression of key GAS VFs such as SLO, Sda1, SpyCEP and SpeB.

Methods:
The GAS strain M1T1 5448 was used. SLO activity was measured by assessing red blood cells hemolysis. Sda1 activity was estimated using a DNA degradation assay. IL-8 degradation was quantified by ELISA as a measure of SpyCEP activity and a colorimetric reaction involving the protease substrate BZ-Pro was employed to assess SpeB activity. Expression of virulence factors was assessed by real-time PCR and/or Western blot.

Results:
Exposure of GAS M1T1 5448 to sub-inhibitory concentrations of clindamycin led to increased activity of the VFs SLO, Sda1 and SpyCEP but to decreased SpeB expression and activity. Sub-inhibitory concentrations of linezolid, tetracyclin and chloramphenicol had the same effect as clindamycin on VFs activity while no increase in activity was observed for gentamycin and tigecyclin. Physiological concentrations of IVIG blunted SLO, Sda1 and SpyCEP activities. The effect of sub-inhibitory clindamycin concentrations on the enhancement of VFs activity was confirmed in two GAS M1 clinical isolate strains resistant to clindamycin. Here, higher clindamycin concentrations were used and a concentration-dependent activity increase of all VFs tested was observed.

Conclusion:
We demonstrate *in vitro* that bacteria exposed to sub-inhibitory concentrations of clindamycin, as found in poorly perfused necrotic tissues, display increased VFs activity and expression. On the other hand we demonstrate *in vitro* that IVIG is efficient in inhibiting GAS VFs involved in the progression and aggravation of invasive infections. Further work including the use of murine *in vivo* models is necessary to assess the role of VFs activity modulation by IVIG and clindamycin in real-time infections.

2090

S. Jordan[1], B. Maurer[1], M. Toniolo[1], BA. Mihel[1], O. Distler[1]

Comparison of performance of new ACR/EULAR and old ACR classification criteria for systemic sclerosis

Division of Rheumatology, University Hospital Zurich, Zurich[1]

Introduction:
The preliminary classification criteria for systemic sclerosis (SSc) lack sensitivity for mild/early SSc patients. Therefore, the new ACR/EULAR (The **A**merican **C**ollege of **R**heumatology/ The **Eu**ropean **L**eague **A**gainst **R**heumatism) classification criteria for SSc were developed. Objective of our study was to evaluate the performance of the new classification criteria for SSc in clinical practice in a cohort of mild/early patients.

Methods:
Consecutive patients with a clinical diagnosis of SSc, based on expert opinion, were prospectively recruited and assessed according to EUSTAR (The **EU**LAR **S**cleroderma **T**rials **a**nd **R**esearch group) and VEDOSS (The **V**ery **E**arly **D**iagnosis **o**f **S**ystemic **S**clerosis) recommendations. In some patients, missing values were retrieved retrospectively from the patients' records. Patients were grouped into established SSc (fulfilling the old ACR criteria) and mild/early SSc (not fulfilling the old ACR criteria). The new ACR/EULAR criteria were applied to all patients.

Results:
Of the 304 patients available for the final analysis, 162/304 (53.3%) had established and 142/304 (46.7%) had mild/early SSc. All 162 established SSc patients fulfilled the new ACR/EULAR classification criteria. The remaining 142/304 patients had mild/early SSc. Eighty out of these 142 (56.3%) patients fulfilled the new ACR/EULAR classification criteria. Patients with mild/early SSc not fulfilling the new classification criteria were most often suffering from Raynaud`s phenomenon, SSc-characteristic autoantibodies and SSc pattern on nailfold capillaroscopy. Taken together, the sensitivity of the new ACR/EULAR classification criteria for the overall cohort was 242/304 (79.6%) compared to 162/304 (53.3%) for the ACR criteria.

Conclusion:
In this cohort with a focus on mild/early SSc, the new ACR/EULAR classification criteria showed higher sensitivity ($p<0.0001$) and classified more patients as definite SSc patients than the old ACR criteria.

2091

D. Li[1], E. Schlaepfer[1], C. Knowlton[2], B. Kim[2], A. Audigé[1], R. Speck[1]

Vpx mediated Degradation of SAMHD1 Does Not Render HSCs more Permissive to Lentiviral Gene Transfer

Division of Infectious Diseases and Hospital Epidemiology , University Hospital of Zürich Zürich [1], Center for Drug Discovery, Department of Pediatrics, Emory University, Atlanta, Georgia, US[2]

Introduction:
Understanding how to achieve efficient transduction of hematopoietic stem cells (HSCs), while preserving their self-renewing capacity, is key for applying lentivirus-based gene engineering methods in Phase I/II clinical trials. The sterile alpha motif (SAM) domain and HD domain-containing protein 1 (SAMHD1) was recently identified as a HIV-1 restriction factor in myeloid and resting $CD4^+$ T cells that interferes with reverse transcription by decreasing the nucleotide pools. HIV-2 and SIV have evolved to counteract the effects of SAMHD1 by their accessory protein Vpx, which targets SAMHD1 for proteasomal degradation. We hypothesized that SAMHD1 also interferes with HIV-1-vector-based HSCs transduction.

Methods:
We used Vpx-mediated degradation of SAMHD1, shRNA to SAMHD1, HIV-2- or SIV- based lentiviral vectors or provided an excess of deoxynucleoside triphosphates (dNTPs) or deoxynucleoside (dNs) to relieve a potential block of SAMHD1 in HSCs. In addition, Alu-PCR was used to identify and characterize the integrated provirus in HSCs and monocyte-derived macrophages (MDMs).

Results:
Our results show that SAMHD1 is highly expressed in HSCs cultured in a medium enriched with cytokines conventionally used for transduction of HSCs. In contrast, uncultured HSCs have poor SAMHD1 expression. Expression levels of SAMHD1 in cultured HSCs are comparable to those found in myeloid cells, including monocytes and MDMs. However, Vpx+ VLPs, dNs or shRNA for silencing SAMHD1 and HIV-2- or SIV-based lentiviral vectors do not relieve a potential block in reverse transcription in HSCs that would result in a higher transduction rate. Notably, while Vpx+ VLPs resulted in a vigorous decrease of SAMHD1 in HSCs, the remaining SAMHD1 level is still remarkably high. Last but not least, Vpx+ VLPs lead to a striking increase of dNTPs in MDMs but not HSCs.

Conclusion:
In summary, HSCs, unlike quiescent cells, express high levels of SAMHD1. However, the Vpx-mediated decrease of SAMHD1 levels was not associated with a higher lentiviral-based transduction rate. These data imply that other restriction factors might be operative in lentiviral transduction of HSCs.

2092

N. Cesarovic[1], M. Arras[1], P. Jirkof[1]

Impact of inhalation anaesthesia, surgery and analgesia on home cage behaviour in mice

Division of Surgical Research, University Hospital Zurich, Zurich[1]

Introduction:
Anaesthesia and analgesia are used frequently in laboratory routine to ensure animal welfare and good scientific outcomes in experiments that may elicit pain or require immobilisation of the animal. However, there is concern regarding the effect of these procedures on animal behaviour in subsequent experiments.

Methods:
Our study determined the impact of short inhalation anaesthesia (sevoflurane, 15 min, 4.9%) and minor surgery with or without pain treatment (carprofen, 5 mg/kg, bid) on spontaneous species-specific home cage behaviours in inbred mice.

Results:
Analysis of 18-hour continuous video recordings showed clear post-procedural changes in spontaneous home cage behaviours, with changes of a moderate level after anaesthesia being marked after surgery. Self grooming, resting and locomotion were the most important behaviours for group separation. Analysis of the temporal distribution of behavioural changes revealed that resting behaviour was altered contradictory to its circadian rhythm as it was decreased in the light phase and increased in the dark phase. Also, locomotion was decreased in the dark phase at 12 to 18 hours after surgery and anaesthesia. In contrast, self-grooming was increased independently of circadian rhythm, being increased for up to 18 hours after surgery and anaesthesia. Following surgery, there was no significant difference in duration of behaviours between animals that were treated with carprofen or left without pain relief.

Conclusion:
In conclusion, it can be assumed that the changes observed in home cage behaviours hint at reduced animal well-being. However, pain or the efficacy of post-operative pain treatment could not be discriminated reliably from the impact of the surgical procedure including inhalation anaesthesia by observing animals' home cage behaviour.
For the interpretation of behavioural research data, the distinct impact of anaesthesia, surgery, pain treatment and other experimental procedures has to be considered. Our results highlight the requirement for knowledge of species-specific circadian rhythms of behaviours as well as the importance of determining the appropriate time of day for behavioural and welfare assessment.

2093

B. Maurer[1], N. Graf[4], B. Michel[1], C. Metzig[2], V. Lanius[2], D. Khanna[3], O. Distler[1]

Prediction of worsening of skin fibrosis in patients with diffuse systemic sclerosis using the EULAR Scleroderma Trials and Research (EUSTAR) registry

Department of Rheumatology, University Hospital Zurich, Zurich, Switzerland[1], Bayer Pharma AG, Berlin, Germany[2], Department of Rheumatology, University of Michigan, Ann Arbor, MI, USA[3], graf biostatistics, Winterthur, Switzerland[4]

Introduction:
To identify predictive parameters for the progression of skin fibrosis within one year in patients with diffuse cutaneous SSc (dcSSc) to enable 1) risk-stratification in clinical practice and 2) improved cohort enrichment in clinical trials with skin fibrosis as the primary endpoint.

Methods:
An observational study using the EUSTAR database was performed. Worsening of skin fibrosis was defined as increase in modified Rodnan skin score (MRSS) >5 points and ≥25% from the baseline to the 2nd visit, which is considered clinically meaningful. Inclusion criteria: dcSSc, ACR criteria fulfilled, MRSS≥7 at 1st visit, valid data for MRSS at 2nd visit, period in between visits 12±2 months. In the univariate analysis, patients with progressive skin fibrosis were compared to non-progressive patients. Predictive markers with $p<0.2$ were included in the multivariate logistic regression analysis. For validation of the regression models, a second cohort with new patients was extracted from the EUSTAR database 11 months after the first data extraction.

Results:

Out of 637 patients fulfilling the inclusion criteria of the original cohort, 9.7% had progressive skin disease. Univariate analysis identified joint synovitis, short disease duration (≤15 months), short disease duration in females/patients without CK elevation, low baseline MRSS (≤22/51), and absence of oesophageal symptoms as potential predictors for progressive skin fibrosis ($p<0.05$).
In the multivariate analysis, by employing combinations of the predictors, 17 models with varying prediction success were generated, allowing cohort enrichment from 9.7% progressive patients in the whole cohort to 44.4% in the optimized enrichment cohort. The model with the highest prediction success rate (n=8/18, 44.4%) had an overall accuracy of 89.9% (98.1% for no progression, 14.3% for progression) (Table1).

Tabl.1 Prediction model for skin progression in dcSSc

Predictors	**p-value**	**OR**	**95%-CI**
Joint synovitis	0.016	2.123	1.147-3.927
Female sex	0.143	0.541	0.238-1.230
Short disease duration* (≤15 months)	0.689	0.752	0.186-3.036
Female sex*short disease duration (≤15 months)	0.033	5.380	1.142-25.342
Low MRSS at baseline (≤22/51)	0.001	6.027	2.113-17.189

Other models with broader inclusion criteria revealed lower prediction success rates, but would simplify the recruiting process (e.g. prediction success rate 23.8% (n=20/84) for a model including low MRSS at baseline (≤22) and short disease duration (≤15 months)).
In the validation cohort, out of 188 patients, 6.5% had progressive skin disease. Short disease duration, low baseline MRSS and joint synovitis were confirmed as independent predictors of progressive skin fibrosis within one year showing a 4.5-fold increased prediction success rate.

Conclusion:
Our study provides novel, evidence-based criteria for the enrichment of dcSSc cohorts with patients who experience worsening of skin fibrosis within one year, which allows improved clinical trial design, but also a risk-stratified diagnostic work-up and treatment of the individual patient.
The study was supported by Bayer Pharma AG.

2094

R. Gerig[2], S. Ihrle[1], JH. Sim[2], C. Röösli[2], A. Eiber[1], A. Huber[2]

Mechanical properties of the incudo-malleolar joint in the middle ear

University of Stuttgart[1], ORL-Klinik, UniversitätsSpital, Zürich[2]

Introduction:
The incudo-malleolar joint (IMJ) is the diarthrodial joint connecting malleus and incus of the middle-ear ossicular chain in mammals. In humans, this joint contains synovial fluid which presumably causes a viscoelastic behavior. Under static loads, occurring for example with the influence of air pressure fluctuations, the IMJ is expected to show a mainly elastic compliance. Under dynamic excitation, additionally the influence of the viscosity of the synovial fluid in the IMJ is supposed to increase as the frequency increases. This viscoelastic characteristic of the IMJ can be integrated into a comprehensive mechanical model to answer questions about anatomical features and function of the IMJ, and to serve as a base for the development and optimization of middle-ear implants. However, the mechanical properties of the IMJ have not been measured, and its role in sound transmission and/or possible protection mechanism is still open.

Methods:
To determine the mechanical properties of the IMJ under static and dynamic excitation, the malleus-incus complex was isolated from fresh human temporal bones. For measurements of the static behavior of the IMJ, the malleus was fixed to a custom-made frame, and the incus was excited by applying a quasi-static force while measuring the resulting spatial displacement subsequently at several points on the incus. For measurements of the dynamic behavior, the isolated malleus-incus complex was excited by an electrodynamic shaker using different test signals and 3-D velocity components were measured at several points on the malleus-incus complex. The measurements were performed using a 3-D Laser Doppler Vibrometry (LDV) system with three independent LDVs. The relative motion between the malleus and incus was calculated, and spatial behavior of the IMJ was characterized. Different intensities and directions of excitation were used, and their influence on the IMJ motion was analyzed as well.

Results:
The force deflection curves obtained from the static measurement show a significant hysteresis loop and a nonlinear characteristic. Both depend on the excitation direction and position of the force application point, i.e. the spatial force and torque. In case of the dynamic measurement, the incus exhibits a spatial relative motion depending on the excitation amplitude, direction and frequency. A state dependent stiffness and damping matrix, describing the behavior of the IMJ, can be derived from those measurements.

Conclusion:
The IMJ shows a viscoelastic and nonlinear behavior under quasi-static and dynamic excitation.

2095

G. Bertolini[1], AA. Tarnutzer[1], KP. Weber[2], D. Straumann[1], S. Marti[1]

Mechanism of rebound nystagmus

Department of Neurology, University Hospital Zurich[1], Department of Ophthalmology at University Hospital Zurich[2]

Introduction:
Impaired cerebellar control causes an increase of the normally weak centripetal eye drift, leading to gaze-evoked nystagmus already at small gaze-angles. Rebound nystagmus, a prominent sign of cerebellar disease, denotes a transient ocular drift in the direction of the former sustained eccentric fixation after returning to primary gaze position. We propose two possible pathomechanisms for the rebound phenomenon, one implying adaptation within the gaze holding system and one based on an external constant eye-velocity input to such system.

Methods:
We tested nine patients with degenerative cerebellar disease, eliciting rebound nystagmus by fixation of an eccentric target positioned at 30° left or right for 20 sec. The curves describing the relation between eye drift velocity and gaze eccentricity were calculated taking the eye drift in the first second upon returning to one of 11 equally spaced horizontal gaze positions between 25° left and 25° right. Two models, representing the two hypothesized mechanisms, were fit to the curves obtained by each subject after sustained fixation to the left and to the right separately. For both models, we then compared the difference of the two fits with the difference of the curves.

Results:
The error computed according to the constant eye-velocity input hypothesis was roughly half of the one obtained with the adaptation hypothesis (median ratio [median absolute deviation]: 0.49 [0.11], p=0.039).

Conclusion:
We hypothesize that the mechanism causing rebound nystagmus in cerebellar patients may depend on the velocity storage, probably loaded by the optokinetic system, which compensates the retinal slip caused by gaze-evoked nystagmus.

2096

E. Unterleutner[1], F. Barchiesi[1], B. Imthurn[1], RK. Dubey[1]

G-protein Coupled Estrogen Receptor mediates Capillary formation and Induces Vasculogenic pathway ALK1/pSMAD1/5/8

Reproductive Endocrinology, UniversityHospital, Zürich[1]

Introduction:
Animal as well as human studies provide evidence that estrogen(s) induce their cardiovascular protective actions, in part, by improving endothelium dependent relaxation and inducing endothelial cell growth and repair. However, the molecular mechanism(s) via which it mediates these effects remains unclear. We have previously shown that Estradiol (E2) induces endothelial growth and capillary formation. Moreover, the effects of E2 on capillary formation are mimicked by its non-permeable analog, BSA-tagged E2. Based on these findings, we hypothesize that the stimulatory effects are potentially mediated via the newly discovered membrane bound estrogen receptor GPER. Hence, in the present study, using HUVECs, we assessed the role of GPER in capillary formation. Moreover, we explored the role of ALK1/pSMAD1/5/8, a prominent angiogenic pathway, in mediating the effects of E2.

Methods:
The role of GPER on capillary formation was assessed using 2D-matrigel based capillary assay and specific GPER -agonist (G1) and -antagonist (G15). Western Blotting was used to evaluate changes in ALK1/pSMAD1/5/8-pathway by GPER.

Results:
Treatment with specific GPER-stimulator G1 (10nm) and E2 (10nm) significantly induced capillary formation. The stimulatory effects of both G1 and E2 were significantly abrogated in presence of specific GPER-antagonist G15 (100nm) or ER-unspecific antagonist ICI (100nm). HUVECs expressed both ALK1 and ALK5, important proteins involved in regulating vasculogenesis. Treatment with G1 (100nm) differentially regulated the expression of ALK1 and ALK5, i.e. up-regulated the expression of pro-angiogenic ALK1 and down-regulated the anti-angiogenicALK5. Treatment with G1 (10nm) and E2 (10nm) was accompanied with increased phosphorylation of SMAD1/5/8, which is downstream of ALK1, moreover, the stimulatory effects were time-dependent with a maximal increase at ≈ 45min. Interestingly G1 (10nm) and E2 (10nm) also induced phosphorylation of SMAD3, which is downstream from ALK5. The stimulating effects of G1 and E2 on SMAD1/5/8 were blocked by GPER-antagonist G15 (100nm), ER-antagonist ICI (100nm) and specific ALK1-antagonist ALK1Fc (100ng/ml), but not with specific ALK5-inhibitor SJN (100nm). Moreover, these abrogatory effects on Smad1/5/8 phosphorylation were also reflected on capillary formation, as the effects of G1 were significantly blocked by ALK1Fc (100ng/ml), but not SJN (100nm). Finally, G1 treatment up-regulated the expression of ID-1, a protein downstream from ALK1/pSMAD1/5/8, but not of PAI-1, which is downstream from ALK5/pSMAD3.

Conclusion:
Our findings provide evidence that GPER plays an important role in mediating the capillary inducing effects by E2. Importantly the effects are mediated via activating the pro-angiogenic pathway ALK1àpSMAD1/5/8àID-1. The finding that SMAD3, a downstream target of ALK5, was also phosphorylated, even though ALK5 and PAI-1 remained unchanged, supports the notion that ALK5 cross-talks with ALK1 and facilitates angiogenesis. However, it is possible that SMAD3 phosphorylation induces vessel resolution and induces barrier function. More studies are required to investigate these possibilities. In conclusion GPER induces

angiogenesis and use of GPER specific agonist may facilitate endothelial recovery thereby promoting vascular protection.

2097

N. Ruangsawasdi[1], M. Zehnder[2], F. Weber[1]

Fibrin Gel Improved Tissue Ingrowth and Cell Differentiation in Human Immature Premolar Implanted in Rats

Cranio-Maxillofacial and Oral Surgery, University of Zürich Center for Dental Medicine, Zurich[1], Preventive Dentistry, Periodontology, and Cariology, University of Zürich Center for Dental Medicine, Zurich[2]

Introduction:
In pulpless immature human premolars implanted in rodents, this study investigated whether Fibrin gel offered advantages over leaving the root canal empty regarding soft tissue ingrowth and cell differentiation.

Methods:
Root canals of extracted human immature premolars (n=12) were accessed and then irrigated with 5% sodium hypochlorite followed by 17% ethylenediaminetetraacetic acid. Root canals were then either left empty or filled with a Fibrin gel (n=6 each) before being placed subcutaneously on top of the calvarial bone of rats (1 tooth per rat) for 12 weeks. After sacrifice, teeth were histologically assessed. Tissue ingrowth was quantified and compared between groups using the Mann-Whitney U test ($P < .05$). Cells adhering to the pulp canal wall were immunohistochemically screened for the presence of bone sialo-protein (BSP) and dentin sialoprotein (DSP).

Results:
More tissue grew into the pulp space when teeth were filled with Fibrin gel ($P < .05$). The presence of Fibrin gel affected not only the extent of tissue ingrowth but also tissue morphology and differentiation of cells contacting the dentinal wall. In the Fibrin gel group, newly formed tissue was similar to normal pulp, constituted of inner pulp, cell-rich zone, cell-free zone, and an apparent odontoblast layer, which stained positive for BSP and DSP. Newly formed blood vessels were also more abundant compared with the initially empty root canals.

Conclusion:
Under the conditions of this study, Fibrin gel improved cell infiltration and cell-dentin interaction. Both are necessary for pulp tissue regeneration.

2098

I. Inci[1], M. Schuurmans[2], S. Hillinger[1], P. Kestenholz[1], C. Benden[2], W. Weder[1]

Lung transplantation for emphysema: Impact of age on short and long-term survival

Thoracic Surgery, University Hospital Zürich[1], Department of Pulmonary Diesease, University Hospital, Zurich[2]

Introduction:
Emphysema is the most common indication for lung transplantation. The majority of patients present with chronic obstructive lung disease (COPD) and less frequently with alpha-1 antitrypsin deficiency (AAT). We analyzed the results of our lung transplantations for emphysema to identify the impact of age on short and long-term outcome.

Methods:
A retrospective analysis was undertaken of the 108 consecutive lung transplants for emphysema performed at our institution from November 1992 to August 2013 (77 COPD, 31 AAT). Retransplantations were excluded.

Results:
The median age was 56.6 years (range,31-68). The 30-day mortality rate was 3.7%. One- and 5-year survival rates in COPD and AAT recipients were comparable(p=0.87, log rank test).
The one- and 5-year survival rates for recipients aged < 60 years were significantly better than the age group of 60 years and older (91% and 79% versus 84% and 54%, p=0.05, log rank test). Since 2007 the one- and 5-year survival for these two age groups were at 96% and 92% versus 86% and 44%, respectively, p=0.04, log rank test).
For following aspects no significant influence on survival rates were found: Use of ECMO during transplantation, waiting list time, sex, size reduction, body mass index, diagnosis COPD or AAT. Age at transplantation (≥60) was a risk factor in univariate analysis (HR 2.1; 95% confidence interval(CI) 1.09 – 4.09, p=0.02). In multivariate analysis (cox regression, backward stepwise) unilateral lung transplantation (HR 0.04; 95%CI 0.01 – 0.2), Zurich Recipient Comorbidity Score (ZRCS) 3 or more (HR 6.3; 95%CI 2.01 – 19.8), and Zurich Donor Score (ZDS) of 3 or more (HR 2.4; 95%CI 1.06 – 5.6) were independent risk factors for mortality.

Conclusion:
COPD and AAT recipients have similar overall long-term survival. Recipients aged >60 years and those with multiple co-morbidities as well as marginal donors with additional co-morbidities were important risk factors for mortality.

2099

K. Seidl[1], M. Leemann[1], Y. Achermann[1], AS. Zinkernagel[1]

Role of SCCmec in Staphylococcus aureus induced endothelial cell cytotoxicity

Division of Infectious Disease and Hospital Epidemiology, University Hospital of Zurich[1]

Introduction:
The expression of the gene conferring methicillin resistance (*mecA*) located on the staphylococcal cassette chromosome *mec* (SCC*mec*) has been shown to interfere with the *agr* quorum sensing system. This system regulates the expression of many toxins thereby affecting *S.aureus* virulence. This study was designed to evaluate the role of SCC*mec* in *S.aureus* induced endothelial cell (EC) cytotoxicity, a surrogate marker for virulence in blood stream infections.

Methods:
We tested a representative set of clinical 40 MRSA isolates from our tertiary hospital (SCC*mec* types II, III or IV) and 40 MSSA isolates for their ability to induce human umbilical cord vein EC (HUVEC) cytotoxicity using an MTT assay. The strains were further compared to isogenic SCC*mec* +/- strain pairs and clinical MRSA isolates of SCC*mec* type I. As a surrogate marker for *agr* activity, the hemolytic activity of all strains was assessed. Oxacillin resistance was assessed by E-tests.

Results:
MRSA strains (SCC*mec* types II, III, and IV) exhibited relatively high EC cytotoxicity (60.4%) that was comparable to EC cytotoxicity induced by MSSA isolates (64.2%). MRSA isolates were significantly less hemolytic as compared to MSSA isolates (p<0.01), indicating a lower *agr* activity in MRSA isolates but there was no direct correlation between hemolytic activity and EC cytotoxicity (R^2=0.11). MRSA SCC*mec* type I isolates that were retrospectively added to the study (n=4) exhibited only little hemolytic activity and induced very low EC cytotoxicity (13.4%). The introduction of an SCC*mec* type I element into an MSSA strain of NCTC8325 background lead to high level oxacillin resistance (MIC512 µg/ml), reduced the hemolytic activity and completely abolished EC cytotoxicity. In contrast to SCC*mec* type I, neither excision of the SCC*mec* II element (strain N315) nor of the SCC*mec* IVa element (USA300 derivative JE2) had an impact on hemolytic activity. In these two MRSA strains with relatively low level oxacillin resistance (32µg/ml and 8µg/ml oxacillin MICs, respectively) excision of the SCC*mec* II or IVa elements had only little impact on cytotoxicity (24% and 3% reductions in cytotoxicity, respectively). Interestingly, inactivation of *agr* had different effects on cytotoxicity in MSSA strain NCTC8325 and MRSA strain JE2 leading to 85% and 50% reductions in cytotoxicity, respectively.

Conclusion:
The low EC cytotoxicity of SCC*mec* type I MRSA strains could be directly linked to the presence of SCC*mec* and it remains to be elucidated to which extent this effect is mediated by the *agr* quorum sensing because the role of *agr* on EC cytotoxicity is limited and strain-dependent. EC cytotoxicity induced by SCC*mec* II-IV isolates, which are predominant in our hospital, was similar to that of MSSA isolates. These findings underline the importance of preventing the spread of MRSA isolates which are as virulent as MSSA isolates but often more difficult to treat due to the oxacillin resistance.

2100

DL. Braun[1], RD. Kouyos[1], B. Balmer[1], C. Grube[1], R. Weber[1], HF. Günthard[1]

Atypical Clinical Presentations Occur in One Third of 293 Patients with a Primary HIV-1 Infection

Division of Infectious Disease and Hospital Epidemiology, University Hospital of Zurich, Zurich[1]

Introduction:
Proportion and disease-spectrum of atypical clinical presentations in primary HIV-Infection (PHI) has not systematically been studied. Unusual presentation of PHI may lead to delayed diagnosis with impact on transmission.

Methods:
Between January 2002 and June 2012 we prospectively enrolled 293 individuals with a well-documented PHI in the Zurich Primary HIV Infection Study, which is an open label, non-randomized, observational, single-center study. PHI was classified as “acute” (acquisition of infection during the last 3 months) or “recent” (acquisition during the last 6 months). At the first visit, a detailed history of symptoms and clinical signs of PHI, a physical examination and standard and specific HIV laboratory parameters were obtained. “Typical” ARS was determined in case of documented or reported fever (temperature > 38° Celsius) plus at least one symptom OR ≥ 2 symptoms (in absence of fever) considered as ARS symptoms in literature. “Atypical presentation” was determined by study-physicians based on patient’s medical history, review of medical chart, lack of any ARS symptoms OR a single symptom only. The date of infection (EDI) for each patient was estimated integrating all available clinical and laboratory data. Time to diagnosis was calculated based on EDI and date of first positive screening test.

Results:
We analysed 293 individuals with PHI, including 271 males. PHI was classified in 245 (84%) individuals as “acute” and in 48 (16%) as “recent”. PHI manifested as typical ARS in 203 (69%) of 293 patients. Overall, PHI presented atypically or with an opportunistic infection (OI) in 90 (31%) of 293 patients, 16 (18%) of them were fully asymptomatic. Patients with atypical PHI presented with a broad spectrum of diseases. Gastrointestinal tract and central nervous system were the most prevalent organ systems for atypical PHI and OI’s. Atypical presentation did not lead to a significantly delayed diagnosis (median time EDI to first positive test without symptoms: 42 days [95% Bootstrap confidence interval 18.4, 65.6]; atypical presentation: 32 days [25.8, 38.2], typical ARS: 29 days [24.8, 33.2]; p= 0.13), but a surgical intervention was required in 6 (6.5%) of 90 patients.

Conclusion:
Atypical presentations and OI’s occur in a substantial proportion of patients with PHI, however, did not result in delayed diagnosis. This may be explained by the severe clinical presentation of these patients leading to a low treshold for HIV testing.

2101

DL. Braun[1], RD. Kouyos[1], R. Ghenzi[1], C. Grube[1], R. Weber[1], HF. Günthard[1]

Increasing rates of STI are Linked to Reduced Condom Use in Patients with Primary HIV-infection

Division of Infectious Disease and Hospital Epidemiology, University Hospital of Zurich, Zurich[1]

Introduction:
In Switzerland, incidence of sexual transmitted infections (STI) is increasing in HIV positive individuals, particularly including an epidemic for sexually acquired acute Hepatitis C virus (HCV) infection in men having sex with men (MSM). Patients with a primary HIV-infection (PHI) represent a highly sexual active population and may contribute to this epidemic, possibly due to changed sexual risk practices influenced by the “Swiss statement” in 2008, postulating that individuals on effective antiretroviral therapy are non-infectious.

Methods:
Between January 2002 and April 2013 we prospectively enrolled 293 individuals with a PHI in the Zurich Primary HIV-1 Infection Study, which is a non-randomized, observational, single-center study. Patients were also included in the Swiss HIV cohort study (SHCS). At study-begin, individuals were actively screened for hepatitis C and B, syphilis, gonorrhea, chlamydia and herpes genitalis. During the study-period, STI-screening was performed based on clinical symptoms, reported sexual risk practices and by yearly serological syphilis and HCV testing. STI were determined by a detailed medical chart review including history, symptoms of STI and screening tests. Condom use is reported in the SHCS database 6 monthly.

Results:
We analysed 293 individuals (271 males). Transmission mode included MSM (79%), heterosexual (20 %) and intravenous drug abuse (1 %). Of all, 49 (17%) individuals had a concomitant STI at presentation. During follow-up period, syphilis was the most prevalent STI with 93 cases, followed by gonorrhoea: 40, chlamydia: 38; acute HCV-infection: 16; herpes genitalis: 8, acute hepatitis B: 2. Incidence rates of syphilis and acute HCV-infections were significantly increasing over the study-period, most pronounced in the latter (figure 1, panel A). For syphilis, there was a significant linkage between incidence and imperfect condom use, whereas for acute HCV-infection such correlation was also found, but only as a trend (figure 1, panel B).

Conclusion:
Increasing incidence rates of STI’s represent a surrogate for changed sexual risk behavior in patients with PHI, may be fostered by the “Swiss statement” that has been endorsed however only for patients in stable partnerships. The ongoing epidemic of acute HCV-infections affecting MSM can not solely be explained by unprotected sex and remains unclear. Risk-group targeted prevention programs, mainly propagation of condom use, are urgently needed.

2102

DL. Braun[1], A. Rauch[2], N. Durisch[1], N. Eberhard[1], QA. Anagnostopoulos[2], B. Ledergerber[1], R. Weber[1], J. Fehr[1]

Silibinin Prior to Triple Therapy Leads to End of Treatment Success in Most Difficult to Treat HIV/Hepatitis C Co-Infected Individuals

Division of Infectious Disease and Hospital Epidemiology, University Hospital of Zurich, Zurich[1], Division of Infectious Diseases, University Hospital Berne, Berne[2]

Introduction:
Efficacy of current hepatitis C virus (HCV) triple therapy, including a protease inhibitor, is limited in HIV/HCV-coinfected patients with advanced liver fibrosis and non-response to previous pegylated interferon plus ribavirin (peginterferon-ribavirin). These patients experience on-treatment failure during triple therapy in up to 50%, and they cannot wait for availability/ affordable next-generation anti-HCV drugs. In a pilot study, we investigated the efficacy of a lead-in therapy with silibinin before triple therapy in difficult-to-treat patients.

Methods:
Inclusion criteria were HIV/HCV coinfection with advanced liver fibrosis and documented failure of previous peginterferon-ribavirin treatment. Intervention was a lead-in therapy with intravenous silibinin 20 mg/kg/day for 14 days. Subsequently, peginterferon-ribavirin combined with telaprevir was initiated for 12 weeks, followed by peginterferon-ribavirin dual-therapy until week 48. The outcome measurement was HCV RNA after silibinin lead-in, at weeks 2, 4, and 12, and at end of treatment.

Results:
We examined six HIV/HCV-coinfected patients. Median age was 49 years (range 38-56). For five individuals the transmission mode was intravenous drug use. Genotype 1a, which is associated with poorer response to triple therapy, was most prevalent (5/6) and all had a fibrosis grade METAVIR F3. All were under successful antiretroviral treatment (HIV-RNA <20c/ml) with a median CD4+ cell count of 574/µl (range 175-686). Mean HCV-RNA decline under silibinin therapy was 2.6log10 copies/ml (range 2-3). Five of six patients were virologically suppressed at weeks 2 and 4, and 6/6 at week 12 of triple therapy. One experienced a viral breakthrough thereafter. At the end of treatment, 5/6 (83%) patients had an undetectable HCV RNA.

Conclusion:
A lead-in with silibinin before triple therapy is highly effective and may increase the probability of HCV treatment success in difficult-to-treat HIV/HCV-coinfected patients with advanced liver fibrosis and previous failure of peginterferon-ribavirin. It might be a treatment alternative where latest direct acting agents against HCV are not available or affordable.

2103

A. Theocharides[2], S. Dobson[1], E. Laurenti[1], F. Notta[1], V. Voisin[1], PY. Cheng[1], M. Minden[1], C. Mullighan[3], E. Torlakovic[1], J. Dick[1]

The Ikaros 6 isoform cooperates with BCR-ABL1 to induce human acute myeloid leukemia in xenografts

University of Toronto, Toronto, Canada[1], University Hospital Zurich, Division of Hematology, Zurich[2], St. Jude Childrens Hospital, Memphis, TN, USA[3]

Introduction:
Historically, our understanding of mechanisms underlying human leukemogenesis are inferred from genetically engineered mouse models. Relatively few models that use primary human cells recapitulate the full leukemic transformation as assayed in xenografts and myeloid transformation is infrequent. We aimed to determine the functional consequence of combinatorial overexpression of *BCR-ABL1* and a dominant negative isoform of IKAROS, Ik6, in human lineage depleted cord blood (LIN-CB) cells.

Methods:
LIN-CB cells were exposed to lentiviruses, and then to retroviral supernatants. Four independent cultures were generated: control, Ik6, *BCR-ABL1* and *BCR-ABL1*-Ik6. Cells were seeded after infection into lympho-myeloid promoting culture conditions. NSG mice were intrafemorally transplanted with transduced LIN-CB and sacrificed at 16-20 weeks post-transplantation or when sick. Engrafted human cells were characterized by flow cytometry and extensive histopathological analysis. Gene expression, gene set enrichment, pathway and network analysis was performed on purified double-transduced cells cultured in vitro.

Results:
We report a humanized experimental leukemia model where xenografts develop aggressive acute myeloid leukemia (AML) with disseminated myeloid sarcomas within 4 weeks following transplantation of cord blood transduced with vectors expressing *BCR-ABL1* and a dominant negative isoform of IKAROS, Ik6. Ik6 induced transcriptional programs in *BCR-ABL1* transduced progenitors that contained repressed B cell progenitor programs, along with strong stemness, proliferation, and granulocyte-monocytic progenitor signatures; a novel combination not induced in control groups.

Conclusion:
Thus, wild type IKAROS restrains stemness properties and has tumor suppressor activity in *BCR-ABL1* initiated leukemia. Although IKAROS mutations/deletions are common in lymphoid transformation, they are found also at low frequency in AML that progress from a prior myeloproliferative neoplasms (MPN) state. Our experimental system provides an excellent model to gain insight into these rare cases of AML transformation and the properties conferred by IKAROS loss of function as a secondary mutation. More generally, our data point to the importance of deregulated stemness/lineage commitment programs in human myeloid leukemogenesis.

2104

CNA. Nombela-Arrieta[1], MGM. Manz[1]

Quantitative Imaging of Hematopoietic Bone Marrow Microenvironment in Health and Disease

Universitätsspital Zürich, Department of Hematology[1]

Bone marrow (BM) cavities are the primary sites of continuous, demand-adapted production of mature hematopoietic cells during adult life. Within BM microenvironments, extremely rare self-renewing hematopoietic stem and progenitor cells enter multistep differentiation pathways to generate a finely-tuned output of all blood cell types. The structural backbone of BM tissues is provided by non-hematopoietic stromal components, which include mesenchymal fibroblastic reticular cells, a dense network of blood vessels, and cells of neural origin. BM stroma plays essential roles in the homeostatic and pathologic regulation of hematopoiesis. A detailed understanding of the hematopoietic hierarchy and, more recently, of BM stromal networks has been obtained through flow cytometric techniques. Nonetheless, insight into the microarchitectural organization and structural dynamics of BM cellular components is very limited to date, due to challenges associated to imaging bone-enclosed marrow cavities.

We have recently applied novel quantitative imaging techniques to perform a comprehensive analysis of the spatial distribution of HSPCs in the BM and analyze their interactions with endothelial cells (*Nombela-Arrieta et al*, Nat Cell Biol. 2013 May;15(5):533-43). Here we apply these powerful technological platforms, in conjunction with multiple reporter mouse strains, to provide a global quantitative 3D overview of BM microstructure with unprecedented resolution. Our studies reveal the existence of highly organized and conserved sinusoidal and arterial networks, which harbor distinct perivascular stromal environments. We have employed advanced image-analysis software to measure morphometric parameters, quantify spatial relationships of hematopoietic cells with stromal structures, and determine the microarchitectural dynamics of BM tissues under inflammatory conditions.

2105

FM. Morsbach[1], SG. Gordic[1], RG. Göttii[1], CG. Gruner[2], HA. Alkadhi[1], RM. Manka[2]

Quantitative Comparison of 2D and 3D Late Gadolinium Enhancement MR Imaging for Cardiomyopathies

Institut für Diagnostische und Interventionelle Radiologie, Universitätsspital, Zürich[1], Klinik f. Kardiologie, UniSpital Zürich[2]

Introduction:
To determine whether the quantification of myocardial fibrosis in patients with Fabry disease and hypertrophic cardiomyopathy (HCM) using a late gadolinium enhancement (LGE) single-breath-hold three-dimensional (3D) inversion recovery magnetic resonance (MR) imaging sequence is comparable with a clinically established two-dimensional (2D) multi-breath-hold sequence.

Methods:
40 consecutive patients (18 men; mean age 50±17) with either Fabry disease (n=18) or HCM (n=22) were enrolled in this prospective study. Studies were conducted on a 1.5-T clinical MR imaging system. Spatial resolution was the same for 3D and 2D images. Datasets were analyzed for subjective image and quantitative evaluation of myocardial mass (grams), fibrotic mass (grams) and total fibrotic tissues percentage. Statistical analysis included Wilcoxon-signed-rank test, student's t-test for paired samples.

Results:
There was no significant difference in subjective image quality between acquisitions (P>0.1) for either disease. In patients with Fabry disease there was no significant differences in myocardial mass between 3D (100.7g±30.8g) and 2D acquisition(99.9g±31.9g; P=0.55), as well as for fibrous tissue mass(3.9g±6.4g vs 4.0±6.4g; P=0.89) and total fibrous percentage(3.4%±5.5%vs3.4±5.5;P=0.89). In patients with HCM there was no significant differences in myocardial mass between 3D (115.5g ± 33.3g) and 2D acquisition (116.7g±33.6g;P=0.48),as well as for fibrous tissue mass (5.6g±8.6g vs 5.7g±8.7g;P=0.6) and total fibrous percentage (4.3%±6.4% vs 4.3%±6.5%;P=0.89). Acquisition time was significantly shorter for 3D sequences (24.9seconds ± 5.2 seconds) as compared to 2D sequence (349.1seconds ± 62.3 seconds, P<0.001).

Conclusion:
3D LGE imaging enables comparable quantification of fibrous myocardial tissue compared to a 2D sequence at a faster acquisition rate.

2106

FM. Morsbach[1], WM. Wurnig[1], HA. Alkadhi[1]

Feasibility and Value of Iterative Reconstructions for Urinary Stone Characterization on Single-Source Dual-Energy CT

Institut für Diagnostische und Interventionelle Radiologie, Universitätsspital, Zürich[1]

Introduction:
To evaluate the feasibility and accuracy of single-source dual-energy CT (SS-DECT) with sequential data acquisition and co-registration motion correction for urinary stone characterization and to evaluate the value of iterative reconstructions (IR) in DECT.

Methods:
Thirty-five urinary stones placed in cylindrical phantoms (diameters 30cm and 40cm) were scanned with 64-slice CT with SS-DE consisting of two sequential acquisitions at 80 and 140kVp, with phantom movement between acquisitions. Images were reconstructed with FBP and IR, and data were coregistered. Two readers evaluated image quality. Image noise and HU values of stones were measured; the dual-energy index (DEI) was calculated.

Results:
The motion correction algorithm achieved a good coregistration. Image quality was significantly higher on IR in the 40cm phantom as compared to FBP ($P<0.05$). Stone visibility was significantly higher for both phantoms on IR images ($P<0.05$). Noise was reduced by 31% in the 40cm phantom with IR ($P<0.001$). The DEI was similar in FBP and IR datasets for both phantoms ($P=0.116$, $P=0.544$). DEI was significantly different between UA-containing stones, cystine and struvite stones, and stones of other compositions ($P<0.001$). Post-processing software classified all stones correctly as UA- or non-UA containing stones. In the 40cm phantom, false-positive colored voxels found in the FBP datasets disappeared on IR images.

Conclusion:
SS-DECT with sequential acquisitions and using co-registration motion correction is feasible and accurate for characterizing urinary stone composition. Use of IR in DECT reduces noise, improves image quality and visibility of stones and helps avoiding false stone classifications.

2107

St. Georgiopoulou[1], F. Aimi[1], I. Kalus[1], F. Lehner[1], I. Bhattacharya[1], K. Drägert[1], P. Limani[4], M. Rüegg[3], MN. Hall[3], N. Lindenblatt[2], E. Haas[1], EJ. Battegay[1], R. Humar[1]

Endothelial mTORC2 is essential for capillary remodeling and de novo angiogenesis in response to FGF2

Division of Internal Medicine, University Hospital, Zurich[1], Division of Plastic and Reconstructive Surgery, Department of Surgery, University Hospital, Zurich[2], Biozentrum, University of Basel, Basel[3], Division of Visceral and Transplant Surgery, University Hospital, Zurich[4]

Introduction:
Endothelial cells receive multiple information from their environment, process these stimuli by diverse signaling pathways and eventually enter and progress along all the stages of angiogenesis, i.e., the biological process that causes the formation of new microvessels. While angiogenic activation of the endothelium is relatively well understood, the relevance of distinct signal transduction pathways between the angiogenic surface receptors and the final effectors of the modified endothelial cellular behavior is incompletely understood. Studies using rapamycin-derived or dual mTORC1/mTORC2 inhibitors have suggested a central function of the kinase mammalian target of rapamycin complex 2 (mTORC2) in angiogenesis. A direct evidence for this role has not been established.

Methods:
To clarify the contribution of mTORC2 in endothelium-controlled angiogenesis we used a transgenic mouse model in this study: Excision of the crucial mTORC2 component Rictor in the endothelium was induced in adolescent mice in vivo and in endothelial cells in vitro to analyze vascular alterations after angiogenic stimulation.

Results:
We demonstrate that Rictor knockout mouse aortic endothelial cells (MAECs) do not form significant capillary-like endothelial networks in response to FGF2. On the other hand, VEGF-stimulation was able to rescue endothelial network formation disabled by Rictor knockout and, unlike FGF2, could form independent endothelial master segment connections when co-cultured with control MAEC. FGF2-stimulated phosphorylation of mTORC2 downstream target Akt-Ser473, PKCα and FGF2-induced endothelial proliferation and migration were markedly diminished in Rictor knockout MAEC.
In vivo, endothelial Rictor knockout ($Rictor^{i\Delta ec}$) did not affect viability or capillary structure. However, capillary diameter increase by exogenously administered FGF2 was delimited by $Rictor^{i\Delta ec}$ as observed through intravital microscopy of the dorsal skinfold chamber. Furthermore, $Rictor^{i\Delta ec}$ efficiently prevented heterogeneous FGF2-induced remodeling of skin capillary vessel structure which in control mice resulted in an aberrant and tortuous vascular bed and dilated microvessels. Likewise, $Rictor^{i\Delta ec}$ markedly reduced neovessel ingrowth in FGF2-loaded Matrigel plugs, whereas FGF2-induced a heterogeneous, expanded and leaky neovasculature in control mice.

Conclusion:
Taken together, we present the first direct evidence that endothelial mTORC2 is specifically required for capillary remodeling and neo-angiogenesis in response to exogenously administered FGF2 in vivo. Our in vitro data strongly point to mTORC2 as central angiogenic signaling mediator of FGF2-induced endothelial responses. The potent ‘normalization’ and mitigation of FGF2-induced neovessel growth by endothelial rictor knockout emphasizes the prospect of targeting mTORC2 in vascular-associated malignancies such as in tumor growth.

2108

A. Mortezavi[2], E. Keller[2], C. Fankhauser[1], PJ. Wild[1], M. Provenzano[2], T. Sulser[1], D. Eberli[2]

Needle biopsy performed in a tertiary care center results in significantly less clinically relevant undergrading of prostate cancer

Institut für klinische Pathologie, UniversitätsSpital Zürich, Zürich [1], Klinik für Urologie, Universitätsspital Zürich, Zürich[2]

Introduction:
Gleason score reported in needle biopsy of the prostate is a key parameter in treatment counseling, considering therapy modalities such as active surveillance. High-grade cancers (e.g. Gleason 4 and 5 patterns) missed at the initial biopsy pose the greatest risk to active surveillance patients in terms of a lost opportunity for cure. This study examines the incidence of clinical relevant up- and downgrading of the Gleason score after radical prostatectomy (RP), according to whether biopsies were assessed in a referral or in a tertiary care center.

Methods:
Data of all patients undergoing RP in our tertiary care center from Mai 2005 to January 2013 were reviewed. Referral and tertiary care center biopsy's Gleason scores were compared with the Gleason scores of their respective embedded prostatectomy specimens (EPS). A clinically relevant upgrade or downgrade, according to the active surveillance inclusion criteria guidelines, was defined as a Gleason score upgrade from 5-6 to ≥7 between the biopsy and the EPS and downgrade from ≥7 to 5-6, respectively. Significance level was assessed by Fischer's exact test (two-sided $p<0.05$).

Results:
A total of 491 patients could be included in this study. Overall, 36% of all cases were upgraded, 7% downgraded and 57% remained identical. When comparing whether the biopsies originated from a referral center or from our institution, 42% vs. 25% were upgraded and 3% vs. 14% were downgraded, respectively. Grade agreement was achieved in 54.6% vs. 61.4% of all cases, respectively ($p<0.001$). Notably, a clinically relevant upgrade was observed in 31% (99/315) of all patients undergoing a biopsy at a referral center vs. 18% (32/176) of all patients diagnosed in our tertiary center, respectively (Odds ratio 2.063, 95% confidence interval 1.134-3.238, $p<0.001$). A clinically relevant downgrade was observed in 1 and 6% of the patients, respectively.

Conclusion:
Tertiary care center biopsies are more accurate than referral center biopsies in determining EPS Gleason score and result in a significantly less clinically relevant undergrading of the disease. However, the risk of overgrading seems higher. Re-evaluation of biopsy specimens in a high caseload center should be considered whenever patients are possibly eligible for active surveillance in order to reduce the rate of missed high-grade prostate cancers.

2109

A. Mortezavi[2], S. Salemi[2], N. Rupp[1], PJ. Wild[1], D. Eberli[2]

Reduced autophagy levels are associated with a higher Gleason score, tumor stage and an increased rate of prostate cancer specific death

Institut für klinische Pathologie, UniversitätsSpital Zürich, Zürich [1], Klinik für Urologie, Universitätsspital Zürich, Zürich[2]

Introduction:
Autophagy is a catabolic cellular process used for degradation of cytoplasmic organelles and preservation of cell viability. In this study we aimed to analyze the level of autophagy in benign and malignant prostate tissue and to evaluate the prognostic properties for patients with primary prostate cancer (PCa).

Methods:
A Tissue microarray containing 479 formalin-fixed, paraffin-embedded prostate tissue cores was stained immunohistochemically for major autophagy proteins ATG5, Beclin1 and LC3b: 41 normal prostate tissues, 382 primary adenocarcinomas (ADC) and 56 prostate cancer metastases or castration resistant prostate cancers. Immunoreactivity was semiquantitatively scored and correlated with pathologic and clinical parameters including survival.

Results:
LC3b expression was significantly upregulated in PCa, especially in metastatic and castration-resistant prostate cancer samples compared to normal prostate tissue (p=0.002). Evaluation of expression in ADCs revealed an inverse association with preoperative serum PSA level (p=0.047), pT-stage (0.033) and Gleason Score (p=0.026). Negative LC3b expression was identified as a novel predictor of prostate cancer specific death after radical prostatectomy (p=0.02). A significant association of ATG-5 and Beclin1 with LC3b expression could be noticed, but no link with clincopathologic parameters.

Conclusion:
A lower LC3b expression in prostate cancer tissue is significantly associated with a higher rate of prostate cancer specific death. Furthermore, there is a significant association of a lower expression in tumors with extraprostatic extension and higher Gleason Scores. This is the first report evaluating autophagy expression levels and their association with the clinical course in prostate cancer patients.

2110

RF. Speck[1], R. Myburgh[1], KH. Krause[2], P. Salmon[3], MS. Pepper[4]

Evidence of a functioanl cure for HIV by gene engineering HIV-resistant CD4+ T cells in humanized mice

Infectious Diseases and Hospital Epidemiology, University Hospital Zurich, Zurich[1], Dept. of Pathology and Immunology, Geneva University Hospitals Centre Medical Universitaire, Geneva[2], Department of Neurosciences, Faculty of Medicine, Centre Medical Universitaire, Geneva [3], Department of Immunology, Faculty of Health Sciences, University of Pretoria, Pretoria[4]

Introduction:
The overall long term goal is to develop a cure for HIV infection involving autologous bone marrow transplantation of gene engineered Hematopoietic progenitor cells (HPCs9. Notably, HIV is dependent on critical host factors for its entry and infection of a host cell; one critical factor is the chemokine receptor CCR5 which in concert with CD4 constitutes the HIV's entry receptor complex for the majority of HIV strains. This gene engineering approach is based on a proof of concept where a patient was cured of HIV after receiving CCR5 deficient bone marrow cells for treatment of leukaemia. This project requires a highly efficient CCR5 targeting "RNA interference" (RNAi) miRNA molecule which efficiently down regulates CCR5 without any off-target effects.

Methods:
We created a novel miRNA mimic called "mirGE". The miRNAs were cloned into an HIV-1 based lentiviral vector system. The potential of the mirGE vector to inhibit HIV *in vitro* was tested on HeLa cells (p24 assay) as wells as macrophages (using a recombinant NL4-3-Luciferase ADA env based HIV virus). The mirGE vector was tested *in vivo* for its ability to knockdown CCR5 as well as inhibit HIV replication through generation of GFP (control) and GFP CCR5-knockdown humanized mice (NSG strain). Human HPCs were transduced, after 3 days the cells were transplanted into the liver of new born mice. In a separate experiment, after transduction the transduced HPCs were sorted into GFP^+ and GFP-negative fractions which were transplanted into separate cohorts of mice (FACS-sorted R5 knockdown and FACS-sorted negative cohorts respectively). After 4 months blood samples from the mice were analysed by flow cytometry to determine transgene expression and engraftment level. Mice were then challenged with R5 tropic HIV and peripheral blood cell subsets were analysed by flow cytometry.

Results:
in vitro: HeLa-R5 cells (expressing CCR5 and CD4) transduced with the mirGE were resistant to multiple rounds of infection with R5 tropic HIV *in vitro*. Upon X4 HIV challenge the survivor cells were killed in a matter of days. Human macrophages were also resistant to HIV infection *in vitro* when transduced with the mirGE vector.
in vivo: The control (GFP) and R5 knockdown mice showed engraftment and development of a human-like immune system, indicating that the transduction did not have deleterious effects on the survival and proliferation of the HPCs. CCR5 expression in the R5-knockdown cohorts was significantly less on GFP^+ $CD4^+$ T cells as compared to the control cohorts. Upon R5 tropic HIV challenge, there was a homeostatic expansion of GFP^+ $CD4^+$ T cells over time in the R5 knockdown cohort indicative that these cells are protected against HIV infection. However, viral loads in these mice were indistinguishable from the control cohorts. 4 months after transplantation of the GFP^+ sorted HPCs, we detected pure GFP^+ $CD4^+$ T cell populations in the blood of the FACS-sorted R5 knockdown mice. Upon infection, these mice had a significantly inhibited viral load compared to the control cohorts over 28 weeks of infection.

Conclusion:
The mirGE miRNA design is very promising for future gene engineering. The mirGE expressing cells were resistant to HIV *in vitro* while remaining infectable by X4 tropic HIV, indicative of the specificity of the CCR5 knockdown. Off target effects of miRNAs is an important safety issue. Experiments *in vivo* are on-going and results thus far suggest that the presence of a majority of gene engineered cells (~80%) is required *in vivo* in order to have an inhibitory effect on HIV over an extended period of time. Therefore, selection strategies that can eliminate only the non-gene engineered cells after transplantation of the manipulated cells are required for the future success of HIV gene therapies.

2111

C. Lutz[1], M. Caj[1], M. Fried[1], G. Rogler[1], M. Hausmann[1]

MyD88 signaling is not essential in intestinal fibrosis in mice

Gastroenterology and Hepatology, University Hospital Zurich, Zurich, Switzerland[1]

Introduction:
Hallmark of fibrosis is an excessive deposition of collagenous extracellular matrix as a consequence of the proliferation and activation of fibroblasts and myofibroblasts. A pivotal role of IL-1R1/MyD88 signaling was suggested in tissue-resident cells leading to lymphocyte recruitment and fibroblast activation. We investigated whether intestinal fibrosis occurs after heterotopic transplantation of small bowel resections lacking functional MyD88.

Methods:
Donor (B6-MyD88$^{-/-}$) small bowel resections were transplanted subcutaneously into the neck of recipients (B6-Tg UBC-GFP) and vice versa. Grafts were explanted 1, 2, 3, 4, 5, 6, 7, 14 and 21 days after transplantation.

Results:
Rapid loss of crypt structures at day one after intestinal transplantation was found in all grafts. Histologic cross sections were stained with EvG to highlight collagen. Freshly isolated samples exhibited very little collagen staining at the submucosal border (10.1 ± 2.3 µm). In contrast, collagen layer thickness was significantly increased at day seven after transplantation in allografts from both B6-MyD88$^{-/-}$ (20.8 ± 2.1 µm, $p < 0.001$) and B6-Tg UBC-GFP (27.3 ± 10.1 µm, $p < 0.001$). Increased collagen expression over time after transplantation was confirmed by Sirius Red staining and real-time PCR (1.1 ± 0.3 arbitrary units in freshly isolated small bowel compared to 198.9 ± 89.4 for B6-MyD88 and 467.3 ± 178.9 for B6-Tg UBC-GFP grafts at day five). Increased collagen was linked with increased expression of TGF-b (1.2 ± 0.4 arbitrary units in freshly isolated small bowel compared to 4.0 ± 1.5 for B6-MyD88$^{-/-}$ and 5.0 ± 3.7 for B6-Tg UBC-GFP grafts at day five).

Conclusion:
Increased collagen and TGF-b were observed in the heterotopic intestinal grafts where B6-MyD88$^{-/-}$ were used as either donors or recipients of small bowel resections. This suggests that MyD88 signaling is not essential for the induction of important profibrotic cytokines and the formation of thickened collagen layers during the pathogenesis of intestinal fibrosis in mice.

2113

K. Wronska[1], J. Reber[1], S. Haller[1], S. Schaefer[2], R. Schibli[3], C. Mueller[1]

Targeted Tumor Therapy Using 177Lu-Folate in Combination with 5-Fluorouracil as a Radiosensitizing Agent

Center for Radiopharmaceutical Sciences ETH-PSI-USZ, Paul Scherrer Institute, Villigen-PSI, Switzerland[1], Division of Nuclear Medicine, Department Medical Radiology, University Hospital of Zurich, Zurich, Switzerland[2], Department of Chemistry and Applied Biosciences, ETH Zurich, Zurich, Switzerland[3]

Introduction:
The folate receptor (FR) is overexpressed in a variety of tumor types including ovarian and lung cancer which makes it an interesting target for tumor therapy. Recently, we performed the world-wide first preclinical radionuclide therapy study in tumor-bearing mice using folic acid as a targeting ligand. For this purpose a novel ^{177}Lu-labeled DOTA-folate conjugate (cm09) was developed. ^{177}Lu-cm09 comprises an albumin-binding entity which is responsible for the excellent tumor targeting characteristics and pharmacokinetics observed in mice. However, long-term experiments indicated damage to the kidneys in mice which were injected with ^{177}Lu-cm09 at a quantity which eradicated tumor xenografts completely. Therefore, it was our aim to reduce the injected activity of ^{177}Lu-cm09 but maintain the therapeutic efficacy by combining it with 5-fluorouracil (5-FU) as a radiosensitizing agent.

Methods:
The DOTA-folate conjugate (cm09) was radiolabeled with ^{177}Lu ($E_{av,\ beta}$ = 134 keV, $T_{1/2}$ = 6.7 d) at a specific activity of 20 MBq/nmol. For the in vitro experiments we used human ovarian cancer cells (IGROV-1) which express the FR. MTT assays were performed to investigate inhibition of the cell viability by ^{177}Lu-cm09 alone and in combination with 5-FU. The in vivo therapy study was conducted with IGROV-1 tumor-bearing nude mice. They received either only ^{177}Lu-cm09 (10 MBq) or a combination of ^{177}Lu-cm09 (10 MBq) with two injections of 5-FU (1 mg)/leucovorin (1 mg). The tumor growth and body weight of treated mice was monitored and compared with untreated controls. Pre-defined endpoint criteria included a tumor volume of >1000 mm^3, body weight loss of >15% and unease of the animals.

Results:
The ^{177}Lu-cm09 was prepared at high radiochemical purity (>97%) and revealed to be stable over several days in solution. The in vitro experiments showed a concentration-dependent inhibition of the cell viability upon exposure of IGROV-1 cells to ^{177}Lu-cm09 (IC_{50} = 5.5 MBq/mL). If ^{177}Lu-cm09 was applied in combination with 5-FU (30 µM) the cell viability was reduced to 50% of controls at a significantly lower activity concentration (IC_{50} = 2.5 MBq/mL) than if it was applied as a single agent. In vivo the tumor growth was more delayed in mice which received ^{177}Lu-cm09 in combination with 5-FU/leucovorin than in mice which received ^{177}Lu-cm09 as a single treatment. The additional effect of 5-FU/leucovorin was also reflected by the increased survival time (36 d) of mice which received the combination therapy compared to mice treated with ^{177}Lu-cm09 alone (28 d) or untreated control mice (23 d).

Conclusion:
In this study the radiosensitizing potential of 5-FU in combination with ^{177}Lu-cm09 was successfully demonstrated in cell viability studies in vitro and in tumor-bearing mice. This new therapy concept would allow reducing the amount of injected ^{177}Lu-cm09 without loss of antitumor efficacy and therewith prevent radiation damage to the kidneys.

2114

A. Theocharides[1], R. Müller[1], Y. Saito[1], M. Manz[1]

Development of a xenograft model for myelofibrosis

University Hospital Zurich, Division of Hematology, Zurich[1]

Introduction:
Engraftment of primary hematopoietic stem and progenitor cells from patients with myelofibrosis (MF) in murine xenograft models is poor. We hypothesized that this is the consequence of rejection and the lack of supportive human growth factors in the bone marrow niche.

Methods:
Purified peripheral blood CD34+ cells from MF patients were transplanted intrahepatically into sublethally irradiated newborn humanSIRPα-transgenic/humanTPO-knockin Rag2-/-gamma-/- mice (humanized mice). It has been demonstrated that the interaction between CD47 expressed on human hematopoietic cells and SIRPα expressed on mouse macrophages is critical for the engraftment of human cells in the xenograft and we hypothesized that hTPO might be an important factor for hMF support.

Results:
CD34+ peripheral blood cells from 4 MF patients were transplanted. 3/4 patient samples generated a human graft in a dose-dependent manner as demonstrated by flow cytometry and immunohistochemistry. 2/3 samples generated a graft with >50% of human cells in the bone marrow (BM) of transplanted mice. The human graft was mainly composed of myeloid cells with a minor proportion of B-cells. The *JAK2*-V617F mutation was detectable in human cells harvested from the mouse BM confirming presence of MF cells in xenografts.

Conclusion:
Humanized mice can support high levels of human MF cell engraftment. The findings constitute a significant improvement compared to previously reported models. The presented MF xenograft model is likely suited to study e.g. the bone marrow niche interactions of human MF cells, clonal evolution in MF, and to test established and novel therapeutics *in vivo*.

2115

P. Forny[1], DS. Froese[1], T. Suormala[1], WW. Yue[2], MR. Baumgartner[1]

Functional Characterization and Categorization of Missense Mutations that Cause Methylmalonyl-CoA Mutase Deficiency

Division of Metabolism and Children's Research Center, University Children's Hospital Zurich, Zurich, Switzerland[1], Structural Genomics Consortium, University of Oxford, Oxford, UK[2]

Introduction:
Mitochondrial methylmalonyl-CoA mutase (MUT, EC 5.4.99.2) catalyzes the reversible isomerisation of L-methylmalonyl-CoA to succinyl-CoA, requiring vitamin B_{12} in the form of adenosylcobalamin (AdoCbl) as cofactor. In humans, this reaction represents an important step in propionate catabolism, funnelling metabolites from the breakdown of valine, isoleucine, methionine and threonine, odd-chain fatty acids and the side chain of cholesterol into the tricarboxylic acid cycle. The importance of the MUT-catalyzed reaction is further underlined by the severe metabolic disorder methylmalonic aciduria (MMA) which is caused by a genetic defect in *MUT,* encoding the MUT enzyme (MIM# 251000, MMA *mut* type), or in one of several proteins involved in the synthesis of its cofactor. Defects in MUT can be further classified according to whether the mutant enzyme exhibits residual activity in the presence of high concentrations of AdoCbl (K_M variants; *mut*$^-$), or no detectable activity (*mut*^{0}).To date almost 250 mutations in *MUT* are known to cause MMA. The clinical importance of these mutations, of which more than half are missense changes, is well known, but their disease causing potential, particularly at the protein level, has not been satisfactorily characterized.

Methods:
We examined 7 *mut*^{0} and 16 *mut*$^-$ patient missense mutations that cover a spectrum of exonic locations, structural domains, clinical phenotypes and ethnic populations in order to determine their influence on *protein stability* and *enzyme function*. The use of two recombinant (*E. coli* and human fibroblasts) expression systems enabled us to study protein integrity while purified mutant proteins served as substrate for a fluorescence-based thermal melting assay providing information about thermolability. By measuring specific MUT activity and the Michaelis-Menten constant (K_M) for AdoCbl, representing cofactor affinity, we delivered key parameters regarding enzyme function.

Results:
Our data enable the stratification of MUT missense mutations into single or multiple categories of biochemical defects. Some mutants revealed (i) reduced protein level due to misfolding (e.g. p.P615T) while others exhibited (ii) increased thermolability (e.g. p.P86L) and altered response to physiological ligands (e.g. p.G426R). All 23 mutants showed (iii) decreased enzyme activity ranging from 0.2 to 85% of mean wild type activity, illustrating a functional impairment conferred by the patient mutations. (iv) Reduced cofactor response in substrate turnover as indicated by elevated K_M values was present to a variable degree in all *mut*$^-$ mutants. We further demonstrated the stabilization of thermolabile MUT mutants by chemical chaperones, lending support to a folding defect in some MUT mutants (e.g. p.Y231N).

Conclusion:
This in-depth mutation study represents a biochemical categorization of MUT mutations that illustrates the tools and principles required for MUT enzyme characterization and guides future interrogation to biochemically catalogue more and/or novel MUT missense mutations.

This work underscores the amenability of mutant MUT to small molecule stabilization and paves the way for the development of target-specific pharmacological chaperones as alternative therapy for patients that do not respond to current treatment, an approach that is gaining wide interest to rescue gene defects from the mutant protein perspective.

2116

C. Feuerstacke[1], C. Stieger[1]

Role of Skeletal Muscle Transport Systems in Statin-Induced Myotoxicity

Klinische Pharmakologie und Toxikologie, UniSpital, Zürich[1]

Introduction:
Statins are widely used in the treatment of hypercholesterolemia. While statins are generally well tolerated, they are associated with myopathies leading in rare, but severe cases to fatal rhabdomyolysis. The exact mechanism of statin-induced myopathies is not completely understood. Statins may adversely affect muscle cells by acting on the plasma membrane with subsequent intracellular signaling or after uptake within the cell. The main aim of this project is to distinguish between cytotoxic effects of statins on muscle cells originating at the plasma membrane from effects originating intracellularly.

Methods:
Muscle cell lines originating from rat (L6) and mouse (C2C12) were stably transfected with the previously described statin transporters OATP1B1 or OATP1B3 using FuGENE® transfection reagents. Clones were selected by measuring the mRNA level using qRT-PCR. Cytotoxicity studies using alamarBlue® were conducted to compare toxicity of statins in non-muscle cells (CHO control and OATP1B1 or OATP1B3 transfected), L6 and C2C12 wild-type cells. Transport studies were performed to measure the uptake of radiolabeled statins into CHO cells transfected with OATP1B1.

Results:
Cytotoxicity studies after 72h of statin treatment show different toxic effects depending on the lipophilicity of the different statins (Pravastatin, Cerivastatin, Simvastatin, Atorvastatin, and Rosuvastatin). In non-muscle cells no difference in toxicity based on IC_{50}-values between wild-type (CHO) and transfected (CHO OATP1B1/ OATP1B3/ OATP2B1) was observed. Statin uptake by OATP1B1 transfected cells was experimentally confirmed at which pravastatin shows similar uptake rates than the model substrate estrone-3-sulfate.

Conclusion:
Statin toxicity is not restricted to muscle cells. Statins show different toxic effects depending on their lipophilicity. The muscle cell lines C2C12 and L6 have been transfected successfully with OATP1B1 and OATP1B3 cDNA.

2117

A. Kostron[1], M. Friess[1], P. Kestenholz[1], D. Schneiter[1], I. Inci[1], S. Hillinger[1], W. Weder[1], I. Opitz[1]

Perioperative outcome for meothelioma patients undergoing induction chemotherapy followed by extrapleural pneumonectomy compared to pleurectomy / decortication

Division of Thoracic Surgery, University Hospital Zurich, Switzerland[1]

Introduction:
To assess the perioperative outcome after extrapleural pneumonectomy (EPP), or pleurectomy / decortication (P/D) following induction chemotherapy for mesothelioma patients.

Methods:
Between September 1999 and December 2013 155 patients received a multimodality treatment consisting of cisplatin-based induction chemotherapy followed by macroscopic complete resection (MCR) by EPP (n= 140), or P/D (extended P/D: 7 or P/D: 8 in the last 2 years). Descriptive statistical analysis was performed comparing perioperative mortality (30d and 90d mortality), postoperative morbidity and duration of hospitalization.

Results:
Patients treated with EPP had more postoperative complications necessitating also substantially more re-operations compared to patients treated with P/D. However, 50% of the P/D group presented with prolonged air leak. Duration of hospitalization was equal in both groups (Table1).

	EPP (140)	**extended P/D & P/D (17)**
Age at surgery	61 (36-72)	65 (45-77)
Duration of Hospitalization	14 (4-38)	14 (8-40)
Days ICU	3 (1-34)	2 (1-6)
Surgery duration	360 (230-600)	455 (210-680)
Number of reoperations	1 (0-20)	0 (0-4)
Mortality		
In hospital mortality	7 (5%)	0
30d mortality	6 (5%)	0
90d mortality	14 (11%)	0
Morbidity	128 (91%)	11 (65%)
Prolonged air leak	0	9 (53%)
Chylothorax	10 (7%)	1 (6%)
Post OP hemorrhage	8 (6%)	0
Patch failure	6 (4%)	0
Empyema	31 (22%)	1 (6%)
Bronchopleural fistula	16 (11%)	0
Pulmonary embolism	3 (2%)	0
Transfusion	59 (42%)	8 (47%)
Seroma	33 (24%)	0
Horner syndrome	13 (10%)	0

Recurrent nerve palsy	7 (5%)	0
Mediastinal shift	37 (27%)	0
Atrial fibrillation	47 (34%)	0
Pneumonia	4 (3%)	0

Conclusion:
Induction chemotherapy followed by MCR is feasible with acceptable morbidity and mortality for MPM patients. P/D seems to be well tolerated although prolonged air leak is a relevant problem.

2118

I. Opitz[1], M. Friess[1], P. Kestenholz[1], D. Schneiter[1], T. Frauenfelder[2], DL. Nguyen-Kim[2], B. Seifert[4], RA. Stahel[3], W. Weder[1]

The Zurich Score: Improved patient selection for mesothelioma patients undergoing surgery after induction chemotherapy. A review of 12 years' experience

Division of Thoracic Surgery, University Hospital Zurich, Switzerland[1], Department of Diagnostic Radiology, University Hospital Zurich, Switzerland[2], Laboratory of Molecular Oncology, University Hospital Zurich, Switzerland[3], Biostatistics Unit ISPM, University of Zurich, Switzerland[4]

Introduction:
The most challenging question in treatment of malignant pleural mesothelioma (MPM) is the selection of patients for aggressive treatment considering the limited prognosis of MPM patients in general. To identify these patient subgroups benefitting most from multimodality (MM) therapy before the treatment starts would be desirable. The identification of selection factors for MPM patients for MM therapy is based on a 12 years' experience analysis of overall survival (OAS).

Methods:
Eligible patients had MPM of all histological subtypes with clinical stage T1-3 N0-2 M0. Induction chemotherapy consisted of cisplatin/gemcitabine (cis/gem) or cisplatin/pemetrexed (cis/pem), followed by extrapleural pneumonectomy (EPP). Multivariate analysis was performed to assess independent prognosticators for OAS. A new selection score based on clinical variables available before surgery was developed.

Results:
From May 1999 to August 2011, 186 MPM patients were intended to be treated with induction chemotherapy followed by EPP. Hematologic toxicity was significantly less frequent after cis/pem in comparison to cis/gem. There were no differences in response or outcome between the regimens. 128 patients underwent EPP with a 30-day of 4.7%. The median OAS of patients undergoing EPP was significantly longer with 22 months (95% CI: 20-24) as compared to 11 months (95%CI: 9-12) for patients treated without EPP. A new prognostic score was defined considering tumor volume, histology, CRP and response after chemotherapy, which identifies patient groups who may benefit from multimodality treatment ($p<0.0005$).

Conclusion:
Induction chemotherapy with cis/gem or cis/pem followed by EPP for MPM of all histological subtypes and irrespective of nodal status results in a median survival of 22 months. If confirmed in an independent cohort, our new Zurich score may allow to better council MPM patients since it identifies patients with a poor prognosis not improved by multimodality treatment.

2119

N. Peter[1], T. Kleinjung[1], L. Horath[1], M. Wichser[1], St. Buechi[3], St. Weidt[2]

PRISM (PICTORIAL REPRESENTATION OF ILLNESS AND SELF MEASURE) AS A NEW ASSESSMENT TOOL FOR SUFFERING IN TINNITUS PATIENTS

Department of Otorhinolaryngology, University Hospital of Zurich, Zurich[1], Department of Psychiatry and Psychotherapy, University Hospital of Zurich, Zurich[2], Clinic for Psychotherapy and Psychosomatics "Hohenegg", Meilen[3]

Introduction:
Chronic subjective tinnitus is a frequent condition that affects the quality of life of millions of sufferers worldwide. The lack of objective measures of tinnitus necessitates the use of self-report questionnaires for evaluating tinnitus severity and annoyance. The analyses of these questionnaires allow medical staff to select adequate treatment modalities and monitor treatment effects. However, the wide range of different questionnaires hampers an international and comparable standard in tinnitus assessment. Furthermore, most of these questionnaires have shortcomings in terms of responsiveness to treatment related changes, insufficient translation and validation in different languages and time-consuming aspects. PRISM (Pictorial Representation of Illness and Self Measure) is a visual method to assess suffering. So far, PRISM has been validated as a marker of burden in different psychological and physical conditions like PTSD, rheumatoid arthritis, chronic urticaria and orofacial pain. The aim of this study is to validate PRISM as a marker of impairment in tinnitus patients in a prospective observational study. The results of PRISM assessment were compared to different standard questionnaires routinely used in tinnitus evaluation.

Methods:
Participating subjects were asked to fulfill an online-base survey including the following questionnaires: Tinnitus Handicap Inventory (THI), TQ (Tinnitus Questionnaire) TBF-12 (German short version of THI), WHOQOL-BREF (WHO Quality of Life-Questionnaire), BDI (Beck Depression Inventory). At the time of consultation in the clinic the subjects were asked to perform an audio-visual task on PRISM using an IPad. Subjects were shown a white panel on the whole display (14.7x19.6cm) representing their life. A yellow circle (diameter 4.9cm) at the bottom right-hand corner represented their "self". Afterwards they were asked to move another smaller red circle (3.5cm) representing their tinnitus in relation to their life at this moment. The answers on the two dimensional PRISM were divided into 3 groups. Comparisons to the questionnaire scores were correlated using t-test and ANOVA (SPSS).

Results:
A total of 130 subjects were included in the analysis (48 women, 82 men) since 2012. The answers on the two dimensional PRISM were divided into 3 groups reflecting different grades of tinnitus severity: In group 1 the red tinnitus-circle was completely placed in the yellow self-circle (most severe); in group 2 the red tinnitus-circle was overlapping the yellow self-circle and was not part of group 1; in group 3 the red tinnitus-circle was placed outside the yellow self-circle (least severe). The different PRISM groups demonstrated a statistically significant correlation with the corresponding gradings in the traditional tinnitus questionnaires.

Conclusion:
PRISM is a new visual method to assess suffering in patients with tinnitus in a short time. We could demonstratea significant correlation between the traditionally used tinnitus-questionnaires and PRISM.

2120

A. Ioannidis[1], GO. Galluci[2], S. Borzangy[2], RE. Jung[1], CHF. Hämmerle[1], HP. Weber[3], GI. Benic[1]

Evaluation of titanium-zirconium narrow diameter dental implants: 3 year of a multicenter randomized controlled clinical trial

Center of Dental Medicine, Clinic of Fixed and Removable Prosthodontics and Dental Material Science, Zürich, Switzerland[1], Department of Restorative Dentistry and Biomaterials Sciences, Harvard School of Dental Medicine, Boston, MA, USA[2], Department of Prosthodontics and Operative Dentistry, Tufts University School of Dental Medicine, Boston, MA, USA[3]

Introduction:
While showing comparable bone tissue response, titanium-zirconium (Ti-Zr) alloy presents significantly higher strength than commercially pure titanium (Ti). Therefore, the indication for the use of reduced diameter Ti-Zr implant could be broadened, by allowing less invasive surgical procedures. Additionally, the operative intervention could be simplified by reduction of drilling steps and need for bone augmentation.
The aim of this randomized controlled clinical study is to test whether the clinical performance of Ti-Zr narrow diameter dental implant placed in single-tooth gaps of anterior and premolar region is comparable to what is achieved using Ti regular diameter implants. In this report the findings 3 years following implant placement will be presented.

Methods:
40 patients in need of a single-implant reconstruction in the anterior or premolar region were enrolled at the University of Zurich (Switzerland) and Harvard School of Dental Medicine (Boston, USA). All single-tooth gaps presented with at least 7 mm of mesio-distal space. According to the randomization, one test (Ti-Zr 3.3 mm diameter) or one control (Ti 4.1 mm diameter) platform-switched implant was inserted in each patient, as type II, III or IV procedure. Osseous defects around implants and thin buccal bone plates were grafted using xenogenic bone mineral and collagen membranes. The healing was attempted with implants in a submerged position. Abutment connection surgeries were performed after three months. Definitive porcelain-fused-to-metal implant-supported crowns were inserted six months following implant insertion and controlled after 1 and 3 years.

Results:
The 3-year implant survival and success rates, change of the radiographic marginal bone level and dimensions of peri-implant soft-tissue after insertion of definitive crowns will be presented and discussed.

2121

O. Evrova[1], J. Houska[1], M. Calcagni[1], E. Bonavoglia[2], P. Giovanoli[1], V. Vogel, J. Buschmann[1]

Bioactive DegraPol electrospun scaffold produced by emulsion electrospinning for tendon repair application – scaffold characterization and release kinetics of biomolecules

Plastic and Hand Surgery, University Hospital Zurich[1], ab medica, Via Nerviano 31, Lainate (Milan), Italy[2]

Introduction:
Emulsion electrospinning is a technique used for production of bioactive scaffolds for tissue engineering applications, offering easy incorporation of growth factors and proteins into electrospun fibers. Carrier system produced by this technique from DegraPol® as a biocompatible material can be applied in the field of tendon repair, delivering PDGF-BB at the site of injury, thus accelerating the healing process and preventing adhesion formation. Characterization of such DegraPol® electrospun scaffold as delivery device is necessary.

Methods:
Electrospinning parameters for production of DegraPol® electrospun scaffolds were determined, yielding polymer fibers with different diameters. These parameters were adjusted for emulsion electrospinning respectively. Fluorescein, FITC-BSA and BSA were chosen as model fluorophore and model protein to assess the release of biomolecules from the electrospun scaffolds. Water-in-oil emulsion was formed from the polymer solution and aqueous protein solution, using different wt % of DegraPol® polymer solution (8 and 10 wt %). The emulsion was produced by magnetic stirring for 2 hours or by using ultrasonication probe at 50 % power for 2 minutes. The produced emulsion was directly electrospun using in-house built electrospinning device, consisting of a programmable syringe pump, a spinning head with a blunt end made of stainless steel tube (1 mm inner diameter and 0.3 mm wall thickness), high voltage power supply and a cylindrical collector. Different flow rates (1 mL/ h and 3 mL/ h) were used to produce fibers with different diameters. The produced scaffolds were placed in 12-well plates containing 3 mL of 1xPBS (pH 7.4) and were incubated under static conditions at 37 °C and 5 % carbon dioxide. At various time points, up to 10 days, the medium was removed and the amount of the biomolecule measured (fluorescence spectroscopy (Fluorescein and FITC-BSA) or BCA protein assay (BSA)) and new medium was added. The incorporation, loading efficiency and cumulative release (%) of the biomolecules of interest were compared as a function of the fiber diameter, wt % of the polymer solution and way of emulsion preparation for the DegraPol electrospun meshes.

Results:
It was found that increase in flow rate during the electrospinning process and thus increase in diameter of the fibers changes the loading of the molecule, with bigger fibers accommodating more molecule of interest. Emulsion preparation by ultrasonication probe allowed for good and quicker emulsion formation, and good distribution of the molecule within the fibers. The release of fluorescein and FITC-BSA or BSA differs drastically, with fluorescein being released in a burst manner, around 96 % within 1 - 2 days. On the other hand, FITC-BSA and BSA showed more sustained release, with 50 - 60 % released within 1 - 2 day and increase in release visible up to 7 days (around 90 %).

Conclusion:
Emulsion electrospinning is an easy technique for incorporation of bioactive molecules on electrospun scaffolds and is applicable for production of bioactive DegraPol® electrospun

scaffolds. These scaffolds are good carriers for different molecules of interest and the release kinetics can be tailored by the electrospinning production parameters.

2122

G. Meier Bürgisser[1], M. Calcagni[1], A. Müller[1], E. Bonavoglia[2], G. Fessel[3], JG. Snedeker[3], P. Giovanoli[1], J. Buschmann[1]

Prevention of Peritendinous Adhesions Using an Electrospun DegraPol Polymer Tube: a Histological, Ultrasonographic and Biomechanical Study in Rabbits

Plastic and Hand Surgery, University Hospital Zurich[1], ab medica, Via Nerviano 31, Lainate (Milan), Italy[2], Department of Orthopedics, Uniklinik Balgrist, Zurich[3]

Introduction:
One of the great challenges in surgical tendon rupture repair is to minimize peritendinous adhesions. In order to reduce adhesion formation, a physical barrier was applied to a sutured rabbit Achilles tendon, with two different immobilization protocols used post-operatively.

Methods:
Thirty New Zealand White rabbits received a laceration on the Achilles tendon, sutured with a 4-strand Becker suture, and half of the rabbits got a DegraPol® tube at the repair site. While fifteen rabbits had their treated hind leg in a 180° stretched position during 6 weeks (adhesion provoking immobilization), the other fifteen rabbits were recasted with a 150° position after 3 weeks (adhesion inhibiting immobilization). Adhesion extent was analysed macroscopically, via ultrasound and histology. Inflammation was determined histologically. Biomechanical properties were analysed.

Results:
Application of a DegraPol® tube reduced adhesion formation by approximately 20 % - independently of the immobilization protocol. Biomechanical properties of extracted specimen were not affected by the tube application. There was no serious inflammatory reaction towards the implant material.

Conclusion:
Implantation of a DegraPol® tube tightly set around a sutured tendon acts as a beneficial physical barrier and prevents adhesion formation significantly – without affecting the tendon healing process.

2123

M. Hochuli[1], I. Aeberli[3], A. Weiss[2], M. Hersberger[2], H. Troxler[2], P. Gerber[1], GA. Spinas[1], K. Berneis[1]

Sugar-sweetened beverages with moderate amounts of fructose, but not sucrose induce fatty acid synthesis in healthy young men – a randomized cross over study

Division of Endocrinology, Diabetes, and Clinical Nutrition, University Hospital Zurich, Zurich[1], Division of Clinical Chemistry and Biochemistry, University Children's Hospital Zurich, Zurich[2], Human Nutrition Laboratory, Institute of Food, Nutrition and Health, ETH Zurich, Zurich[3]

Introduction:
The impact of sugar sweetened beverages (SSB) on lipid metabolism when consumed in moderate amounts by normal weight subjects is debated. The aim of the study was to investigate the effect of different types of sugars in SSB on fatty acid metabolism (*i.e.* fatty acid synthesis and oxidation) in healthy young men.

Methods:
Thirty-four normal weight men were studied in a randomized crossover study. Four isocaloric three-week interventions with SSB were performed in random order: Medium fructose (MF, 40 g/day); high fructose (HF, 80 g/day), sucrose (HS, 80 g/day), and glucose (HG, 80g/day). Fasting total plasma fatty acid composition was measured after each intervention. Acylcarnitines were measured in the fasting state and after a euglycemic hyperinsulinemic clamp in 9 subjects.

Results:
The relative abundance of palmitate (16:0), and the molar fatty acid ratio palmitate/linoleic acid (16:0/18:2) as markers of fatty acid synthesis were increased after HF (relative abundance of palmitate: 22.97±5.51 % [percent of total fatty acids by weight ±SD]) and MF (26.1±1.7%) compared to HS (19.40±2.91 %, $p<0.001$), HG (19.43±3.12 %, $p<0.001$) or baseline (19.40±2.79 %, $p< 0.001$). After HS and HG, the relative abundance of palmitate was equal to baseline. Fasting palmitoylcarnitine was significantly increased after HF and HS (HF, HS *vs* HG: $p = 0.005$), decreasing after inhibition of lipolysis by insulin in the clamp.

Conclusion:
When consumed in moderate amounts, fructose but not sucrose or glucose in SSB increases fatty acid synthesis (palmitate), while fasting long-chain acylcarnitines are increased after both fructose and sucrose, indicating an impaired beta-oxidation flux.

2124

S. Salemi[1], A. Mortezavi[1], T. Sulser[1], D. Eberli[1]

The Role of Autophagy in the Differentiation of Adipose Derived Stem Cells to Functional Smooth Muscle Cells for Urologic Tissue Engineering

Laboratory for Urologic Tissue Engineering and Stem Cell Therapy, Department of Urology, University Hospital Zurich, Switzerland. [1]

Introduction:
Tissue engineering utilizing using smooth muscle cells may provide a treatment option for diseases with smooth muscle pathology such as bladder dysfunction, urinary incontinence, and erectile dysfunction. As autologous smooth muscle cells (SMC) should not be harvested from organs with end-stage disease and tissue regeneration requires large amount of functional SMC, there is urgent need for other cell sources. Adipose derived stem cells (ADSC) can be harvested easily and can be differentiated into SMC tissue engineering. We have shown that autophagy, a conserved lysosomal degradation pathway, is required for cell survival and differentiation of human blood and skin SC. ADSC undergoing differentiation to SMC efficiently remodel their cytoskeleton and shape in an energy-consuming process. We investigated the functional role of autophagy during differentiation and remodeling of ADSCs to SMC *in vitro*.

Methods:
Rat ADSCs were characterized by immunocytochemistry (ICC) and FACS. ADSC were induced towards SMC using MCDB induction medium for 1 to 6 weeks. The changes in gene and protein expression level for SMC specific markers: calponin, smoothelin, α-SMA, MyH11; and autophagy genes: LC3, Atg5, Beclin1, were investigated by ICC and WB.

Results:
Upon induction, up regulation of Atg5-Atg12 and free Atg5 was observed during 4 - 6 weeks. This was supported by an increase in conversion of cytosolic LC3I to membrane-bound LC3II protein. At the same time the contractile proteins calponin, MyH11 and smoothelin were up regulated during 1 - 3 weeks and decreased after 5 - 6 weeks of differentiation detected by WB and ICC.

Conclusion:
Our study demonstrates that autophagy plays an important role in ADSC differentiation to SMC. This finding might lead to novel supporting strategies for ADSC use in clinics, since autophagy can be easily influenced by FDA approved drugs.

2125

S. Salemi[1], A. Mortezavi[1], M. Horst[2], R. Gobet[2], T. Sulser[1], D. Eberli[1]

The role of authophagy in neuropathic bladder remodeling

Laboratory for Urologic Tissue Engineering and Stem Cell Therapy, Department of Urology, University Hospital Zurich, Switzerland. [1], Division of Pediatric Urology, Department of Pediatric Surgery, Children's Hospital Zurich, Switzerland.[2]

Introduction:
Neurogenic bladder dysfunction is the result of disease or injury to the neural pathways and commonly occurs in patients with meningomyelocele or after spinal cord injury. During the pathogenesis the smooth muscle cells (SMC) shift from contractile SMC phenotype towards a synthetic type. In muscular disorders increased autophagy is known to protect cells from deterioration by compensating for defects in lysosome function. However, the the accumulation of autophagosomes can also impair cell function over time. Autophagy may play an important role in remodeling of bladder SMC in children with neuropathic bladder. In this study we investigated the role of autophagy in neuropathic bladders in the pediatric population.

Methods:
Full thickness bladder biopsies were taken from children with neuropathic disorder. Samples obtained from healthy donors without urological problems were used as control. A piece of bladder tissue was snap frozen for genetic analysis and another piece was fixed for immunostaining. Samples were stained with SMC lineage associated markers calponin, smoothelin, α-SMA and autophagy proteins LC3, Atg5 and Beclin l.

Results:
We found that the ATG5 protein, a key regulator of autophagy, is upregulated in neuropathic muscle tissue compared with normal bladder. This was repetitively shown in WB and immunostaining. Neuropathic bladder muscle exhibited a punctated immunostaining pattern for LC3 in subset of SM confirming accumulation of autophagosomes. Pronounced elevation of ATG5 in SM in neuropathic bladder tissue co-localized with a downregulation of the key contractile proteins smoothelin and calponin. At mRNA level an increased expression of Atg5 (47.9 ± 9 SD, fold) and Beclin 1 (19.8 ± 3.1) gene was observed in neuropathic bladder samples compared to normal bladder.

Conclusion:
Our study reveals that autophagy is important factor in the remodeling of SMC and functionality of bladder SM tissue in neuropathic bladder. Since autophagy can be influenced by oral medication this research might lead to novel strategies preventing the remodeling and deterioration of neuropathic bladder tissues.

2126

IL. Leonardi[1], FN. Nicholls[2], BT. Tewes[3], RG. Greinwald[3], GR. Rogler[1], IFW. Frey-Wagner[1]

Oral administration of DSS induces a cecum localized colitis in rabbits

Division of Gastroenterology and Hepatology, USZ, Zurich, Switzerland; [1], Central Biological Laboratory, USZ, Zurich, Switzerland[2], Dr. Falk Pharma GmbH, Research & development, Freiburg, Germany[3]

Introduction:
The therapeutic effect and the underlying mechanisms of the helminth species *T. suis*, that has shown promising results for treatment of inflammatory bowel disease (IBD) in human studies, cannot be studied in mice and rats as *T. suis* fails to colonize the rodent intestine whilst hatching in humans and rabbits. Since a suitable rabbit IBD model is currently not available, we developed a rabbit colitis model by administration of dextran sodium sulphate (DSS).

Methods:
White Himalayan rabbits (n = 12) received 0.1 % DSS in the daily beverage for 5 days. Clinical symptoms were monitored daily and rabbits were sacrificed at different time points. A genome wide expression analysis was performed with RNA isolated from cecal lamina propria mononuclear cells and epithelial cells.

Results:
Rabbits receiving 0.1% DSS in the daily beverage have a delayed and reduced weight gain and develop disease symptoms such as reduced food uptake and diarrhoea from day 5 on. To monitor the symptoms we developed a disease activity index (DAI) that increased up to 2.1 ± 0.4 (n = 6) at day 10 (controls DAI < 0.5). At the microscopic level, DSS administration induced an acute cecum localized inflammation that mimics features of ulcerative colitis such as crypt architectural distortion, stunted villous surface and inflammatory infiltrate in the lamina propria. The histopathology score reached a peak of 14.2 ± 4.9 (n = 4) at day 10 (baseline < 8). Interestingly, DSS administration did not affect other sections of the intestine. Expression profiling revealed an enrichment of IBD related genes in both lamina propria mononuclear cells and intestinal epithelial cells. Innate inflammatory response, Th17 signalling and extracellular matrix remodelling were among the significantly affected biologically relevant pathways.

Conclusion:
We show here the development of a reproducible and reliable model of colitis in the rabbit by administration of 0.1% DSS in the daily beverage for five days. Localization of the inflammation in the cecum and its similarities with human IBD make this rabbit DSS model particularly suitable to study the therapeutic effects of *T. suis in vivo*

2127

P. Limani[1], Ch. Tschuor[1], A. Schlegel[1], E. Kachaylo[1], M. Linecker[1], JH. Jang[1], S. Georgiopoulou[2], JM. Lehn[3], R. Graf[1], B. Humar[1], PA. Clavien[1]

Inositol trispyrophosphate (ITPP) and its anti-hypoxic potential in colorectal metastases of the liver

Division of Visceral and Transplant Surgery, University Hospital, Zurich[1], Division of Internal Medicine, University Hospital, Zurich[2], Laboratoire de Chimie Supramoléculaire ISIS, Collège de France, Strasbourg/F[3]

Introduction:
The hypoxic response in the core of growing malignancies not only promotes angiogenesis, but also a number of other processes associated with aggressive tumour behavior. Hence, reduction of hypoxia per se might be more efficient than purely antiangiogenic approaches. The recently designed molecule ITPP promotes oxygen release from hemoglobin. In this study, we assessed whether ITPP can prevent hypoxia and tumor growth in a mouse model of colorectal cancer (CRC) liver metastasis.

Methods:
Two syngeneic orthotopic mouse models of hepatic CRC metastasis were established by selective portal vein injection of CRC cells. Small animal MR imaging was used to follow metastatic development in vivo. Oxygen dissociation kinetics from hemoglobin were determined by tonometry. Localization of hypoxic areas was achieved by pimonidazole stainingon histological sections.

Results:
ITPP treatment increased oxygen release from hemoglobin in mice. Compared to controls, mice treated with ITPP had a significant survival benefit of 20 days (57 days versus 37 days, $p<0.01$, $n=6$), along with a reduced tumor burden ($p<0.01$). In tumors, ITPP had an antihypoxic effect as demonstrated by a down-regulation of HIFs and a reduction in pimonidazole staining. Furthermore, ITPP appears to counteract the hypoxic response in terms of the Warburg effect, inflammatory changes, and the epithelial-mesenchymal transition. Additionally, circulatory markers indicating metastatic activity and invasiveness were decreased in animals treated with ITPP. Ex vivo studies confirmed a reduced invasiveness and a diminished tumorigenic potential of ITPP-treated cancer cells. Notably, after cessation of treatment with ITPP, we observed a more benign phenotype for a period of at least one month.

Conclusion:
ITPP is a potent inhibitor of the hypoxic tumor response. Its anti-hypoxic action seems to favor a more benign tumor phenotype that is accompanied by reduced tumor invasiveness and increased survival. A direct comparison with current antiangiogenic therapies will reveal whether ITPP holds promise as a new class of anti-hypoxic agents.

2128

C. Zhu[1], N J. Kräutler[1], B. Li[1], I. Abakumova[1], P. Schwarz[1], C. Tiberi[1], P. Pelczar[2], E J. Rushing[1], M. Heikenwälder[3], G. Rogler[4], A. Aguzzi[1]

Inappropriate enteric lymphotoxin β receptor signaling causes iron-deficient anemia

Institute of Neuropathology, University Hospital of Zurich, Switzerland[1], Institute of Laboratory Animal Science, University of Zurich, Zurich[2], Institute of Virology, Technische Universität München/ Helmholtz-Zentrum München, Germany [3], Klinik für Gastroenterologie und Hepatologie, UniversitätsSpital Zürich, Zurich[4]

Introduction:
The crosstalk between lymphoid and stromal cells is accomplished largely through the lymphotoxin β receptor (LTβR), which is indispensable for lymphoid organogenesis. Lymphoid cells express membrane-bound $LT\alpha_1\beta_2$ heterotrimers that signal through LTβR on lymphoid organizer stromal cells, and stromal LTβR signaling attracts further lymphoid cells by inducing cytokines and chemokines. However, ectopic LTβR signaling leads to inflammation in non-lymphoid organs.

Methods:
We used a bacterial artificial chromosome (BAC) contains milk fat globule epidermal growth factor 8 (Mfge8) promoter and created transgenic mice expressing lymphotoxin α and lymphotoxin β specifically in Mfge8-expressing stromal cells (Mfge8-LTα and Mfge8-LTβ). Mfge8-LTα and Mfge8-LTβ mice are bred to get Mfge8-LTαβ expressing lymphotoxin α and lymphotoxin β. The phenotypes of the Mfge8-LTαβ mice and their wild type, Mfge8-LTα, Mfge8-LTβ littermates are analyzed macroscopically, histologically and biochemically.

Results:
Mfge8-LTαβ mice, but neither Mfge8-LTα nor Mfge8-LTβ mice, showed macroscopically growth retardation and splenomegaly, developed iron deficiency and anemia. Histology studies revealed the Mfge8-LTαβ villi is shortened, associated with ectopic lymphoid follicles and increased cellularity and apoptotic cells in the lamina propria. Further studies revealed that duodenal LTβR signaling repressed iron absorption-related genes (DMT1+IRE, Dcytb and Ferroportin) leading to impaired iron absorption. The resulting anemia in Mfge8-LTαβ mice caused elevated erythropoietin, which consequently resulted in splenomegaly with extensive but ineffective extramedullary erythropoiesis. The iron deficiency anemia in Mfge8-LTαβ mice was curable by parenteral iron supplementation or by depleting/antagonizing LTβR.

Conclusion:
This study demonstrates a novel pathway of iron homeostasis regulation by duodenal LTβR signaling, and suggests that LTβR antagonists may be useful in curing anemia symptom found in selected bowel pathologies.

2129

N. Aellig[1], GA. Kullak-Ublick[1], N. Corti[1]

Rifampicin and Phenprocoumon – A Challenging Combination

Department of Clinical Pharmacology and Toxicology, University Hospital Zurich[1]

Introduction:
Rifampicin is well-known to cause drug interactions due to strong inducing effects on drug metabolising enzymes. Phenprocoumon is metabolised by cytochrome-P450-enzymes and case reports on reduced anticoagulant effects when adding rifampicin exist. However, data on this interaction is scarce and no guideline on managing this drug-drug combination exists.

Methods:
We retrospectively analysed four cases with concomitant administration of phenprocoumon and rifampicin assessing changes of phenprocoumon dose, target international normalized ratio (INR) and therapeutic failure or bleeding complications.

Results:
Mean phenprocoumon dose was increased 1.5-fold in two patients, in one case no substantial dose adjustment was made at all after adding rifampicin treatment. In these three cases no steady target INR could be achieved during the entire treatment period with rifampicin. Target INR was reached eventually in the fourth patient after mean increase of phenprocoumon dose by 4-fold. Time to achieve target INR after stopping rifampicin was 14 and 28 days respectively in two patients. One patient was hospitalized because of occurrence of an ischemic stroke while INR was subtherapeutic despite dose increase of phenprocoumon.

Conclusion:
Concomitant administration of phenprocoumon and rifampicin is a challenge to treating physicians because of high risk of insufficient anticoagulation leading to severe thromboembolic events. Close INR monitoring is necessary during at least 3-4 weeks after concurrent rifampicin therapy is started or stopped. No empirical phenprocoumon dosage recommendation can be made because of high interindividual variability of INR changes. A substantial dose increase up to 4 to 5-fold may be necessary to reach therapeutic INR.

2130

M. Nuvolone[1], S. Sorce[1], P. Pelczar[3], E. Rushing[1], F. Lavatelli[2], G. Palladini[2], G. Merlini[2], A. Aguzzi[1]

Generation of a conditional transgenic mouse model of immunoglobulin light chain (AL) amyloidosis.

Institute of Neuropathology, University Hospital of Zurich[1], Amyloidosis Research and Treatment Center, Foundation Scientific Institute San Matteo, Department of Molecular Medicine, University of Pavia, Pavia[2], Institute of Laboratory Animal Science, University of Zurich, Zurich[3]

Introduction:
The molecular mechanisms underlying AL amyloidosis remain elusive, in part due to the paucity of reliable animal models for this dismal disease. Generation of transgenic mice overexpressing human amyloidogenic light chains (aLCs) is technically hampered by the intrinsic toxicity of these proteins, which could result in embryolethality or selection against high expressor lines. To overcome this limitation, we aimed at generating a conditional transgenic mouse in which the expression of an aLC can be regulated in a spatial and temporal manner using the Cre-loxP system.

Methods:
The cDNA encoding an aLC was sub-cloned in the 3' region of an expression vector consisting (5'→3') of a ubiquitous promoter and a reporter gene-stop cassette flanked by two loxP sites. Transgenic mice obtained by pronuclear injection were crossed with different cre-deleter lines to express aLC in a spatially and temporally regulated manner.

Results:
Transgenic mice obtained by pronuclear injection showed ubiquitous expression of the reporter gene, but no expression of aLC, as expected. Crossing with cre-deleter mice resulted in the generation of mice with tissue-specific or ubiquitous expression of aLC and detectable serum levels of aLC. Mice are in follow up for the identification of amyloid deposits and phenotypic abnormalities.

Conclusion:
We have generated a transgenic mouse in which the expression of aLC can be activated in a regulated manner. This newly developed conditional transgenic mouse could prove instrumental to deepen our current mechanistic understanding of AL amyloidosis.

2131

T. Gorski[1], J. Krützfeldt[1]

Do myoblasts from different mouse strains differentiate into brown adipocytes?

Klinik für Endokrinologie, Diabetologie und Klinische Ernährung, UniversitätsSpital Zürich[1]

Introduction:
Due to the presence of uncoupling protein 1 (UCP1) in the inner mitochondrial membrane, brown adipocytes present impaired respiratory chain efficiency and dissipate energy as heat. Increasing the amount of BAT, recently shown to be present in humans, and the expression of UCP1 could be a means of enhancing energy expenditure, thereby counteracting obesity. While UCP1-expressing cells are found in BAT and in pockets within white adipose tissue depots, there is growing evidence that these cells can also be present in skeletal muscles. This is not surprising when considering that myocytes and brown adipocytes share the same embryonic origin. In the present study, we investigated the potential of myoblasts isolated from mice with different predisposition levels to obesity – the obesity-prone C57Bl/6 and the obesity-resistant Sv/129 – to differentiate into adipocytes *in vitro* under different stimuli.

Methods:
Myoblasts were isolated from the hindlimbs of three Sv/129 and three C57Bl/6 mice and sorted by fluorescence-activated cell sorting. The cells were then cultured and expanded. After cells reached confluence, adipogenic differentiation was induced for 2 days with medium supplemented with insulin, T3, isobutylmethylxanthine, dexamethasone, indomethacin and rosiglitazone, followed by 8 days of treatment with medium containing insulin and T3. Additionally, we tested the effects of adding the following known promoters of brown adipocyte formation: isoproterenol, activin receptor type IIb inhibitor, bone morphogenetic protein 7, FGF21 or atrial natriuretic peptide to the adipogenic cocktail. In a third experiment, myoblasts of C57Bl/6 mice were transfected with PRDM16, PPARg2, CEBPb, a combination of PRDM16 and CEBPb, a combination of PPARg2 and PRDM16, or a control DNA plasmid. After cells reached confluence, adipogenesis was induced as previously described, but also including rosiglitazone in the medium used during days 2-10. To test the ability of subpopulations of myoblasts to form adipocytes, myoblasts isolated from Sv/129 and C57Bl/6 mice were single-sorted into 96-well plates. Eighty-eight colonies formed by these single-sorted cells – 46 from C57Bl/6 mice and 42 from Sv/129 mice – underwent the same adipogenic induction protocol. After all experiments, cells were fixed and stained with oil red O (ORO) to identify possible formation of adipocytes.

Results:
Used solely or in combination with different compounds known to stimulate brown adipogenesis, the adipogenic induction cocktail was not able to promote the differentiation of myoblasts from any of the analyzed mouse strains into adipocytes, as verified by microscopy and ORO staining. Similarly, none of the colonies derived from single-sorted myoblasts showed formation of adipocytes after 10 days of adipogenic induction. On the other hand, a small fraction of cells transfected with PPARg2, CEBPb, a combination of PRDM16 and CEBPb, or a combination of PPARg2 and PRDM16 was able to differentiate into adipocytes after a 10-day adipogenic induction.

Conclusion:
In the absence of specific transcription factors (PPARg2 and CEBPb) primary mouse myoblasts do not spontaneously differentiate into adipocytes, even in the presence of several stimulating compounds. Therefore our data highlight the importance of PPARg2 and CEBPb in this process. PRDM16 alone was not able to promote adipogenic differentiation. Further

studies should address whether spontaneous adipocyte formation occurs from earlier developmental stages of muscle progenitors.

2132

A. Mizbani[1], J. Krützfeldt[1]

Identification of microRNAs involved in the activation of adult skeletal muscle stem cells

Klinik für Endokrinologie, Diabetologie und Klinische Ernährung, UniversitätsSpital Zürich[1]

Introduction:
Skeletal muscle has the ability to regenerate efficiently after heavy exercise or damage. This process is shown to be dependent on the proper function of muscle adult stem cells, named satellite cells or myogenic progenitors (MP). Upon injury these cells exit the quiescent phase and proliferate, making both myoblasts, which finally differentiate into myotubes, and undifferentiated cells which reconstitute the stem cell pool.
MicroRNAs (miRNAs) are a class of small noncoding RNAs that downregulate the expression of their target genes by inhibiting mRNA translation or inducing mRNA degradation. It is getting increasingly evident that miRNAs are essential regulatory factors in the muscle regeneration process.
The aim of this study is to identify novel miRNAs involved in skeletal muscle regeneration. With further understanding of the involved pathways, we hope to find targets for treating diseases related to impaired muscle regeneration, like muscular dystrophies, sarcopenia, and fibrosis.

Methods:
We use cardiotoxin (CTX) injections into Tibialis anterior (TA) muscles of mice as a model for muscle regeneration. MPs were sorted from regenerating and also from adult skeletal muscle, and the RNA was subjected to Ilumina deep sequencing. Regulated miRNAs were identified based on the normalized read numbers, and their tissue specificity and expression levels in regenerating and adult skeletal muscle were examined by northern blot analysis and real time PCR. The role of candidate miRNAs for proliferation of myoblasts was examined in vitro and in vivo by EdU assay. Overexpression of miRNAs was done in myoblast cultures using transfection with miRNA mimics. The effect of miRNA inhibition and overexpression on expression of muscle-specific genes was measured by real time PCR. Histological characterization of regenerating muscle with inhibited miRNA was done by H&E staining and immunofluorescence on tissue sections. Finally, transcriptome profile of cultured myoblasts with and without inhibition of miRNA was determined by Ilumina deep sequencing to find the significant changes in gene expression and identify the miRNA targets.

Results:
Based on the data from initial screenings we selected one miRNA for its remarkable enrichment in activated MP, freshly isolated or cultured in vitro. Our preliminary findings indicate that inhibition of this miRNA in regenerating muscle could downregulate early myogenic regulatory factors and upregulate adult muscle markers, suggesting a potential role in preventing the premature differentiation of myoblasts. So far we observed no difference in proliferation rate of MP after inhibition of the miRNA. Based on the results of the RNA sequencing data we are currently evaluating several candidate target genes.

Conclusion:
We identified a novel miRNA significantly upregulated in skeletal muscle progenitors early after their activation. The expression of this miRNA in proliferating myoblasts is much higher than all other tissues tested. Our functional studies so far suggest a role for this miRNA in regulating the onset of differentiation in proliferating myoblasts.

2133

K. Turcekova[1], J. Krützfeldt[1]

Regulation of skeletal muscle differentiation by a distinct subset of microRNAs

Klinik für Endokrinologie, Diabetologie und Klinische Ernährung, UniversitätsSpital Zürich[1]

Introduction:
MicroRNAs (miRNAs) are a class of conserved small non-coding RNAs which function as negative posttranscriptional regulators of mRNAs. Imperfect complementarity for target recognition sites enables single miRNA regulation of many mRNAs possibly resulting in changes of synthesis of thousands of proteins. Albeit many aspects of skeletal muscle biology are under extensive investigation, identification and understanding of single miRNA function remains challenging. One of the reasons is that in muscle tissue some miRNAs might be expressed at saturated levels and can function redundantly. In this project, we aim to study the impact of deletion of the miRNA pathway in adult skeletal muscle cells *ex vivo* by means of deletion of Dgcr8, a protein essential for miRNA generation.

Methods:
A double transgenic mouse line, $Dgcr8^{flox/flox}$ x $Pax7^{CE/+}$ was generated. Fluorescent activated cell sorting (FACS) was used to isolate primary mouse myoblasts and to study apoptosis and proliferation. Muscle differentiation was determined by Western blot and qRT-PCR upon differentiation of primary myoblasts to myotubes.

Results:
miRNA profiles decreased with a half-time of approximately 2-3 days after deletion of Dgcr8. When the progressive decrease of miRNA expression reached over 90%, we observed a reduction in cell number, increased apoptosis and altered cell morphology as the predominant phenotypic changes of proliferating myoblasts. Proliferation, measured by the rate of EdU incorporation, was not changed. By subjecting cells to the myogenic differentiation conditions, we observed defects in terminal myotube formation. MiRNA depleted myoblasts were still able to fuse and form myofibers, but we observed reduced differentiation capacity, concomitant with dysregulation of MyHC and myogenin at the protein level. The re-introduction of single miRNAs was not able to fully rescue the differentiation defect. However, combining the analysis of highest expressed miRNAs in myotubes with their regulation of mRNAs in miRNA depleted myoblasts, we identified a subset of miRNAs which have a positive effect on impaired myogenesis in miRNA deprived cells. We are currently in the process of identifying the miRNA targets that are involved.

Conclusion:
We were able to confirm the critical role of the miRNA pathway for muscle cell viability and differentiation. Furthermore, we identified a subgroup of miRNAs essential for normal myogenesis that might act cooperatively.

2134

A. Galimov[1], J. Krützfeldt[1]

An FGF-microRNA pathway provides a link between mitochondrial activity and muscle differentiation

Klinik für Endokrinologie, Diabetologie und Klinische Ernährung, UniversitätsSpital Zürich[1]

Introduction:
Mitochondrial dysfunction such as the production of radical oxygen species is critical for the development of insulin resistance in skeletal muscle. The detrimental effects of excess mitochondrial activity already occur at early stages of muscle cells, e.g. during muscle regeneration and repair. The mechanisms that link mitochondrial function to alterations of muscle cells are, however, incompletely understood. Therefore, we asked whether microRNAs (miRNAs) can regulate mitochondria activity in primary myoblasts.

Methods:
Mitochondria function was induced in primary murine myoblasts by serum starvation or inhibition of glycolysis (deoxy-D-glucose incubations) and examined using cell-permeable fluorescent dyes (TMRE, mitotracker). miRNA regulation was analysed using microarrays, qRT-PCR and northern blotting. miRNA function in myoblasts was inhibited by transfection of pharmacological inhibitors (antagomirs). Receptor-mediated signaling pathways were activated by recombinant peptides (FGF, IGF1, TGFbeta, TNFalpha).

Results:
Activation of mitochondria function in myoblasts by serum starvation or inhibition of glycolysis increased muscle differentiation. miRNA profiling revealed that serum starvation significantly regulated expression levels of miRNAs (downregulation by ~50%), which were also decreased by incubations with deoxy-D-glucose (~30%). Inhibition of these miRNAs in myoblasts increased muscle differentiation, while induction of miRNAs by activation of the FGF receptor had the opposite effect. We are currently determining the targets of FGF-activated miRNAs.

Conclusion:
Activation of miRNAs by FGF signaling regulates myoblast differentiation. Mitochondrial dysfunction could impact on myogenesis by inhibition of this pathway**.** miRNAs might be an interesting target for strategies to improve muscle regeneration in conditions of mitochondrial stress such as type 1 or type 2 diabetes mellitus.

2135

T. Piegeler[1], M. Schläpfer[1], RO. Dull[2], B. Beck-Schimmer[1], RD. Minshall[2]

Mechanistic insight regarding a possible inhibition of malignant cell metastatic potential by amide-linked local anesthetics

Institut für Anästhesiologie, UniversitätsSpital Zürich, Zürich[1], Department of Anesthesiology, University of Illinois at Chicago, Chicago, IL, USA[2]

Introduction:
Expression and secretion of matrix-metalloproteinases (MMP) by malignant cells are thought to play a crucial role in solid tumor metastasis. Circulating cytokines, such as tumor necrosis factor alpha (TNF-alpha), activate the kinases Src, Akt and Focal Adhesion Kinase (FAK) essential for MMP secretion and function. We recently demonstrated that ropivacaine and lidocaine block TNF-alpha-induced Src activation in malignant cells and therefore evaluated whether these agents might also inhibit activation of Akt and FAK in malignant cells, thus attenuating MMP release.

Methods:
Cell lysates from NCI-H838 lung adenocarcinoma cells were incubated with ropivacaine or lidocaine (1nM-100µM) in absence or presence of TNF-alpha (20ng/ml) for 20 minutes. Activation/phosphorylation of Akt (threonine 308) and FAK (tyrosine 397) were evaluated by Western blot. The influence of ropivacaine and lidocaine on TNF-alpha-induced MMP-9 secretion by NCI-H838 cells at 4 hours was assessed by ELISA in cell culture supernatant. Additionally, the effect of Wortmannin (100nM, blocks Akt activation) and FAK-inhibitor FI14 (5mM) on MMP-9 release was evaluated. Statistical analysis was conducted by two-way ANOVA with Bonferroni post-hoc testing.

Results:
Ropivacaine (1nM) and lidocaine (10µM) both significantly reduced TNFalpha-induced activation of Akt (ropivacaine: 40% reduction, $p=0.01$, $n=6$; lidocaine: 40%, $p<0.01$, $n=11$) and FAK (ropivacaine: 42% reduction, $p<0.01$, $n=7$; lidocaine: 51%, $p=0.04$, $n=8$) in NCI-H838 cells. MMP-9 secretion triggered by TNF-alpha was attenuated by 36% in presence of 1nM ropivacaine ($p<0.01$, $n=6$) and 52% in presence of 10µM lidocaine ($p<0.01$, $n=6$). The inhibition of MMP-9 release by the amide-LAs was similar to that observed in presence of Wortmannin or FI14.

Conclusion:
Ropivacaine and lidocaine – at clinically relevant concentrations – reduced the release of MMP-9 by malignant cells via inhibition Akt and FAK activation. Although our findings were determined entirely in vitro, they provide significant insight into a potential mechanism by which amide-LAs might attenuate metastasis of malignant cells.

2136

RD. Kouyos[1], A. Rauch[2], DL. Braun[1], S. Yerly[3], J. Böni[4], T. Klimkait[5], V. Aubert[6], B. Ledergerber[1], HF. Günthard[1]

Higher risk of sexually acquired HCV-coinfection in MSM with wide HIV transmission bottleneck

Division of Infectious Disease and Hospital Epidemiology, University Hospital of Zurich[1], University Hospital Bern, Bern, Switzerland[2], University Hospital Geneva, Geneva[3], University of Zurich, Zurich[4], University of Basel, Basel[5], University of Lausanne, Lausanne[6]

Introduction:
Even though the mechanisms responsible for the recent dramatic increase of sexually transmitted HCV among HIV-infected MSM remain largely unknown, an important role of high-risk sexual behaviors has been suggested. At the same time such high-risk behaviors have been linked with a broad transmission bottleneck in HIV as they might lead to mucosal breaches, which could facilitate the transmission of several genetically distinct viruses in one transmission event.

Methods:
We assessed the association between the width of the HIV transmission bottleneck and the incidence of HCV coinfections in HIV-infected MSMs from the Swiss HIV Cohort Study. As a proxy for the width of the transmission bottleneck we used the fraction of ambiguous nucleotides in GRTs from recently infected MSMs. We have previously shown that a high fraction (>0.5%) of ambiguous nucleotides during recent infection corresponded to a high viral diversity, which in turn indicated a broad transmission bottleneck. Accordingly, the HIV transmission bottleneck was considered to be broad if the fraction of ambiguous nucleotides exceeded 0.5% in GRTs from recent (less than one-year-old) infection and narrow otherwise. Recent infection was determined by Acute Retroviral Syndrome and by negative and positive HIV-serology less than 1 year apart. The impact of the HIV-transmission bottleneck on HCV incidence was quantified as Hazard Ratios (HR) determined from uni- and multivariable Cox-proportional hazards models.

Results:
We considered 558 MSMs, who were HCV-negative at baseline and for which a GRT sampled during recent infection (<1 year post seroconversion or ARS) was available. Of those individuals, 130 (23.3%) exhibited a broad transmission bottleneck and 26 (4.7%) had an incident HCV infection. The total incidence rate of HCV infections was 8.9/1000 person-years. Individuals with a broad HIV-transmission bottleneck exhibited a threefold higher hazard of an incident HCV infection than individuals with a narrow HIV transmission bottleneck (HR[95%CI]=3.0[1.4,6.6] , $p<0.001$). This effect remained robust when adjusting for time (year of enrolment), geography (lab performing the GRT), and age: In the corresponding multivariable model the hazard of an HCV coinfection was increased by an HR of 3.2[1.5,6.9] if the HIV-transmission bottleneck was broad.

Conclusion:
Our results indicate that the currently occurring sexual spread of HCV is focused on those MSMs that are also prone to exhibit a broad transmission bottleneck at HIV transmission. This suggests that high-risk behavior and mucosal barrier impairment may play an important role in the sexual transmission of HCV.

2137

A. Lau[1], D. Goniotaki[1], P. Pelczar[2], S. Hornemann[1], A. Aguzzi[1]

Examining the Communication between Domains of the Prion Protein

Institute of Neuropathology, University Hospital of Zurich, CH-8091 Zurich, Switzerland[1], Institute of Laboratory Animal Science, University of Zurich, CH-8091 Zurich, Switzerland[2]

Introduction:
Prion diseases are fatal neurodegenerative diseases that include bovine spongiform encephalopathy and Creutzfeldt-Jakob disease. A conformational change of the cellular prion protein PrP^{C} to a form rich in β-sheets (PrP^{Sc}) is involved in the disease. Recently, it was shown that the PrP antibody POM1 was able to induce toxicity, mimicking the toxic pathways used during prion diseases. The antibody binds the C-terminal globular domain of PrP^{C} and yet, the N-terminus was shown to be responsible for toxicity. In contrast, it is well known that the N-terminus of PrP^{C} has neuroprotective properties. We intend to examine the interactions of the C-terminus and N-terminus of PrP and analyze how the N-terminus decides to exert a protective or toxic effect.

Methods:
If the toxicity of the N-terminus relies on a subtle conformational change of the C-terminus that is relayed to the N-terminus, the presence of a large protein in between the domains would most likely interfere with this communication. Thus, a mutant form of PrP^{C} will be generated to include the large protein EGFP in between the N-terminal and C-terminal domains of PrP (termed PrP-EGFP-PrP). Biochemical characterization will be performed to ensure proper expression, folding, and cellular localization. Techniques will include PNGaseF digestion, trypsin digestion, and TritonX-114 fractionation.
To examine whether POM1 is able to induce toxicity when PrP-EGFP-PrP is expressed, cerebellar organotypic cultured slices will be used. We will establish the use of lentiviruses to produce transgenic mice and slices will be derived from these mice.

Results:
A construct containing the coding sequence for PrP-EGFP-PrP was produced using the Gibson assembly. After transfection into HEK cells, initial biochemical characterization indicates that the mutant protein is expressed on the surface of cells, is associated with membrane fractions, and undergoes cleavage events. Furthermore, the PrP-EGFP-PrP coding sequence has been inserted into a lentiviral vector using the Gateway cloning system and lentiviruses will soon be produced.

Conclusion:
Establishment of a protocol to produce transgenic mice using lentiviruses will enable us to quickly test the PrP-EGFP-PrP mutant in slice culture. We expect that the toxicity induced by POM1 will be abrogated due to the presence of EGFP. This will help us to understand more about the mechanism of communication between the N-terminus and C-terminus of PrP.

2138

A. Wirsching[1], E. Melloul[2], R. Graf[1], PA. Clavien[1], M. Lesurtel[1]

Temporary Portal Vein Occlusion does not compromise Liver Regeneration of the occluded lobes

Department of Surgery, Swiss Hepato-Pancreato-Biliary Center, University Hospital Zurich, Switzerland[1], Department of Surgery, CHUV, Lausanne[2]

Introduction:
Liver lobe volume manipulation using temporary portal vein embolization (PVE) could contribute to make liver surgery or transplantation safer. In mice, we previously showed that temporary PVE is as efficient as permanent PVE or portal vein ligation to induce hypertrophy of the non-occluded lobes. However, recovery of the occluded lobes after revascularization remains to be assessed.
Study Aims: To assess histological and functional recovery of embolized liver lobes after temporary PVE.

Methods:
Forty BL6/male mice underwent 70% portal vein embolization using either powdered absorbable material (temporary PVE) or embospheres (permanent PVE). Fourteen days after temporary PVE, revascularization of the occluded lobes was confirmed by MRI angiography and hypertrophied non-occluded lobes were resected. In the permanent PVE group, non-occluded lobes were resected at the same time point. Mice undergoing 30% hepatectomy without previous PVE served as controls. Liver regeneration was assessed by liver-to-body weight ratio (LBW-R) and Ki-67 immunohistochemistry, liver function by bilirubin serum levels, liver injury by AST and ALT serum levels and fibrosis by sirius red staining.

Results:
Survival after non-occluded lobe resection was 100% in the temporary PVE group compared to 81% after permanent PVE. Twenty-four hours after resection, AST, ALT and bilirubin serum levels were significantly higher in the permanent PVE group compared to the temporary PVE group ($p < 0.05$ and < 0.001, respectively). Periportal fibrosis was observed almost exclusively after permanent PVE. After seven days, non-occluded lobe resection induced 156 and 263% liver hypertrophy of the occluded lobes in the temporary and permanent PVE groups, respectively. Mean liver-to-body-weight-ratios of temporary PVE, permanent PVE and 30% hepatectomy groups at postoperative day 7 reached 3.51, 3.54 and 4.2 respectively. Ki-67 positive hepatocytes in the temporary and permanent PVE groups were significantly increased 48 and 72h after resection compared to the 30% hepatectomy controls ($p < 0.001$).

Conclusion:
While temporary PVE induces hypertrophy of non-occluded lobes, revascularized liver lobes are functional and able to hypertrophy after resection of the non-occluded lobes.

2139

A. Sharma[1], S. Bender[1], A. Broggini-Tenzer[1], O. Riesterer[1], M. Pruschy[1]

Identification of Novel Targets for Radiosensitization of Non–Small Cell Lung Cancer by Secretome Analysis

Laboratory for Molecular Radiobiology, University Hospital Zurich, Switzerland[1]

Introduction:
Inherent and acquired resistance to the cytotoxic effects of ionizing radiation (IR) is increasingly recognized as a significant impediment to the efficacy of radiotherapy. Primary therapeutic response of IR is imparted by genomic instability and DNA damage, however IR also triggers multiple intracellular signaling processes that lead to the secretion of various para- and autocrine factors into the tumor microenvironment. These secreted factors then loop back (autocrine fashion) to modulate multiple pathways eventually driving acquired resistance. Here we investigated treatment-dependent secretion of various auto- or paracrine factors, which might drive acquired rescue mechanisms and determine the overall radiation sensitivity of the tumor.

Methods:
Exhaustive secretome analysis was performed using antibody arrays for a wide range of secretory factors impacting different phenotypes. Secretion kinetics of selected factors was determined across different established tumor cell lines in response to increasing doses of ionizing radiation and in murine blood serum, derived from irradiated tumor xenograft-carrying mice. To determine the relevance of the specific targets, proliferation and clonogenic survival assays in response to IR were performed with siRNA-targeted tumor cell lines and in presence of respective small molecule inhibitors.

Results:
We performed an exhaustive IR-dependent secretome analysis (>300 factors) and investigated in detail the effect of increasing doses of IR on the expression and tumor cell secretion of amphiregulin, transforming growth factor-α and ALCAM, which represent top hits in the array screening. All these factors were secreted in a dose dependent way from several non–small cell lung cancer (NSCLC) cell lines in response to IR. No changes were observed at the transcriptional level implying potential modulation at the posttranslational level. Interestingly, irradiation induced a dose-dependent increase in cleavage of the proform of ADAM17 (Disintegrin and metalloprotease domain 17) to active ADAM17 which resulted in enhanced ADAM17 activity and correlated with subsequent substrate shedding. Ex vivo analysis of murine blood serum derived from irradiated tumor xenograft-carrying mice support our in vitro results. Targeting ADAM17 with the small molecular inhibitor TMI-005 and siRNA-mediated silencing confirmed that ADAM17 is driving a prosurvival response with subsequent treatment resistance. Pharmacologic inhibition or siRNA-mediated downregulation of ADAM17 in combination with IR reduced proliferation and clonogenicity of the NSCLC cells. Analysis of in vivo experiments is ongoing.

Conclusion:
Our findings demonstrate that IR significantly activates ADAM17, which results in shedding of multiple survival factors, growth factor pathway activation and treatment resistance in NSCLC cells. We provide a sound rationale for positioning ADAM17 inhibitors as radiosensitizers to improve the treatment of NSCLC.

2140

DE. Haralampieva[1], SO. Salemi[1], TH. Betzel[3], IV. Dinulovich[2], ST. Kraemer[3], TU. Sulser[1], CH. Handschin[2], SI. Ametamey[3], DA. Eberli[1]

Non-Invasive Tracking Of Muscle Precursor Cells For Muscle Tissue Engineering

Urology department, USZ, Zurich, Switzerland[1], Biozentrum Basel, Basel, Switzerland[2], Radiopharmacology, ETHZ, Zürich, Switzerland[3]

Introduction:
Organ transplantation is the gold standard for the treatment of terminally damaged organs. This method has drawbacks including shortage of donor organs and high morbidity of immunosuppressive therapy. Regenerative medicine offers an alternative using autologous stem cell therapy for skeletal muscle diseases. In this study we investigated the possibility of using a mutated dopamine D2-receptor (D2R) and PET Imaging for precise localization and long-term *in vivo* tracking of the implanted cells.

Methods:
Human muscle precursor cells (hMPCs) were isolated from muscle biopsies and expanded. The cells were genetically modified to express a mutated D2R, as D2R tracers are already used in clinics. The infected hMPCs were characterized via immunocytochemistry and FACS using muscle-specific markers and visualized with PET.

Results:
For the *in vivo* evaluation 30 million modified hMPCs were suspended in collagen and injected *s.c.* in nude mice. After 2 and 4 weeks the newly-formed muscle tissues were visualized by PET and harvested for autoradiography, histology and histomorphometry.
Transduction of hMPCs allowed precise detection by PET Imaging *in vitro*. The morphology after harvesting revealed no differences to non-transduced cells, confirming that using modified hMPCs does not alter the muscle phenotype or contractility.
PET Imaging of engineered muscles allowed cell tracking after transplantation and provided us with additional insights about their survival *in vivo*. Autoradiography confirmed the presence of the transduced cells in the engineered tissue.

Conclusion:
PET Imaging may offer a novel method for non-invasive visualization and detection of autologous stem cells after injection for treatment of muscle diseases.

2141

C D. Schuh[1], E. Craigie[1], D. Hänni[2], A. Hall[1]

Multiphoton imaging of intracellular structure and function in the renal proximal tubule

Institute of Anatomy, University of Zurich[1], Center for Microscopy and Image Analysis, University of Zurich[2]

Introduction:
The renal proximal tubule (PT) is a highly specialized epithelium that is adapted to perform solute transport. PT cells are densely packed with endosomes, lysosomes and mitochondria, and damage to any of these organelles can impair solute transport causing renal Fanconi syndrome (FS). We have used a multiphoton microscope (MPM) to image intracellular structure and function in the PT in live kidney tissue.

Methods:
Kidney slices (220µm) were made from C57Bl/6J mice using a vibrotome and were imaged using an upright Olympus MPM. Dyes were loaded using an oxygenated perfusion system heated to 37C. Endosomes were identified by uptake of cascade blue-labeled dextran. Lysosomes were stained with lysotracker. Mitochondria were identified by NADH auto-fluorescence or with Rhodamine-123.

Results:
We were able to simultaneously image endosomes, lysosomes and mitochondria within PT cells. S_1 and S_2 PT segments were identified by differences in lysotracker signal. We found that the intracellular environment within PT cells is highly dynamic, with rapid movement of endosomes and lysosomes, and fusion/fission of mitochondria. Both endosomes and lysosomes showed bidirectional movement along the entire length of mitochondria to the basolateral membrane. In some cells, mitochondrial membrane potential was observed to flicker rapidly, and mitochondria could be selectively depolarized within single cells with targeted phototoxicity.

Conclusion:
In summary, we have developed an imaging tool-kit to track the function, movement and interactions of key intracellular organelles in the PT; by investigating the effects of targeted insults we aim to gain insights into the pathogenesis of diseases such as FS.

2142

B. Gjoksi[1], C. Ghayor[1], F. Weber[1]

The potential of N-methylpyrrolidone (NMP) to prevent osteoporosis and enhance bone regeneration in vivo

Departement of Cranio-Maxillofacial and Oral Surgery, Univeristy Hospital Zurich, Zurich [1]

Introduction:
Osteoporosis is a chronic, skeletal disease highly prevalent in post-menopausal women influenced by hormonal factors causing a huge burden on health care in an aging society. We previously demonstrated that NMP is a bioactive drug which enhances bone regeneration *in vivo* and acts as an enhancer of bone morphogenetic protein (BMP) *in vitro.* NMP also inhibits osteoclast differentiation and attenuates bone resorption.
The present study used animal models established for the evaluation of enhanced osteoporosis through double ovariectomy (OVX) and treated systemically with different doses of (NMP). With this treatment we want to describe the preventive effect of NMP on bone mass loss.

Methods:
Female Sprague-Dawley rats with an approximate weight of 220-250g were randomly divided into sham-operated group (Sham) either treated or not with NMP and four ovariectomized subgroups as OVX (control), OVX treated with three different graded doses of NMP. Bilateral ovariectomy or Sham operations were performed as previously designated and the weight of the animals was measured weekly. We assessed the pharmacological effects of NMP against osteoporosis by evaluating the body weight, serum biochemical parameters, bone mineral density (BMD), dynamic histomorphometry of bone and bone histomorphology

Results:
As predicted, in OVX rats the increase in body weight, serum osteocalcin levels and decreases of BMD were significantly reversed by NMP treatment. Additionally, the effect of the three different treatment dosages of NMP correlated dose-dependently with their effect on bone resorption. Mineral apposition rate (MAR) showed the protective activity of NMP through promotion of bone formation and suppression of bone resorption.

Conclusion:
These results suggest that NMP has a remarkable antiosteoporotic activity, and may be a promising candidate for treatment of postmenopausal osteoporosis induced by estrogen deficiency.

2143

SM. Frei[1], MR. Spalinger[1], A. Fürst[2], E. Jehle[3], M. Fried[1], G. Rogler[1], MM. Scharl[1]

Pathogen-Associated Molecular Pattern Contribute to Fistula-Associated Epithelial-Mesenchymal Transition in Intestinal Epithelial Cells While Interleukin-22 Antagonizes TGF-?-Induced Effects

Division of Gastroenterology and Hepatology, University Hospital Zurich, Switzerland[1], Department of Surgery, Caritas-Krankenhaus St. Josef, Regensburg, Germany[2], Department of Surgery, Oberschwaben-Klinik, Ravensburg, Germany[3]

Introduction:
An important complication of Crohn's disease (CD) is the development of perianal and intestinal fistulae. Therapeutic outcome using conventional drugs such as antibiotics, immunosuppressive agents and biologics is poor and surgical intervention is often required. Chronic inflammation, failure of the intestinal barrier function and a bacterial imbalance may contribute to the induction of epithelial-mesenchymal transition (EMT) and the consequent formation of fistula tracts. Tumor necrosis factor alpha (TNF-α), transforming growth factor beta (TGF-β) and interleukin (IL)-13 synergistically contribute to the migration and invasiveness of intestinal epithelial cells (IEC). The underlying extracellular matrix is broken down to enable IEC to invade. Here, we investigated the impact of pathogen-associated molecular patters (PAMPs) such as muramyldipeptide (MDP) on the induction of EMT in a three-dimensional multicellular model of HT-29 IEC and matrix destruction in human fistula tissue.

Methods:
Multicellular three-dimensional HT-29 IEC constructs were exposed to MDP (100 ng/ml) or IL-22 (50 ng/ml) for one, five and seven days and observed microscopically as well as on a molecular level. Monolayer IECs were challenged to IL-22, TGF-β or a combination thereof. Human perianal fistula tissue was assessed for matrix metalloproteinases (MMPs) using immunohistochemical procedures.

Results:
After exposure to MDP for seven days, the spheroids lost the well-defined globular shape and the epithelial cells separated indicating the onset of EMT. This was not seen in untreated control spheroids. In accordance with these microscopic findings, MDP treated spheroids up-regulated mRNA levels of EMT-related genes, including *SNAIL1* ($p < 0.05$), *TGF-β* ($p < 0.05$) and *IL-13* ($p < 0.05$) after treatment for seven days. In contrast to MDP, interleukin (IL)-22 did not induce EMT in spheroids. When IECs were co-treated with IL-22 and TGF-β, the effects of TGF-β were abrogated, but a further enhanced mRNA expression of *β6-Integrin* ($p < 0.001$) was observed. Furthermore, we found that MMP-3 was highly expressed around fistula tracts in human CD fistula tissue while only few stained cells were found in the surrounding inflamed tissue.

Conclusion:
Here, we demonstrate that PAMPs might contribute to the onset of EMT and therefore to the development of CD fistulas. The observed effects are indicative for an antagonistic effect of IL-22 on TGF-b. We therefore hypothesize that IL-22 might exert a protective effect in the pathogenesis of CD-associated fistulas. An excessive expression of MMP-3 around the fistula tracts might contribute to the invasive growth of the EMT cells into deeper tissue layers. In summary, our data suggest that bacterial pathogens likely impact the pathogenesis of CD-associated fistulas.

2144

M. Rottmar[1], M. Wurnig[1], A. Boss[1], D. Eberli[2]

Magnetization transfer (MT)-MRI characterizes in vivo fiber formation of muscle precursor cells

Institute of Diagnostic and Interventional Radiology, University Hospital Zurich, Zurich[1], Department of Urology, University Hospital Zurich, Zurich[2]

Introduction:
Cell based therapies using e.g. muscle precursor cells (MPCs) show great promise to treat stress urinary incontinence. For translating such approaches into clinics, non-invasive in-vivo imaging modalities are needed. The aim of this study was thus to assess the muscle fiber formation of hMPCs *in vivo* using magnetization transfer (MT) MRI in a mouse model in correlation to histology and immunohistochemistry.

Methods:
hMPCs were mixed with collagen and injected subcutaneously into nude mice and monitored via MRI (4.7 T scanner) for 4 weeks. Thereafter, the engineered muscle tissue was assessed by histology, immunohistochemistry and western blot. For MT measurements a 3D-spoiled gradient-echo sequence (repetition time TR/echo-time TE 20.4ms/4.7ms) was applied with/without a systematically varied MT prepulse (off-resonance frequency 50Hz to 37'500Hz, flip angle 800°).

Results:
At 2'500Hz, MT measurements showed magnetization transfer ratios (MTR) of 25.0% at day 1, decreasing to 14.1% at day 7 and increasing strongly to 42.9% by day 14, approximating the MTR of 49.9% from the skeletal muscle reference. A similar trend could be observed over the range of off-resonance frequencies. Cell differentiation and myofiber formation could be confirmed by histology, immunohistochemistry and western blot.

Conclusion:
hMPCs form muscle tissue *in vivo* and MT-MRI is able to directly assess muscle fiber formation describing the myogenic differentiation process. The results will be transferable to the clinical setting as a non-invasive biomarker for the assessment of muscle tissue regeneration in patients.

2145

G. Iotzova-Weiss[1], SN. Freiberger[1], I. Kleiber-Schaaf[1], P. Johansen[1], L. French[1], GFL. Hofbauer[1]

TLR4 is a negative regulator of keratinocyte proliferation

Dermatologische Klinik, Universitätsspital Zürich, Zürich[1]

Introduction:
Our current study investigates the role of TLR4 in the proliferation capacity of normal keratinocytes. Our results using a blocking monoclonal antibody (HTA125) against TLR4 showed an unexpected, pronounced proliferation of keratinocytes, assessed by BrDU proliferation assay. In addition, we abrogated the interaction between TLR4 and its accessory protein MDII using a specific blocking peptide for MDII and we detected an induction of proliferation. We observed that with the subsequent growing of normal primary keratinocytes and keratinocytes derived from patients with SCC up to full confluence and differentiation, the expression of TLR4 increased significantly. This correlates with the differential TLR4 expression within the layers in normal skin and skin from patients with SCC. We found that the tumor SCC13 cell line, stably expressing TLR4 showed lower proliferation capacity in vitro and decreased tumor growth in vivo. Moreover, the overexpression of TLR4 led to phosphorylation of ERK1/2 and increased protein level of ATF3. TLR4 knockdown induced cellular proliferation in keratinocytes in vitro and increased tumor growth in vivo.
Our results show that TLR4 is a negative regulator of keratinocyte proliferation and may be associated with the progression of SCC of the skin. Better understanding of the regulatory role for TLR4 is the basis for a later use in a therapeutic setting to stop keratinocyte proliferation such as in squamous cell carcinoma of the skin and to induce keratinocyte proliferation such as in wound healing

Methods:
BrDU proliferation Assay; transient and stable transfection; PCR, immunobloting; application of tumor cells in mice

Results:
Our results using a blocking monoclonal antibody (HTA125) against TLR4 showed an unexpected, pronounced proliferation of keratinocytes, assessed by BrDU proliferation assay. In addition, we abrogated the interaction between TLR4 and its accessory protein MDII using a specific blocking peptide for MDII and we detected an induction of proliferation. We observed that with the subsequent growing of normal primary keratinocytes and keratinocytes derived from patients with SCC up to full confluence and differentiation, the expression of TLR4 increased significantly. This correlates with the differential TLR4 expression within the layers in normal skin and skin from patients with SCC. We found that the tumor SCC13 cell line, stably expressing TLR4 showed lower proliferation capacity in vitro and decreased tumor growth in vivo. Moreover, the overexpression of TLR4 led to phosphorylation of ERK1/2 and increased protein level of ATF3. TLR4 knockdown induced cellular proliferation in keratinocytes in vitro and increased tumor growth in vivo.

Conclusion:
Our results show that TLR4 is a negative regulator of keratinocyte proliferation and may be associated with the progression of SCC of the skin. Better understanding of the regulatory role for TLR4 is the basis for a later use in a therapeutic setting to stop keratinocyte proliferation such as in squamous cell carcinoma of the skin and to induce keratinocyte proliferation such as in wound healing

2146

Ms. Bombardo Ayats[1], Ms. Sonda[1], Mr. Graf[1]

Epigenetic acetylation mechanisms are activated during progenitor cell-based regeneration in the adult pancreas.

Swiss HPB Center, Visceral & Transplantation Surgery, University Hospital Zurich[1]

Introduction:
Acute pancreatitis continues to be a clinical challenge with mortality rates as high as 43%. Regeneration of pancreatic acinar cells is critical for the recovery of the injured organ but its molecular mechanisms are not completely understood. This regenerative process involves an initial de-differentiation of acinar cells to a progenitor-like state followed by cell division and consequent re-differentiation. As acinar cell de-differentiation is characterized by a robust change in gene expression, we analyzed whether epigenetic mechanisms regulate this event.

Methods:
Pancreatitis was induced by repetitive injections of cerulein in wild type C57BL/6 mice. *In vivo* regulation of acetylation levels, histone deacetylase (HDAC) expression and the regenerative potential of pancreatic acinar cells were evaluated over a period of one week by immunohistochemistry, western blotting and qRT-PCR.

Results:
After experimental pancreatitis, pancreatic acinar cells showed a transient increase of acetylation levels of nuclear proteins. The timing of this regulation paralleled the up-regulation of progenitor markers and preceded cell proliferation. Moreover, pancreatic regeneration was characterized by a time-dependent expression of selected members of class I HDACs. Specifically, HDAC 2 and 3 transcripts were the most robustly regulated during pancreatitis and showed an expression pattern opposite to the changes in acetylation levels.

Conclusion:
Our results indicate that pancreatic gene expression following pancreatitis correlates with a time-dependent regulation of acetylation levels in acinar cells and a differential expression of class I HDACs members. Current investigations using pharmacological inhibitors and genetic approaches aim to elucidate the role of selective HDACs in acinar cells and their potential to modulate pancreatic regeneration.

2147

Ms. Bombardo Ayats[1], Mr. Graf[1], Ms. Sonda[1]

Epigenetic acetylation mechanisms are activated during progenitor cell-based regeneration in the adult pancreas.

Swiss HPB Center, Visceral & Transplantation Surgery, University Hospital Zurich[1]

Introduction:
Acute pancreatitis continues to be a clinical challenge with mortality rates as high as 43%. Regeneration of pancreatic acinar cells is critical for the recovery of the injured organ but its molecular mechanisms are not completely understood. This regenerative process involves an initial de-differentiation of acinar cells to a progenitor-like state followed by cell division and consequent re-differentiation. As acinar cell de-differentiation is characterized by a robust change in gene expression, we analyzed whether epigenetic mechanisms regulate this event.

Methods:
Pancreatitis was induced by repetitive injections of cerulein in wild type C57BL/6 mice. *In vivo* regulation of acetylation levels, histone deacetylase (HDAC) expression and the regenerative potential of pancreatic acinar cells were evaluated over a period of one week by immunohistochemistry, western blotting and qRT-PCR.

Results:
After experimental pancreatitis, pancreatic acinar cells showed a transient increase of acetylation levels of nuclear proteins. The timing of this regulation paralleled the up-regulation of progenitor markers and preceded cell proliferation. Moreover, pancreatic regeneration was characterized by a time-dependent expression of selected members of class I HDACs. Specifically, HDAC 2 and 3 transcripts were the most robustly regulated during pancreatitis and showed an expression pattern opposite to the changes in acetylation levels.

Conclusion:
Our results indicate that pancreatic gene expression following pancreatitis correlates with a time-dependent regulation of acetylation levels in acinar cells and a differential expression of class I HDACs members. Current investigations using pharmacological inhibitors and genetic approaches aim to elucidate the role of selective HDACs in acinar cells and their potential to modulate pancreatic regeneration.

2148

D. Scheiner[1], D. Fink[1], D. Perucchini[1], C. Betschart[1]

Urogynaecologic operations in Switzerland between 1998 and 2013

Gynecology, University Hospital of Zurich, Zurich[1]

Introduction:
The lifetime risk of undergoing surgery for a pelvic floor disorder such as pelvic organ prolapse (POP) or urinary incontinence (UI) is 11%. The aim of this study is to evaluate the most performed urogynaecological procedures in Switzerland as well as patient's and hospital stay characteristics.

Methods:
Retrospective analysis of 1,216,705 continuously collected ASF data (Sevisa AG) of the Swiss association of hospitals in ob/gyn ("Arbeitsgemeinschaft Schweizerische Frauenkliniken"). Each record corresponds to a hospitalized patient at one of the participating hospitals (45 to 75) and includes the kind of procedure, i.e. POP and UI procedures (colporrhaphia anterior, CA; colporrhaphia posterior, CP; levator plasty; sacrospinal ligament fixation, SSLF; enterocele repair, E; abdominal sacrocolpopexy, ASC; stress urinary incontinence procedures), demographics, risk factors, morbidity and complications. 2007, about 40% of all inpatient cases in Switzerland were covered, and 50 of the 71 Swiss teaching hospitals participated in 2010. 2005, an adapted questionnaire was introduced, addressing the changes in the field of ob/gyn, and inter alia the different midurethral slings (retropubic TVT and transobturator TOT). Hospitalisation rates and prevalence of operations are based on the year of 2007 (ASF coverage of 40 %) and the Swiss Federal Statistical Office (FSO 2007: 3,073,700 women at the age of 20 and above). Statistics were undertaken by means of ANOVA and X2 test, as appropriate. Values as a percentage or as mean ± standard deviation.

Results:
40,768 hospitalizations were analyzed. In 2007, the hospitalization rate was 162/1,000 women in acute care hospitals and 59/1,000 in women's clinics, while the prevalence of urogynaecologic procedures was 2.34/1,000 women. 3.35 % of all ASF cases were urogynaecologic procedures. Their prevalence increased from 1998 by 2.61 % to 4.1 % in 2013. POP surgery was performed in 57.2 %, UI surgery in 32.3 %, and concomitant procedures for POP and UI in 10.2 %. Most common POP surgery was CP (47.2 %), followed by CA (42.0 %), SSLF (17.4 %), E (6.4 %), and ASC (0.7 %). Mesh implantations were recorded since 2005 (7.1 %). In 41%, POP surgery was combined with vaginal hysterectomy. The average age increased continuously from 61.0 ± 13.3 to 64.4 ± 13.6 years ($p < 0.0001$), whereas the hospital stay declined from 11.8 ± 4.8 to 5.2 ± 3.9 days ($p < 0.0001$). Patients who underwent POP surgery were older (65.5 ± 12.4) than patients with concomitant procedures (63.0 ± 13.0) or solely incontinence surgery (59.2 ± 13.5), resp. ($p < .001$). The hospitalization time was longest for concomitant (9.4 ± 4.7) and POP operations (8.4 ± 4.1), and shortest for UI surgery (4.9 ± 4.9), resp. ($p < 0.0001$).

Conclusion:
Urogynecology operations account for an increasing proportion of hospitalizations. Pelvic organ prolapse and urinary incontinence procedures are usually addressed separately. The average age of patients is increasing while the hospital stay decreases.

2149

M. Meerang[1], A. Boss[2], E. Felley-Bosco[3], O. Lauk[1], S. Arni[1], B. Bitanihirwe[1], R. Stahel[3], W. Weder[1], I. Opitz[1]

Evaluation of Tumor Imaging Techniques for Malignant Pleural Mesothelioma orthotopic Rat Model

Division of Thoracic Surgery, University Hospital Zürich, Zürich[1], Department of Radiology, University Hospital Zürich, Zürich[2], Laboratory of Molecular Oncology, University Hospital Zürich, Zürich [3]

Introduction:
An orthotopic rat tumor model for malignant pleural mesothelioma (MPM) provides clinical similarity to patients. The model is useful for several applications such as drug testing and surgical intervention. For non-invasive and repetitive visualization of tumor burden, a reliable imaging method is required. Here, we compared 2 techniques namely bioluminescence (Bli) imaging and magnetic resonance (MR) imaging.

Methods:
Immune competent rats (n=5) were implanted subpleurally with 500,000 syngeneic rat MPM cells transfected with luciferase. At day 8 or 10 after the inoculation, MRI was performed using 4.7 Tesla small animal MR scanner equipped with a ^{1}H whole-body rat coil. Image data sets were acquired with T2-weighted fast spin-echo sequences in transverse orientation. Bli was measured by bioluminescent imager following intra-peritoneal injection of Bli substrate (D-Luciferin). Tumor burden was expressed either as volume (mm^3) calculated from sequential MR images or as maximum Bli intensity (photon/second).
Finally the tumor burden was correlated (Pearson correlation) with macroscopic tumor (ellipsoid) volume performed during autopsy at the same day.

Results:
In all rats, a single tumor nodule was found at the inoculation site with a median volume of 52 mm^3 (36 – 278). Tumor burden quantified from MR images correlated significantly with tumor volume measured ($p<0.0001$; $r=0.99$). However, signal intensity of Bli did not correspond with tumor volume measured neither by the macroscopic observation ($p=0.50$; $r=-0.41$) nor by MRI ($p=0.50$; $r=-40$).

Conclusion:
Our results showed that MRI allowed reliable assessment of MPM tumor burden in the present model. This non-invasive imaging technique could also be performed repetitively. Bli has been shown to be a sensitive detection method; however reliable quantitation could be influenced by several factors such as the expression level of luciferase in cells or the variable absorption of its substrate, D-luciferin. Moreover, these discrepancies could be due to the fact that bioluminescence represents amount of tumor cells however MRI and macroscopic tumor volume could represent both tumor and stromal compartment. These factors have to be taken into consideration for the interpretation.

2150

M. Meerang[1], B. Bitanihirwe[1], M. Friess[1], K. Bérard[1], A. Soltermann[3], E. Felley-Bosco[2], B. Seifert[4], R. Stahel[2], W. Weder[1], I. Opitz[1]

NF2/Hippo Pathway Dysregulation as Predictors of Survival for Mesothelioma Patients Treated with Multimodal therapy

Division of Thoracic Surgery, University Hospital Zürich, Zürich[1], Laboratory of Molecular Oncology, University Hospital Zürich, Zürich [2], Institute of Surgical Pathology, University Hospital Zürich, Zürich[3], Division of Biostatistics, Institute for Social and Preventative Medicine, University of Zürich, Zürich[4]

Introduction:
Malignant pleural mesothelioma (MPM) caused by asbestos exposure is one of the most aggressive neoplasms. Multimodal regimen tailored by the stage of disease such as induction chemotherapy followed by extrapleural pneumonectomy provides good survival outcome. MPM is resistant to chemotherapy thus tumor relapses remain significant clinical problem. Activation of the Hippo signaling pathway has been reported in a wide range of cancers including MPM. Moreover, the tumor suppressor Neurofibromatosis type II (NF2) has been reported to be lost in nearly half of MPM patients, causing constitutive activation of Yes-Associated Protein 1 (YAP), the main downstream effector of Hippo pathway. Therefore, we hypothesized that Hippo pathway dysregulation may provide prognostic information for MPM and shed new light on individualized therapy for this dreadful disease.

Methods:
Paired samples of MPM patients (n = 153) were collected pre- and post-induction chemotherapy and assembled in tissue micro arrays. Expression levels of key components of the Hippo pathway (NF2, YAP, survivin and connective tissue growth factor (CTGF)) were evaluated by immunohistochemistry in both cytoplasmic and nuclear fractions and semi-quantitatively scored. Nuclear survivin and proliferation marker (Ki-67) were scored as labeling index (%). The data obtained were then correlated to overall survival (OAS) and progression free survival (PFS).

Results:
Kaplan-Meier survival curves revealed an association of nuclear survivin labeling index assessed in pre-chemotherapy tissues with PFS ($p=0.051$). Nuclear YAP score and nuclear survivin labeling index was significantly reduced in post-chemotherapy compared to pre-chemotherapy tissue. We also observed strong correlation between proliferation index (Ki-67) and nuclear survivin ($p<0.0005$). Cytoplasmic and nuclear YAP score did not show correlation with survival.

Conclusion:
YAP works as a transcriptional co-activator in the nucleus, it enhances transcription of target genes such as survivin and CTGF to induce tumor growth and suppress apoptosis. We will confirm, in an independent MPM cohort, the prognostic significance of nuclear survivin. NF2 and CTGF assessment is currently ongoing. Finally, dissecting the dysregulation of this pathway may hold great chance to discover predictors of survival and effective treatment for patients.

2151

PK. Kambakamba[1], CT. Tschuor[1], PK. Kron[1], KS. Slankamenac[1], PAC. Pierre Alain[1], ML. Lesurtel[1]

Impact of Epidural Analgesia on Perioperative Kidney Function in Hepatic Surgery.

University Hospital Zurich, Department of Visceral Surgery, Zurich[1]

Introduction:
Postoperative acute kidney failure occurs in 10 to 16% of liver resections and is dramatically associated with morbidity and mortality. Epidural analgesia (EDA) comes along with sympatholysis, consecutive vasodilatation, and may induce a drop of the mean arterial pressure below a certain threshold which compromises renal blood pressure autoregulation and leads to kidney injury. We hypothesized that EDA is a risk factor for postoperative acute liver failure after liver surgery.

Methods:
The incidence of acute kidney injury (AKI) according to the AKI criteria was investigated in a series of 453 patients who underwent liver resection with or without EDA from 2002 to 2007. Uni- and multivariate analysis was performed including the usual preoperative (diabetes, cardiovascular disease, chronic renal disease, ALT) and intraoperative (blood transfusions, colloids, diuretics, catehcolamines, oliguria, hepaticojejunostomy) predictors of post-hepatectomy renal failure.

Results:
In 80% of liver resections (n=364) an EDA was used. Thirty percent of patients with EDA experienced a procedure-associated adverse event including hypotension (74%), which resulted in an early postoperative withdrawal of EDA in 6%. Overall postoperative morbidity was comparable in both groups (51 vs. 44%, p=0.6). Ninety percent of patients with EDA did not need any postoperative opioids. AKI occurred in 8% of the patients. The EDA group had a significantly higher incidence of AKI (9% vs. 2%, p=0.02). No significant difference was observed between the 2 groups in case of minor liver resections (1% vs. 3%, p=0.6), while EDA was remarkably associated with AKI in case of major liver resections (15% vs. 2%, p=0.02). The need for postoperative hemofiltration was rare (2%) and was not significantly different between the 2 groups (3% vs. 1%, p=0.3 for all, and 4% vs. 3%, p=0.6 for major resections). On multivariate analysis, EDA was an independent risk factor for AKI after major liver resections (p=0.03).

Conclusion:
EDA is a risk factor for postoperative acute kidney failure after major hepatectomy. While patients undergoing minor hepatectomy seem to benefit from the analgesic potential of EDA without increasing risk for AKI, patients undergoing major hepatectomy need to be chosen carefully.

2152

E. Becker[1], C. Stanzel[1], K. Atrott[1], G. Rogler[1], I. Frey-Wagner[1]

Effects of isotretinoin treatment on epigenetic programming in T cells

Gastroenterology and Hepatology, University Hospital Zurich, Zurich, Switzerland[1]

Introduction:
Retinoids are essential nutrients involved in the maturation of the immune system. The majority of *in vitro* and *in vivo* studies provided evidence that retinoid treatment exhibits anti-inflammatory properties and is effective acne therapy. However, there is a controversial discussion about a causal relationship between isotretinoin treatment and the onset of inflammatory bowel disease (IBD). Some patients have claimed that they developed acute intestinal inflammation during isotretinoin treatment or had an onset of IBD weeks or even years after cessation of the medication. We have previously shown that isotretinoin treatment has no adverse effects in two mouse models of inflammatory bowel disease[1]. Here we investigated the influence of isotretinoin treatment on genetic imprinting in two T cells subsets as a potential mediator of long-term effects of isotretinoin treatment on the immune system.

[1] Effects of retinoids in mouse models of colitis: benefit or danger to the gastrointestinal tract?
Frey-Wagner I, Fischbeck A, Cee A, Leonardi I, Gruber S, Becker E, Atrott K, Lang S, Rogler G.
Inflamm Bowel Dis. 2013 Oct; 19(11):2356-65

Methods:
Balb/c mice were treated with isotretinoin (30 mg/kg bodyweight) or vehicle orally for 2 weeks and kept for further 4 weeks to study potential direct and long-term effects. Naive T cells and regulatory T cells were isolated directly after the treatment period and at the end of the study by magnetic cell sorting. After isolation of genomic DNA, microRNA and mRNA, samples were sequenced with the Illumina technique to study changes in methylation patterns, microRNA and mRNA expression. For predicting target genes of determined microRNAs the software Target Scan and Traget Scan Custom were used. For identification of pathways significantly affected by isotretinoin treatment the software Meta Core® was applied.

Results:
Analysis of epigenetic modifications in naive and regulatory T cells revealed potential long-term effects in both T cells subsets. In regulatory T cells mainly the methylation pattern was altered in T cells isolated four weeks after cessation of treatment. In naive T cells on the other hand predominantly microRNA expression was altered in T cells isolated after four weeks without treatment. Pathway analysis by Meta Core® revealed that pathways of immune responses, concerning antigen presentation and T helper cell differentiation were affected. Further functional analysis of affected pathways is currently under investigation.

Conclusion:
Preliminary results identified changes in methylation pattern and microRNA expression in naive and regulatory T cells which might mediate potential long-term effects after isotretinoin treatment, yet differences between the different T cell subsets were far more pronounced than differences induced by isotretinoin treatment.

2153

E. Becker[1], C. Stanzel[1], S. Schmidt[3], K. Atrott[1], L. Biedermann[1], A. Rehman[2], D. Jonas[2], C. Von Mering[3], G. Rogler[1], I. Frey-Wagner[1]

Effects of isotretinoin treatment on murine gut microbiota composition

Gastroenterology and Hepatology, University Hospital Zurich, Zurich, Switzerland[1], Department of Environmental Health Sciences, University Medical Center, Freiburg, Germany[2], Department of Molecular Life Sciences, University of Zurich, Zurich, Switzerland[3]

Introduction:
In-vitro and *in-vivo* data have shown that retinoid treatment promotes an anti-inflammatory milieu with few adverse effects towards the gastrointestinal (GI) tract, yet there is current debate about a causal relation between retinoid treatment and inflammatory bowel disease (IBD). Patients have claimed that they developed acute intestinal inflammation during isotretinoin treatment or to develop inflammatory bowel disease (IBD) weeks or even years after cessation of the medication. We have previously shown that isotretinoin treatment has no adverse effects in two mouse models of inflammatory bowel disease[1]. Since the gut microbiota can metabolize retinoids, we investigated whether administration of retinoids might change the gut microbiota composition in a way that is favorable for the development of IBD.

[1] Effects of retinoids in mouse models of colitis: benefit or danger to the gastrointestinal tract?
Frey-Wagner I, Fischbeck A, Cee A, Leonardi I, Gruber S, Becker E, Atrott K, Lang S, Rogler G.
Inflamm Bowel Dis. 2013 Oct;19(11):2356-65

Methods:
Balb/c mice were treated with isotretinoin (30 mg/kg bodyweight) or vehicle orally for 2 weeks and kept for further 4 weeks to study potential direct and long-term effects. Fecal samples were collected before treatment, directly after the treatment period and four weeks later for analysis of gut microbiota composition by 16S rRNA gene sequencing on the GS-Flx 454 platform. Sequencing data were analyzed with the software QIIME to determine OTUs, calculate the relative abundance for each group and time point and to general principal coordinate analysis plots.

Results:
Principle coordinate analysis showed no formation of clusters neither depending on treatment nor on time point of investigation indicating no fundamental differences between the gut microbiota composition of isotretinoin or vehicle treated animals or between the different time points studied. Some differences with regard to alpha and beta diversity between the different treatment groups as well as between the different time points studied were observed and are currently under further investigation.

Conclusion:
Preliminary results with QIIME showed no substantial differences between isotretinoin and vehicle treated animals indicating that isotretinoin treatment had no fundamental effect on the composition of the murine gut microbiota. We are currently investigating the variations in alpha and beta diversity that were observed between groups exposed to isotretinoin and vehicle, as well as between the different time points.

2154

Y. Plutino[1], F. Barchiesi[1], B. Imthurn[1], R. Dubey[1]

Activation of Intracellular Calcium Triggers DHT-induced phopshoSmad1/5/8 Signaling in EPCs

Clinic for Reproductive Endocrinology, Department of Obstetrics and Gynecology, University Hospital of Zurich[1]

Introduction:
Clinical data suggest that androgens may induce cardiovascular protection in men, hence it is essential to investigate the mechanism(s) by which androgens (dihydrotestosterone; DHT) induce their vaso-protective actions. Because endothelial damage and dysfunction is associated with cardiovascular disease (CVD), and Endothelial Progenitor Cells (EPCs) protect against CVD by repairing damaged ECs. Hence in the present study we assessed the role of DHT on angiogenesis. More importantly we assessed the impact on Smad1/5/8 pathway and the underlying mechanisms involved in its activation and angiogenesis.

Methods:
In vitro two dimensional gel-based system was used to assess EPC mediated angiogenesis. Western blotting was used to detect changes in protein levels upon DHT treatment. Calcium signalling inhibitors such as U73122 (Phospholipase C inhibitor) and BAPTA-AM (calcium chelator) were applied to study the role of calcium in mediating DHT-dependent Smad1/5/8 phosphorylation. Fluo-4 (2uM) loaded EPCs were used to measure changes in intracellular calcium levels with fluorescence microscopy.

Results:
EPCs expressed ALK1 and ALK5 receptors for TGFβ pathway. Treatment with DHT 100nM induced Smad1/5/8 phosphorylation in a time-dependent manner. A maximal upregulation of Smad1/5/8 phosphorylation was observed at 30 minutes, suggesting the involvement of non-genomic mechanisms. Treatment with DHT also induced Id-1, downstream target of Smad1/5/8, moreover this effect was evident after 4h. A similar stimulatory effect was observed for Endoglin, an accessory protein. Because calcium is implicated in early cell growth signaling we assessed its participation in DHT induced Smad1/5/8 phosphorylation. Calcium has been shown to mediate Smads signaling in part. Indeed, the stimulatory effects of DHT on Smad1/5/8 phosphorylation were abrogated by calcium inhibitors such as U73122 1uM (Phospholipase C inhibitor) and calcium chelator BAPTA-AM 50uM. Moreover, using calcium-sensitive agents as fluo-4 we found that DHT increases intracellular calcium levels in EPCs within minutes.

Conclusion:
Our findings provide evidence that DHT induces angiogenesis by EPCs and these effects potentially involve non-genomic activation of Smad1/5/8 via ALK1 and downstream target Id-1. More importantly, we demonstrate that DHT induced ALK1/Smad1/5/8 phosphorylation by triggering increase in intracellular calcium. In conclusion, our findings suggest that DHT might modulate EPCs function through activation of ALK1/Smad1/5/8 pathway, mediated by intracellular calcium changes. The growth stimulatory effects of DHT on EPC-mediated capillary formation may in part be responsible for protective actions of DHT on the vasculature.

2156

M. Weisskopf[1], G. Bucklar[3], J. Blaser[2]

Tools in a Clinical Information System Supporting Clinical Trials at a Swiss University Hospital

Clinical Trials Center, University Hospital Zurich, Zurich, Switzerland[1], Research Centre for Medical Informatics, University Hospital Zurich, Zurich, Switzerland[2], Department of Informatics and Communications University Hospital Zurich, Zurich, Switzerland[3]

Introduction:
Issues concerning inadequate source data of clinical trials rank 2nd in the most common findings by regulatory authorities. The increasing use of electronic clinical information systems (CIS) by healthcare providers offers an opportunity to facilitate and improve the conduct of clinical trials and the source documentation.

Methods:
In 2011/2012 a set of tools was developed and implemented into the CIS of the University Hospital Zurich (USZ) to support clinical research, including

1. a trial registry for documenting metadata on the clinical trials conducted at the hospital,
2. a patient-trial-assignment-tool to tag patients in the electronic medical charts as participants of specific trials,
3. medical record templates for the documentation of study visits and trial related procedures,
4. online queries on trials and trial participants,
5. access to the electronic medical records for clinical monitors,
6. an alerting tool to notify of hospital admissions of trial participants,
7. queries to identify potentially eligible patients in the planning phase as trial feasibility checks and during the trial as recruitment support, and
8. predefined sets of orders for vital signs, laboratory analyses, drug prescriptions and treatments to facilitate the complete and accurate performance of study visit procedures.

Results:
The number of approximately 100 new registrations per year in the voluntary CIS trial registry now matches the numbers of the existing mandatory USZ trial registry. Likewise, the yearly numbers of patients tagged as trial participants as well as the use of the standardized trial record templates increased to 2073 documented trial-enrolments and over 200 reports generated/month in the year 2012. Accounts for 32 clinical monitors have been established in the first two years monitoring a total of 49 trials in 16 clinical departments. Within one year, 79 running trials (22% of all active trials registered in the CIS) have activated the hospital admission alert option, generating approximately 85 alerts per month.

Conclusion:
The popularity of the presented CIS tools demonstrate their potential to facilitate the conduct of clinical trials. Future studies on monitoring and inspection findings will have to evaluate their impact on quality and safety.

2157

A. Aguzzi[1], A. Ahlm[1], K. Arroyo[1], M. Bieri[1], B. Li[1], G. Manco[1], B. Piccapietra[1], L. Takacs[1], C. Tournaire[1], A. Varol[1], S. Yakushev[1]

High-throughput automated genotyping of transgenic laboratory animals

Institute of Neuropathology, University Hospital of Zurich, CH-8091 Zurich, Switzerland[1]

Introduction:
Transgenic animals are widely used to model and investigate human diseases and are a common tool in research and development of the new therapeutic targets. The control of the inheritance of the transgene is imperative for the high quality of the data and becomes inseparable from the effective animal keeping. Current evolution of regulatory and quality requirements and concomitant evolution of cost challenges researchers and administration to improve the efficiency of the animal keeping. Centralization, automation and increase in throughput of the genotyping procedure might give an opportunity to moderate personnel working hours and costs of animal keeping for individual research groups as well as the institutions.
The Institute of Neuropathology developed an automated and high-throughput workflow for genotyping of the laboratory animals – iMice.

Methods:
iMice platform includes 4 main units:
1. Web interface that allows users to request sampling and genotyping of individual animals and view detailed results
2. An instrument for simplified sampling of the biopsies, which consists of the robotic 96-well plate filler with the palmtop computer, connected to the iMice and iRats databases
3. Genotyping facility equipped with automated liquid handling robot, cyclers, capillary electrophoresis to analyze PCR products and a depository of biopsies
4. Database to track, organize, store and link information
The users of iMice submit information about the transgene, strain and conditions for genotyping PCR linked to the strain. Subsequently the specified animal can be semi-automatically biopsied on request in to the 96-well plate prefilled with the lysis buffer. Afterwards it is transferred to the PCR facility, where the lysate is analyzed with the desired PCRs. For the liquid handling of the PCR components we programmed the JANUS automated liquid handling robot, which is linked to the iMice database. PCR cycling is performed in the cycler programmed for the specific conditions or in the Real Time PCR cycler. To analyze the presence of the PCR product we are using capillary electrophoresis equipment, which transfers the results of the analysis as well as an image to the iMice database and links the results with the corresponding biopsy and animal.

Results:
High-throughput automated genotyping platform iMice is currently used to analyze about 3000 biopsies per month for 190 transgenes, which significantly reduces the workload from 5 to 3 days per week. The price per PCR for USZ clients is 5.50CHF.

Conclusion:
Currently we are adapting the iMice platform for the multiplex Real Time PCR genotyping using 384-well plates. This will allow us to increase the throughput and reduce the time of analysis with minimal or no change in costs. In addition, units of iMice platform, such as biopsy sampler and automated PCR facility may be cloned and integrated to the database giving an opportunity for UZH/ETH researchers to profit from iMice and encourage the collaboration with USZ sharing mice facilities.

2158

Z. Gai[1], C. Hiller[1], S.H. Chin[2], D. Konrad[3], A.. Kullak-Ublick[1]

Uninephrectomy augments the effects of high fat diet induced obesity on gene expression in mouse kidney

Department of Clinical Pharmacology and Toxicology, University Hospital Zurich, CH-8091 Zurich[1], Division of Pediatric Endocrinology and Diabetology, University Children's Hospital, Zurich[2], Children's Research Centre, University Children's Hospital, Zurich[3]

Introduction:
Obesity has been reported as an independent risk factor for chronic kidney disease, leading to glomerulosclerosis and renal insufficiency.

Methods:
To assess the relationship between a reduced nephron number and a particular susceptibility to obesity-induced renal damage, mice underwent uninephrectomy (UNX) followed by either normal chow or high-fat diet (HFD) and were compared with sham-operated control mice.

Results:
After 20 weeks of dietary intervention, HFD-fed control mice presented characteristic features of progressive nephropathy, including albuminuria, glomerulosclerosis, renal fibrosis and oxidative stress. These changes were more pronounced in HFD-fed mice that had undergone uninephrectomy. Analysis of gene expression in mouse kidney by whole genome microarrays indicated that high fat diet led to more changes in gene expression than uninephrectomy. HFD affected mainly genes involved in lipid metabolism and transport, whereas the combination of UNX and HFD additionally altered the expression of genes belonging to cytoskeleton remodeling, fibrosis and hypoxia pathways. Canonical pathway analyses identified the farnesoid X receptor (FXR) as a potential key mediator for the observed changes in gene expression associated with UNX-HFD.

Conclusion:
In conclusion, HFD-induced kidney damage is more pronounced following uninephrectomy and is associated with changes in gene expression that implicate FXR as a central regulatory pathway.

2159

SN. Freiberger[1], G. Iotzova-Weiss[1], PF. Cheng[1], MP. Levesque[1], R. Dummer[1], K. Skak[2], GFL. Hofbauer[1]

Investigating the Mechanism of Action of Ingenol Mebutate in Squamous Cell Carcinoma

Department of Dermatology, University Hospital Zurich, Switzerland[1], LEO Pharma A/S, Biologicak Research, Ballerup, Denmark[2]

Introduction:
Squamous cell carcinoma (SCC) is the second most common human cancer and the second leading cause of skin cancer death in the US. Many SCCs arise in lesions previously diagnosed as actinic keratosis (AK). The treatment opportunities for AK are either therapy with liquid nitrogen, photodynamic therapy and topicals (5-FU, imiquimod, diclofenac) or excision of the lesion. The application period of these therapies lasts from several weeks to several months being burdensome for the patients due to repeated daily applications. They can cause localized inflammation and ulceration, some flu-like side effects, or even scars. Recently a new drug for topical treatment of AK, ingenol mebutate, was approved which has the advantage of being applied for the short period of two or three days and causes a short period of local skin reactions. The mechanism of action has been shown to be inducing cell death and eliciting a specific PKC-dependent immune reaction. Although, direct effects of Ingenol Mebutate on keratinocytes and AK/SCC cells have not been elucidated. We aimed to investigate if ingenol mebutate has specific selective effects on SCC cells compared with healthy keratinocytes.

Methods:
Direct effects on cell functionality were addressed by analyzing viability and proliferation by MTT assay and BrdU incorporation. We performed a gene expression microarray to analyze differential gene expression patterns upon treatment in keratinocytes and SCC cells. Protein kinase C and ERK1/2 were blocked by either a specific inhibitor or siRNA . Gene expression was analyzed by RT-PCR.

Results:
We found a direct effect of ingenol mebutate on viability and proliferation of both keratinocytes and SCC cells. Treatment of keratinocytes and SCC cells lead to an activation of protein kinase C delta (PKCd) and ERK1/2. Inhibition of PKCd or ERK1/2 by a specific inhibitor therefor rescues the drug-dependent loss of cell viability and proliferation capacity. In a gene expression microarray we found most genes affected at a drug concentration of 100 nM. From these genes we selected some highly upregulated genes, DEFB4A, IL1R2, IL13RA2, S100A7A, MMP1 to investigate the overall mechanism of action of the drug. In further experiments we found the expression of these five genes were fully inhibited by blocking PKC.

Conclusion:
Ingenol mebutate induces a direct effect on keratinocytes and SCC cells, dependent on PKCd and ERK1/2 signaling. Further experiments will show in which extend the selected genes from the microarray are involved in these processes and whether they play an essential role in the mechanism of action of ingenol mebutate.

2160

M. Einsiedler[1], V. Chandrasekar[1], T. O'Connor[1], S. Yaganoglu[1], A. Lau[1], A. Aguzzi[1]

Glia-Dependent Non-Cell Autonomous Toxicity in Prion Disease

Neuropathology, Neuropathology, Zürich[1]

Introduction:
Prion diseases are infectious neurodegenerative disorders that can affect humans (e.g. Creutzfeldt-Jakob disease (CJD)) and a broad range of animals, including bovine spongiform encephalopathy (BSE) in cattle and scrapie in sheep. Currently, the molecular mechanisms that lead to neurotoxicity in prion diseases are poorly characterized; however, the expression of the cellular prion protein PrP^C is absolutely necessary for neurodegeneration. Recent publications suggest that the pathology of neurodegenerative diseases is mainly non-cell autonomous, meaning that neuronal cell loss is influenced by mutant protein expression or toxicity in neuronal and non-neuronal cell types in the vicinity of the affected neurons. This also seems valid for prion-mediated neurodegeneration since toxicity in primary neurons can only be achieved in the presence of glial cells.

Methods:
In slice culture, the PrP antibody POM1 appears to mimic prion-induced neurotoxicity; therefore, this antibody was used to induce neurodegeneration in *Tga20* primary cortical neurons that overexpress PrP^C. The neurons were treated with POM1 in the presence or absence of glial cells or with astrocyte-conditioned medium. For the evaluation of neurodegeneration, cell viability assays were done. To further characterize POM1-induced cell death, experiments with embryonic stem cell (ESC) derived neurons will also be performed. Using fluorescently labeled neurons or cells that express a fluorescent marker under the control of a neuronal promoter, more subtle changes like neurite outgrowth and soma size will be detected by microscopy. To identify the astrocyte secreted factor leading to neuronal cell death, depletion of specific molecule classes from the astrocyte media and further downstream analyses will be performed. In addition, the examination of signaling pathways involved in POM1-mediated toxicity will be done with RNA sequencing and results will be confirmed with qRT-PCR and western blot.

Results:
POM1 treatment of a pure neuronal culture has no effect on cell viability. However, in an astrocyte-neuron co-culture and in the presence of astrocyte conditioned media, POM1-induced neurodegeneration was observed. This leads to the suggestion that POM1-mediated cell death is non-cell autonomous and astrocytes may secrete one or more factors that enable POM1 neurotoxicity.

Conclusion:
One of the limiting factors for the treatment of prion diseases and many other neurodegenerative diseases is that the signaling pathways that underlie neurodegeneration are poorly understood. POM1 treatment of an astrocyte-neuron co-culture seems to a useful model to mimic prion disease in a high-throughput manner. Moreover, the signaling pathways involved in prion diseases might play a role in other neurodegenerative diseases and improve the treatment options for these diseases as well.

2161

M. Einsiedler[1], V. Chandrasekar[1], T. O'Connor[1], S. Yaganoglu[1], A. Lau[1], A. Aguzzi[1]

Glia-Dependent Non-Cell Autonomous Toxicity in Prion Disease

Pathology, Neuropathology, Zürich[1]

Introduction:
Prion diseases are infectious neurodegenerative disorders that can affect humans (e.g. Creutzfeldt-Jakob disease (CJD)) and a broad range of animals, including bovine spongiform encephalopathy (BSE) in cattle and scrapie in sheep. Currently, the molecular mechanisms that lead to neurotoxicity in prion diseases are poorly characterized; however, the expression of the cellular prion protein PrP^C is absolutely necessary for neurodegeneration. Recent publications suggest that the pathology of neurodegenerative diseases is mainly non-cell autonomous, meaning that neuronal cell loss is influenced by mutant protein expression or toxicity in neuronal and non-neuronal cell types in the vicinity of the affected neurons. This also seems valid for prion-mediated neurodegeneration since toxicity in primary neurons can only be achieved in the presence of glial cells.

Methods:
In slice culture, the PrP antibody POM1 appears to mimic prion-induced neurotoxicity; therefore, this antibody was used to induce neurodegeneration in *Tga20* primary cortical neurons that overexpress PrP^C. The neurons were treated with POM1 in the presence or absence of glial cells or with astrocyte-conditioned medium. For the evaluation of neurodegeneration, cell viability assays were done. To further characterize POM1-induced cell death, experiments with embryonic stem cell (ESC) derived neurons will also be performed. Using fluorescently labeled neurons or cells that express a fluorescent marker under the control of a neuronal promoter, more subtle changes like neurite outgrowth and soma size will be detected by microscopy. To identify the astrocyte secreted factor leading to neuronal cell death, depletion of specific molecule classes from the astrocyte media and further downstream analyses will be performed. In addition, the examination of signaling pathways involved in POM1-mediated toxicity will be done with RNA sequencing and results will be confirmed with qRT-PCR and western blot.

Results:
POM1 treatment of a pure neuronal culture has no effect on cell viability. However, in an astrocyte-neuron co-culture and in the presence of astrocyte conditioned media, POM1-induced neurodegeneration was observed. This leads to the suggestion that POM1-mediated cell death is non-cell autonomous and astrocytes may secrete one or more factors that enable POM1 neurotoxicity.

Conclusion:
One of the limiting factors for the treatment of prion diseases and many other neurodegenerative diseases is that the signaling pathways that underlie neurodegeneration are poorly understood. POM1 treatment of an astrocyte-neuron co-culture seems to a useful model to mimic prion disease in a high-throughput manner. Moreover, the signaling pathways involved in prion diseases might play a role in other neurodegenerative diseases and improve the treatment options for these diseases as well.

2162

M. Linecker[1], E. Kachaylo[1], P. Limani[1], AC. Piguet[2], C. Tschuor[1], DA. Raptis[1], M. Foti[3], R. Graf[1], JF. Dufour[2], A. Vuck[1], P. Kambakamba[1], P. Kron[1], B. Humar[1], PA. Clavien[1]

The impact of exercise and ω3- fatty acids on ischemia reperfusion injury and regeneration of fatty liver

Visceral and Transplantation Surgery, University Hospital Zürich, Zürich[1], Hepatology, Department of Clinical Research, Berne[2], Department of Cellular Physiology and Metabolism, Geneva[3]

Introduction:
The Western life style is associated with a surge in the number of patients that present with obesity and/or fatty liver (steatosis). Hepatic lipid accumulation increases the risk of hepatocellular carcinoma and hence contributes to an increased demand for liver surgery. However, steatosis enhances the sensitivity of liver towards ischemia reperfusion injury (IRI) and slows its regeneration (LR), thereby increasing postoperative complications. Both exercise and ω3- polyunsaturated fatty acids (n3-PUFAs) are known to reverse steatosis, but their effects on IRI and regeneration in fatty livers are less clear.

Methods:
We are investigating the impact of daily exercise and n3-PUFA on hepatic IRI and regeneration in lean mice and mice with high fat diet-induced steatosis. Whilst exercise increases energy expenditure, the effects of n3-PUFAs on energy metabolism need clarification. Experimental steatosis was induced by feeding mice a high fat diet for 6 weeks. Mice were consecutively treated for 4 weeks through caloric restriction (fat content reduction 60 to 45kJ%) combined with either n3-PUFA supplementation (20% of the 45kJ%) or daily exercise (1h).

Results:
Both treatments markedly reduced steatosis and IRI, whilst their impact on regeneration after 70% hepatectomy needs further analysis. In a *second* step, we are investigating key molecules governing fat metabolism including the PI3K-PTEN-mTOR pathway, FOXA2 and GPR120 to identify potential downstream mechanisms of the anti-steatotic n3-PUVA action. *Thirdly*, we aim on the therapeutic potential of this treatment towards NAFLD-NASH-HCC progression in inducible PTEN -/- mice and in a syngeneic HCC mouse model.

Conclusion:
Any intervention that can safely reduce hepatic fat accumulation and mitigate IRI without negatively affecting the regenerative capacity would be most welcome in the clinic. Inasmuch n3-PUFA acids can substitute the beneficial effects of exercising is another point of interest, as regular exercise will always remain limited in its therapeutic potential due to matters of compliance and the critical health state of obese individuals. The identification of key pathways underlying the beneficial effects of n3-PUFAs may provide new alternatives for a therapeutic intervention.

2163

K. Grabliauskaite[1], S. Sonda[1], E. Saponara[1], T. Reding Graf[1], R. Graf[1]

Loss of p21WAF1/Cip1 accelerates senescence and acinar-to-ductal metaplasia formation during pancreatitis

Department of Surgical Research, University Hospital Zurich[1]

Introduction:
Transdifferentiation of pancreatic acinar cells into ductal-like lesions, a process defined as acinar-to-ductal metaplasia (ADM), is observed during organ regeneration following pancreatitis. ADM is found in association with pre-malignant PanIN lesions and correlates with an increased risk of pancreatic adenocarcinoma (PDAC). Human PDAC samples show down-regulation of $p21^{WAF1/Cip1}$, a key regulator of cell cycle and cell differentiation. Here we investigated whether $p21^{WAF1/Cip1}$ down-regulation is implicated in controlling the early events of acinar cell trans-differentiation and ADM formation.

Methods:
Pancreatitis was induced in wild type (WT) and $p21^{WAF1/Cip1}$ deficient ($p21^{-/-}$) mice by multiple injections of cerulein. Recovery from pancreatitis was analyzed in mice one week after termination of cerulein treatment. The expression of proliferation markers, cell cycle regulators, and the severity of tissue inflammation and fibrosis were analyzed by immunohistochemistry, western blotting and qRT-PCR.

Results:
During pancreatitis, we found that $p21^{WAF1/Cip1}$ was strongly up-regulated in WT acinar cells but absent in cells forming ADM. $p21^{-/-}$ mice showed a significant increase in the number and size of ADM. In addition, the loss of $p21^{WAF1/Cip1}$ did not increase cell replication rates but resulted in a compensatory activation of positive and negative cell cycle regulators. Furthermore, loss of $p21^{WAF1/Cip1}$ resulted in increased expression and re-localization of b-catenin during both pancreatitis and subsequent recovery phase. Finally, loss of $p21^{WAF1/Cip1}$ was accompanied by increased DNA damage and development of senescence.

Conclusion:
Our findings reveal that $p21^{WAF1/Cip1}$ is a gate-keeper of acinar cell de-differentiation, ADM formation and prevents activation of senescence program during pancreatic regeneration.

2164

K. Grabliauskaite[1], S. Sonda[1], E. Saponara[1], T. Reding Graf[1], R. Graf[1]

Acinar-specific TGF-b signalling regulates acinar cell regeneration

Department of Surgical Research, University Hospital Zurich[1]

Introduction:
TGF-ß signalling is implicated in regeneration and fibrosis of pancreatic cells. However, the function of TGF-ß signalling is strongly context-dependent and an acinar cell specific role of this molecule in modulating regeneration has not been completely investigated before. In this study we aimed to determine the contribution of TGF-ß signalling to acinar cell regeneration during pancreatitis by using mice deficient in TGF-ß receptor II (TGFßRII$^{fl/fl}$?) in acinar cells.

Methods:
Pancreatitis was induced in control and PTF1a-Cre^{Tg}; TGFßRII$^{fl/fl}$ mice by multiple injections of cerulein. The expression of proliferation markers, cell cycle regulators, and the severity of tissue inflammation and fibrosis were analysed by immunohistochemistry, western blotting and qRT-PCR.

Results:
Our analyses revealed formation of extended acinar-to-ductal metaplasia (ADM) in TGFßRII$^{fl/fl}$ mice together with increased expression of AKT, a protein involved in ADM development. Smad3 activation, which is capable to inhibit AKT, was not observed in TGFßRII$^{fl/fl}$ compared to control group animals. Furthermore, the lack of TGF-ß receptor II resulted in an increased number of proliferating acinar cells. Concurrently, the expression of the cell cycle inhibitor p16INK4a, a TGF-ß signalling target, was selectively reduced. In addition, we observed higher stellate cells activation and stronger fibrosis accompanied by a robust inflammation in TGFßRII$^{fl/fl}$ mice compared to control animals.

Conclusion:
Our data revealed that TGF-ß signalling prevents excessive ADM formation and inhibits activation of acinar cell cycle. Additionally, loss of TGF-ß signalling in acinar cells potentiates fibrogenic processes during pancreatitis, suggesting the existence of a regulatory feedback between acinar and stellate cells.

2165

L. Rigassi[1], Y. Plutino[1], F. Barchiesi[1], N. Simigdala[2], B. Imthurn[1], R. Dubey[1]

Regulation of microRNAs in Endothelial Progenitor Cells (EPCs) by Sex Steroids

Clinic for Reproductive Endocrinology, Department of Obstetrics and Gynecology, University Hospital of Zurich[1], The Institute of Cancer Research, London[2]

Introduction:
Recent studies provide evidence that small non-coding RNAs termed microRNA (miRNA) are involved in many clinically relevant biological and pathophysiological processes. They regulate cell differentiation, proliferation, migration and apoptosis in many cell types, including the cardiovascular system. Importantly, miRNAs also serve as mediators for several growth factors and inhibitors. Vascular remodeling associated with cardiovascular disease involves endothelial damage/dysfunction and abnormal growth of smooth muscle cells (SMCs). Moreover, miRNAs are known to influence EC function and SMC growth. Therefore, it is feasible that processes associated with vaso-protection and vascular repair are mediated by miRNA modulation. Since sex steroids like estrogen are known to protect women against vasoocclusive disorders by promoting endothelial repair/recovery and inhibiting SMC growth, we hypothesize that the vasoprotective actions of sex steroids may in part be mediated via modulation of miRNAs. In the present study, using EPCs (known to participate in EC repair), we investigated and screened the miRNAs that are regulated by male and female sex hormones DHT and Estradiol. Moreover, we assessed the role of nuclear receptor, membrane receptor and non-receptor pathways in regulating specific miRNAs. Finally, differential regulation by male and female hormones was also documented.

Methods:
Human EPCs were treated with or without Estradiol (E2), DHT, membrane ER (GPER) agonist G1 or E2 metabolite 2-Methoxyestradiol (2-ME) prior to small RNA extraction. Using Illumina HiSeq (Functional Genomics Centre at UZH/ETHZ), we generated small RNA libraries and focused our analysis on significantly regulated miRNAs.

Results:
MicroRNAs were regulated by both male and female sex steroids. E2 increased the expression of miR-146a/b, while decreasing the level of miR-494 and miR-335. DHT stimulated miR-494, miR-376a and miR-877 and downregulated miR-151b, miR-409 and miR-146a. Interestingly, expression of many miRNAs was differentially regulated by E2 and DHT (miR-494, miR-376a, miR-877 and miR-146a). G1 largely mimicked the effects of E2 on miRNAs modulation compared to control with differential regulation of only two miRNAs. 2-ME, an endogenous E2 metabolite with no binding affinity for ER was used to assess the role of ER-independent pathway. Compared to E2, 2-ME upregulated miR-376a, miR-494 and miR-877 and reduced miR-151b, miR-409 and miR-501. Interestingly, 2-ME and DHT had similar effects on the modulation of miRNAs in EPCs, except for two miRNAs that were differentially regulated.

Conclusion:
Here, we provide evidence that sex steroids modulate miRNA expression in EPCs, suggesting a role for miRNAs in mediating E2 and DHT actions in vascular remodeling. Interestingly, female and male hormones regulated miRNAs expression in contrasting fashion, implying that they may differentially influence EPC function. This notion is supported by the fact that 2-ME (known to inhibit EPC function) mimics the effects of DHT on expression of miRNAs. We also demonstrate that both membrane ERs and ER-independent pathways are involved as both G1 and 2-ME regulated miRNAs. Finally, G1 mimicked the effects of E2 on miRNAs, suggesting a role or cross-talk between membrane and nuclear ER

in miRNA regulation. In conclusion, miRNAs regulated by sex-steroids may influence/define their effects on the cardiovascular system and needs to be further investigated.

2166

A. Cee[1], K. Atrott[1], M. Fried[1], G. Rogler[1], I. Frey-Wagner[1]

Tissue specific overexpression of Nrf2 worsens acute but not chronic intestinal inflammation.

Gastroenterolgy, University Hospital Zürich, Zürich[1]

Introduction:
The transcription factor NF-E2-related factor 2 (Nrf2) is an important modulator of the cellular antioxidative response. So far its cytoprotective function has been well established, yet some recent studies indicate negative effects of Nrf2 overexpression. In inflammatory bowel disease (IBD) the regulation of reactive oxygen species (ROS) detoxification is of high interest, because the mucosa of IBD patients is infiltrated by macrophages leading to a massive overproduction of ROS. This oxidative burst contributes to tissue destruction and epithelial permeability, but at the same time is required for effective antibacterial defense.
In previous studies we showed a worsening of experimental DSS induced acute colitis in mice overexpressing Nrf2 either in epithelial cells or the myeloid cell lineage. To gain a better insight into the role of Nrf2 overexpression on mucosal inflammation, we studied now the effect of Nrf2 overexpression in a chronic model of colitis.

Methods:
For this purpose we used transgenic mice conditionally expressing a constitutively active form of Nrf2 (caNrf2) either in epithelial cells (VilCre-CMVcaNrf2 mice) or in the myeloid cell lineage (LysMCre-CMVcaNrf2 mice). To induce chronic mucosal inflammation we crossbred those animals into IL-10 knockout mice that spontaneously develop colitis. Animals were monitored for the occurrence of rectal prolapse. Mice were sacrificed and body weight, colon length and spleen weight were assessed.

Results:
No difference was found in the prolapse rate of male VilCre-CMVcaNrf2/IL-10-/- mice compared to controls, whereas female VilCre-CMVcaNrf2/IL-10-/- mice showed a trend towards less prolapse occurrence (15% versus 21%). Also for male mice overexpressing Nrf2 in myeloid cells no differences in in prolapse rate could be observed. Again female mice had slightly reduced rate of prolapses that was not significantly different from control (15% versus 24%).
After eight weeks animals that had not yet developed a prolapse were euthanized. No differences in body weight, colon length and spleen weight were observed in VilCre-CMVcaNrf2/IL-10-/- or in LysMCre-CMVcaNrf2/IL-10-/- mice. The histological scoring of H&E stained sections of distal colon did not differ between VilCre or VilCre-CMVcaNrf2 mice with IL-$10^{-/-}$ background, whereas female LysMCre-CMVcaNrf2 mice showed a significant reduced histological score compared to control.

Conclusion:
In contrast to an acute DSS induced model of mucosal inflammation there is no evidence for a worsening of inflammation in animals overexpressing Nrf2 in epithelial cells or myeloid cells with an *IL-$10^{-/-}$* background. This finding indicates that the deleterious effect of an induced antioxidative response are limited to acute insults of the colon and does not influence the outcome of a chronic inflammation.

2167

A. Kashyap[1], E. Delamarche[2], P. Schraml[1], G V. Kaigala[2], A. Soltermann[1]

Local DNA extraction from tissue sections using the Microfluidic Probe for mutation profiling of tumors

Institute for Surgical Pathology, University Hospital Zurich[1], IBM Research GmbH, Ruschlikon[2]

Introduction:
The intra and inter-tumoral heterogeneity within a malignant tumor manifests by close spatial co-existence of different cell populations (cancerous and native) and their respective microenvironments. This heterogeneity is a consequence of uncontrolled growth, for example through multimodal pathways, differentiation trees, clonal evolution. Most of the data analyzed and abstracted from these often-scarce samples, have information on the target cells diluted with non-target cells, thereby influencing the accuracy of the information. A reduced accuracy translates to challenges in selection of treatment modalities and application of personalized medicine strategies. Local molecular profiling is one method through which these challenges can potentially be addressed.

Methods:
Traditionally, localized profiling on tissue sections is performed by needle biopsies (punch core) or laser microdissection which usually involves some form of direct contact with the tissue. The sampled tissue is then digested and the molecule of interest (e.g. DNA, RNA) isolated for further analysis, steps that constitute a workflow. A non-contact localized DNA extraction assay from tissue sections was developed by the co-adaption of the associated pathology workflow and the Microfluidic Probe (MFP). The MFP is a non-contact, scanning technology developed at IBM, which spatially confines nanoliter volumes of chemicals hydrodynamically on biological surfaces at the *micrometer* length-scale in an aqueous environment.

Results:
By means of developing chemical, fluidic and thermal systems in concert with the MFP, decellularization was achieved on cell-block sections in an area of 100 × 100 μm within 1 min of confinement of the chemical system. Further, it was also shown that the DNA extracted from the resulting local sample was compatible with amplification and Sanger sequencing for mutation analysis. Using the developed assay, the BRAF V600E mutation, which is of prognostic significance in melanoma and non-small cell lung cancer (NSCLC), was detected in less than 150 cells from a cell block section with BRAF V600E+ cells. A preliminary study of the application of the developed assay was further carried out on NSCLC tumor sections, showing its applicability on native tumor tissue.

Conclusion:
The described work provides a platform to perform non-contact local profiling of single tumor sections, which has the potential of yielding a higher sensitivity, specificity and selectivity of information to aid cancer research and diagnosis.

2168

US. Herrmann[1], A. Schütz[3], D. Saban[1], M. Nuvolone[1], H. Shirani[2], D. Huang[4], B. Li[1], B. Ballmer[1], A. Aslund[2], J. Mason[2], EJ. Rushing[1], H. Budka[1], P. Hammarstrom[2], A. Böckmann[5], KP. Nilsson[2], A. Caflisch[4], B. Meier[3], S. Hornemann[1], A. Aguzzi[1]

The antiprion activity of polythiophenes is specified by regioregular ionic bonds to amyloid

Institute of Neuropathology, University Hospital Zurich, CH-8091 Zurich[1], Department of Chemistry, University of Linköping, Sweden[2], Department of Chemistry and Applied Biosciences, ETH Zurich, 8093 Zurich[3], Department of Biochemistry, University of Zurich, CH-8057 Zurich[4], IBP, UMR 5086 CNRS/Université de Lyon 1, 69367 Lyon, France[5]

Introduction:
Prion diseases are untreatable and fatal neurodegenerative diseases involving the accumulation of misfolded endogenous prion protein (PrP^{Sc}). *In vitro* evidence suggests that prion fibrils have an in register beta-sheet conformation, but the *in vivo* conformation of prion fibrils is not defined; hence developing specific inhibitors remains challenging. Luminescent conjugated polythiophenes (LCPs) are small, easily synthesizable fluorochromes that bind to ordered protein aggregates and suppress prion replication *in vitro*. Here we explored the structure-activity relationship of LCPs administered to prion-infected mice via osmotic minipumps.

Methods:
We administered a panel of structurally diverse LCPs into the brains of prion-infected mice using osmotic minipumps and monitored prion incubation times. Based on preliminary findings, we designed LCPs with modified side chains and tested their efficacy in preventing prion-mediated toxicity *in vivo*. Using these data and solid-state nuclear magnetic resonance analyses, we developed an *in silico* model of LCP-prion fibril binding with the assumption of an in register beta-sheet structure. We predicted the efficacy of newly designed LCPs to prevent prion toxicity with this model and tested these predictions *in vivo*.

Results:
LCPs with certain terminal functional groups showed increased prion incubation times when applied in mice prophylactically (+36%; p=0.031). We confirmed these findings with second generation LCPs and demonstrated that these functional groups are critical for LCP anti-prion function. Solid-state nuclear magnetic resonance analyses and atomistic simulations revealed that these residues interacted with complementary, regularly spaced cationic residues of amyloids. These parameters were then used to design improved binders with dramatically improved potency *in vivo (+87.5%; p<0.001)*.

Conclusion:
These results support the in-register β-sheet structural model of the misfolded prion protein PrP^{Sc}, and demonstrate the feasibility of rational chemical design of drugs against protein aggregation diseases.

2169

E. Eschmann[1], PE. Beeler[1], J. Blaser[1]

An Ongoing Cluster Randomized Trial to Assess the Effect of Specific Alerts in Potassium-Increasing Drug-Drug Interactions

Medical Informatics Research Centre, Directorate of Research and Education, University Hospital, Zurich[1]

Introduction:
Alerts for preventing hyperkalemia (serum potassium ≥5.5mEq/l) during potassium-increasing drug-drug-interactions (DDIs) are often ignored due to their low specificity. This retrospective analysis aimed at the development of highly specific alerts. The impact of the novel alerting concept will be assessed in a prospective clinical trial.

Methods:
Data of all inpatients admitted to the University Hospital Zurich between 12/1/2009-12/31/2011 were included. Generalized additive models were used to identify crucial interacting parameters. Their efficacy to detect potassium-increasing DDIs inducing hyperkalemia was retrospectively validated. Alert thresholds were defined by applying Youden's J statistic on ROC curves. ROC curves were compared with Delong's test.

Results:
We analyzed 1.5 million drug orders of 76,467 patients and identified 8,431 potassium-increasing DDIs resulting in 151 hyperkalemias. Table 1 compares common alerts (A_{none}, A_{K+}) and novel alerts (A_{opt}, B_{K+}, B_{opt}). The A-alert rules (A_{none}, A_{K+}, A_{opt}) were applied at onset of each potassium-increasing DDI. In contrast, B-alert rules (B_{K+}, B_{opt}) were computed at onset of the DDI and again for each serum potassium level measured during the DDI.
Table 1. Comparison of 5 alerting concepts.

Triggering event	Alerting for	Label	Parameters considered	Sensitivity	Specificity
start of DDI	risk of hyper-kalemia during the entire period of DDI	A_{none}	none	100.0%	0.0%
		A_{K+}	last serum potassium before onset of DDI ≥4.2mEq/l	54.8%	68.6%
		A_{opt}	9 patient parameters	59.4%	71.6%
start of DDI and each serum potassium measurement during DDI	risk of hyper-kalemia within the next 48h	B_{K+}	current serum potassium ≥4.4mEq/l	70.5%	76.5%
		B_{opt}	11 patient parameters	75.6%	72.4%

The commonly used alert A_{none}, i.e. systematically alerting at onset of each potassium-increasing DDI, is unspecific. The A_{K+} concept restricting alerts to the presence of potassium levels above a threshold provides increased specificity and limited sensitivity.
Compared to A_{K+}, the proposed novel alerts A_{opt}, B_{K+} and B_{opt} increase both sensitivity and specificity: Including 8 patient parameters in addition to the last serum potassium level significantly improved the effectiveness (A_{opt} vs. A_{K+}; p=0.024). Focusing on short-term predictions of hyperkalemia occurring within the next 48h further increased sensitivity and specificity (B_{K+} vs. any A alert; p<0.05). However, short-term predictions considering further patient parameters in addition to the current serum potassium level did not provide significant improvements (B_{opt} vs. B_{K+}: p=0.056).
Therefore, the alerting concept B_{K+} is currently investigated in a cluster randomized trial. From 1/1/2014 to 12/31/2014, the 14 clinics of the intervention group will provide

hyperkalemia warnings displayed as non-interruptive bar within the top section of the electronic health record. In the 15 clinics of the control group the hyperkalemia warnings will remain suppressed.

Conclusion:
Specificity of electronic hyperkalemia warnings may be improved by focusing on periodic short-term predictions based on serum potassium monitoring. An ongoing cluster randomized trial will assess whether this concept reduces alert fatigue and increases patient safety.

2170

RC. Gerosa[1], S. Boettcher[1], MG. Manz[1]

The regulatory role of non-hematopoietic bone marrow cells in steady-state and during hematopoietic stress

Division of Hematology, University Hospital Zurich, Zurich[1]

Introduction:
Hematopoietic stem cells (HSC) are characterized by the general hallmarks of "stemness", i.e. self-renewal and multipotency. They are located in the bone marrow (BM) surrounded by different types of supportive cells. Accumulating evidence suggests that important HSC-extrinsic regulatory mechanisms have evolved to maintain stemness but also to guide HSC differentiation according to the fluctuating demand for mature cells. We set out to study how the BM microenvironment supports the hematopoietic system in adaptation to infection.

Methods:
After stimulation with LPS or polyIC to mimick gram-negative bacterial or viral infection in wild-type (WT) mice, respectively, we isolated different non-hematopoietic BM cell populations and determined their gene expression profiles compared to steady-state WT mice using microarray analysis.

Results:
We focused primarily on soluble factors to identify potential extrinsic regulators of the hematopoietic system during the adaptation to infection. We revealed that Il6 is significantly and specifically upregulated during LPS stimulation by a BM stromal cell population called CARs (CXCL12-abundant reticular cells).

Conclusion:
Given the available data on Il6 function on early hematopoietic stem and progenitor cells (HSPCs), we hypothesize that Il6 upregulation during bacterial infection eventually leads to promote HSC differentiation into hematopoietic progenitors. We could confirm the microarray data using qRTPCR and are currently functionally validating *in vivo* the importance of Il6 with regard to its ability to support hematopoiesis in steady-state and during inflammation. The mechanisms regulating HSCs extrinsically are of high relevance as these findings might lead to new therapeutic applications to treat diseases.

2171

AKK. Lakkaraju[1], H. Budka[1], P. Liberski[2], A. Aguzzi[1]

Molecular mechanisms involved in the development of spongiform phenotype and neurotoxicity in prion infections.

1. Institute for Neuropathology, Universitatsspital Zurich, Switzerland[1], 2. Medical University of Lodz, Lodz, Poland[2]

Introduction:
Mammalian cellular prion protein (PrP^C) is a GPI anchored protein expressed on the cell surface of most cells. It has been implicated in several transmissible spongiform encephalopathies or prion diseases, like: Creutzfeldt-Jakob disease (CJD) etc. It is one of the hallmark diseases of the protein folding disorders (PMA) where the cellular PrP^C is converted into a toxic aggregate (PrP^{SC}). The prion encephalopathies are commonly characterized by the neuropathological changes, which include astrocytosis, neuronal loss and development of amyloid plaques. A characteristic feature of prion-infected brains is the presence of spongiform encephalopathy characterized by the presence of large membrane bound vacuoles. Previous studies have suggested that the vacuolation phenotype observed in the infected brains is a result of functional depletion of mahogunin, an E3 ubiquitin ligase. However, recent in vivo studies have shown that changes in the levels of mahogunin do not play a significant role in the pathogenesis of prion infections. Significant evidence has been developing that prion infections are associated with activation of ER stress and by using specific inhibitors against ER stress the symptoms of prion infections can be alleviated. A set of proteins regulating the endolysosome maturation have been shown to be downregulated by ER stress according to various micro array data available on Geoprofiles and our preliminary experimental results. More recent studies have shown that mice lacking either PIKFYVE or SAC3 proteins develop vacuoles and exhibit a spongiform phenotype. Both PIKFYVE and SAC3 are found in a complex along with VAC14 and regulate the endosome fusion. PIKFYVE is a PtdIns mono-phosphate (PIP) kinase which phosphorylates PtdIns(3)P to generate PI(3,5)P2. PI(3,5)P2 is thought to be a key player in the regulation of endomembrane homeostasis regulating the fusion and fission of endosomes. We hypothesize that the vacuolation phenotype is a result of modulation of the endo-lysosomal machinery, which ultimately leads to development of toxicity and appearance of spongiform phenotype. Understanding the molecular mechanism of these events would give us an enlightened view of prion infections and would help us in targeting specific factors that are involved in causing neurotoxicity.

Methods:
To understand the molecular mechanism involved in the formation of spongiform vacuoles we will be using BL6 mice and infect them with Rocky mountain laboratory lysate (RML) prions. Similar experiments will also be performed on the organotypic slice cultures prepared from the brains of BL6 mice, followed by the infection with RML or treatment with anti-prion antibody (POM1) that was shown to mimic prion infection. The brain sections from mice will be monitored by immunohistochemistry, electron microscopy for the loss of PIKfyve protein. *In vitro* biochemical assays will be done in the cell lines to understand mechanistic details of the role of PIKfyve in generating spongiform phenotype.

Results:
The initial results from western blot analysis suggest that PIKfyve protein is downregulated upon prion infection or in samples treated with POM1 antibody. These results suggest that vacuolation phenotype observed could be a result of alteration of the endosomal maturation pathway.

Conclusion:
From the initial results we have obtained we can hypothesize that the appearance of the spongiform phenotype could be possibly because of the depletion of PI(3,5)P2 which requires PIKfyve for its synthesis. Molecular dissection of the pathways associated with PI(3,5)P2 could help us in understanding the vacuolation phenotype observed in prion infections and also shed light on the neurotoxicity induced by prions.

2172

K J. Nytko[1], K J. Pruschy[1]

Dynamic Changes of Tumor Hypoxia under Treatment with Ionizing Radiation

University Hospital Zurich, Radiation Oncology, Laboratory for Molecular Radiobiology, Clinical Research Priority Program (KFSP) Tumor Oxygenation[1]

Introduction:
Hypoxia is a hallmark of many solid malignancies and confers resistance to radiotherapy as well as other treatment regimens. Tumor hypoxia correlates with high aggressiveness, increased metastatic potential and overall poor prognosis. Independent of the cellular genotype, hypoxic cells are more radiation resistant than normoxic cells. Better understanding of tumor oxygenation before and during treatment with ionizing radiation could potentially lead to the development of improved diagnostics and new therapeutic options.

Methods:
We investigated the dynamics of tumor hypoxia in response to low dose fractionated irradiation and high dose hypofractionation *in vitro* and *in vivo,* using *the* lung carcinoma cell line A549, which was stably transfected with an oxygen-dependent luciferase reporter gene. Blood samples and tumor specimens were collected from xenograft-bearing mice undergoing high dose and fractionated irradiation for secretome and immunohistochemistry studies. Moreover, novel antisignalling agents were tested in combination with ionizing radiation towards the development of new combined treatment modalities.

Results:
Cells treated with high dose irradiation (20 Gy) did not show changes in oxygen-dependent luciferase activity up to 24 hours after irradiation *in vitro*. In contrary, the hypoxia-mimicking agent DMOG increased oxygen-dependent luciferase activity already 2 hours after treatment start in these cells. In tumor xenografts irradiated with 20 Gy, oxygen-dependent luciferase activity was transiently upregulated between days 6-8 after treatment start. No changes or a transient decrease in the oxygen-dependent luciferase activity was observed at the early time points (days 1-5) after high dose irradiation. Tumor xenografts treated with a low dose fractionation regimen (5x3Gy) were monitored daily during treatment and showed fluctuating changes in oxygen-dependent reporter gene activity. The secretion of several angiogenic factors were induced 48 hours after high dose irradiation in mice carrying tumor xenografts.

Conclusion:
Since tumor hypoxia is one of the major factors causing radiation resistance, better understanding of tumor oxygenation during and in response to treatment could lead to improved treatment planning and outcome. Using our bioluminescence-hypoxia reporter in vivo system we could monitor the dynamics of tumor hypoxia with high temporal and spatial resolution. A differential treatment response with regard to hypoxia could be determined in response to high dose and fractionated irradiation. The differential secretion of angiogenic factors in response to high dose irradiation points to the development of a combined treatment modality with ionizing radiation and novel antisignaling agents, which could overcome treatment resistance, especially in hypoxic tumors.

2173

YV. Valko[1], EW. Werth[1], CB. Bockisch[1], PV. Valko[1], KW. Weber[1]

Polysomnography detects benign paroxysmal positional vertigo

Universitätsspital Zürich[1]

Introduction:
Benign paroxysmal positional vertigo (BPPV) is the most common cause of dizziness. Calcium carbonate crystals of the vestibular organ (otoconia) become dislodged from the otolithic membrane and freely float within the endolymphatic fluid of the semicircular canals. Head movements may cause the otoconia to move and to overstimulate the vestibular receptors, thereby causing disabling episodes of vertigo accompanied by nystagmus. Despite the availability of highly effective canalolith repositioning procedures, the condition remains underdiagnosed, which too often means unnecessary long-lasting suffering and dangerous falls. While it is well known that changes of head position in bed often elicit BPPV, video-polysomnography (PSG) has not yet been considered as a tool to detect unrecognized BPPV. Thus, in this study we aimed at evaluating whether PSG has the potential to recognize the occurrence of positional nystagmus.

Methods:
We performed whole-night video-PSG in a patient with frequent nocturnal BPPV attacks. We used a conventional 16-channel recording system containing a built-in, three-dimensional sensor for measurement of body position and movements. The electrode of the left electrooculography (EOG) (E1-M2) was placed at the left outer canthus and slightly above the horizontal plane, and the right EOG (E2-M2) was placed at the right outer canthus and slightly below the horizontal plane in order to detect horizontal and vertical eye movements.

Results:
A 59-year-old woman was admitted to our emergency department because of repeated attacks of rotational vertigo, triggered by head movements while in bed. Supine roll test to the left revealed apogeotropic horizontal nystagmus with a latency of several seconds. Supine roll test to the right caused even stronger apogeotropic nystagmus, establishing the diagnosis of left lateral canal cupulolithiasis. Brain magnetic resonance imaging did not reveal any structural abnormality. During whole-night-PSG, we observed six episodes of apogeotropic positional nystagmus precipitated by change of body position. Several episodes with changes of head position but unaltered body position also triggered positional nystagmus. The EOG pattern of positional nystagmus appeared to be highly distinctive – it occurred only during wakefulness, showed a delay of several seconds and a characteristic reversal after change of head position.

Conclusion:
This case provides the first evidence that PSG can detect BPPV in the sleep laboratory. The typical EOG pattern of positional nystagmus should therefore be brought to the attention of sleep specialists, because this cumbersome condition is highly prevalent yet often overlooked, while the diagnosis is easy and treatment is safe, inexpensive and highly effective.

2174

T. Skaria[1], G. Schoedon-Geiser[1]

Wnt5A is a crucial factor for the pro-inflammatory response of human vascular endothelial cells to IL-4

Inflammation Research Unit, Division of Internal Medicine, University Hospital Zurich, Switzerland[1]

Introduction:
Interleukin- (IL-) 4 has recently emerged as an “alternative” inflammatory mediator in Th2 cell mediated immune response to parasitic infections, autoimmune responses and allergy. IL-4 has been associated with tumor inflammation and metastasis in cancers. IL-4 affects functions of the vascular endothelium through mechanisms not fully understood. The present study aims to identify genes and processes regulated by IL-4 signalling in human vascular endothelial cells.

Methods:
Human coronary artery endothelial cells (HCAEC) were treated with recombinant human (rh) IL-4, 4 ng/ml; rhIL-6, 20 U/ml (Peprotech, USA) for 8h. Gene expression profiles were achieved using whole genome 4X44K V2 microarrays (Agilent Tech. Inc.) as described (Schaer C. *et al.*, 2013, *Cell Death Differ.)*. Data acquisition and analysis was conducted as described (Pereira C. *et al.*, 2010, *PLoS One)*. Regulated genes were validated by qRT-PCR. Gene ontology (GO) classification and pathway analyses were conducted using Metacore GeneGO (Thomson Reuters, http://portal.genego.com). HCAEC barrier function was measured using electrical cell substrate impedance sensing (ECIS).

Results:
GO clustering of IL-4 regulated genes according to biologic processes revealed ‘Immune response_Oncostatin M signaling via JAK-Stat in human cells’ as the most significant pathway. Genes significantly up regulated, e.g. *CCL2, IL6ST* and *MMP1* are mainly associated with immune responses involving monocyte-endothelial interactions and *VEGF* involved in endothelial permeability. ‘Development_Regulation of epithelial-to-mesenchymal transition (EMT)’ was the second most significant biological process affected by IL-4. Among genes significantly up- regulated in this pathway map is *Wnt5A*, recently identified as an inflammatory mediator in the vascular system (Pereira *et al*., 2008, *Arterioscler Thromb Vasc Biol.*). The ‘Cytoskeleton remodeling_TGF, Wnt and cytoskeletal remodeling’ pathway was the third most significant biological process affected by IL-4 in HCAEC. Significantly up- regulated genes in this pathway again include *Wnt5A*, *VEGFA* and *FZD*, that latter being involved in Wnt signaling. Among the genes significantly down regulated by IL-4, *LIMK* and *CFL1*, and *KDR* are mainly involved in cytoskeleton remodeling and endothelial permeability, respectively. Refined analysis showed that Wnt5A and VEGF act as the ligands that could trigger and mediate the downstream signaling cascade responsible for remodeling actin cytoskeleton. In a recent study, identical pathways were detected as the biologic process most significantly regulated by paracrine Wnt5A signaling in HCAEC (in preparation). Since IL-4 strongly up-regulated *IL-6* in HCAEC and IL-6 has been suspected to increase endothelial permeability, we investigated if IL-6 impairs barrier integrity of HCAEC monolayers. IL-6 did not significantly alter the barrier properties of HCAEC monolayer in a life real-time analysis by ECIS. In contrast, we identified Wnt5A as mediator of increased permeability of HCAEC monolayers.

Conclusion:
IL-4 signaling strongly induces the expression of Wnt5A in vascular endothelial cells. Downstream targets of Wnt5A are genes involved in cytoskeleton rearrangements and in

endothelial barrier function. Our data indicate that Wnt5A plays a critical role in pro-inflammatory processes associated with increased IL-4 production.

2175

T. Sonati[1], J. Falsig Pedersen[2], R. Reimann[1], S. Hornemann[1], P. Baral[3], B. Wieland[3], M. Swayampakula[3], M. James[3], A. Aguzzi[1]

The flexible tail of the prion protein mediates the toxicity of anti-prion antibodies

Institute of Neuropathology, University Hospital of Zurich, Zurich, Switzerland[1], IRBM-Promidis, Pomezia, Italy[2], Department of Biochemistry, School of Translational Medicine, University of Alberta, Edmonton, Canada[3]

Introduction:
The cellular prion protein (PrP^C) is an extracellular, membrane-anchored protein that is highly abundant in the nervous system, and consists of two domains, an N-terminal flexible tail (FT) and a C-terminal globular domain (GD). Widespread deposition of an aggregated and misfolded isoform of PrP^C, denoted as PrP^{Sc}, is a distinctive hallmark of fatal infectious prion diseases and is accompanied by dramatic neuronal loss. While it is well established that PrP^C is required for PrP^{Sc}-mediated toxicity in prion infections, which suggests a crucial interaction between PrP^{Sc} and PrP^C, the mechanisms by which aggregated prions are lethal to neurons remain a mystery.

Methods:
Fab fragments were generated by ficin digestion and further purified by protein A elution and size exclusion chromatography. Single chain antibodies and recombinant mouse prion proteins were expressed in Escherichia Coli and purified according to standard procedures. Biological effects of antibodies and their derivatives were assessed in brain slice cultures and *in vivo* mostly by quantifying neuronal markers and MRI-lesion profiles respectively. The exact epitope of a toxic GD antibody was determined by X-ray and NMR analyses and affinity binding constants by SPR experiments. Organotypic cerebellar slice cultures were prepared using a vibratome from 9-11 day-old mouse pups (350 µm thick brain sections) according to Falsig and Aguzzi 2008.

Results:
Recently, we established the first ex vivo model of prion disease using cerebellar organotypic cultured slices, which recapitulates all of the major pathological features of a genuine prion infection. Moreover, we mimicked prion-induced neuronal death ex vivo and in vivo with antibodies, and monovalent Fab and single chain Fv derivatives directed against certain epitopes of the GD. The latter approach (“the antibody model”) eliminates the need to work with infectious prions and shortens the timeframe of neurotoxicity. The antibody model and prion infections were characterized by calpain activation and a ROS burst. Furthermore, neuronal death was blocked by pharmacological ROS scavengers and calpain inhibitors, indicating that neuronal death is mediated by similar signaling pathways in both models. GD antibody-mediated neurotoxicity was also prevented by pretreatment with antibodies against the FT and by shortening of the FT, thus designating the FT as the effector module of neuronal death. Congruently, blockade of the FT with specific antibodies was beneficial in genuine prion infections and in mice expressing a truncated toxic PrP variant.

Conclusion:
We have shown that GD antibody-induced neurotoxicity is a good model to study PrP-dependent neurotoxicity that is uncoupled from PrP^{Sc} replication/infectivity. Our results uncovered two PrP modules, the GD as the receptor module of toxic ligands and the FT as the effector module of toxicity. We believe that therapeutic agents interfering with these domains may be a novel option for future drug development to treat prion-mediated neurodegeneration.

2176

PE. Dijkman[1], L. Frese[1], B. Weber[1], A. Driessen-Mol[2], MY. Emmert[1], J. Sherman[3], J. Gruenenfelder[1], N. Cesarovic[1], B. Sanders[2], P. Zilla[3], V. Falk[1], FPT. Baaijens[2], SP. Hoerstrup[1]

Off-the-shelf Decellularized Tissue-Engineered Heart Valves Repopulate and Remodel rapidly in pre-clinical animal models

Division of Surgical Research, University Hospital of Zurich, Zürich, Switzerland[1], Department of Biomedical Engineering, Eindhoven University of Technology, Eindhoven, The Netherlands[2], Cardiovascular Research Unit, Cape Heart Centre, University of Cape Town, South Africa[3]

Introduction:
Xenogenic valve starter matrices are associated with the risk of immunogenic reactions or disease transmission while the availability of allogenic matrices is limited. Living tissue-engineered heart valves (TEHVs) have been successfully created from biodegradable synthetic scaffolds, but are associated with logistical hurdles. Recently, we demonstrated the feasibility of decellularized TEHVs (dTEHVs), based on biodegradable synthetic materials, as an alternative off-the-shelf starter matrix for guided tissue regeneration. Here, we study the functionality and host repopulation capacity of dTEHVs in both an ovine and a non-human primate model.

Methods:
dTEHVs were engineered by decellularization of in-vitro grown TEHVs, based on PGA/P4HB scaffolds seeded with either ovine or human vascular-derived cells. In-vivo pulmonary valve performance was evaluated after trans-apical implantation into the orthotopic pulmonary position of sheep and non-human primates. Control implants were analyzed to validate cell removal and preservation of extracellular matrix. Valves were explanted from sheep after 1 day, 8, 16, and 24 weeks and from primates after 4 and 8 weeks and analyzed for repopulation and remodeling of the dTEHVs by histology, biochemical assessment of tissue composition, and biaxial mechanical tests.

Results:
In sheep valve leaflets became rapidly repopulated with endogenous cells, with first signs of cell infiltration after 5 hours post OP. Moreover, the implants remodeled over time with increasing collagen density and the presence of elastic fibers and endothelialized surfaces, starting in the valvular wall and followed by the leaflets. Mechanical analyses of explanted leaflets showed a trend towards increased anisotropic properties over time, resembling remodeling towards native-like valvular properties. In-vivo performance of dTEHVs was excellent up to 8 weeks, although mild-to-moderate insufficiency developed thereafter. The small valvular insufficiency was also detected in the non-human primates. The dTEHVs revealed mobile and thin leaflets, however, relative leaflet shortening was observed in the primates and beyond 8 weeks follow-up in sheep.

Conclusion:
Here we demonstrate the rapid cellular repopulation and remodeling capacity of dTEHVs with excellent initial valve performance. Changes in valve geometry and therewith enhancing more physiological loading of the leaflets, might overcome the observed reduction in leaflet size over time and therewith preventing valvular insufficiency. These homologous, non-immunogenic, off-the-shelf biomaterials may ultimately overcome the limitations of currently used valve replacements.

2177

K. Drägert[1], I. Bhattacharya[1], E. Haas[1], P. Seebeck[2], U. Held[3], A. Azzi[4], S. Brown[4], M. Hall[5], R. Humar[1], E. Battegay[1]

Adipocyte-specific knockout of rictor impairs anti-contractile properties of PVAT and increases mean arterial pressure in mice

Division of Internal Medicine, University Hospital, Zurich[1], Zurich Integrative Rodent Physiology, University of Zurich, Zurich[2], Horten Center for Patient-Oriented Research and Knowledge Transfer, University of Zurich, Zurich[3], Chronobiology and Sleep Research Group, Institute of Pharmacology and Toxicology, University of Zurich, Zurich[4], Biozentrum, University of Basel, Basel[5]

Introduction:
Mammalian target of rapamycin (mTOR) is a kinase and found in two distinct complexes: mTORC1 and mTORC2. The latter is activated by growth factors (e.g. insulin) and characterized by its adaptor protein RICTOR. mTORC2 controls essential functions in white adipose tissue, while its role in brown-like perivascular adipose tissue (PVAT) is less characterized. PVAT is an important regulator of the vascular tone and we have shown that mTORC2 is required for normal PVAT function. In the present study we focussed on adipose mTORC2's contribution to blood pressure regulation and investigated the diurnal expression of mTORC2 phosphorylation targets and circadian clock genes in PVAT.

Methods:
Experiments were performed with male adipose-specific *rictor* knockout mice (*rictor*$^{ad-/-}$) and control littermates (15-25 weeks of age). Vascular function was assessed *ex vivo* using aortic rings with or without PVAT treated with 5-hydroxytrypthamine (5-HT; 10^{-9}- $3x10^{-6}$ mol/l). Blood pressure recordings were performed using radiofrequency transmitters monitoring hemodynamic parameters over 7 days (n = 5-6). mRNA and protein levels were analyzed using qRT-PCR and Western Blot.

Results:
In *rictor*$^{ad-/-}$ mice, vascular maximal contractions of aortic rings in the presence of PVAT were 2-fold higher after stimulation with 5-HT compared with control mice (43.4% ± 6.8% vs. 26.0% ± 3.5%, n=13). Removal of PVAT resulted overall in increased contraction reaching similar levels in both groups of mice. Blood pressure recordings revealed a significant increase of the mean arterial pressure (MAP; 103.9 ± 1.1 vs. 98.5 ± 1.4 mm Hg) and diastolic arterial pressure (DAP; 94.6 ± 1.4 vs. 90.2 ± 0.6 mm Hg) in *rictor*$^{ad\ -/-}$ mice, while systolic arterial pressure and pulse pressure were not significantly changed. Interestingly, MAP and DAP were slightly elevated in dark as compared to the light period. Expression levels of clock genes were similar in PVAT. Interestingly, mTORC2 phosphorylation targets such as *FoxO1* and *Sgk1* showed diurnal expression pattern which were abolished in *rictor*$^{ad-/-}$ mice.

Conclusion:
mTORC2 in adipose tissue regulates mean arterial pressure potentially by affecting diurnal expression and activation of phosphorylation targets such as *Foxo1*.

2178

D. Kenkel[1], A. Boss[1], M. Wurnig[1], D. Nanz[1], C. Rossi[1]

Whole-body diffusion tensor imaging (DTI)

Department of Diagnostic and Interventional Radiology, University Hospital of Zürich, Switzerland[1]

Introduction:
The purpose of this study was to demonstrate the feasibility of whole-body DTI

Methods:
We performed a whole body DTI on 8 healthy individuals at a 3T Ingenia from Philips showing the mean diffusivity (MD) and fractional anisotropy (FA) values of different tissues and compared them to the values of DTI perfomed by other group focusing specific regions.

Results:
The values of FA and MD obtained in this study are qualitatively consistent with literature values.

Conclusion:
In this study we showed the feasibility of whole body DTI, which might be useful for further studies investigating for example muscle disease such as dystrophy or myositis.

2179

YL. Kok[1], C. Oberle[1], NK. Campbell[1], F. Di Giallonardo[1], C. Leemann[1], H. Kuster[1], B. Joos[1], D. Braun[1], HF. Günthard[1], KJ. Metzner[1]

Replication Capacity of Primary HIV-1 Isolates From Acutely Infected Patients in Macrophages

Division of Infectious Diseases and Hospital Epidemiology, University Hospital Zurich, University of Zurich, Zurich[1]

Introduction:
R5-tropic HIV-1, which utilises the CCR5 chemokine receptor for entry into host cells, generally replicates well in activated primary $CD4^+$ T cells, but its replication capacity in monocyte-derived macrophages (MDMs) is lower and highly variable. The former phenotype in MDMs is likely a result of the physiology of these cells whereas the intrinsic replication capacity of the virus in MDMs may explain the latter observation. Several studies have shown that HIV-1 strains, into which HIV-1 *Env*, or regions containing it, derived from acutely infected patients was cloned, did not replicate efficiently in MDMs. To investigate the replication capacity of wild type R5-tropic HIV-1 in MDMs, we have used primary HIV-1 isolates generated from patients of the Zurich Primary HIV Infection (ZPHI) Study.

Methods:
Primary HIV-1 isolates were generated by co-culturing $CD4^+$ T cells of patients from the ZPHI Study during the acute phase of infection with activated mixed donor $CD8^-$ PBMCs. The 12 patients, 10 of whom were men who have sex with men, selected for this study were all infected with HIV-1 subtype B. R5 tropism was tested with an MT-2 assay and genotypic analysis. To determine the replication capacity of these primary HIV-1 isolates in MDMs, we isolated $CD14^+$ monocytes from 4 different donors that were subsequently differentiated into MDMs. The remaining $CD8^-CD14^-$ PBMCs were mixed and activated. Both cell populations were infected with primary HIV-1 isolates in triplicates per donor. Replication capacity in MDMs was estimated relative to that in $CD8^-$ $CD14^-$ PBMCs. The V1, V2 and V3 loops of *Env* were sequenced with Illumina MiSeq.

Results:
All primary HIV-1 isolates were confirmed to be R5-tropic, except for one, which was a dual-tropic virus. The relative replication capacity of the primary HIV-1 isolates in MDMs ranged from 0.4–22.4% (controls: $HIV\text{-}1_{JR\text{-}FL}$ (R5): 67.0%; $HIV\text{-}1_{NL4\text{-}3}$ (X4): 0.05%). By grouping the primary HIV-1 isolates according to their relative replication capacity in MDMs, we found 7 with low (5%), 2 with intermediate (5–15%), and 3 with high (15%) relative replication capacity. Analysis of the amino acid sequence of the V1, V2 and V3 loops of *Env* of the primary HIV-1 isolates revealed no clear pattern which one could correlate with their replication capacity in MDMs.

Conclusion:
The primary HIV-1 isolates derived from the ZPHI Study replicated in MDMs to a broad degree. A clear pattern in the amino acid sequence of the V1, V2 and V3 loops of *Env* of the primary HIV-1 isolates to predict their replication capacity in MDMs was not evident, suggesting that a redundant combination of amino acid residues in *Env* may be involved and/or the responsible amino acid residues might be located elsewhere in the HIV-1 genome.

2180

JF. Glaus Garzon[1], K. Léger[2], K. Bartnicka[1], I. Jurisica[3], M. Hottiger[2], R. Wenger[1], L. Borsig[1]

The Role of Hypoxia and Inflammation in the Tumor Microenvironment of Colon Carcinoma

Institute of Physiology, University of Zurich, Zurich[1], Institute of Veterinary Biochemistry and Molecular Biology, University Zurich, Switzerland[2], University of Toronto, Toronto, Canada[3]

Introduction:

Colon carcinoma represents one of the most frequent cancers, associated with high mortality, mainly due to liver metastasis. Development of hypoxic zones within the tumor is linked to poor prognosis.

Methods:

We established an orthotopic syngeneic model of colon carcinoma by injecting MC-38 cells constitutively expressing GFP into the cecum of C57BL/6 mice. We injected MC-38GFP cells with silenced HIF-1α expression. Mice developed primary tumors after four weeks of the injection. Tumors were harvested at this time point for further analysis using flow cytometry and histology.

Results:

The preliminary results show that the mice injected with MC-38GFP-HIF1α -KD cells developed smaller tumors than mice injected with MC-38GFP-Mock cells. The percentage of neutrophils was decreased in primary tumors of mice injected with silenced HIF-1α MC-38GFP cells. The percentage of macrophages in HIF-1α tumors was increased. In addition, differences in phenotype (M1 markers versus M2 markers) have been detected. This phenotypic difference must be confirmed by cytokine profiling. Histological analysis of pimonidazole staining reveals that Mock tumors have an increased percentage of hypoxic zones compared to HIF1α-KD tumors.

Conclusion:

Based on deep sequencing data of MC-38GFP cells and protein-protein-interaction network analysis, we are investigating the link between inflammation and hypoxia in tumor development and metastasis and validating identified targets.

2181

A. Hegglin[1], S. Mikkat[2], M. Russ[2], M. Kreutzer[2], B. Vollmar[3], P. Giovanoli[1], MO. Glocker[2], N. Lindenblatt[1]

Rho-GDI 2-connected signalling during skin graft revascularization – a proteomic study

Plastic and Hand Surgery, University Hospital Zurich[1], Proteome Center Rostock, Medical Faculty and Natural Science Faculty, University of Rostock[2], Institute for Experimental Surgery, University of Rostock, Rostock, Germany[3]

Introduction:
Despite extensive research activities in the field of Tissue Engineering (TE), the clinical practice is still missing skin substitutes for full-thickness skin grafts (FTSG). The main responsibility for this failure is seen in an insufficient revascularization, which itself is still poorly understood on the molecular level.

Methods:
Autologous FTSGs were transplanted in the dorsal skinfold chamber of C57BL/6J wild-type mice (n=30) and harvested after 0, 1, 3, 5 and 10 days (n= 6 animals/time-point). The differences in protein expression were studied by applying 2D gel analysis. In total, ~1200 spots were assembled in a 2D reference gel, of which 80 spots were differentially expressed and resulted in the identification of 46 non-redundant proteins. These proteins were grouped according to their biological role. Representative proteins of group of importance with respect to transplant revascularization were validated by either Immunofluorescence (IF) or by Western Blotting (WB) and yielded in a remarkable consistency of the expression differences that were observed during the time courses.

Results:
In total, approx. 1200 spots were assembled in a 2D reference gel, of which 80 were found differentially expressed according to spot density analysis. Mass spectrometric peptide mass fingerprinting as well as sequencing of partial peptides by mass spectrometric fragmentation resulted in the identification of 46 non-redundant proteins. These proteins were grouped in biological clusters of which representative protein expression was confirmed by either immunofluorescence analysis (IF) or by Western blotting (WB) and yielded in a remarkable consistency of the expression differences that were observed during the time courses.

Conclusion:
Most prominent protein expression changes affected proteins from the L-arginine-NO pathway and, for the first time, pointed towards Rho-GDI 2-connected signalling pathways during engraftment. Our study shows that despite the complexity of proteomic data interpretation it is possible not only to reassign protein expression profiles to already known pathways but as well to discover new interconnections between known molecules.

2182

Y. Saito[1], L. Kovtonyuk[1], H. Takizawa[1], MG. Manz[1]

Impact of commensal microbiota on hematopoietic stem and progenitor cell homeostasis

Division of Hematology, University Hospital Zurich, Zurich[1]

Introduction:
Most of hematopoietic stem and progenitor cells (HSPCs) reside in the adult hematopoietic bone marrow (BM). However, at any given time, about 1% of HSPCs leave the BM, enter systemic circulation, perambulate peripheral tissues, and some re-home to the BM. It has been suggested that invading pathogens in peripheral tissues induce migration arrest of HSPCs and promote HSPC proliferation and differentiation to ensure local supply of myeloid effector cells. Besides pathogens, commensal microbiota is also known to control quantity and quality of the immune cell pool of peripheral tissues in steady-state. However, it remains unclear if commensal microbiota controls BM HSPC pools and their migration to peripheral tissues.

Methods:
We use C57BL/6 GF mice that are bread and housed in sterile isolators and recolonized C57BL/6 GF mice are used as controls. Sex- and age-matched mice are used in the studies. The number of colony-forming units in the peripheral blood, BM, and spleen are analyzed after 12-14 days of culture.

Results:
We observe that the size as well as the faction of HSPCs is similar in the BM of germ-free (GF) and conventional environment control mice. In contrast, lineage$^-$cKit$^+$Sca-1$^+$ (LSK) cells that contain HSPCs are significantly increased in circulation whereas numbers of LSK cells are reduced in the spleen of GF mice compared to controls. Accordingly, the number of immature hematopoietic progenitor cells that generate CFU-GEMM is significantly increased in the peripheral blood and significantly decreased in the spleen whereas it is similar in the BM of GF versus control mice.

Conclusion:
These data suggest that commensal microbiota regulate egress from and/or homing of HSPCs to circulation and peripheral tissues in steady-state.

2183

JH. Jang[1], Y. Yamada[1], I. De Meester[2], S. Arni[1], P. Limani[3], W. Weder[1], W. Jungraithmayr[1]

Inhibition of CD26/DPP4 decreased lung tumor growth

Division of Thoracic Surgery, University Hospital Zurich[1], Medical Biochemistry, University Antwerp[2], Division of Visceral and Transplant Surgery, University Hospital, Zurich[3]

Introduction:
Lung cancer is the most common cause of death in men worldwide among cancer patients, accounting for 1.38 million deaths annually. In spite of improved treatment in surgery, radiation, and chemotherapy, the five year survival is poor. Besides primary lung cancers, most of metastatic malignant neoplasms form secondary lung tumors identified in 30-50% of cancer patients. Although prevalence varies among primary cancers, the formation of metastasis has high impact in clinic.
CD26 is multifunctional transmembrane glycoprotein constitutively expressed on most of hematopoetic cells, but it is also found on lung epithelial and endothelial cell surfaces. CD26 comprises exopeptidase activity which cleaves N-terminal dipeptides with proline or alanine preferentially. CD26 involves in other protein functions of fibroblast activating protein (FAP), plasminogen, adenosine deaminase, and tyrosine phosphatase. Additionally it encloses extracellular matrix binding activity to collagen and fibronectin associated with FAP. A role of CD26 in tumor biology has been suggested according to its functional properties by many researchers in various cancers. As multifunctional CD26 is expressed ubiquitously and even soluble form of CD26 abundantly exists in circulation and body fluid, the suggested mechanisms and data were complicated and contradictory. Moreover the importance of CD26 activity as dipeptidyl peptidase 4 (DPP4) was mostly neglected in lung cancer studies.
During the last decade, diversified scientific interest has focused on CD26/DPP4, describing its involvement in the fields of immunology and diabetology. Pharmaceutical inhibition of DPP4 ameliorates diabetes by increasing incretin hormones. Nowadays, various commercially available DPP4-inhibitors such as Vildagliptin or Sitagliptin are in clinical praxis for diabetic patients.

Methods:
Pharmaceutical effect of CD26/DPP4 inhibitor (Vildagliptin) on tumor cell lines (MC38, CT26, HT29, LLC, Ekvx, H460) was tested in vitro for 3 days with different doses (0.025-3.2µg/µl) of Vildagliptin. The viability and growth of cell line was determined by MTT assay daily. In vivo experiment was performed in mouse lung tumor model established by inferior vena cava injection of syngeneic cell lines ($1x10^5$ cells of MC38 or LLC) to BL/6 male mice. 3 weeks after tumor cell line injection, lung tumor was harvested for quantification. To study an inhibitory mechanism of tumor growth, Vildagliptin was given in vitro for western blotting of apoptosis, autophagy, and ER stress markers.

Results:
MTT assay showed an inhibitory effect of Vildagliptin on tumor cell line growths with dose dependent manner for 3 days. All tumor cell lines had less than 50% growth of vehicle treated groups 3 days after Vildagliptin treatment in vitro. In line with the observation in vitro, mouse lung tumor developed by inferior vena cava injection of syngeneic cell line showed reduction of tumor size by Vildagliptin treatment significantly. Intra cellular stress markers (cleaved caspase 3, ATF4) were elevated by cytotoxic and non-cytotoxic doses of Vildagliptin. And non-cytotoxic dose of Vildagliptin significantly reduced Oct4 which is cancer stem cell marker in MC38 and LLC cell lines in vitro.

Conclusion:
Applying clinically approved medication to another indication is an economic and practical way of drug redisposition. CD26/DPP4 inhibitors (Vildagliptin, Sitagliptin) are well established and clinically proved as a safe treatment for diabetes. The drug redisposition of Vildagliptin reduced tumor growth in vitro and in vivo by inducing intra celllular stress and decreasing stemness. Hereby, we show a new therapeutic concept, drug redisposition of Vildagliptin, for lung tumor treatment in mice.

2184

B. Ammann[1], R. Knols[1], P. Baschung Pfister[1], RA. De Bie[2], ED. De Bruin[3]

Application of principles of exercise training in sub-acute and chronic stroke survivors: a systematic review

Directorate of Research and Education, Physiotherapy & Occupational Therapy Research, University Hospital Zurich, Zurich, Switzerland[1], Maastricht University, Department of Epidemiology, CAPHRI School for Primary Health and Primary Education, Maastricht, the Netherlands[2], ETH, Zurich; Department of Health Sciences and Technology[3]

Introduction:
An increasing amount of evidence refers to the salutary effects of physical exercise training in stroke survivors. The consistent application of exercise training principles are important to ensure that an adequate dose and type of exercise is applied to achieve the desired outcome. The aim of this systematic review was to evaluate the consideration of principles of physical exercise training and the patients' adherence to exercise prescription in RCTs focusing on exercise training to improve strength and/or endurance in sub-acute and chronic stroke survivors.

Methods:
A systematic literature review focusing on physical exercise training to improve muscular strength and/or endurance as primary outcome. The Cochrane library's risk of bias (ROB) tool was used to judge the methodological quality.

Results:
One of 33 trials met all (six of six) criteria on the ROB. Failure to report blinding in patients and participants and failure to report allocation concealment were the most prevalent methodological shortcomings. Twelve reports (36%) focused on aerobic, 7 (22%) on resistance and 14 (42%) on combined interventions of aerobic and resistive strength exercise. Twenty-five reports (76%) included chronic, 7 reports (21%) sub-acute stroke survivors and one report included both types of patients. Eighty-eight % of the trials reported *specificity*, 70% *progression*, 39% *overload*, 30% *initial values*, 39% *reversibility* and 18% *diminishing returns*. One RCT described all principles of physical exercise training and 14 (43%) all FITT-components. The patient's adherence to the exercise prescription was correctly described in 3 reports (9%).

Conclusion:
The trials reviewed were of moderate methodological quality. Together, they suggest sub-acute and chronic stroke patients to benefit from physical exercise training. However, incomplete and inconsistent reporting of exercise training principles and training components limit the use and reproducibility of the physical exercise programs and hinder the understanding of the patients' adherence to the physical exercise prescription. Therefore, future trials implementing principles of exercise training in intervention programs would allow practitioners and researchers a precise elaboration and documentation of the planned exercise program in order to achieve optimal training outcomes for their stroke patients.

2185

VJ. Jacomella[1], GP. Gerber[2], MK. Mosimann[1], MH. Husmann[1], CT. Thalhammer[1], IW. Wilkinson[3], KB. Berneis[2], BA. Amann-Vesti[1]

Small dense low density lipoprotein particles are associated with poor early outcome after angioplasty in peripheral artery disease

Klinik für Angiologie, Universitätsspital Zürich[1], Klinik für Endokrinologie, Diabetologie und Klinische Ernährung, UniversitätsSpital Zürich[2], Clinical Pharmacology Unit, University of Cambridge, UK[3]

Introduction:
In patients suffering from symptomatic peripheral artery disease (PAD), percutaneous revascularization is the treatment of choice. However, restenosis may occur in 10 to 60% in the first year depending on a variety of factors. Small dense low density lipoprotein (sdLDL) particles are associated with an increased risk for cardiovascular events, but their role in the process of restenosis is not known. We conducted a prospective study to analyze the association of sdLDL particles with the outcome of balloon angioplasty in PAD. The composite primary endpoint was defined as improved walking distance and absence of restenosis.

Methods:
Patients with angiographically documented PAD of the lower extremities who were scheduled for lower limb revascularization were consecutively recruited for the study. At baseline and at three month follow-up triglyceride, total cholesterol, LDL and HDL cholesterol and ankle-brachial index (ABI) were measured. LDL size and subclasses were determined by using non-denaturing polyacrylamide gradient gel electrophoresis (GGE) of plasma. Walking capacity was evaluated by using the walking questionnaire (SF-35). Three months after the intervention duplex sonography was performed to detect restenosis.

Results:
Sixty-four patients (53% male) with a mean age of 68.6 ± 9.9 years were included. The proportion of small- dense LDL particles (class III and IV) was significantly lower in patients who reached the primary end-point compared with those who did not. Patients with improved walking distance and without restenosis had a significantly higher LDL size at baseline (266±11.1nm vs. 260.6±11.1nm, p=0.046) and at follow-up (266.7±11.1nm vs. 261.6±9.3nm, p=0.044) than patients without improvement.

Conclusion:
Small-dense LDL particles are associated with worse early outcome in patients undergoing percutaneous revascularization for symptomatic PAD.

2186

B. Li[1], S. Hornemann[1], C. Zhu[1], G. Meisl[2], T. P.J.Knowles[2], A. Aguzzi[1]

Sensitive prion infectivity titration with an automated homogeneous-phase bioassay: Digital Prion Infectivity Assay (dPIA)

Institute of Neuropathology, University Hospital of Zurich, Switzerland[1], Department of Chemistry, University of Cambridge, UK[2]

Introduction:
Measurements of prion infectivity in animal organs and biological fluids are typically performed by titration of serial dilutions with bioassays or cell-based scrapie cell end-point assays (SCA). Infectivity titers in those assays are calculated with the spearman-karber formula, based on the median infective dose model (ID_{50}) which requires serial dilutions of the prion-containing sample to the end-point titration. However, the animal assay is time-consuming and requires vast number of animals and is therefore expensive and ethically problematic, whereas the SCEPA needs intensive cell culture and is labor-intensive. Therefore, it is imperative to develop new assays to determine the prion infectivity in a faster, more sensitive and more economical way.

Methods:
Prion susceptible cells (mouse neuronal cell line) are seeded in 384-well plates and exposed to serial diluted prion infectious samples. After about 8 days cell culture without medium change, the cells are confluent and PrP^{Sc} level in the cell lysates is measured by homogeneous-phase time-resolved fluorescence resonance energy transfer (TR-FRET). The FRET signals are analysed by the “dPIA global fitter” software based on Poisson statistics with four fitting parameters, and then the infectious prion titer (propagons/well) are reported automatically by the software.

Results:
1) We established the miniaturized cell-based homogenous-phase dPIA in a 384-well format which requires minimal manipulation of cells and infectious samples. 2) We developed the “dPIA global fitter” software to calculate and report the infectious prion titer automatically. 3)We validated the dPIA with standard mouse prion inoculums.

Conclusion:
A novel sensitive, fast and convenient cell-based bioassay dPIA has been established. The dPIA system will be fully robotized on our automatic platform and applicable for high-throughput projects related to prion infectivity studies.

2187

P. Dametto[1], C. Bridel[2], A. Lakkaraju[1], L. Villiger[1], T. O'Connor[1], U. Herrmann[1], P. Pelczar[4], T. Rülicke[5], D. McHugh[3], A. Adili[6], A. Aguzzi[1]

MEMBRANE TETHERING OF THE FLEXIBLE TAIL OF THE PRION PROTEIN TRIGGERS UNFOLDED PROTEIN RESPONSE AND NEURODEGENERATION

Institute of Neuropathology, University Hospital Zurich, Zurich[1], Department of Clinical Neurosciences, Geneva University Hospital, Geneve [2], Institute of Experimental Immunology, University of Zurich, Zurich[3], Institute of Laboratory Animal Science, University of Zurich, Zurich[4], Institute of Laboratory Animal Science, University of Veterinary Medicine Vienna, Vienna[5], Institute of Virology, Technische Universität München (TUM)/ Helmholtz-Zentrum, München[6]

Introduction:
The cellular prion protein (PrP) is a membrane GPI-anchored glycoprotein, the conversion of which into a misfolded and aggregated conformer defined as prion (PrP^{Sc}) is the central event in prion pathogenesis. PrP consists of a flexible N-terminal tail (FT, aa 23-128) hinged to a membrane-anchored globular domain (GD, aa 129-231). Ligation of the GD with antibodies induces rapid neurodegeneration, which is prevented by deletion or functional inactivation of the FT. While these findings indicate that the FT is an allosteric effector of neurotoxicity, its mechanism of action is unknown. We speculate that anti-GD antibody induces FT juxtaposition to lipid membranes, which may underline the aforementioned toxicity. To explore the latter, we generated transgenic mice expressing the FT fused to a GPI anchor, but lacking the GD (PrPΔ141-225, or 'FTgpi' mice).

Methods:
FTgpi sequence was cloned into the "half-genomic" pPrPHG backbone and injected into pronuclei of Prnp+/+ mice. The two selected lines (FTgpi155 and FTgpi177) were crossed with *Prnp*$^{o/o}$ mice to obtain offspring lacking PrP. The phenotypes of these mouse lines were characterized macroscopically, histologically, and biochemically. HPL cells were stably transfected with pBMN-FTgpi and pBMN-PrP constructs and co-stained with POM11, an antibody against the FT of PrP. Biochemical assessment of endoplasmic reticulum (ER) stress proteins was performed by RT-PCR and Western blot.

Results:
FTgpi mice developed a progressive, inexorably lethal neurodegeneration, characterized by a massive loss of cerebellar granule neurons, widespread atrophy, and intense astrocytosis. Immunofluorescence and FACS analysis showed that only a minor fraction of FTgpi reaches the plasma membrane whereas most of FTgpi is retained in the ER. This is not entirely surprising as FTgpi is completely unstructured and exhibits hydrophobic properties which are likely to be targeted by quality control processes in the ER. Therefore, the next question to address was "does FTgpi induce ER-stress and unfolded protein response (UPR)?" Proteomic data indicated that FTgpi triggered a conspicuous UPR, activating the PERK pathway and leading to phosphorylation of eIF2α and overexpression of CHOP, which in turn induce apoptosis if chronically activated. In contrast, mice expressing untethered, soluble FT (sFT) did not develop any pathology, suggesting that the forced proximity of the FT to cellular membranes suffices to drive toxicity.

Conclusion:
An earlier article was published this year: "Sustained translational repression by eIF2α-P mediates prion neurodegeneration" by Mallucci G. et al (Nature). Here it was shown that prion infected mice display increased level of phosphorylated PERK, eIF2α and overexpression of CHOP, exactly as in the FTgpi mice. Moreover, the FTgpi phenotype is

morphologically and biochemically similar to that triggered by anti-GD antibodies. Therefore, the requirement of an intact FT for the toxicity of antiprion antibodies, and the similarities between the signaling pathways evoked by prions and FTgpi, suggest that the FT is the effector of neurotoxicity in most prion-related conditions, and that FTgpi may be a useful tool for further investigation of the mechanisms of toxicity underlying human prion diseases.

2188

IT. Tritschler[1], JS. Schroeder[1], MW. Weller[1]

The TGF-beta superfamily coreceptor TbRIII modulates both Smad1/5/8 and Smad2 signaling pathways in gliomas

Department of Neurology, University Hospital Zurich, Switzerland[1]

Introduction:
Glioblastoma is the most common primary brain tumor in adults and is rather resistant to multimodal treatment approaches. The existence of glioma-initiating cells (GIC) represents a principle hurdle in glioma treatment as they may survive treatment and repopulate the tumor. Members of the transforming growth factor beta (TGF-beta) superfamily such as TGF-beta itself and the bone morphogenetic proteins (BMP) have been shown to be involved in the regulation of the malignant phenotype of glial tumors. TGF-beta receptor type III (TbRIII) is an accessory TGF-beta receptor and a component of the TGF-beta signaling complex. Importantly, TbRIII may influence GIC acting as modulator of canonical and non-canonical TGF-β signaling.

Methods:
We characterized TbRIII mRNA expression and protein levels in panels of eight long-term glioma cell lines (LTC), 4 glioma-initiating cell lines (GIC) and in human brain-derived microvascular endothelial cells. In selected glioma cell lines and GIC we examined TbRIII expression upon modulation of TGF-beta levels. Beyond, we investigated TbRIII dependent modulation of Smad signal transduction.

Results:
Glioma cells exhibit heterogeneous patterns of TbRIII mRNA expression which correlate with the respective protein levels. Treatment with TGF-beta downregulates and inhibition of TGF-beta dependent signal transduction by the TGF-beta receptor inhibitor SD-208 upregulates TbRIII expression on a transcriptional level. SiRNA mediated knockdown of TbRIII results in upregulation of TGF-beta-mediated phosphorylation not only of SMAD2 and SMAD3, but also of SMAD1/5/8.

Conclusion:
TbRIII modulates TGF-beta dependent signal transduction in glioma cells involving SMAD2, SMAD3 and SMAD1/5/8 signaling acting as a negative regulator of autocrine TGF-beta signaling. This may open up new perspectives of biomarker-driven exploratory clinical trials focusing on the microenvironment in glioblastoma.

2189

S. Bengs[2], A. Weber[3], S. Lang[2], S. Vavricka[1], P. Frei[2], M. Halama[4], M. Fried[2], G. Rogler[2], M. Scharl[2]

PTPN2 (TC-PTP), PTPN9 (PTP-MEG2) and PTPN23 (HD-PTP) are involved in the regulation of the JAK-STAT and MAPK/ERK pathway in colorectal cancer (CRC)

Gastroenterology and Hepatology, City Hospital Triemli, Zürich[1], Gastroenterology and Hepatology, University Hospital Zurich, Zurich[2], Pathology, Institute of Clinical Pathology, University Hospital Zurich, Zurich[3], Clinic for Gastroenterology, Zurich-Fluntern, Zurich[4]

Introduction:
Tyrosine phosphorylation (TP) is an important process in mammalian cells and plays a critical role in the activation of oncogenic progression. One family, which is involved in regulation of TP, are protein tyrosine phosphatases (PTP). PTPN2 (TC-PTP), PTPN9 (PTP-MEG2) and PTPN23 (HD-PTP), are non-transmembrane PTPs (PTPN) and involved in epithelial tumorgenesis, e. g. in breast cancer as they regulate growth factor signalling. PTPNs are also involved in the regulation of immune functions, where IL-6 has been associated with the development of colorectal cancer (CRC). Here, we investigated whether expression of PTPN2, PTPN9 and PTPN23 is altered in colorectal cancer (CRC) and regulates IL-6 mediated tumorigenic events.

Methods:
Expression of PTPN2, PTPN9 and PTPN23 in primary tumors (n = 12) of CRC patients was examined by immunohistochemistry (IHC). Clinical and pathologic characteristics were correlated analyzed. mRNA and protein levels were assessed by real-time RT-PCR and Western Blot in HT-29 intestinal epithelial cells (IEC).

Results:
PTPN2 was higher expressed in the nuclei of CRC cells as compared to the nuclei of non-cancer cells. In contrast, PTPN9 staining was more intense in the cytoplasm in cancer cells as in non-cancer cells. For PTPN23 increased protein levels were observed in the nuclei as well as in cytoplasm of CRC cells when compared to normal intestinal epithelia cells. To assess, how PTPN2, PTPN9 and PTPN23 regulate tumorigenic gene expression events, transient single knockdowns of these PTPNs in HT-29 IECs were performed and treated with IL-6 (50 ng/ml) to stimulate the JAK-STAT and MAPK/ERK signalling cascades. IL-6 treatment results in increased mRNA levels of PTPN9 ($p<0.05$ vs. control) and PTPN23 ($p<0.001$ vs. control) as compared to the non-treated control transfected cells, whereas PTPN2 expression was reduced ($p<0.001$ vs. control). Elevated levels of ITGB6 and Ets-1 transcription factor were observed in all PTPN knockdown cells with IL-6 treatment, indicating a possible involvement of these PTPNs in EMT and cell proliferation.

Conclusion:
We demonstrate that expression of PTPN2, PTPN9 and PTPN23 is increased in CRC cells compared to healthy colon tissue parts. Expression of those PTPNs is regulated by IL-6 which leads to an altered Ets-1 and ITGB6 expression pattern. Our data indicate that PTPN2, PTPN9 and PTPN23 are involved in EMT and cell proliferation and might therefore play a role for CRC development.

2191

R. Müller[1], A. Theocharides[1], M.G. Manz[1]

hSIRPα-tg-hTPO-Expressing RAG2-/-, IL2Ry-/- immunodeficient mice - a xenograft model for human polycythemia vera

Division of Hematology, University Hospital Zurich, Zurich, Switzerland[1]

Introduction:
Xenotransplantation of human hematopoietic malignancies into immune-deficient mice represents the most appropriate *in vivo* model system for human malignant hematopoiesis. We hypothezised that mouse strains expressing human cytokines and key factors of xenogeneic cell acceptance like hSIRPalpha would represent suitable models for the assessment of human less aggressive hematologic neoplasms *in vivo.*

Methods:
Polycythemia vera (PV) patient samples were collected after informed consent at the Division of Hematology, Zurich University Hospital. Newborn hSIRPα-tg-hTPO-knockin mice on the $Rag2^{-/-}$/$IL2Ry^{-/-}$-BALB/C background received sublethal irradiation and CD34+ cells were transplanted intra-hepatically 24 hours later. Mice were sacrificed 8 weeks after transplantation and engraftment was analyzed by flow cytometry. To verify engraftment of human malignant hematopoiesis we quantified allele-burden of JAK2V617F point mutation in mouse BM.

Results:
By transplantation of 4-10x10^5 CD34+ cells into newborn hSIRPα-tg-hTPO-$Rag2^{-/-}$/$IL2Ry^{-/-}$ mice we could detect engraftment of hCD45+ cells in BM at week 8 (median 4.43%) with a high proportion of human myeloid cells detected by hCD45/hCD33 co-staining (median 3.07 %). JAK2V617F AS-PCR was used to quantify human malignant hematopoiesis. In tested BM samples of engrafted mice we found JAK2V617F positive alleles with a frequency of 2-12% (median 8%).

Conclusion:
We could show engraftment of PV-CD34+ cells that extends previous reported engraftment levels in other model organisms. hSIRPα-tg-hTPO-$Rag2^{-/-}$/$IL2Ry^{-/-}$ mice thus represent a suitable model for assessing human less aggressive hematological neoplasms *in vivo* and testing targeted therapies in the future.

2192

R. Reimann[1], T. Sonati[1], S. Hornemann[1], A. Aguzzi[1]

Safety assessment of potentially therapeutic anti-prion antibodies

Neuropathology, University Hospital Zürich[1]

Introduction:
Any treatment opportunity for the fatal neurodegenerative disease Creutzfeld Jakob caused by the infectious particle prion is lacking. Passive immunotherapies are one of the strategies of potential, as mice expressing anti-prion antibodies are protected from peripheral prion inoculation and positive survival effects in mice have been reported by chronic intraventricular and intravenous treatment regimens . However, the observation of rapid and extensive apoptosis in hippocampal and cerebellar neurons after stereotactic injection of anti-prion specific monoclonal antibodies in vivo warned against the development of passive immunotherapies in Creutzfeld Jakob disease. This finding could not be reproduced later, what revitalised the hope of using anti prion antibodies in immunotherapy. Recently, we proved the epitope specific neurotoxic potential of anti-prion antibodies in extensive *in vivo* and *ex vivo* studies. The controversy about the toxicity of anti-prion antibodies calls further investigations of their safety assessment prior clinical trial start.

Methods:
Anti-prion antibodies are stereotactically injected into the left hippocampus of male C57BL/6 mice (A/P: -2 mm, ML: 1.3mm, DV: -1.4mm from Bregma). For control, antibodies pre-incubated with a three-fold molar excess of a recombinant murine prion protein were injected into the right hippocampus. The read out is based on volumetric analysis of diffusion weighted Magnetic Resonance Images. Dose-response assessment for toxicological studies is performed by the use of Benchmark Dose Software from the United State Enviromental Protection Agency (EPA). The non observed Adverse Level (NOAL) is defined as the lowest dose at which there is no significant increase in the frequency or severity of adverse affect levels, where as the Benchmark Dose Level (BMDL) is the lower border of the 95% confidence interval of the Benchmark Dose Response (BMR). We defined latter as an increase in lesion volume of 5% over control injection.

Results:
In order to solve the controversy about the toxicity of the antiprion antibody D13, initially reported to be toxic and later as untoxic at very low concentrations (2µg) we have evaluated dose-response curves for risk assessment. No lesion was found at 48 hours post injection of 2µg into wild type (*wt*) mice. However, 6µg and 12µg of D13 (purity ~90%, as evaluated by silver-stained SDS-PAGE) produced large, hyperintense lesions in the hippocampus and/or cortex of 4 out of 5 mice observed on diffusion weighted images. Injection of D13 blocked with recombinant PrP was innocuous.
Based on a dose response curve analyse we determined the NOAL as 3.35 µM and the BMR as 5.235 µM. In lesion areas 48 hours post injection neurons presented with nuclear condensation or fragmentation. The apoptotic nature of lesion was then confirmed based on Terminal deoxynucleotidyl transferase dUTP nick end labelling (TUNEL) assays of paraffin sections from mice injected with 6µg D13.

Conclusion:
Despite reports on the neurotoxicity of anti-prion antibodies, immunotherapy still represents a potential therapy for Creutzfeld Jakob disease. We have shown that toxicity of anti-prion antibodies is epitope specific offering a safe therapeutic window. However based on the precaution principle, the potential toxicity of every anti-prion antibody intended to treat Creutzfeld Jakob disease and entering clinical studies has to be addressed carefully. With

our data we solved a controversy in the literature, provided toxicological index values about D13 and established a testing regime of antiprion antibodies prior intended to enter clinical trials.

2193

A. Senatore[1], M. Hermann[2], P. Pelczar[2], A. Aguzzi[1]

MODELING GENETIC PRION DISEASES LINKED TO EXTRA OCTAPEPTIDE REPEATS: PATHOGENIC MECHANISMS AND OCTAPEPTIDE LIGAND BASED THERAPY

Institute of Neuropathology, University of Zurich, Zurich[1], Institute of Laboratory Animal Science, University of Zurich, Zurich[2]

Introduction:
Familial prion diseases account for approximately 10–15 % of human prion diseases and are caused by dominantly inherited germ line mutations in the prion protein gene, *PRNP*. More than 30 different pathogenic point or insertion mutations in the *PRNP* gene have been identified. Insertions occurs solely in the octapeptide-repeat (OR) region which is located in its flexible N-terminal tail and normally contains one ninepeptide followed by four PHGGGWGQ octapeptide segments.
Expansions of the octarepeat domain are directly linked to the development of prion disease and recent data indicated a critical role for the OR containing flexible tail as the effector domain of PrP-mediated neuronal death. However, little is known about the underlying pathogenic mechanisms. It is thought that mutant PrP with supernumerary OR is inherently unstable, prone to misfolding and aggregation and may cause disease because of gain of toxic functions leading to oxidative stress. Also, extra OR PrP mutants may lead to the formation of a 'seed' to recruit additional mutant proteins, eventually generating infectious PrP molecules responsible for a transmissible disease. Octapeptide ligands have been found to prevent the toxicity of ligand targeting the C-terminal globular domain of the protein and prolong the life of mice expressing the a toxic PrP(C) deletion mutant but their possible beneficial effect in arresting the toxicity and/or infectivity of extra OR PrP mutants has not been assessed so far.

Methods:
We selected two insertion mutations described in humans carrying 9 and 12 additional OR and used golden gate cloning strategy and a Zinc Finger Nucleases (ZFNs)-based mouse transgenesis approach to generate supernumerary OR PrP mutants and model the associated genetic prion diseases in mice.

Results:
Extra-9 and extra-12 OR mouse-human (MoHu) PrP chimeric constructs have been created which harbor the human insertional mutations in the OR flanked by the N- and C-terminus of murine PrP. These constructs have been expressed in cell lines to characterize their cellular metabolism and the formation of insoluble mutant PrP aggregates. Transgenic mice are being generated by targeting the extra OR (MoHu)PrP constructs to the mouse *gt(ROSA26)Sor (ROSA26)* locus by using specific ZFN pairs. As the ROSA26 targeting vector has been constructed with a floxed CAT stop cassette upstream the PrP open reading frame, this will allow the temporally and spatially regulated expression of the extra OR PrP mutants by Cre-lox system. As next step, clinical evaluation and behavioral tests of the double transgenic Cre/extra OR (MoHu)PrP mice will be paralleled by biochemical and histological analyses to phenotype the extra OR-dependent pathology.

Conclusion:
The generation of these conditional transgenic mice expressing supernumerary OR PrP mutants will provide an invaluable model to dissect the pathogenic mechanisms and assess the potential infectivity of the extra OR PrP mutants. Finally, these mice will used be to test *in vivo* the therapeutic potential of octapeptide ligands in counteracting the extra OR-induced disease.

2194

JW. Deuel[1], F. Vallelian[1], DJ. Schaer[1]

Lipid degradation catalyzed by free heme is a hallmark of endothelial hemoglobin toxicity.

Klinik und Poliklinik für Innere Medizin, UniversitätsSpital, Zürich[1]

Introduction:
Intravascular Hemoglobin (Hb) is released during a variety of conditions such as hemolytic anemias, blood transfusion, atherosclerosis and infection. Free Hb can trigger cardiovascular instability and oxidative damage within the vasculature. Haptoglobin, the natural Hb scavenger protein, as well as hemopexin, the natural heme scavenger protein, can protect endothelial cells from Hb mediated toxicity. However, the molecular mechanisms of endothelial Hb toxicity remained unclear. Side reactions of Hb with lipid components have been proposed as a mode of action.

Methods:
We used a co-incubation model of an engineered lipoprotein containing reactive phosphatidyl choline and apoA1 lipoprotein (rHDL) with Hb to monitor the biochemical reactions, generation of bioactive compounds and their biological impact on endothelial cells. The biochemical reactions of Hb mediated lipid peroxidation and its modulation by haptoglobin and hemopexin were analyzed by spectrophotometry. This method allowed the simultaneous recording of the iron redox state and the oxygen concentration in the reactions without using any perturbing detection reagents. Exposing human umbilical vein endothelial cells (HUVEC) to the identical reactions correlated the biochemical reaction kinetics to biologic processes in the endothelium. Biologic parameters were endothelial monolayer integrity measured by electric cell-substrate impedance sensing (ECIS), apoptosis induction and gene expression.

Results:
Spectrophotometry revealed a rapid depletion of oxygen when Hb was added to rHDL. This peroxidatve reaction was accompanied by the generation of higher oxidative iron states (Fe^{3+} and Fe^{4+}) and release of modified lipid peroxidation products. Reaction kinetics, diverse effects of hydrophilic and lipophilic radical scavengers and heme capturing strategies allowed us to identify heme release from Hb as the crucial trigger of the reaction sequence. Hemopexin captures free heme while haptoglobin prevents heme release by structurally stabilizing Hb. These two scavenger proteins effectively prevent accumulation of free heme and the toxic reaction sequence by synergistic mechanisms. Translation of our biochemical model into the biological system allowed us to allocate distinct toxic and protective effects to the principle biochemical reaction components.

Conclusion:
In our study we could for the first time unambiguously correlate biochemical reactions of free Hb with toxic effects in a biological system. Heme release from extracellular Hb was identified as the most critical trigger of lipid peroxidation and subsequent generation of cytotoxins. Diverse and synergistic protective mechanisms of the two natural scavengers hemopexin and haptoglobin could be characterized and explain the strong protection exerted by the two proteins against Hb toxicity in vivo.

2195

C. Corrò[1], M. Rechsteiner[1], H. Moch[1]

Non-invasive identification of VHL mutations in plasma by deep-sequencing with subsequent assessment of mutant pVHL functionality in FFPE by FRET in ccRCC patients

Surgical Pathology, University Hospital, Zurich[1]

Introduction:
Clear cell renal cell carcinoma (ccRCC) is the most common type of renal cell carcinoma (RCC), a malignant tumor affecting adult kidney caused by inactivation of von Hippel-Lindau (VHL) tumor suppressor gene. So far, non-invasive tools are not available to determine the mutation and functional status of VHL for the detection, staging and monitoring of ccRCC response to treatment. Therefore, the study aims to establish an ultra-deep-sequencing approach to detect VHL mutations in circulating tumor DNA (ctDNA), and a FRET assay in FFPE tissue cuts to determine mutant pVHL functionality. The final purpose of the project is to integrate the information obtained by ultra-deep-sequencing and FRET technology in order to identify and monitor ccRCC cases; this would be useful tool in clinical diagnostics.

Methods:
Thirdy-two patients with ccRCC have been selected from our University Hospital Zürich-RCC patient cohort. In order to avoid possible false negative, which could arise from lower stages and no metastatic condition, patients who present metastasis and higher tumor stage were chosen as starting point in the research. The workflow consists of ctDNA extraction and purification form 1ml of plasma and serum, following DNA quantification and DNA fragment distribution analysis to determine the amount and quality of isolated DNA. If enough DNA is present, DNA target amplification and quantification will be carried out before starting sequencing.

Results:
Usable amount of circulating DNA was isolated from 1ml of serum and plasma (in Heparin). Fragment distribution analysis showed no degradation or low DNA quality in the samples. The Cancer Hotspot Panel from Ion Torrent offers a partial coverage of the coding region of VHL. For this reason, it was used for control samples as proof of principles. On the contrary, the Comprehensive Cancer Panel, which offers a complete coverage of the coding region of VHL, was used for patient samples. Following the target amplification process, only amplified DNA derived from serum samples reached high enough concentrations (11pM) to proceed with deep-sequencing. Both, control and patient plasma samples have not been amplified as serum. A possible explanation for this observation, which was confirmed in colon cancer samples, is that heparin influences PCR reaction. The amplified serum samples were further used for ultra-deep sequencing. Patient n°68 showed an insertion of thymidine at the position c.365 in VHL exon 2. Sanger sequencing of DNA derived from primary tumor of the same patient showed an insertion of cythosine at the same position. To further investigate this mutation the DNA of the primary tumor will be used as input for the deep-sequencing. In order to perform FRET technique on FFPE tissue cuts, reliable antibodies for pVHL and HIF have first to be chosen and tested in Western Blot, ELISA and immunohistochemistry.

Conclusion:
The project is at the initial stage and the following points will be additionally developed: ongoing collection of serum and plasma of patients included in the study (after surgery and during treatment), increase coverage and reads number of deep-sequencing, determine filter and thresholds for variant calling of reads present as low as 0.5%, establishment of Western Blot, ELISA, immunohistochemistry for FRET.

2196

KC. Brunner[1], CHF. Hämmerle[1], MÖ. Özcan[1]

Fatigue Strength and Weibull Characteristics of Inlay-retained Resin-bonded Fixed Dental Prosthesis

Clinic for Fixed & Removable Prosthodontics and Dental Material Science[1]
Introduction:

Advances in adhesive technologies enabled the dental profession to restore the missing teeth in a minimal invasive fashion with resin-bonded fixed dental prosthesis (RBFDP) without sacrificing the hard and soft dental tissues using metal-free material options ranging from reinforced polymers to reinforced all-ceramics. Yet, information on their durability under fatigue conditions is scarce. The objectives of this study were to evaluate the load bearing capacity of RBFDPs made of different materials after cyclic loading, and classify the failure types after loading.

Methods:
Sound human mandibular first premolars and first molar pairs (N=60, n=10 per group) were randomly divided into six experimental groups to receive one of the following RBFDP types: a) Resin composite only, b) Direct E-glass fiber-reinforced composite (FRC), c) Indirect E-glass FRC, d) Lithiumdisilicate glass-ceramic, e) Yttria-stabilized tetragonal zirconia (Y-TZP), f) Metal-ceramic. Box preparations were made in abutment teeth using standardized ultrasonic burs. The teeth were conditioned employing an etch-and-rinse adhesive system and the indirect RBFDPs (c-f) were cemented adhesively. The specimens were subjected to cyclic loading for x1.200.000 in water alternating between 5 and 55 °C (Zurich Chewing Simulator). They were then loaded to failure from the occlusal surface in the Universal Testing Machine (cross-head speed: 1 mm/min). Failure types were classified as irreparable or repairable depending on the location and size. Data were analyzed using ANOVA and Bonneferroni tests (a=0.05). Weibull modulus for each group was calculated based on parametric distribution analysis of censored data for maximum fracture load.

Results:
Mean load bearing capacity (N) of Groups d (1274±270), e (1567±363) and f (1544±787) were significantly higher than those of other groups (601±130 - 819±270 N) ($p<0.05$). Early debondings occurred in 2 specimens in Group e. While in this group, predominantly abutment and/or connector fractures were observed, Groups a to d demonstrated mainly reparable failure types with cracks or chipping in the veneering material at maximum load. Weibull modulus was the highest in Group d (m=5.3) followed by Group a (m=5.1). Other groups presented Weibull moduli (m) ranging between 1.4 and 3.3.

Conclusion:
Considering load bearing capacity, repairable failure types and Weibull moduli, lithium disilicate seem to be more durable than those of other material options for RBFDPs. Direct and indirect polymeric materials with and without FRC reinforcement presented similar results. Due to early debondings and catastrophic irreparable failure types, Y-TZP RBFDPs should be indicated with caution in the posterior region.

2197

DG. Goniotaki[1], AL. Lakkaraju[1], SS. Sorce[1], AG. Aguzzi[1]

Inhibition of metabotropic glutamate receptor 5 (mGluR5) is protective against prion-induced toxicity

Neuropathology, University Hospital of Zurich, Zurich[1]

Introduction:
Prion diseases are a group of fatal, neurodegenerative disorders affecting both human and animals, occurring on genetic, sporadic or infectious grounds. However, the physiological role of PrP^C as well as the molecular pathways associated with prion toxicity and neuronal death, are still largely unknown.
Glutamate is the main excitatory neurotransmitter in the mammalian central nervous system (CNS). It can induce fast synaptic signaling though ionotropic glutamate receptors (iGluRs) or modulate cell excitability and synaptic transmission through metabotropic glutamate receptors (mGluRs). The latter form a family of eight receptors that are subdivided into three major groups.
Recently interaction of PrP^C with mGluR5 was shown to be the effector of the Abeta-oligomer induced toxicity in Alzheimer's disease.
We tested the hypothesis that selective inhibition of mGluR5 can be protective against prion protein-induced toxicity.

Methods:
Experiments were carried out on cultured organotypic slice cultures prepared from p5-p11 tga20 mice.
Prion toxicity was triggered not only by prion infection (RML6) but also by exposure to toxic anti-PrP antibodies (POMs), a group of antibodies binding to the globular domain of PrP^C, whose mechanism of action is mimicking prion infections.
The slice culture model allows reproduction of the classical hallmark of prion disease (prion replication, inflammation, spongiosis, neurodegeneration), as well as thorough pharmacological manipulation.
Inhibition of mGluR5 was performed by addition of a selective mGluR5 inhibitor MPEP (2-methyl-6-(phenylethynyl)-pyridine) in concentrations ranging from 10nM to 10mM.
Morphometric assessment of granule cell death was performed with NeuN immunofluorescence on fixed slices.

Results:
Our preliminary results indicate a significant neuroprotection against both prion-infection and anti-PrP antibody mediated toxicity, shown as a rescue of granular cell death, upon addition of MPEP (10nM-1uM).

Conclusion:
These results indicate that inhibition of mGluR5 can be protective against prion-induced toxicity in slices. Additional experiments with an alternative mGluR5 inhibitor (CTEP) are to be performed in slices as well as *in vivo* experiments with both MPEP and CTEP. Experiments will also be repeated in genetic model of mGluR5 inhibition (mGluR5 knockout mice).

2198

S. Sorce[1], M. Nuvolone[1], A. Keller[1], J. Falsig[1], A. Varol[1], P. Schwarz[1], H. Budka[1], A. Aguzzi[1]

The NADPH oxidase enzyme NOX2 contributes to the pathology of prion diseases

Institute of Neuropathology[1]

Introduction:
The formation and aggregation of misfolded prion proteins (PrP^{Sc}) in the brain cause neurodegeneration, and lead to neurological dysfunctions, severe disabilities and death. The group of diseases due to the accumulation of infectious prion deposits is known as Transmissible Spongiform Encephalopathies, since the main neuropathological hallmark of these disorders is the presence of vacuoles in affected brain regions. Signs of oxidative stress have been found in Transmissible Spongiform Encephalopathies. However, the exact source of reactive oxygen species (ROS) is unknown.

Methods:
Here, we analyzed the contribution of NOX2 enzyme to prion diseases by studying *post-mortem* brain samples of Creutzfeldt–Jakob disease (CJD) patients and by comparing the development of prion disease in NOX2-deficient and wild-type mice. Survival analysis after prion inoculation, as well as time-dependent occurrence of neuropathological changes and behavioural alterations were investigated.

Results:
Our results indicate that NOX2 is markedly expressed in affected brain regions of CJD patients. The morphology of NOX2-positive cells corresponds mainly to microglia, and a particular strong localization of NOX2 was observed around spongiform vacuoles, typical hallmarks of prion disease pathology. Moreover, immunofluorescence and confocal imaging confirmed that NOX2 expression is restricted to microglial cells. Accordingly, NOX2 was undetectable in cerebellar slices after microglia depletion. NOX2 expression was upregulated in prion-inoculated mice or organotypic cerebellar slice cultures. Genetic ablation of NOX2 in mice significantly reduced motor deficits during the development of prion disease and completely abrogated the production of ROS at the terminal stage. This effect was associated with prolonged survival rates in NOX2-deficient mice.

Conclusion:
Our results therefore indicate that NOX2 enzyme is a major source of reactive oxygen species, which contribute to the pathogenesis of prion diseases. Compounds able to inhibit NOX2 activation might offer a new therapeutic possibility for the treatment of these disorders.

2199

F. Wehrle[1], B. Latal[2], R. Huber[2], R. O'Gorman[3], L. Kaufmann[4], A. Hüsser[5], C. Verrey[5], C. Hagmann[1]

Impaired Executive Functions in Complex Tasks in Children and Adolescents Born Very Preterm

Division of Neonatology, University Hospital Zurich, Zürich[1], Child Development Centre, University Children's Hospital, Zurich[2], Center for MR Research, University Children's Hospital, Zürich[3], Department of Psychiatry and Psychotherapy A, General Hospital, Hall in Tyrol, Austria[4], Department of Psychology, University of Zurich, Zürich[5]

Introduction:
Many studies have found impaired performance in executive functions (EF) in patients formerly born very preterm (VPT) [1]. Most evidence derives from studies in early and middle childhood. EF play a pivotal role for academic achievement and personal autonomy. Demands in both domains and, in parallel, the dependence on EF ability continuously increase in later childhood and adolescence [2]. This study therefore aims to investigate the pattern of EF deficits in older children and adolescents born very preterm and to compare them with healthy term-born peers.

Methods:
Forty-one VPT children and adolescents (age: *M* = 12.9 [*SD* = 1.7, *range* = 10.4-16.6] years) with normal general cognitive abilities and 38 healthy term-born (TB) peers (age: *M* = 12.7 [*SD* = 1.8, *range* = 10.0-16.9] years) were examined. Various EF components (*i.e.*, planning, inhibition, working memory, cognitive flexibility) were assessed with a computer-based test battery (Cambridge Neuropsychological Testing Automated Battery, CANTAB). Additionally, parents reported on their children's EF ability in the school and home environment using the Behavior Rating Inventory of Executive Functions, BRIEF (German version).

Results:
Mixed-model ANOVAs with birth status (VPT vs. TB) as between-subjects factor and difficulty levels of EF tasks as within-subject factor revealed a significant interaction between birth status and difficulty level for planning ability ($F(3, 231) = 3.120$, $p = .03$), working memory, ($F(2, 154) = 2.307$, $p = .10$) and inhibition ($F(3, 216) = 3.946$, $p = .03$): Performance of VPT and TB participants was comparable in lower difficulty levels but poorer for VPT participants in higher difficulty levels. Parents of VPT participants rated EF abilities of their children poorer than parents of TB participants (*e.g.*, global EF ability: $t(78) = 3.002$, $p = 0.004$) with more VPT participant's scores lying above the cut-off for clinically relevant EF problems ($c(1) = 7.671$, $p = .006$).

Conclusion:
Executive function deficits persist into adolescence in VPT patients with normal general cognitive ability. Particularly, when tasks become more complex, VPT participants experience more EF difficulties than their peers. As EF demands in school become increasingly more complex in later childhood and adolescence, EF deficits may hinder optimal development in former VPT patients.

References:
[1] Mulder et al., Dev Neuropsychol 2009, for a review
[2] Burnett et al., Early Hum Dev 2013

2200

L V. Kovtonyuk[1], R. Radpour[1], H. Takizawa[1], M G. Manz[1]

Aging-associated intrinsic and extrinsic factors control hematopoietic stem cell behaviour

Division of Hematology, University Hospital Zurich, Zurich[1]

Introduction:
Life-long self-renewing hematopoietic stem cells (HSCs) continuously replenish mature blood cells. Upon aging, HSCs reduce self-renewal capacity, skew towards myeloid differentiation, and show less efficient bone marrow (BM)–homing ability. Recently, we have demonstrated that at any given time young adult HSCs consist of actively cycling and dormant pools, and that aged HSCs tend to be dormant in a permissive environment, suggesting that a cell-intrinsic drive towards dormancy is imprinted on HSCs through increased proliferative history. Here we address the questions how extrinsic and intrinsic factors determine HSC behaviour and what their molecular signature and relative contribution are in HSC cell fate decision.

Methods:
Recently, we have established in vivo single HSC divisional tracking with CFSE (5(6)-carboxyfluorescein diacetate *N*-succinimidyl ester), and subsequent isolation of different divisional classes of HSC-containing cell fractions (LKS) based on CFSE dilution for in vivo HSC functional readout. CFSE-labeled young (8-12 week old), aged (>2 year old) and young LKS that were previously serially transplanted were transferred into non-irradiated young or aged recipients, respectively. To test biological function of HSC with distinct divisional histories, dormant (0-divided at 8 weeks) or cycling LKS or c-MPL+ Flt3- LKS (>5-divided at 8 weeks) were isolated and transplanted into lethally irradiated mice. The transplanted mice were monthly bled to follow long-term donor engraftment and lineage repopulation. To dissect aging-associated extrinsic factors, we performed antibody based protein arrays and transcriptome analysis with total BM of young versus aged animals, and bioinformatical analysis to narrow down key candidate proteins.

Results:
BM analysis at 8 weeks after tracking showed that young LKS proliferated faster than old LKS, while both young and aged LKS appear to be more dormant in an old environment. Young HSC, irrespective of environment and cycling activity, demonstrated balanced lineage repopulation. Dormant aged HSCs favor myelopoiesis independent of the environment. In contrast, cycling aged HSCs that had been exposed to a young environment showed balanced lineage repopulation as do young HSCs, indicating that the young external factors can modulate aging-associated lineage skewing in a cell cycle dependent manner. Similar biology as in aged HSCs was observed in HSCs with extensive divisions during serial transplantation. Expression levels of some chemokines, cytokines, growth factors and cell surface receptors were altered in aged BM, suggesting their possible role in HSC behavior.

Conclusion:
These findings demonstrate that HSC turnover and differentiation are controlled by cell-intrinsic and -extrinsic factors: extensive proliferative history imprints a cell dormancy program on HSCs that is associated with myeloid-biased differentiation; lineage skewing of HSC during aging can be modulated via environmental cues. Understanding of how HSC cell cycle and fate is determined and altered with aging will open a new avenue for regenerative medicine.

2201

P. Kellner[1], M. Müller[1], P. Eugster[1], M. Schläpfer[1], B. Beck-Schimmer[1]

Long-term sedation with sevoflurane offers protective effects in a rat model of acute lung injury

Anesthesiology, USZ, Zurich[1]

Introduction:
In acute lung injury (ALI) and acute respiratory distress syndrome (ARDS) disruption of alveolo-capillary barriers result in lung edema, respiratory failure and the need of mechanical ventilation. Despite continuous efforts, no effective pharmacological treatment has been established yet and mortality rates remain high. Sedation needed to tolerate mechanical ventilation is usually performed with intravenous agents like propofol. The invention of the Anaesthetic Conserving Device (AnaConDa®) made the use of volatile anesthetics a valuable option for sedation in intensive care units (ICU).
Volatile anesthetics (especially sevoflurane) demonstrated anti-inflammatory properties and a facilitated oxygenation in ALI models (1), these were however limited to short-term application.
In this study we evaluated for the first time the effects of long-term administration of sevoflurane in an ALI model in rats.

Methods:
Anesthetized adult male Wistar rats (weight: 364±28 g) were tracheotomized and instrumented with an arterial and a central venous line. Lipopolysaccharide from E.coli (LPS, 0.3 µg/kg, dissolved in phosphate buffered saline, PBS) was instilled intratracheally to induce ALI. Control animals received PBS alone. Animals were continuously ventilated and sedated with propofol (10 mg/kg/h) or sevoflurane (1,3 Vol%, 0.5 MAC) for 6, 12, 18 or 24 h.
Arterial blood gases were analyzed every 3h. At the end of the experiment animals were sacrificed, bronchoalveolar lavage fluid (BALF) and plasma samples were harvested.
Oxygenation index (paO2/FiO2) was calculated. Inflammatory cells in BALF were quantified and cytokine levels (IL-6, CINC-1, MCP-1) were determined in BALF and plasma by ELISA. To assess integrity of the alveolo-capillary barrier albumin and total protein were measured in BALF. Results are presented as means ± SD and were analyzed by ANOVA, Tukey post hoc test and Bonferroni correction. $P<0.05$ is considered significant.

Results:
Blood oxygenation was better in the sevoflurane/LPS vs. propofol/LPS group (9h: 465±34 vs. 405±73; 12 h: 456±43 vs. 383±60; 15 h: 451±38 vs. 368±52; 18 h: 433±46 vs. 321±76; 21 h: 429±35 vs. 295±65; 24 h: 415±61 vs. 243±58 mmHg, p after 9h <0.01, all other p< 0.001).
Cell count (in 10^6 cells/ml) in BALF was lower in sevoflurane/LPS vs. propofol/LPS animals (12h: 21.4±3.2 vs. 31.8±14.1; 18h: 28.1±10.0 vs. 44.2±5.1; 24h: 27.9±7.2 vs. 49.8±13.5, all $p<0.001$).
Peak values of IL-6 and CINC-1 in BALF were reached at 6h and were attenuated in the sevoflurane/LPS vs. propofol/LPS group (IL-6: 9.2±2.3 vs. 18.8±7.0 ng/ml, $p<0.001$ and CINC-1: 2.7±0.7 vs. 4.0±0.8 ng/ml, $p<0.001$). MCP-1 peaks (at 18h) were not affected by sevoflurane.
In the blood, MCP-1 after 24h was lower in the sevoflurane/LPS vs. propofol/LPS (277±116 vs. 476±177 ng/ml, $p<0.05$). CINC-1 was not affected by sevoflurane.
Albumin and whole protein concentration in BALF was increased in ALI animals, but remained unaffected by sevoflurane.

Conclusion:
Long-term application of sevoflurane improves blood oxygenation and decreases inflammatory reaction in ALI in rats. Sevoflurane may therefore be an interesting sedative in patients suffering from ALI in the future.
References
Anesthesiology. 2009 Dec; 111(6):1238-48

2202

F. Wehrle[1], A. Hüsser[5], A. Buchmann[6], B. Bea[2], R. Huber[2], R. O'Gorman[3], K. Kaufmann[4], H. Speckbacher[3], C. Verrey[5], C. Hagmann[1]

Volume of Cerebellum and Thalamus Is Associated with Working Memory Performance in Children and Adolescents Born Very Preterm

Division of Neonatology, University Hospital Zurich, Zürich[1], Child Development Centre, University Children's Hospital, Zurich[2], Center for MR Research, University Children's Hospital, Zürich[3], Department of Psychiatry and Psychotherapy A, General Hospital, Hall in Tyrol, Austria[4], Department of Psychology, University of Zurich, Zürich[5], Department of Neurology, University Hospital Zurich, Zürich[6]

Introduction:
Children and adolescents born very preterm (VPT) are at increased risk for altered brain development [1] and impaired cognitive performance such as working memory [2]. Decreased regional brain volume in VPT infants has been associated with later working memory deficits [3]. Little is known on regional brain volumes and working memory in older children and adolescents after VPT birth. This study therefore aims to identify associations between regional brain volume and working memory performance in VPT children and adolescents and to compare them to healthy term-born peers.

Methods:
Thirty-three VPT children and adolescents (age: 12.7 [*1.5, 10.4-15.8*] years) and 34 term-born peers (age: 12.4 [*1.7, 10.0-15.8*] years) were examined. Three-dimensional T1- and T2-weighted MR images were acquired on a 3T GE scanner. Regional brain volumes were calculated using FreeSurfer 5.3.0. Working memory was assessed using the spatial working memory (SWM) task of the Cambridge Neuropsychological Testing Automated Battery (CANTAB).

Results:
No significant group differences ($p > .05$) in regional brain volume were apparent after controlling for intracranial volume (ICV). The total amount of errors (M, [*SD*]) in the SWM task was not different ($p = .840$) between VPT participants (20.1, [*15.3*]) and term-born peers (20.1 [*14.2*]). There was a significant associations between regional brain volumes and working memory performance in VPT participants: After controlling for ICV, the number of errors in the SWM task correlated negatively with the volume of the cerebellar white matter on the right ($r = -.359$, $p = .043$), the cerebellar white matter on the left (trend level; $r = -.315$, $p = .079$), the thalamus on the right (trend level; $r = -.331$, $p = .065$) and the thalamus on the left side ($r = -.437$, $p = .012$). In term born peers, no correlation was found.

Conclusion:
Working memory performance is specifically linked to thalamic and cerebellar volumes in VPT adolescents but not in term-born controls. This implies a specific anatomical correlate of working memory in adolescents at risk for altered brain development.

References:

[1] De Kieviet et al., Dev Med Child Neurol 2012, for a review
[2] Mulder et al., Dev Neuropsychol 2009, for a review
[3] Beauchamp et al., Brain 2008

2203

C. Eberhardt[1], M. Wurnig[1], A. Wirsching[2], M. Lesurtel[2], A. Boss[1]

Assessment of tissue diffusion and pseudo-diffusion of abdominal organs by intravoxel incoherent motion MRI in a cohort of C57Bl/6 mice

Institute for Diagnostic and Interventional Radiology, University Hospital Zürich, Zürich [1], Department of Visceral and Transplant Surgery Research, University Hospital Zürich, Zürich[2]

Introduction:
Intravoxel Incoherent Motion (IVIM)-MRI is increasingly applied for characterization of organ lesions, assessment of diffuse parenchymal pathologies and therapy monitoring. Required IVIM reference parameters for translational research were determined in a large cohort study of C57Bl/6 laboratory mice (n=50).

Methods:
Anesthetized mice were measured in a 4.7T small animal MR imager with a diffusion-weighted spin-echo echo-planar imaging sequence (*b*?values 0, 13, 24, 55, 107, 260, 514, 767, 1020 s/mm^2). Using a two-step approach to IVIM analysis, tissue diffusion D_t and perfusion fraction f_p were initially retrieved for *b*>100 using a linear fit to the log-transformed signal intensities, subsequently the pseudo-diffusion D_p was calculated from a bi-exponential fit to all measurement points.

Results:
Tissue specific diffusion parameters were for the liver D_t=1.2±0.2 x 10^{-3} mm^2/s; D_p=39.6±18.5 x 10^{-3} mm^2/s; f_p=15.4±6.8, for renal cortex D_t=1.5±0.2 x 10^{-3} mm^2/s; D_p=24.8±18.5 x 10^{-3} mm^2/s; f_p=11.8±5.9, and for renal medulla D_t=1.6±0.2 x 10^{-3} mm^2/s; D_p=35.0±22.8 x 10^{-3} mm^2/s; f_p=16.2±5.9. Spleen was characterized by D_t=0.6±0.2 x 10^{-3} mm^2/s; D_p=45.1±24.0 x 10^{-3} mm^2/s; f_p=10.8±5.8 and small bowel by D_t=1.1±0.2 x 10^{-3} mm^2/s; D_p=15.8±8.4 x 10^{-3} mm^2/s; f_p=18.9±8.7.

Conclusion:
We obtained relatively stable results for D_t, whereas D_p and f_p showed higher variability, which may be attributed to residual body motion and physiological tissue variability. The reported values may serve as reference parameters for future studies on small animal disease models using IVIM for tissue characterization.

2204

Y. Yamada[1], J. Jang[1], I. Inci[1], W. Weder[1], W. Jungraithmayr[1]

The CD26-costimulatory pathway is critical for Th17-mediated lung allograft acceptance

Division of Thoracic Surgery, University Zurich, Zurich, Switzerland[1]

Introduction:
The molecule CD26, a type II transmembrane glycoprotein, is expressed on activated T and B cells leading to classical T-cell co-stimulation and plays an important role in regulating $CD4^+$ T cell activation in autoimmune diseases. Recently, Th-type 17-differentiated $CD4^+$ T cells have been shown to be phenotypically characterized by a high expression of CD26. Here, we hypothesize that the co-stimulatory blockade of CD26 during acute rejection (AR) results in reduced $CD4^+$ Th-17 cell alloreactivity, thereby promoting mouse lung transplant (Tx) acceptance.

Methods:
In vitro experiments (n=4): mixed lymphocyte reaction (MLR) was performed between sorted CD4+ T cells from C57BL/6 mice as targets (T) and splenocytes from BALB/c being effectors (E) in a E:T ratio of 1:2 upon CD26-inhibition using the reversible inhibitor Vildagliptin in increasing concentrations. *In vivo* experiments (n=11): MHC class I and II complete mismatched mice, BALB/c (donors) and C57BL/6 (lung Tx recipients) were used. $CD26^{-/-}$ recipient mice were used for gain of function experiments. Inhibition of CD26 in the recipient was achieved by daily sc. application of 10 mg/kg BW of Vildagliptin from the time of until day 5. Macroscopy, histology, immunohistochemistry (IHC for $CD3^+$ T cells) and IL-17A levels (ELISA) were analyzed.

Results:
Levels of IL-17A were significantly reduced in MLR experiments when increasing the concentrations of Vildagliptin ($p=0.003$) . Upon Tx, macroscopically, allografts from untreated mice (control) show severe AR, histologically A4, from Vildagliptin-inhibited mice show attenuated AR, histologically A1, and from $CD26^{-/-}$ mice show minimal AR, histologically A2.

Conclusion:
Based on our *in vitro* experiments showing that CD26-inhibition results in a reduction of $CD4^+Th17^+$ derived IL-17A, we unravel that *in vivo* blockade of the CD26-costimulatory pathway leads to AR macroscopically as well as to a reduced infiltration of alloreactive CD3 T^+ cells and an attenuation of AR. These findings identify CD26 as an important, yet underestimated co-stimulatory molecule in Th17-mediated lung allograft rejection.

2205

L. Peter[1], Th. Reding[1], G.M. Seleznik[1], S. Sonda[1], R. Graf[1]

Effects of p21 deficiency in murine autoimmune pancreatitis

Swiss HPB Centre, Visceral & Transplantation Surgery, University Hospital Zurich, Switzerland[1]

Introduction:
The cell cycle inhibitor p21 has been already described as a mediator of autoimmunity in several diseases such as lupus nephritis and rheumatoid arthritis. In two independent mouse models of autoimmune pancreatitis (AIP) (MRL/Mp; *Tg(ELa1-Lta,b)* we found p21 up-regulated in pancreas compared to healthy animals. Thus, we started to investigate the role of p21 in AIP development.

Methods:
In order to study the role of p21 in AIP we have combined a transgenic mouse model, that spontaneously develops AIP (*Tg(ELa1-Lta,b);* **LT**) with mice deficient in p21 (**p21$^{-/-}$**) to get p21$^{-/-}$ x *Tg(ELa1-Lta,b)* (**LTp21$^{-/-}$**). The wild type (**wt)** controls, and all genotype groups were bred on a mixed C57BL/6 x 129SV background. First, the immune profile of the four genotypes (LTp21$^{-/-}$; LTp21$^{+/+}$; p21$^{-/-}$ and wt) was established at 12 months of age, when LT mice already have an autoimmune phenotype. We assessed whether p21 affects recruitment of immune cells using immunohistochemistry and qPCR.

Results:
Macrophages, B-cells and T-cells, as well as the degree of fibrosis and number of proliferating and apoptotic cells in pancreatic tissue were quantified. Immunohistochemical analysis showed a significant, three fold reduction of the number of macrophages in pancreatic tissue of LTp21$^{-/-}$ compared to LTp21$^{+/+}$ mice. On the other hand, p21 deficiency did not affect the overall number of B- and T-cells in the AIP background. We found less mitotic acinar cells in LTp21$^{-/-}$ than in LTp21$^{+/+}$ mice. qPCR results showed significant differences in inflammatory cytokine and chemokine expression. Genes involved in B-cell activation and attraction, as well as fibrosis (e.g. *Cxcl13, α-Sma*) were increased in LTp21$^{-/-}$ mice. Genes implicating macrophage activation and apoptosis, (*Emr1, Larc and Bcl-2*) were dependent on the presence of p21. In currently ongoing experiments we are testing if the onset of autoimmunity is affected in LTp21$^{-/-}$. Total IgG production in the pancreas, as well as circulating autoantibody levels against pancreatic self-antigens will be quantified. Finally, using immunohistochemistry, number, mass and cellular composition of tertiary lymphoid organs (TLOs) in the pancreas will be examined.

Conclusion:
Autoimmune pancreatitis is characterized by different inflammatory processes. Lack of p21 affects these cellular processes selectively: while the phagocytic cells are dependent on the presence of p21, the humoral immune response is not affected.

2206

A. Wyss[1], T. Raselli[1], K. Atrott[1], I. Frey-Wagner[1], AW. Sailer[2], G. Rogler[1], B. Misselwitz[1]

The role of EBI2 and oxysterols in the pathogenesis of inflammatory bowel diseases (IBD) and the generation of lymphoid structures in mouse intestine

Gastroenterology and Hepatology, University Hospital Zurich, Zurich[1], Novartis Institutes for BioMedical Research, Basel[2]

Introduction:
The oxysterol 7alpha,25-dihydroxycholesterol (7alpha,25-OHC) is a chemoattractant for immune cells expressing Epstein-Barr virus-induced gene 2 (EBI2) and directs their migration. EBI2 is a G-protein coupled receptor which is primarily expressed in lymphoid tissue and leukocytes. Mice lacking EBI2 or enzymes responsible for production of 7alpha,25-OHC show severe defects in the generation of T cell dependent antibody responses. Recently EBI2 was identified as a risk gene for inflammatory bowel diseases (IBD). Furthermore, EBI2 was found amongst genes upregulated in the ileum of CD patients with mutations in NOD2 compared to CD patients with a NOD2 wildtype genotype.

Methods:
We used mice with and without a functional EBI2-7alpha,25-OHC system in models of acute and chronic colitis. Colitis was induced by administration of 2-3% DSS for 7 days (acute) or 4 cycles of 7 days interspersed with 10 days recovery periods (chronic) in EBI2 and CH25H knockout mice and wildtype controls. Disease severity was determined by colonoscopy, colon length, histopathological analyses, MPO activity and expression of typical inflammation markers.

Results:
In the acute colitis model expression of EBI2 and both enzymes responsible for 7alpha,25-OHC synthesis, CH25H and CYP7B1, were significantly upregulated in the colon after DSS treatment. In chronic DSS colitis histological scoring revealed significantly stronger mucosal inflammation in CH25H knockout mice as compared to wildtype controls (4.0±0.4 and 2.8±0.8, $p < 0.05$). The number of lymphoid structures detected in colon tissue was significantly lower in both EBI2 and CH25H knockout mice as compared to wildtype controls ($p < 0.01$ and $p < 0.05$).

Conclusion:
The development of the intestinal lymphoid tissue and the intensity of inflammation in chronic DSS colitis seem to depend on an intact EBI2–7alpha,25-OHC system. These findings may establish EBI2-mediated cell migration as an important step in IBD pathogenesis and development of the gut immune system.

2207

K. Schilcher[1], F. Andreoni[1], S. Uchiyama[1], T. Ogawa[1], RA. Schuepbach[2], AS. Zinkernagel[1]

Increased NET-mediated Staphylococcus aureus clearance through inhibition of nuclease activity by clindamycin and immunoglobulin

Division of Infectious Disease and Hospital Epidemiology, University Hospital Zurich, Zurich[1], Division of Surgical Intensive Care, University Hospital Zurich, Zurich[2]

Introduction:
The Gram-positive human pathogen *Staphylococcus aureus* causes a variety of human diseases such as skin infections, pneumonia, and endocarditis. The nuclease Nuc1 is one of the major *S. aureus* virulence factors. By degrading DNA it allows the bacterium to avoid neutrophil extracelluar trap (NET)-mediated killing. The aim of this study was to test whether the protein synthesis inhibitor clindamycin or pooled human immunoglobulin blocks nuclease activity and whether this blockage translates into enhanced *S. aureus* clearance.

Methods:
S. aureus wild-type and a nuclease deficient strain were grown in the absence or presence of sub-clindamycin concentrations. Furthermore bacterial supernatants were incubated with pooled human immunoglobulin. We analysed extracellular nuclease activity and its inhibition by a DNA cleavage reporting assay and NETs degradation. The impact of nuclease activity on bacterial host clearance was tested by total neutrophil and NETs-mediated killing assays. Further we performed quantitative RT-PCR on *nuc1* of LAC wild-type grown in presence and absence of sub-clindamycin.

Results:
We found that addition of the protein synthesis inhibitor clindamycin to *S. aureus* LAC cultures decreased *nuc1* transcription and subsequently blunted nuclease activity. Further we observed reduced NETs degradation through Nuc1 inhibition translating into increased NET-mediated clearance. Similarly pooled human immunoglobulin specifically inhibited nuclease activity in a concentration-dependent manner. We also showed that in three clinical clindamycin-resistant *S. aureus* strains, sub-clindamycin did not inhibit Nuc1 expression or nuclease activity.

Conclusion:
Inhibition of nuclease activity by sub-clindamycin and immunoglobulin enhanced *S. aureus* clearance and should be considered when treating *S. aureus* infections.

2208

GM. Seleznik *[1], Th. Reding*[1], S. Sonda[1], M. Souter[1], M. Heikenwalder*[2], R. Graf*[1]

Lymphotoxin promotes acinar cell reprogramming and accelerates pre-neoplastic conversion in Kras induced pancreatic tumorigenesis

Swiss HPB Centre, Visceral & Transplantation Surgery, University Hospital Zurich, Switzerland[1], Institute of Virology, Technische Universität München–Helmholtz Zentrum München, Munich, Germany[2]

Introduction:
Pancreatic inflammation is a well-known risk factor for pancreatic ductal adenocarcinoma (PDAC) development in humans. PDAC initiation is linked to activating mutations in KRAS oncogene. Pancreatic acinar cell transdifferentiation results in acinar-to-ductal metaplasia (ADM), which can give rise to pancreatic intraepithelial neoplasia (PanIN), the most common precursors of PDAC. However little is known about the mechanisms how inflammatory damage promotes ADM and PanIN development.

Methods:
Here we establish a new genetic model (LTKP) by intercrossing the commonly used $p48^{+/Cre};Kras^{+/G12D}$ (KP) model for pancreatic tumorigenesis, to a novel transgenic mouse developing spontaneous pancreatic inflammation, reminiscent of human pancreatitis due to overexpression of Lymphotoxin (LT). Immunohistochemistry along with RT-PCR were used to obtain an inflammatory signature. *In vitro* transdifferentiation experiments were performed to investigate the role of LT on ADM development.

Results:
Overexpression of Lymphotoxin in mice harbouring a constitutively active form of Kras mutation in the pancreas (LTKP) dramatically accelerates the development of premalignant PanIN lesions compared to KP animals. Already at the age of 6 weeks highly proliferating cells, extensive ADM and PanIN development are observed in LTKP mice. This coincides with a significant upregulation of inflammatory genes and increased activated (GTP-bound) Kras. These molecular and phenotypic changes are only observed around 16 weeks in Kras animals. *In vitro* experiments show that LT overexpression in wt acinar cells is sufficient to initiate spontaneous transdifferentiation, furthermore acinar cells derived from LTKP-animals form ADMs significantly faster than cells from KP-animals.

Conclusion:
We conclude that Lymphotoxin may contribute to the initiation of spontaneous and pancreatitis-accelerated PDAC precursor formation: By (1) inducing inflammatory environment and by (2) regulating acinar cell transdifferentiation, leading to accelerated pre-malignant PanIN lesion development.

2209

CF. Waschkies[1], T. Reding Graf[1], GM. Seleznik[1], U. Ungethüm[1], R. Graf[1]

Magnetic Resonance Imaging of the Pancreas in a Transgenic Mouse Model of Pancreatic Carcinogenesis

Pancreatitis-Research Laboratory / Division of Visceral and Transplantation Surgery, University Hospital Zurich, Zurich[1]

Introduction:
To date, MRI has been appreciated in the clinical assessment of various pancreatic diseases such as pancreatitis and in the diagnosis of pancreatic cysts and tumors. However, only few preclinical studies infer upon MRI to assess and monitor pancreatic tissue changes in the commensurate animal models. Pancreatic inflammation is a risk factor for pancreatic ductal adenocarcinoma development in humans, and its initiation is linked to activating mutations in KRAS oncogene (p48+/Cre;Kras+/G12D, refered to as KP model here). Recent studies propose a stepwise process starting from acinar cells undergoing ductal reprogramming through premalignant pancreatic intraepithelial neoplasia lesions leading to tumor formation. In the present study we report on the potential of preclinical MRI to visualize the murine pancreas and changes associated with cellular transformations in a mouse model of pancreatic carcinogenesis.

Methods:
MR imaging was performed on a 4.7T/20 cm Bruker PharmaScan unit equipped with transmit/receive a 40 mm bird-cage resonator. T1- (FLASH, TE/TR 5/410ms, FA 80°, NA 6 and TE/TR 3.5/16.2ms, FA 15°, NA 96, in a single slice, respectively) and T2-weighted images (turboRARE, TE/TR 33/2000ms, factor 8, NA 16) were acquired in 18 image slices at a spatial resolution of 117x117x700um^3. Two wildtype and two KP mice were fasted 2-6h prior the MR examination to reduce peristaltic motion. During MRI mice were intubated, mechanically ventilated and maintained under 2.4% isoflurane anesthesia in a 1:5 oxygen:air mixture. Animals were placed supine onto a heated animal bed and fixed by adhesive tapes to reduce respiratory motion at the level of the pancreas. A venous catheter was inserted into the tail vein and a bolus of 50uL Gd-DOTA (Dotarem®, Guerbet S.A.) was injected for contrast-enhancement. Throughout the MRI procedure body temperature of the animals was kept at 37°C and respiratory motion was continuously monitored.

Results:
High-resolution abdominal images were obtained with commensurate image quality. The pancreas was identified and outlined anatomically by locating the head of the pancreas using the posterior border of the stomach, spleen and kidney as anatomical landmarks and tracing it through subsequent posterior slices. In the KP mice the pancreas was found to be substantially enlarged and to extend laterally into the right side of the animal, confirmed by autopsy after the MRI examination. Dotarem facilitated delineation of the pancreas by changing contrast to surrounding structures. Furthermore, KP pancreas presented as heterogenous in T2- and T1-weighted images; however, focal changes <200um in diameter were only clearly distinguished in MRI on ex vivo preparations of the pancreas. Heterogeneity in the pancreatic mass of the KP mice is consistent with histological findings of acinar and ductal metaplasia in this animal model.

Conclusion:
Our preliminary data point towards MRI providing a non-invasive in vivo technique to assess carcinogenic tissue transformation in murine pancreas in transgenic mouse model of pancreatic carcinogenesis.

2210

M.G. Dietrich[1], R.A. Zuellig[1], B.A. Hemmings[2], G.A. Spinas[1], R. Lehmann[1], O. Tschopp[1], M. Niessen[1]

PKBα regulates pancreatic β-cell mass

Endocrinology, Diabetes & Clinical Nutrition, University Hospital of Zurich, Switzerland[1], Friedrich Miescher Institute (FMI) for Biomedical Research, Basel, Switzerland[2]

Introduction:
Loss of PKBα or PKBβ in mice results in increased or decreased glucose tolerance, respectively, whereas loss of PKBγ has no effect. The regulation of β-cell mass is normal in these mouse models indicating that no single isoform is required *in vivo* in pancreatic islets. The aim of this study is to test how gain-of-function (GOF) for PKB isoforms affects regulation of proliferation, growth, apoptosis, and insulin production in human islets.

Methods:
Human islets (7 donors) were obtained from the Juvenile Diabetes Research Fund (JDRF) and the European Consortium for Islet Transplantation's (ECIT) "Islets for Research Distribution Program". Intact (4 donors) or dissociated islets (3-4) donors were cultured on extracellular matrix (ECM)-coated dishes. GOF was induced by overexpressing PKBα or PKBβ (GFP as control) from adenoviral vectors. Proliferation and apoptosis were assessed by BrdU incorporation and TUNEL. Insulin secretion (GSIS) and insulin content were assessed with intact islets. Insulin was measured by ELISA. β-Cell size was determined after dissociation of islets. At least 50 intact islets or 2000 cells from dissociated islets in triplicate were evaluated.
Data were normalised to GFP control and presented as mean ± SE and were analysed by student's t test.

Results:
In intact islets, PKBα increased overall proliferation to 3.21 ± 0.78 fold ($p < 0.005$) and PKBβ to 1.4 ± 0.19 fold ($p < 0.05$). Only PKBα increased β-cell proliferation significantly after dissociation of the islets (PKBα: 3.52 ± 0.38 fold ($p < 0.005$); PKBβ: 2.1 ± 0.58 fold). Only 15.4% +/- 1.4% of all proliferating cells were β-cells. β-cell size was significantly increased by PKBα (1.56 ± 0.12 fold ($p < 0.005$)) and PKBβ (1.45 ± 0.08 fold ($p < 0.005$)). In intact islets IL-1β increased apoptosis 2.36 ± 0.33 fold ($p < 0.005$). PKBα prevented the IL-1β-induced increase in apoptosis ($p < 0.05$), whereas PKBβ had no effect. After dissociation of islets IL-1β did not affect apoptosis. 76% +/- 5.9% of the apoptotic cells were β-cells. Only PKBα decreased significantly basal apoptosis of β-cells by 60% ($p < 0.01$) whereas PKBβ had no effect.
In dissociated islets, PKBα increased the percentage of insulin-positive cells by 10.8% +/- 2.1% ($p < 0.005$). PKBβ had no effect.
No significant increase of insulin content and no change in GSIS were detected.

Conclusion:
Our findings indicate significant differences between intact and dissociated human islets, with respect to the potency of IL-1β to induce apoptosis, possibly due to cellular interactions in intact islets. Overall PKBα appears to be more potent than PKBβ in regulating human islet mass as it protects β-cells from apoptosis and increases the percentage of β-cells to non-β-cells.

2211

K. Schlesinger[1], S. Sonda[1], R. Graf[1]

3,3',5-Triiodothyronine Improves Pancreatic Regeneration in Murine Acute Pancreatitis

USZ, Viszeralchirurgie[1]

Introduction:
Acute pancreatitis (A.P.) is an inflammatory disease with a high morbidity and mortality. Sustained inflammation leads to tissue damage and over time, a loss of function, which is exacerbated by the limited regenerative capacity of the pancreas. Damage to the acinar cell, triggers a transient dedifferentiation with loss of amylase. Thyroid hormone, 3,3',5-Triiodothyronine (T3), is a potent mitogen initiating a proliferative response in a number of organs. Our initial investigations were to elucidate the molecular role of T3 *in vivo* on the exocrine pancreas of healthy mice. Further, we used a cerulein-induced A.P. mouse model to investigate the potential of T3 to improve pancreas regeneration in this pathology.

Methods:
In vivo models using healthy mice given T3 with and without cerulein-induced A.P. Biochemical and immunohistochemical analyses were carried out to determine the mitogenic effects of T3 in healthy pancreas. T3 was also applied during disease progression of A.P and compared with untreated mice over a time-course of one week.

Results:
We found that T3 elicits a mitogenic effect in the healthy exocrine pancreas in a time-associated manner without inducing cellular damage or inflammation. T3 triggers a decrease in α-amylase levels and increased gene expression of Notch signalling mediators. This is indicative of pancreatic dedifferentiation, yet without the occurrence of acinar-to-ductal metaplastic (ADM) lesions. In the context of A.P., T3 significantly increases expression of proliferative markers in acinar cells. T3 reduces ADM lesion formation, which is suggestive of T3 improving pancreatic regeneration.

Conclusion:
We conclude that T3 significantly increases the replicative capability of the exocrine pancreas in healthy mice. T3 also significantly increases acinar proliferation during acute pancreatitis, whilst reducing ADM lesions. Therefore, T3 may have a therapeutic role to improve pancreatic regeneration.

2212

K. Frontzek[1], P. Georgiadis[1], T. Sonati[1], S. Sorce[1], P. Schwarz[1], A. Aguzzi[1]

A novel fluorescence-based live-imaging assay for sensitive detection of neuronal cell loss in hippocampal organotypic slice cultures

University Hospital Zurich, Institute of Neuropathology, Zurich, Switzerland[1]

Introduction:
Neuronal cell loss is a mutual hallmark of neurodegenerative diseases such as Parkinson's, Huntington's and prion disease. Its assessment usually relies on post-hoc immunohistochemistry of fixed tissue samples using neuron-specific markers with high read-out variability or a plethora of typically indirect assays that depend on cellular release of stress-induced proteins or loss of mitochondrial membrane potential and many more. Recently, we showed that monoclonal antibodies targeting the globular domain of the cellular prion protein (PrP^C-GD) induced widespread neuropathological changes similar to prion disease, i.e. neuronal loss, microglial activation and astrogliosis. Our goal was to establish a direct and sensitive live-imaging assay of neuronal cell loss in anti-PrP^C-GD antibody-induced neurotoxicity that eventually leads to reduced read-out variability of neuronal cell loss compared to previously used post-hoc immunohistochemistry.

Methods:
Transgenic mice from the commercially available strain Thy1.2/YFP16, Tg(YFP16), selectively express yellow fluorescent protein (YFP) in CA1 pyramidal neurons under the Thy1.2 expression cassette and were further crossed to tga20 prion protein overexpressing and $Prnp^{0/0}$ animals. *Ex vivo* hippocampal organotypic slice cultures (hOCS) from Tg(YFP16) animals were imaged repeatedly using confocal laser-scanning microscopy and pharmacological treatments of hOCS were performed using the PrP^C-GD targeting antibody POM1. Semi-automatic detection of neuronal cell counts was done using Imaris software. All pharmacological treatment schemes were repeated in non-fluorescent hOCS and quantified by conventional morphometry of fluorescently labeled neuronal nuclei as described before. The read-out variability between both methods was compared using the F-test of equal variances. Furthermore, POM1-treated hOCS underwent post-hoc immunohistochemical stainings of for the pre- and postsynaptic proteins Synapsin I, Synaptophysin and PSD-95.

Results:
Pharmacological manipulation of hippocampal Tg(YFP16) OCS with POM1 reliably reproduced our previously reported findings of PrP^C-mediated neurotoxicity from cerebellar OCS and hippocampal *in vivo* experiments. Semi-automated quantification of YFP^+ CA1 pyramidal neurons in Tg(YFP16) hOCS resulted in 50% of the performed experiments in increased read-out sensitivity when compared to post-hoc immunohistochemical morphometry in non-YFP hOCS. Live-imaging of Tg(YFP16) hOCS additionally allowed the construction of slice-based slopes for neuronal cell loss. Furthermore, PrP^C-antibody mediated neurodegeneration in the hippocampus was associated with a redistribution of synaptic proteins such as Synaptophysin, Synapsin I and PSD-95.

Conclusion:
Our newly developed assay allows for a more sensitive assessment of neuronal cell loss in PrP^C-antibody induced toxicity than hitherto used post-hoc morphometry. Further investigations of the observed synaptic protein redistribution after treatment with PrP^C-GD directed antibodies may broaden the knowledge about synaptic dysfunction as induced by infectious prions. Robust and reliable assays of neurodegeneration might improve screenings for novel, putatively neuroprotective and neurotoxic compounds in prion disease.

2213

A. König[1], D. Cadosch[1], M. Werner[1], HP. Simmen[1], A. Wanner[1], C. Cinelli[1]

Prospective isolation of perivascular stem cells for the treatment of critical size bone injuries

Division of Trauma Surgery, University Hospital Zurich, Zurich[1]

Introduction:
Multipotent mesenchymal stem cells (MSCs) can be isolated from different adult tissues (e.g. bone marrow and adipose tissue) and represent an interesting source of cells for therapeutic applications. MSCs consist of a heterogenous population of stem/progenitor cells, which exhibit osteogenic, chondrogenic, and adipogenic potentials. An interesting subpopulation is represented by the perivascular cells (pericytes), which can be prospectively identified by the expression of CD146, NG2, and PDGF-Rbeta and absence of hematopoietic, endothelial, and myogenic cell markers.

Methods:
We isolated CD146+ NG2+ and CD45- cells from adipose tissue from C57BL/6 mice by magnetic activated cell sorting. We tested the potential of these cells to differentiate to osteoblast and their regenerative capacity in a mouse model of critical size bone defect.

Results:
Upon seeding on scaffolds (e.g. cancellous bone, tricalcium-phosphate) CD146+ NG2+ and CD45- isolated cells were differentiated for two weeks in osteogenic medium. Alizarin red staining and QRT-PCR confirmed the capacity of these cells to generate osteoblasts and induce calcium deposition (mineralization).
In a last step, as a proof of principle, we tested the regenerative capacity of these cells in a mouse model for femoral segmental critical-sized defect. This model is based on a 3.5-mm-long segmental bone defect where the bone fixed by a titanium microlocking plate with four locking screws (RISystem AG).
The freshly isolated cells were seeded on a collagenous bone scaffold which upon overnight cultivation in vitro was inserted in the segmental bone gap. A control
group with collagenous bone scaffold but without cells was used. Eight weeks upon operation the bones were isolated and analyzed by micro-computer tomography. In the animals which obtained a collagenous bone graft with perivascular stem cells an evident stronger mineralization was present as compared with the scaffold only controls.

Conclusion:
Perivascular stem cells (CD146+NG2+CD45-) isolated from ASCs are able to contribute to bone regeneration and might represent a valuable alternative for improving bone healing in critical size bone injuries.

2214

M. Brock[1], TJ. Haider[2], J. Vogel[2], M. Gassmann[2], M. Kohler[1], S. Ulrich[1], LC. Huber[1]

The tumor suppressor CDKN1A (p21) is targeted by the microRNA family miR-130 in hypoxia-induced pulmonary hypertension

Division of Pulmonology, University Hospital, Zurich[1], Institute of Veterinary Physiology, Vetsuisse Faculty and Zürich Center for Integrative Human Physiology (ZIHP), University of Zürich, Switzerland[2]

Introduction:
Increased proliferation of pulmonary artery smooth muscle cells (PASMCs) causing vascular remodelling of the small pulmonary arteries is one of the hallmark features in the pathogenesis of pulmonary hypertension (PH). We recently demonstrated that the microRNA (miRNA) family miR-130 (i.e. miR-130a and miR-301a) is upregulated in the murine model of hypoxia-induced PH. In the current study the effect of miR-130 on the proliferation of PASMCs was investigated.

Methods:
For inhibition of the miR-130 family miRNA seed blockers were designed. BrdU proliferation assay was employed in PASMCs transfected with miRNA precursor molecules or seed blockers. Expression of cyclin-dependent kinase inhibitor 1A (CDKN1A, p21) was measured on RNA and on protein level. Reporter gene assay was used to proof direct miRNA-target interaction. To induce experimental PH the hypoxia mouse model (10% oxygen for 5 weeks) was used.

Results:
Proliferation of PASMCs was significantly increased by overexpression of miR-130a and miR-301a (by 37.9% and 62.4%, respectively) and decreased by transfection of seed blockers (reduction of 65.4%). Inhibition of the miR-130 family increased the expression of CDKN1a (by 55.7% on mRNA level, and by 72.2% on protein level). Reporter gene assays showed that miR-130 family directly targets CDKN1A. Expression of CDKN1A in lungs of hypoxic mice was found reduced as compared to normoxic controls (from 0.7±0.4 to 0.16±0.09, $p<0.01$, expression was normalized to beta-actin). Restoration of CDKN1A expression in mice was achieved by application of miR-130 seed blockers (from 0.16±0.09 to 0.51±0.28, $p<0.05$).

Conclusion:
Our results show that the miR-130 family triggers proliferation of PASMCs probably through repression of CDKN1A and that levels of CDKN1A could be restored in hypoxic mice by application of seed blockers. These data emphasize the potential role of miR-130 in pulmonary vascular remodelling.
This abstract was presented at the annual meeting of the Swiss Society of Pulmonology 2014.

2215

HC. Wong[1], HE. Kohrt[2], JA. Shizuru[2], AMS. Müller[1]

Maximizing Graft-Versus-Leukemia effects by WT1-vaccination of donors and stringent selection of allograft components

Experimental Hematology Division, University Hospital Zürich, Zürich[1], Division of Blood and Marrow Transplantation, Stanford University, Stanford, USA[2]

Introduction:
Allogeneic hematopoietic cell transplantation (HCT) is the only curative treatment option for many patients with aggressive leukemias, but is associated with high treatment-related morbidity and mortality. Despite the aggressiveness of this cellular therapy a substantial proportion of patients relapse and die of their disease. A major goal for allogeneic HCT is to engineer donor grafts to contain only cell types required to rescue blood production, recover immune function, provide curative graft-vs-leukemia (GVL) effects, but avoid deleterious graft-vs-host disease (GVHD). The goal of this study was to enhance the anti-tumor activity of immune cells in the donor by applying a vaccination against the tumor-associated peptide WT1, and select specifically these cells for transplantation into the recipient.

Methods:
The potency of isolated donor cell subsets to exert GVL was dissected in MHC-matched mouse models, that had genetic disparities in multiple minor antigens - a setting that resembles best transplantations as performed in humans. To enhance GVL activity donors were vaccinated with tumor-peptide WT1 plus incomplete Freunds adjuvants (IFA). Grafts consisted of purified hematopoietic stem cells (HSC [$cKit^+Thy1.1^{lo}Lin^-Sca1^+$]) and were augmented with $CD4^+$, $CD8^+$, naïve or memory $CD4^+$ and $CD8^+$ T cells, or WT1-tetramer+$CD8^+$ T cells ($CD8_{WT1}$). HSC +/- T-cell subsets were infused into lethally irradiated recipients. The luciferase-expressing FBL3 cell line, a myeloid leukemia, was inoculated on d0 or 14 post-transplant, and tumor growth was measured by bioluminescence imaging.

Results:
To model tumor persistence recipients were given tumor cells on the day of HCT. (i) HSC+$CD4^+$+$CD8^+$ T cells grafts from vaccinated donors rescued most recipients, while those from unvaccinated donors resulted in rapid death from leukemia; (ii) HSC+$CD8^+$, HSC+memory, or HSC+$CD8_{WT1}$ T cells from vaccinated donors provided improved but non-curative protection compared to HSC alone; (iii) HSC+$CD4^+$ T-cell grafts (vaccinated or unvaccinated) lead to rapid death; however, (iv) $CD4^+$ T-cells were required to fortify tumor eradication by $CD8^+$ T cells.
To model early relapse, tumor cells were infused on d14 post-transplant. (I) Now also a high proportion of recipients of HSC+$CD4^+$+$CD8^+$ from vaccinated donors died of leukemia. We hypothesize the lack of tumor antigens present at the time of T-cell infusion may have resulted in expansion of a different T-cell repertoire during lymphopenia and thereby diminished tumor-specific activity. (II) All subgroups given combinations of naïve/memory $CD8^+$ and $CD4^+$ T cells displayed prolonged survival compared with HSC recipients, but no long-term cure. (III) The best survival was observed in recipients of HSC+$CD8_{WT1}$ grafts supplemented with low numbers of $CD4^+$ T cells. This benefit was due to *in vivo* expansion of tumor-specific T-cells early post-transplant in absence of other competing CD8 T-cell clones and boosted by an additional d7-vaccine.

Conclusion:
Dynamics of donor effector populations are complex. Modalities to promote tumor specific $CD8^+$ T-cell expansion may be critical to maximize GVL effects. Immunogenic maneuvers such as vaccinations are powerful tools to enhance the potency of specific effectors. Our

approach of stimulating and activating tumor-specific immune responses already in the donor and continuing their expansion in the host (using donor and post-transplant vaccinations) is novel. However, before such manipulative approaches can be translated into clinical practice, dynamics and interactions of expanding donor populations must be clearly understood.

2216

F. Scholkmann[1], S. Kleiser[1], M. Pastewski[1], T. Hapuarachchi[2], C. Hagmann[3], JC. Auchère[3], M. Wolf[1]

Using nonlinear data analysis and data mining to assess physiological changes in preterm infants measured with near-infrared spectroscopy, pulse oximetry and electrocardiography

Biomedical Optics Research Laboratory, Division of Neonatology, University Hospital Zurich, 8091 Zurich, Switzerland[1], Department of Medical Physics and Bioengineering, University College London, London, UK[2], Division of Neonatology, University of Zurich, Zurich, 8091, Switzerland[3]

Introduction:
The physiological significance of the cerebral autoregulatory state as well as fluctuations in peripheral capillary (SpO_2) and cerebral tissue (StO_2) oxygenation in preterm neonates are receiving more and more attention. The goal of the present study was to show that data analysis techniques for nonlinear dynamical systems represent a powerful framework for investigating the characteristics of these fluctuations and their interdependence.

Methods:
To this end, StO_2, SpO_2 and the heart rate (HR) were measured on preterm neonates for several hours. For the present study we selected data sets from four neonates which provide a good signal-to-noise ratio. As an additional parameter, the fractional tissue oxygenation extraction (FTOE) was calculated. To characterize the fluctuations in StO_2, SpO_2, FTOE and HR, two methods were employed: (i) phase-space modeling and application of the recurrence quantification analysis (RQA), and (ii) maximum entropy spectral analysis (MESA). The correlation between StO_2 and SpO_2 as well as FTOE and HR were quantified by (i) nonparametric nonlinear regression based on the alternating conditional expectation (ACE) algorithm, and (ii) the maximal information-based nonparametric exploration (MINE) technique.

Results:
We found that (i) each neonate showed individual properties of StO_2, SpO_2, FTOR and HR characteristics, (ii) a ~60 min oscillation could be observed in all of the signals (possibly related to sleep stage transitions), (iii) the nonlinear correlation strength between StO_2 and SpO_2 as well as FTOE and HR was specific for each neonate and showed a high value for a neonate with a reduced health status, indicating an impaired cerebral autoregulation.

Conclusion:
In conclusion, the results demonstrate that our novel data analysis framework is suitable for analyzing complex physiological signals, enabling novel insights into the characteristics of hemodynamic and oxygenation changes in preterm infants.

2217

An. Kegel[1], Wk. Lai[1], Sa. Reidt[1], No. Dillier[1]

Measuring the real-life localization performance of hearing impaired persons in the laboratory

Laboratory for Experimental Audiology, University Hospital Zurich, Zürich[1]

Introduction:
Our auditory environment is complex – for normal hearing and hearing impaired people as well. There is a variety of hearing objects like speech, music, warning signals embedded in an also variable sounding background. It is hard to localize in this complex environment.
Therefore the task for hearing research is to develop hearing devices which are appropriate working according to these complex hearing conditions and show their benefit in the laboratory.
Hearing instruments could support localization by enhancing the audibility of localization cues on one hand, while making it difficult on the other because these enhancements may change the natural cues used for localization.
An explorative approach was taken to develop a test which would provide a valid, reliable, objective and efficient procedure to measure the localization ability of hearing impaired persons. This test involves the detection of realistic acoustic warning signals in realistic listening situations reproduced in controlled lab conditions.
Hypothesis: Differences are expected in the localization ability between normal hearing persons and hearing instrument users as well as CI-users, the latter two while wearing their devices.

Methods:
The VALE (**V**irtual **A**coustic **L**ocalization **E**xperiment)-Test was developed for measuring the identification from different hearing objects in different realistic listening situations.
The test environment provides a variety of realistic listening situations in a circle of 12 loudspeakers with different alarm signals as targets. The alarm signals could be either static or moving. In every measurement, accompanying head movements are also recorded.
The outcome measures are:

- RMS (**r**oot **m**ean **s**quare) errors, which describe the error in detection the angle between the object was presented and perceived
- front back confusions, which describe the error in detection the object in front of you instead of behind - or the other way around
- effort/costs to use the acoustic information for localization with help of the head movement measures

Five normal hearing participants, five participants with (moderate hearing loss) and hearing instrument in noise reduction setting and five participants with (severe hearing loss) and CI in noise reduction setting participated in the test.
The following scenes are presented:

- A public square with a braking tram (moving target)
- A railway station with a horn from a luggage car (static target)
- A street with a bicycle bell (static target)

The task of the participant was to press one of 12 possible buttons on a touchscreen indicating the direction from which the target was detected.

Results:
There are differences in localization ability between normal hearing people, hearing instrument- and CI-users regarding to RMS-errors, front back confusions, costs for localization and head movement measures.

Conclusion:
The VALE (**V**irtual **A**coustic **L**ocalization **E**xperiment) is an appropriate tool for hearing instrument verification. It is sensitive for a variety of hearing losses and provides test procedures in varying difficulties.

2219

J. Mwinyi[1], K. Vokinger[1], A. Jetter[1], U. Breitenstein[2], C. Hiller[1], GA. Kullak-Ublick[1], A. Trojan[2]

Impact of variable CYP Genotypes on Breast Cancer Relapse in Patients undergoing adjuvant Tamoxifen Therapy

Clinical Pharmacology and Toxicology, University Hospital Zürich[1], Breast Center Zürich, Switzerland [2]

Introduction:
Tamoxifen is frequently used for the treatment of hormone receptor positive breast cancer (BC). Mainly CYP2D6 is responsible for the transformation to therapeutically active metabolites, but CYP2C19, CYP2C9 and CYP2B6 also are involved. We investigated the impact of polymorphisms within the genes encoding these CYP enzymes on the relapse free time (RFT) in breast cancer patients.

Methods:
Ninety-nine hormone receptor positive breast cancer patients, who had undergone adjuvant tamoxifen therapy, were genotyped for seventeen common variants within the genes encoding *CYP2D6*, *CYP2C9*, *CYP2C19*, and *CYP2B6* using TaqMan and PCR/RFLP technology. Kaplan-Meier and Cox regression analyses were performed to elucidate the impact of genetic variants on RFT. Furthermore, CYP2D6 metabolic activity was determined in a subset of 50 patients by assessing dextromethorphan/dextrorphan urinary excretion ratios. CYP2D6 activity was compared to the *CYP2D6* allelic combinations to evaluate the predictive value of the CYP2D6 genotyping results on phenotype.

Results:
Although a trend towards longer RFTs in carriers of *CYP2D6* allele combinations encoding for extensive and ultrafast metabolizer phenotypes was observed, none of the investigated genetic variants had a statistically significant impact on RFT. The combined analysis of five major *CYP2D*6 variants was useful for the discrimination between poor and non-poor metabolizers.

Conclusion:
Comprehensive CYP2D6 genotyping has a good predictive value for CYP2D6 activity. Common variants in *CYP2C9, CYP2C19, CYP2D6* and *CYP2B6* did not have a significant impact on the RFT in this cohort of BC patients.

2220

LD. Frick[1], Y. Böge[1], F. Böhm[1], J. Friemel[1], L. Quagliata[2], LM. Terracciano[2], M. Heikenwälder[3], A. Weber[1]

Biliary/progenitor-cell markers and liver-specific Wnt target genes define distinct subgroups of hepatocellular carcinoma

Institute of Surgical Pathology, University Hospital Zurich[1], Institute of Pathology, University Hospital Basel, Basel, Switzerland[2], Institute of Virology, Technische Universität München, Munich, Germany[3]

Introduction:
Beta-catenin is the most commonly mutated oncogene in hepatocellular carcinoma (HCC), whereas the expression of biliary/progenitor-cell markers has been associated with poor prognosis. However, the relationship between Wnt-β-catenin activation and progenitor-cell phenotype is unclear.

Methods:
Based on preliminary results from murine liver tumors, in which a negative association between the biliary/progenitor cell marker A6 and β-catenin activation was observed on immunohistochemistry, a tissue microarray array analysis of two separate cohorts of hepatocellular carcinoma patients was performed. Results were further validated using immunohistochemistry of large tissue sections and data mining of publicly available whole-genome expression data.

Results:
A negative association was found between positivity for any of five liver progenitor-cell markers and expression of glutamine synthetase, a sensitive marker for beta-catenin mutation, in an initial tissue microarray analysis of 90 HCC patients. This could be confirmed in a validation cohort with 150 patients. In focal nodular hyperplasia of the liver, both cytokeratin 7, a biliary marker, and glutamine synthetase were overexpressed, but co-immunostaining of whole slides showed a complementary pattern of expression on the level of individual cells. Analysis of publicly available gene expression data showed that biliary and progenitor cell markers were almost exclusively upregulated in hepatocellular carcinoma without beta-catenin mutation. Furthermore, glutamine synthetase and other liver-specific Wnt targets were negatively associated with biliary markers and α-fetoprotein in a meta-analysis of over a thousand patients.

Conclusion:
Expression of biliary/liver progenitor cell markers and liver-specific markers of beta-catenin activation showed a negative association and define distinct subgroups of hepatocellular carcinoma.

2221

EX. Keller[1], C. Acevedo[1], A. Mortezavi[1], P. Kardas[2], J. Samaridis[2], T. Sulser[1], HH. Hirsch[2], M. Provenzano[1]

Antibody response against BK virus large tumor antigen as an independent predictor of biochemical recurrence after radical prostatectomy

Deparment of Urology, University Hospital Zürich, Zürich[1], Department Biomedicine (Haus Petersplatz), University of Basel, Basel[2]

Introduction:
Infectious agents, including viruses, have been ranked among inflammatory-related factors that are important for prostate cancer (PCa) development. However, virus involvement in prostate carcinogenesis remains to be demonstrated. In this study, we aimed at defining the role of Polyomavirus BK (BKV), a urotheliotropic virus that becomes latent in the urinary tract, in this malignancy by testing a humoral immune response against BKV proteins VP1 and L-Tag in patients with PCa at first diagnosis.

Methods:
A total of 264 consecutive PCa patients undergoing radical prostatectomy were enrolled in the study. Humoral responses (IgG level) against BKV-specific VP1 and L-Tag were analyzed by enzyme immunoassay (EIA) in sera of patients collected before surgery. Antibody titers were correlated to 5-year follow-up clinical data focusing on evidence of biochemical recurrence (BR) after surgery. Recurrence free survival (RFS) was the primary endpoint and was evaluated by Kaplan-Meier survival curves. In addition, a multivariate Cox regression analysis was modeled including established prognostic factors of BR (pathologic stage, Gleason score and surgical resection margin status). Association of the serology results with patients' clinicopathologic parameters was the secondary endpoint and was evaluated by Pearson's Chi-square tests or Mann-Whitney U test, as indicated.

Results:
Patients with a modest L-Tag-IgG titer showed a significantly lower RFS, as compared to patients with higher L-Tag-IgG titers (5-year RFS rate 65% vs. 75%, p=0.021). In the multivariate analysis, a weak anti-L-Tag IgG response independently predicted BR (HR 2.58, 95% CI 1.38-4.83, p=0.003). In contrast, differences in RFS when testing anti-VP1 IgG levels were not significant. Validity of established prognostic factors of BR could be verified. Baseline clinicopathologic parameters did not significantly differ after stratification for the serology results.

Conclusion:
A weak antibody response against BKV L-Tag before surgery is associated with a worse clinical outcome after radical prostatectomy for prostate cancer. On the contrary, antibody response against BKV VP1 cannot predict the course of the disease. This undoubtedly hints at a causative role of BKV L-Tag in the onset and progression of PCa and suggests the use of L-Tag as a potential biomarker for the follow-up of this disease. Furthermore, boosting anti-L-Tag IgG levels by vaccination means could allow a better immune-mediated control of the disease after prostatectomy.

2222

S. Sanchez[1], J. Mata Pavia[1], S. Lindner[1], E. Charbon[2], M. Wolf[1]

Last generation near infrared imaging system

KFSP Tumor Oxygenation project, Neonatologie, UniversitätsSpital, Zürich[1], TU Delft[2]

Introduction:
It is well known that tumor hypoxia is associated with adverse prognosis and tumor progression. In addition, hypoxia often substantially reduces effectiveness of therapy in particular for radio- and chemotherapy.
Unfortunately tumor oxygenation is not measured routinely, because no method is available that is non-invasive, reliable and repeatable.
The aim of this project is to develop such a method based on near-infrared imaging.

Methods:
An unprecedented high spatial resolution will be enabled by increasing the number of detectors to 16384, which is two orders of magnitude higher compared to previous imaging systems. In addition, the measurements will be time resolved, i.e. the arrival times of the photons will be determined with 100ps time resolution. The detector is based on a single photon avalanche diode array, which has the sensitivity to detect single photons. This detector camera is combined with the spectral capabilities of supercontinium lasers that produces ultrashort light pulses of 15ps duration and enables to freely select different wavelengths
The large data sets generated by the instrument are analyzed by a multi-core computer using a finite element method software package (Nirfast) optimized for parallel processing of time resolved data.
To reconstruct 3D images, the external shape of the tissue under investigation needs to be determined. A respective setup was developed and is based on time of flight measurements by the same imager. To further improve the imaging, the software takes advantage of MR and CT images, which are available from patients. This information will be used to define boundary conditions for accurate image reconstruction.

Results:
The system to measure the external shape of imaged tissue has been completed providing an accuracy of 1mm. The imager was also tested in tissue-like phantoms. A spatial resolution of 5mm has been achieved. Image reconstructions have been tested and examples will be presented. The performance of a new measurement method based on optical contrast at different wavelengths will be discussed in the context of its application to clinical cases as well.

Conclusion:
In the future a clinical setup will be designed to position and control the imager at the bed-side allowing the acquisition of data in patients. The imager will be optimized for this purpose and will be applied in clinical studies of tumor oxygenation within the framework of the KFSP Tumor Oxygenation generating tomographic images with a resolution in the order of millimeters.

2223

DM. Heuberger[1], M. Ender[1], RA. Schuepbach[1]

Co-receptor Dependent Activation of Protease Activated Receptors by Clotting Proteases.

Division of Surgical Intensive Care, University Hospital Zurich, Zurich[1]

Introduction:
Protease-activated receptors (PARs) are G-protein coupled seven transmembrane proteins, sensing for extracellular proteolytic activity. Clotting enzymes are prototypical agonists for PAR involved in a variety of biological processes ranging from platelet activation, vascular barrier regulation or regulation of apoptosis. All members of the receptor family (PAR1-4) are uniquely activated by protease cleavage of the N-terminal domain. Upon cleavage a neo-N-terminus is unmasked that serves as a tethered ligand activating PAR and induces transmembrane signaling. Efficient activation of cells surface expressed PAR requires recruitment of clotting proteases towards the cell membrane. In PAR1 and PAR3 activation via the prototypical clotting protease thrombin occurs through a direct PAR-thrombin binding interaction followed by cleavage of PAR. In contrast, PAR1 activation via the activated protein C (APC) depends on the endothelial protein C receptor – APC binding interaction allowing to bring APC and PAR1 together. We wondered whether other cell surface clotting (co-) receptors facilitate PAR cleavage and activation by clotting proteases.

Methods:
To determine whether co-receptors improve the efficiency of clotting proteases to cleave PAR, a cleavage reporter assay, was used. The assay bases on chimeric PAR expression constructs that carry a secreted alkaline phosphatase (AP) tag at the extracellular N-terminus of PAR. In case the AP-PAR molecule is cleaved, AP-activity is removed from the cell surface and released into the supernatant allowing to simply quantifying cleavage events by measuring cell bound and released AP-activity by the colorimetric substrate p-Nitrophenyl Phosphate. The AP-PAR constructs alone or together with the clotting protease binding proteins tissue factor (TF), thrombomodulin (TM) and endothelial protein C (EPCR) were transiently overexpressed in HEK T293 cells and clotting proteases were tested for PAR cleavage efficiency.

Results:
The screening experiment confirmed known co-receptor dependence, such as TF promoting PAR1 cleavage by FVIIa, EPCR boosting PAR1 and PAR3 cleavage by APC and Xa. We found a novel co-receptor function for thrombomudulin a cell surface thrombin receptor. When present, thrombomodulin facilitated thrombin mediated cleavage of PAR4 and PAR2. In addition unexpected inhibitory effects of EPCR on PAR cleavage by non EPCR binding proteases were observed.

Conclusion:
In our screening experiments in an overexpression system relaying on cleavage reporter assay we showed that the thrombomodulin boosts the efficiency of thrombin to cleave PAR2 and PAR4. Since thrombin and PAR2 have been found to be key players in chronic inflammation we speculate that this interaction might be of clinical importance.

2224

NC. Corti[1], SW. Weiler[1], MH. Hofer[2], TH. Hess[2], SW. Wehrli[2]

Colistimethate sodium and Colistin Pharmacokinetics in Ambulatory Hemodialysis – A Case Report

Clinical Pharmacology and Toxicology, University Hospital Zürich[1], Department of Internal Medicine, Cantonal Hospital of Winterthur[2]

Introduction:
Colistin is a polymyxin antibiotic for the treatment of Gram-negative infections, including *Pseudomonas aeruginosa*, *Klebsiella, Enterobacter* and *Acinetobacter* with concentration-dependent killing properties. A target plasma concentration > 2.5 mg/L has been suggested for most pathogens based on the minimal inhibitory concentration (MIC) breakpoints. After intravenous application of the prodrug colistimethate sodium (CMS), 60%-80% is excreted unchanged by the kidneys and the rest is hydrolyzed to its active form colistin (A and B), which itself is only minimally renally excreted. Dose reductions according to the degree of renal impairment are indicated due to CMS accumulation. However, product information does not give dosing recommendations for ambulatory intermittent hemodialysis (HD) and pharmacokinetic data of CMS and colistin in patients with severe renal impairment and HD with modern high flux filter are scarce.

Methods:
Pharmacokinetics of Colistin and CMS were assessed in a 48 kg female patient with endstage renal disease due to ANCA-Vasculitis undergoing HD three times weekly. The patient is also suffering from ANCA-Vasculitis related pulmonary disease with bronchiectasia. She has therefore been treated with Colistin® intravenously daily for chronic pulmonary infection with a multiresistant *Pseudomonas aeruginosa*. Sampling was performed over three days, i.e. twice during HD days and once on a non-HD day in between. 1.5 million units (MioU) Colistin® were infused over 30 minutes after the end of each HD session and 1 MioU was administered on the day without HD. HD was performed as postdilution Online Hemodiafiltration with the polynephron highflux filter *Elisio 19H* with a surface of 1.9m^2 for 4 hours with the following settings: blood flow 350-380 mL/min, dialysate flow 500 mL/min, total ultrafiltration rate 65-75 mL/min, net ultrafiltration rate 5-6 mL/min (1.5-1.8%). Peripheral blood samples were taken before and at the end of each Colistin® infusion with 3-4 samples taken additionally over the dosing interval to determine C_{min}, C_{max}, AUC_t, clearance and elimination half life. Peripheral blood samples were also taken before, during and after each HD session with additional samples from the prae- and postfilter line to determine HD clearance and fraction removed. Samples were immediately placed on ice, centrifuged and then frozen (-80°C) before analysis. Plasma concentrations of CMS and free colistin were determined by liquid chromatography–mass spectrometry.

Results:
Overall mean peak and trough concentrations of CMS were 20.4 mg/L and 3.1 mg/L, and of colistin 0.1mg/L and 2.2mg/L, respectively. Comparable colistin exposure was found during all three dosing intervals with steady plasma levels of 3.3-3.5 µg/mL of colistin on the non-HD day and 2.4-3.1 µg/mL on HD days. The higher Colistin® dose of 1.5 MioU administered shortly after the end of each HD compensated for the colistin removal of 71% - 75% during a HD session. Colistin half life was 2.3 hours and mean clearance was 59 mL/min during HD. Between HD sessions the plasma concentration time curve of CMS showed a rapid decline with hardly any CMS detectable before start of HD. Mean half life and clearance were 2 h and 20.2 mL/min for CMS, and 155 h and 1.5 mL/min for colistin, respectively.

Conclusion:
Colistin is significantly removed by HD. Target colistin plasma concentrations of >2.5mg/ml were reached with a Colistin® dosing regimen of 1.5 MioU administered shortly after HD and 1 MioU administered on non-HD days.

2226

K. Fritsch[1], P. Bourgine[2], E. Piccinini[2], M G. Manz[1], I. Martin[2], H. Takizawa[1]

Maintenance of human hematopoiesis and hematopoietic stem cells in in vivo engineered bone organs

Division of Experimental Hematology, University Hospital Zurich[1], Department of Biomedicine and Surgery, University Hospital Basel[2]

Introduction:
Lifelong self-renewal and multilineage repopulation capacity of hematopoietic stem cells (HSCs) are maintained in a specialized microenvironment in the bone marrow (BM), the so-called “niche” that provides HSCs with vital factors for HSC maintenance. Genetically modified animals have revealed that the mouse HSC niche consists of various cell types including endothelial cells, osteoblasts, macrophages, adipocytes, Schwann cells, Nestin+ mesenchymal stromal cells (MSCs), and CXCR12 abundant reticular cells. However, little is known about the cellular and molecular component of the human niche.

Methods:
We took a developmental tissue engineering approach which allows to differentiate human adult BM derived MSCs into a cartilage template ex vivo, and upon in vivo implantation develop bone organs through in vivo endochondral ossification. Ex vivo generated human cartilage templates were implanted subcutaneously in the back of immunodeficient mice, and 4 weeks after, a third party donor of human CD34+ cells were injected to reconstitute human hematopoiesis. The implanted ossicle were isolated and analyzed on histology and flowcytometry to characterize in vivo bone maturation and maintenance of human HSC and hematopoiesis in vivo, respectively. To identify the putative human niche factors that are expressed in the ossicle and responsible for human HSC maintenance, total RNA were isolated from in vitro expanded MSCs, in vitro differentiated ossicles and in vivo developed ossicles, and subjected to quantitative PCR.

Results:
Histological analysis at 3 months post implantation showed that human ossicles implanted into immunodeficient mice developed vascularization and mature bone in all cases analyzed (42 vascularized/42 implanted). Flowcytometric analysis 3 months post transplantation showed comparable or better development of human hematopoiesis with phenotypic HSC and progenitor engraftment and maintenance in the human ossicles compared to mouse BM. The gene expression profiling showed that the in vivo developed human ossicle express higher levels of CXCL12, Thrombopoietin and Wnt5b than the original in vitro expanded and in vitro differentiated template.

Conclusion:
Our data indicate that adult BM MSC can develop ectopic bone organs in vivo through an endochondral ossification process and support allogenic human hematopoiesis and HSCs, possibly via local expression of human HSC niche factors. The functional bone organ system that is transplantable and engineerable will serve as a platform that allows to study physiology and pathophysiology of human hematopoiesis and HSC in vivo.

2227

E. Saponara[1], S. Sonda[1], G. Seleznik[1], K. Grabliauskaite[1], T. Reding[1], R. Graf*[1]

Serotonin regulates cytoskeletal remodeling during the formation of pancreatic acinar-to-ductal metaplasia

1Swiss HPB Centre, Visceral & Transplantation Surgery, University Hospital Zurich, Switzerland[1]

Introduction:
Acinar-to-ductal metaplasia (ADM) forms during pancreatic regeneration following pancreatitis. ADMs are associated with pre-malignant lesions during pancreatic carcinogenesis. ADM transition depends on cytoskeletal remodeling of acinar cells. We previously demonstrated that serotonin (5-hydroxytryptamine, 5-HT) promotes acinar cell secretion by regulating actin cytoskeletal rearrangments. We now investigated whether 5-HT-mediated cytoskeletal remodeling regulates the formation of ADM lesions.

Methods:
Cytoskeletal remodeling and development of ADM lesions were evaluated in mice wild type (WT) and deficient in peripheral 5-HT (tryptophan hydroxylase-1 knocked-out, TPH-1$^{-/-}$) using two models of cerulein-induced pancreatitis (two injections on consecutive days and six injections on alternate days). The therapeutic effect of 5-HT signalling manipulation to prevent cytoskeletal remodelling and ADM formation was evaluated *in vitro* using a 3D culture system of pancreatic explants from mice expressing the activating Kras (G12D) mutation.

Results:
Lack of 5-HT *in vivo* or inhibition of its uptake *in vitro* resulted in increased cell-cell adhesion. In both cerulein regimens, WT mice developed typical ADM lesions four days after the induction of pancreatitis. Conversely, TPH-1$^{-/-}$ mice were characterized by stronger cell-cell adhesion and showed smaller ADM foci with incomplete acinar cell trans-differentiation. *In vitro,* inhibition of intracellular 5-HT up-take completely prevented the formation of ADMs in Kras explants.

Conclusion:
These data indicate that cytoskeletal remodeling mediated by intracellular 5-HT is critical for the formation of ADM lesions. Thus, inhibition of 5-HT uptake may constitute a novel pharmacological intervention to interfere with ADM formation and prevent the spreading of pancreatic pre-malignant lesions.

2228

H. Giral[1], M. Keel[1], A. Kratzer[1], C. Tournaire[2], T F. Lüscher[1], A. Aguzzi[2], U. Landmesser[1]

Identification of miRNAs regulating inflammatory leukocyte recruitment: functional high-throughput screening (HTS)

Clinic of Cardiology, University Hospital Zurich[1], Institute of Neuropathology and Clinical Pathology, Department of Pathology, University Hospital Zurich[2]

Introduction:
Cardiovascular disease (CVD) remains a leading cause of mortality worldwide and its incidence is expected to rise in the next decades highlighting the need for novel therapeutic approaches.
Inflammatory activation is a key mechanism promoting development and progression of atherosclerosis. Recruitment and extravasation of blood monocytes to the lesion and subsequent differentiation to macrophages are a hallmark of the disease. This multistep process is driven by a vast set of proteins including adhesion molecules, integrins and chemokines expressed on endothelial cells (EC) and monocytes. Blockage of monocyte entry by targeting chemokines or their receptors prevents or retards atherogenesis in mouse models of atherosclerosis and it is a promising therapeutic target to attenuate the progression of the disease.
MicroRNAs (miRNA) are small non-coding RNAs able to regulate a wide range of biological processes by post-transcriptional mechanisms. Typically a miRNA exerts modest inhibition on many mRNAs within one or a few biological pathways. Dysregulation of miRNAs has been associated with the pathogenesis of cardiovascular disease. Our increasing ability to manipulate miRNA expression, through the use of mimics and inhibitors, has raised the possibility to use them as therapeutic tools. In the proposed project we perform an unbiased approach for identification of the most potent miRNA modulating the inflammatory response on atherosclerosis.

Methods:
A functional high-throughput screening with mimic and inhibitory miRNA libraries was performed in EC (HAEC) and monocytes (THP-1 cells). Two different human microRNA libraries (mirVana libraries- Ambion), including 2019 miR-mimics and 2019 inhibitors of miRNAs each, were transfected in HAEC or THP-1 cells with individual miRNA mimics (or inhibitors) on each well of a 384-well plate. Transfections were performed via liposome-miRNA complexes with the commercial reagent RNAiMAX that has been optimized to use in our cell lines. The cells are incubated during 36 hours after transfection to allow both mimics and inhibitors to act.
The screening was performed under inflammatory stimulation by treatment of HAEC with TNF-α (1 ng/ml) during 6 hours. In order to accomplish a reliable screening minimizing variability and random errors we use a Janus pipetting robot (Perkin Elmer). As a functional assay we performed a monocyte adhesion assay by measuring the attachment of fluorescently-labeled THP-1 cells to stimulated ECs with an Envision microplate reader.

Results:
We present the optimization of a functional HTS assay developed to identify miRNAs involved in the recruitment and adhesion of monocytes to ECs. This methodology has been designed to perform an unbiased analysis of most know human miRNAs (miRBase V19 – 2019 miRNAs) by inducing exogenous expression (mimics) or by blocking the endogenous miRNAs (inhibitors).

Conclusion:
We have designed and optimized a functional high-throughput screening to identify miRNAs that regulates cell adhesion of monocytes to endothelial cells under inflammatory stimuli. The newly identify miRNAs will be further studied to select putative therapeutic targets that induce the stronger modulation of this inflammatory process minimizing deleterious side effects.

2230

GA. Kullak-Ublick[1], WE. Thasler[2], J. Mwinyi[1]

Bile acid induced changes in the expression of miRNAs and genes involved in drug metabolism and disposition

Clinical Pharmacology and Toxicology, University Hospital Zürich[1], Department of Surgery, University of Munich, 81377 Munich, Germany[2]

Introduction:
Bile acids (BAs) are essential for the absorption, transport, and distribution of dietary lipids, vitamins and xenobiotics. As transcription factor ligands (e.g. of FXR) they influence signaling pathways regulating lipid, glucose, and energy homeostasis (1). First studies indicate that BAs are also able to influence the expression of microRNAs (miRNAs), a class of small noncoding RNAs that is able to inhibit protein translation (1,2). Several different hepatic disease states as well as the intake of certain hepatotoxic drugs can induce cholestasis, a condition associated with elevated bile acid levels in hepatocytes.
We aimed to comprehensively investigate the impact of BAs on the human mRNAome and miRNAome, focusing on the question, to which extent elevated BAs may have the potential to influence the expression of genes involved in drug metabolism and disposition and signaling pathways driven by miRNAs.

Methods:
Two batches of primary human hepatocytes were treated with 50µmol chenodeoxycholic acid (CDCA) or vehicle (DMSO) for 48 hours. Global mRNA and miRNA profiling was performed using next generation sequencing. Adapter ligated RNA samples were reverse-transcribed and enriched by PCR. After cluster generation (TruSeq PE Cluster Kit v3-cBot-HS (Illumina)) sequencing was performed on the Illumina HiSeq 2000 (TruSeq SBS Kit v3-HS (Illumina)). RNA-reads were quality-checked (fastqc) and aligned to the genome (tophat v1.3.3). The paired t-test was used to compare the average mRNA and miRNA expression values.

Results:
702 genes were significantly decreased, 1345 genes and 71 miRNAs were significantly increased in expression in BA treated cells. Besides classical FXR targets involved in BA transport and metabolism (e.g. CYP7A1, BSEP) that served as positive controls for repression and induction by BAs, respectively, many genes coding for proteins involved in drug metabolism appear to be affected and in many cases down regulated by BAs. Examples include genes encoding members of the CYP1A, CYP2C and CYP3A and the SLC transporter family as well as members of the GST, SULT, and UGT family. Notably members of the miRNA families 320 and 548 appeared to be strongly regulated by CDCA.

Conclusion:
BAs have the potential to significantly modulate the expression of genes involved in the biotransformation of drugs and, thus, may have a significant impact on drug metabolism and disposition. The detection of differentially expressed miRNA molecules extends the spectrum of regulatory pathways influenced by BAs.

1. Song et al., J Lipid Res. 2010 Aug;51(8); (2) Castro et al., J Hepatol. 2013 Jan;58(1):119-25

2231

T. Claro da Silva[1], J. Mwinyi[1], GA. Kullak-Ublick[1], C. Hiller[1]

Vitamin D3 Alters Expression of Intestinal Drug Transporters, Metabolizing Enzymes and miRNAs in Caco-2 Cells

Department of Clinical Pharmacology and Toxicology, University Hospital, Zurich, Switzerland[1]

Introduction:
Vitamin D_3 (1,25-dihydroxyvitamin D_3) is the active form of vitamin D and is employed pharmacologically to treat rickets, osteoporosis and hyperparathyroidism, among other diseases. It is also being evaluated for breast cancer prevention in high risk patients (1). The extensive use of vitamin D in the clinic and the rise in reported cases of intoxication (2) highlight the need for a better understanding of its off-target effects. In the present study, we have examined the impact of vitamin D treatment on levels of intestinal drug transporters and metabolizing enzymes, as well as on microRNAs (miRNAs), using the human-derived intestinal cell line Caco-2 and RNAseq for global profiling. Our goal was to uncover vitamin D_3-dependent alterations in regulatory pathways that may affect physiology and drug disposition.

Methods:
Caco-2 cells were treated with 500 nM vitamin D_3 or vehicle (EtOH) for 48h. Cells were harvested and total RNA isolated using the guanidinium thiocyanate-phenol-chloroform extraction method. At the Functional Genomic Center Zurich, small RNAs were separated by gel extraction, and then small and total RNAs were reverse-transcribed and amplified by PCR. Subsequently, next-generation sequencing on the Illumina HiSeq 2000 (TruSeq SBS Kit v3-HS (Illumina)) was performed and the resulting mRNA and miRNA expression profiles were analyzed with the paired t-test method.

Results:
Vitamin D_3 treatment significantly altered expression of 2375 genes and 54 miRNAs, encompassing (upregulated/downregulated): SLC transporters (13/32), phase I and phase II metabolizing enzymes (20/28) and miRNAs (41/13). Several of the altered genes encode transporters and enzymes involved in vitamin D, glucose and xenobiotic metabolism (*e.g.*, CYP3A4 and OATP1A2), while miR-7, miR-658 and miR-4258 were among the miRNAs mostly affected by treatment.

Conclusion:
Vitamin D_3 modulates the expression of miRNAs and genes critical for drug disposition. While further studies are required, we speculate that some of the observed effects may underlie drug-drug interactions during vitamin D therapy.
REFERENCES:
1. K.D. Crew. Vitamin D: are we ready to supplement for breast cancer prevention and treatment? ISRN Oncol. 2013:483687 (2013).
2. F. Granado-Lorencio, I. Blanco-Navarro, B. Perez-Sacristan, E. Donoso-Navarro, and R. Silvestre-Mardomingo. Serum levels of 3-epi-25-OH-D3 during hypervitaminosis D in clinical practice. J Clin Endocrinol Metab. 97:E2266-2270 (2012).

2232

D. Natsiou[1], T. Mitsiadis[1], L. Jimenez-Rojo[1]

3D in vitro culture for the expansion of dental epithelial stem cells

Department of Craniofacial Development and Regeneration, Insitute of Oral Biology, University of Zurich[1]

Introduction:
Teeth are covered by enamel which is the hardest tissue in the body and protects dentin and dental pulp from external harmful agents. Erupted teeth cannot regenerate damaged enamel. The cells that produce enamel, the epithelium-derived ameloblasts, disappear after tooth eruption. Thus, it will be important to find alternative source of stem/progenitor cells that have the ability to regenerate enamel. Some studies have shown that the epithelium of the third unerupted molar can have the potential to differentiate in enamel-secreted ameloblast. However, in order to use these cells as sources for dental tissue engineering, there is the need of expanding them *in vitro* and further characterised them. Mouse incisors are an ideal model for the study of dental epithelial stem cells because their incisors grow continuously due to a population of dental epithelial stem cells residing in the so-called cervical loop. The aim of this project is to develop a 3D *in vitro* culture system for the expansion and characterization of dental epithelial stem cells using the mouse incisor as a model. In addition, we aimed to expand epithelial stem cells from the molars, which resemble more to human teeth.

Methods:
In order to establish the optimal conditions for the 3D *in vitro* culture of dental epithelial/progenitors cells, epithelial cells from cervical loops isolated from postnatal mouse incisors were cultured under non-adherent conditions without and with Matrigel and with different combination of growth factors. After 7 days in culture, formed dentospheres were harvested, fixed, embedded in agarose and processed for paraffin embedding. 5µm sections were obtained and immunohistochemistry assay were used to characterise the dentospheres. In order to assess the potential of the dentospheres to give rise to dental tissues *in vivo*, recombinants of E14,5 dental mesenchyme with GFP+ dentospheres were transplanted under the kidney capsule of immunocompromised mice and analysed by µCT after 4 weeks. Lastly, epithelial cells from the molars were cultured under the same culture conditions as the cervical loop and proceed accordingly.

Results:
Firstly, we observed that the isolated cells from the cervical loop can form dentospheres. We observed that with the combination of bFGF/EGF larger diameter and higher numbers of dentospheres were formed in comparison to the other growth factors. With the addition of Matrigel the diameter of the dentospheres was 3 times bigger than without. Preliminary results from the *in vivo* assay to assess the potential of dentospheres showed the formation of mineralised tissue. Additionally, the epithelium of the molar shown that can form dentospheres with the combination of bFGF/EGF and Matrigel. The dentospheres from both cervical loop and molars expressed epithelial markers like K14, stem cells markers like Sox2 and other markers like Notch2.

Conclusion:
The sphere-forming assays have been widely used to identify tissue-specific stem cells. Hereby; we have established a sphere culture system for dental epithelial stem cells. Our experiments showed that unerupted molar epithelium has the ability to grow as spheres, indicating the presence of stem/progenitor cells in mouse molars. Further characterization of the dentospheres will clarify if dental epithelial stem cells keep their identity and potential

after *in vitro* expansion. This would indicate their possible use as a source of cells for enamel regeneration. Thus, these findings would contribute significantly to the emerging field of Regenerative Dentistry.

2233

GM. Seleznik[1], Th. Reding[1], J. Browning[3], S. Segerer[4], S. Sonda[1], M. Heikenwalder*[2], R. Graf*[1]

Comparative effectiveness of immune-cell depletion and a targeted therapy against LTbR-signaling in the treatment of autoimmune pancreatitis

Swiss HPB Centre, Visceral & Transplantation Surgery, University Hospital Zurich, Switzerland[1], Institute of Virology, Technische Universität München–Helmholtz Zentrum München, Munich, Germany[2], Department of Microbiology, Boston University School of Medicine, Boston, USA[3], Division of Nephrology, University Hospital Zurich, Zurich, Switzerland[4]

Introduction:
The long-term management of autoimmune pancreatitis (AIP) is still elusive. Currently, the treatment options for AIP are limited. The only therapy that has been established and accepted so far is corticosteroids, but the relapse rate is significant (15-60%). We previously demonstrated that acinar specific Lymphotoxin expression in mice (Tg(Ela1-Lta,b)) induces autoimmunity with features reminiscent of human AIP. This includes formation of tertiary lymphoid organs, increased serum IgGs, anti-nuclear antibodies and immune-complex glomerulonephritis. In this model we have previously shown that in contrast to corticosteroids, which only diminished inflammation, inhibition of Lymphotoxin beta receptor signaling (LTßR-Ig) also abrogated autoimmunity.

Methods:
The aim of the study is to investigate the effectiveness of LTßR pathway inhibition compared with depletion of specific subset of immune cells (B-cells and CD4+ T-cells), which are suggested to play a pathological role in AIP development. Therefore, *Tg*(Ela1-Lta,b) mice with established AIP were treated with anti-CD20 mAb (Rituximab), anti-CD4 mAb in order to deplete B- and CD4+ T-cells respectively and with LTßR-Ig fusion protein. Histology, autoantibody production, cytokine and chemokine expression, TLO integrity and extrapancreatic manifestations (in kidneys) were tested, and compared to LTßR-Ig treatment. Furthermore, macrophage and T helper cell polarization was evaluated upon different treatments.

Results:
LTßR-Ig and anti-CD20 treatment led to a significant decrease in autoantibody production and inflammatory cell infiltration. The molecular mechanism of this beneficial effect possibly involves the down regulation of Stat3 and non-canonical NF-kb activation. Additionally, in contrast to anti-CD20 and anti-CD4 treatments, blocking LTßR-signaling reverted acinar cell proliferation and acinar-to-ductal metaplasia formation and also disrupted the formation of TLOs. Anti-CD4 treatment resulted in reduced Th1 and Th2 polarization; however this did not ameliorate AIP.

Conclusion:
In this unique genetic mouse model of AIP, we demonstrate that therapy with LTßR-Ig and anti-CD20 antibody is superior to CD4+ T-cell depletion. With these targeted therapies we reveal novel anti-inflammatory and anti-autoimmune mechanisms. Assessing numerous parameters associated with AIP pathogenesis, LTbR-Ig achieved the greatest improvements. Therefore, inhibition of the LTbR-signaling pathway could become an alternative or supplementary approach for AIP treatment.

2234

A. Kratzer[1], N. Kraenkel[1], MF. Mueller[2], H. Giral[2], J. Manz[1], G. Treichel[1], P. Jakob[2], TF. Luescher[2], U. Landmesser[2]

miR-223 and miR-181a as potential role players in monocyte subpopulations from patients with acute and stable coronary syndrome

Center of Molecular Cardiology, University of Zurich[1], Clinic of Cardiology, University Hospital Zurich[2]

Introduction:
Coronary artery disease (CAD) is a chronic low-grade inflammatory vascular disease, whereas acute myocardial infarction (MI) is a form of sterile injury involving immune cell recruitment and wound healing. Experimental studies have suggested potentially important roles of inflammasome activation in both CAD and MI. In the present study we therefore examine activation of the caspase-1 recruiting inflammasome in three monocyte subsets from patients with stable CAD or an acute coronary syndrome (ACS) as compared to healthy subjects. The monocyte subsets were defined as classical (CD14++CD16-), intermediate (CD14++CD16++) and non-classical (CD14+CD16++) monocytes. Intermediate monocytes have been more closely associated with classical monocytes, having been recently negatively associated with cardiovascular disease outcome. Inflammasomes are differently regulated in monocyte subpopulations of patients with CAD as compared to healthy donors.

Methods:
Peripheral blood mononuclear cells were isolated from patients with stable CAD or ACS and healthy subjects. Using FACS sorting, monocyte subpopulations were isolated based on their CD14 and CD16 expression. Analysis of inflammasome-related mRNA and miR-223 expression was performed by real-time PCR. Inflammasome activation was further examined by flow cytometry (e.g. caspase-1). The endothelial repair and wound-healing capacity of these monocyte subgroups was measured using a scratch assay and human aortic endothelial cells.

Results:
CD14+ cell numbers were significantly increased in patients with CAD and ACS. Both CAD and ACS patients had more non-classical monocytes. NLRP3 inflammasome expression was significantly lower on non-classical monocytes compared with the other monocyte subpopulation in all study groups. Its expression was significantly altered in patients with CAD and ACS, especially in classical monocytes. miR-223, that inhibits NLRP3, was dysregulated in these subpopulations, showing a decreased expression in classical monocytes. Another inflammation-associated miRNA, miR-181a being associated with M1 macrophage differentiation, has been significantly upregulated in classical and intermediate monocytes of CAD patients. Caspase-1 activity was significantly increased in intermediate and non-classical subgroups from acute and stable CAD patients. Additionally, we found a significant decrease in the wound-healing capacity of intermediate and non-classical monocytes of CAD patients.

Conclusion:
The NLRP3 inflammasome is upregulated in monocyte subgroups of patients with CAD and ACS, associated with dysregulated miR-223. Another “pro-inflammatory role player”, miR-181a was identified to be upregulated in classical and intermediate monocytes. There is an increased caspase-1 activity, an effector of NLRP3 inflammasome, in particular in the intermediate and non-classical monocyte subgroups of CAD patients**.** Careful characterization of regulation and activation of inflammasome, including potential role a certain miRNAs in CAD and ACS may provide novel targets for therapeutic intervention.

2235

A. Renganathan[1], J. Kresoja-Rakic[1], N. Echeverry[1], G. Ziltener[1], B. Vrugt[3], I. Opitz[2], R. Stahel[1], E. Felley-Bosco[1]

GAS5 long non coding RNA in malignant pleural mesothelioma

Laboratory of Molecular Oncology, Clinic and Policlinic for Oncology, University Hospital Zurich[1], Thoracic Surgery Department, Molecular Oncology Laboratory, University Hospital Zürich, Zürich, Switzerland[2], Institute of Surgical Pathology, Department of Pathology, University Hospital Zurich, Switzerland[3]

Introduction:
Malignant pleural mesothelioma (MPM) is an aggressive cancer with short overall survival. Long noncoding RNAs (lncRNA) are a class of RNAs more than 200 nucleotides that do not code for protein and are part of the 90% of the human genome that is transcribed yet less well characterized. Earlier experimental studies showed *GAS5* (growth arrest specific transcript 5) lncRNA deletion in asbestos driven mesothelioma. The function of GAS5 is not well known, but it has been shown to act as glucocorticoid receptor decoy and microRNA "sponge". Thus our aim is to investigate the possible role of the GAS5 in the growth of MPM.

Methods:
Primary MPM cultures grown in serum-free condition in 3% oxygen or MPM cell lines grown in serum medium were used. Doxycycline inducible short hairpin GAS5 clones were generated from ZL55SPT cells. Gene expression was quantified by qPCR. To investigate *GAS5* promoter, 1kb sequence was inserted into pGL3 reporter plasmid and reporter activity was determined after transfection into MPM cells. Cell cycle length was determined by EdU incorporation assay. Localization of GAS5 lncRNA was identified by *in situ* hybridization. Expression of podoplanin and ki67 was identified by immunohistochemistry.

Results:
GAS5 expression was lower in MPM cell lines compared to normal mesothelial cells. GAS5 was upregulated upon growth arrest induced by inhibition of Hedgehog or PI3K/mTOR signaling in *in vitro* MPM models. The increase in mRNA was accompanied by increased promoter activity. Silencing GAS5 increased the expression of glucocorticoid responsive genes GILZ and SGK1 and shortened the length of the cell cycle. Drug induced growth arrest was associated with GAS5 accumulation in the nuclei. Surprisingly, GAS5 was expressed at higher level in tumor tissue compared to non-tumoral tissue, was abundant in tumor quiescent cells and it was correlated to podoplanin expression.

Conclusion:
Drug induced growth arrest increases GAS5 expression and decreasing levels of GAS5 shortens cell cycle *in vitro.* The higher GAS5 expression in MPM tissue compared to non-tumoral tissue is associated with cell quiescence and podoplanin expression. Because podoplanin and GAS5 mRNA sequence contain the same microRNA targets, this supports GAS5 lncRNA having an important role in growth-arrest and microRNA-"sponge" in MPM.

2236

SJ. Schreiner[1], T. Kirchner[3], A. Gietl[1], SC. Steininger[1], M. Wyss[3], E. Gruber[1], A. Buck[2], S. Leh[1], R. Nitsch[1], K. Prüssmann[3], C. Hock[1], A. Henning[4], PG. Unschuld[1]

INVESTIGATING REGIONAL RELATIONSHIPS BETWEEN AMYLOID-BETA AND BRAIN METABOLISM IN HEALTHY ELDERLY CONTROLS

Division of Psychiatry Research and Psychogeriatric Medicine, University of Zürich, Switzerland[1], Division of Nuclear Medicine, University of Zürich, Switzerland[2], Institute for Biomedical Engineering, University and ETH Zurich, Zürich, Switzerland[3], Max Planck Institute for Biological Cybernetics, Tübingen, Germany[4]

Introduction:
Deposition of amyloid-β (Aβ) in the brain is a hallmark of Alzheimer's disease (AD), but its consequences regarding brain metabolism are largely unknown. Regional Aβ accumulation can be assessed with Pittsburgh compound-B positron-emission-tomography (PiB-PET) and magnetic resonance spectroscopic imaging (MRSI) non-invasively quantifies regional brain metabolite levels. This study aims to investigate potential regional effects of Aβ accumulation on brain metabolite levels in healthy controls and will be extended to clinical cohorts with mild cognitive impairment and AD.

Methods:
MRSI was performed at high field strength of 7 Tesla to increase signal-to-noise ratio and spatial resolution, and was applied to a pilot-cohort of healthy, cognitively normal elderly adults (n=14). Individual cortical Aβ load was quantified based on PiB-PET late frame signals. Regional correlation of PiB-PET signals with the respective metabolite-levels of MRSI was performed based on tissue-specific probability maps.

Results:
As this is an on-going study, recruitment of clinical cohorts will continue. The newest results regarding the relationship of individual cortical Aβ load with regional metabolite concentrations will be presented.

Conclusion:
Investigating the regional association between deposition of Aβ and corresponding brain metabolite levels will allow us to draw conclusions about regional Aβ-associated neuronal stress. This study will characterize the metabolic signature of asymptomatic brain amyloidosis, and will help to evaluate MRSI as a potential AD biomarker.

2237

I. Bhattacharya[1], A. Perez Dominguez[1], K. Drägert[1], R. Humar[1], E. Battegay[1], E. Haas[1]

Hypoxia enhances the effect of tumor necrosis factor in adipocytes by elevating the expression of inducible nitric oxide synthase and cyclooxygenase-2

University Hospital of Zurich, Switzerland[1]

Introduction:
In obesity, adipose tissue mass increases massively leading to increased inflammation and the formation of hypoxic areas. Inflammation and hypoxia together may impair adipocyte function. However, molecular mechanisms are not clear. In the present study, using an in-vitro cell culture model, we investigated whether tumor necrosis factor (TNF)α, an inflammatory molecule, and hypoxia affect the expression of inducible nitric oxide synthase (iNOS) and cyclooxygenase (COX) 1/ 2 in 3T3-L1 adipocytes.

Methods:
3T3-L1 adipocytes were stimulated with TNFα (10 ng/ml) in the presence of hypoxia (1% O_2) or normoxia (21% O_2). Gene and protein expression of iNOS and COX-1/2 were examined using RT-PCR and Western blotting, respectively. The expression of these molecules was also analysed in preadipocytes, vascular smooth muscle cells (VSMCs) and endothelial cells (ECs). Moreover, the release of nitrite and prostaglandinE_2 (PGE_2) was also measured from the conditioned media.

Results:
In 3T3-L1 adipocytes, stimulation with TNFα increased the gene expression of iNOS and Cox-2 in normoxia. Under hypoxic conditions, iNOS and Cox-2 gene expression increased by 7-fold after 24 h stimulation with TNF as compared with normoxia. The protein expression of iNOS and COX-2, but not COX-1, was significantly increased with TNFα in the presence of hypoxia. The levels of nitrite and PGE_2 were also elevated upon TNFα stimulation in hypoxic conditions. The expression of other pro-inflammatory genes such as interleukin-6 (IL-6), serum amyloid A (SAA) and RANTES were not similarly enhanced. Interestingly, the expression of iNOS and COX-2 remained unchanged in preadipocytes, VSMCs and ECs.

Conclusion:
These findings suggest that inflammation together with hypoxia specifically affect adipocytes, probably leading to increased oxidative stress and impaired adipose tissue metabolism.

2238

E. Kachaylo[2], Ch. Tschuor[2], P. Limani[2], P. Ramadori[1], M. Foti[1], B. Humar[2], R. Graf[2], PA. Clavien[2]

DEFICIENT MICRORNA-21 INDUCTION PROMOTES SMALL-FOR-SIZE SYNDROME FOLLOWING EXTENDED HEPATECTOMY IN MICE

Département de Physiologie Cellulaire & Métabolisme, Faculté de Médecine, Centre Médical Universitaire, Genève, Suisse[1], Laboratory of the Swiss Hepato-Pancreatico-Biliary (HPB) Center, Department of Surgery, University Hospital Zurich, Switzerland[2]

Introduction:
Extensive liver resection can lead to hepatic failure known as the Small-For-Size Syndrome (SFSS). Using a novel mouse model, we have recently demonstrated experimental SFSS develops due to a p21-dependent delay before mitosis. This was associated with suboptimal induction of Foxm1b, a direct repressor of p21 and an essential driver of cell cycle progression following hepatectomy (pHx). Here, we explored whether alterations in miR-21, usually induced by pHx and a proposed regulator of Foxm1b, may be causally involved in the development of SFSS.

Methods:
SFSS was induced by extended (86%) pHx and compared to standard (70%) pHx. Liver regeneration was monitored by weight gain, proliferative activity, cyclin levels. Q-PCR, immunochemistry and immunoblots were used to assess molecules associated with the putative miR21-Foxm1b-p21 axis. miR-21 mimics were delivered via liposomal injection.

Results:
miR-21 expression peaked at 16 hours post 70%pHx. Following 86%pHx, miR-21 induction was deficient and paralleled by a reduced activation of Stat3, a direct transcriptional activator of miR-21. Btg2, an inhibitor of Foxm1b and predicted to be repressed by miR-21, was overexpressed following 86%pHx relative to 70%pHx. Injection of miR-21 mimics before 86%pHx improved liver weight gain, hepatic function, and Foxm1b expression whilst reducing p21 levels.

Conclusion:
miR-21 appears to constitute an important upstream regulator of the Foxm1b-p21 axis following hepatectomy. Its insufficient induction delays liver regeneration and is associated with the development of the SFSS. miR-21 mimics can mitigate experimental SFSS, suggesting therapeutic potential.

2239

P. Pagella[1], A. Woloszyk[1], E. Neto[2], M. Lamghari[2], T. Mitsiadis[1]

Cross-talk between sensory innervation and mesenchymal stem cells for orofacial regeneration in a microfluidics co-culture system.

Institute of Oral Biology, Department of Craniofacial Development and Regeneration, University of Zurich[1], INEB – Instituto de Engenharia Biomédica, NEWTherapies Group, Universidade do Porto, Porto, Portugal[2]

Introduction:
Innervation plays a key role in the development and the maintenance of the various orofacial organs. Increasing evidence is supporting an active role for innervation in the regulation of stem cells proliferation, mobilization and differentiation in different compartments, during development and adult life. As regenerative medicine aims to reconstitute fully functional organs and tissues, it is fundamental to understand how stem cells of various origins interact with nerve fibres innervating the different organs.
Bone marrow stromal cells are widely used for regenerative medicine studies, including regeneration of orofacial tissues; however, these cells are isolated from non-orofacial bones. A possible alternative for orofacial regeneration could be represented by dental pulp cells, isolated from the tooth pulp. In this study we aim to compare the interactions between fibres innervating the orofacial complex, originated from the trigeminal ganglion, and bone marrow stromal cells and dental pulp cells. For this purpose we co-culture trigeminal ganglia and mesenchymal stem cells in a microfluidics co-culture system that allows culturing various cells types in different culture media while allowing the contact of axons with mesenchymal cells. We analyse the attraction/repulsion effect of mesenchymal cells on axons and the response of mesenchymal cells to trigeminal innervation.

Methods:
Trigeminal ganglia were dissected from mouse embryos (day 14.5-16.5 p.c.) and co-cultured with human bone marrow stromal cells or human dental pulp cells in a microfluidics co-culture platform. The co-culture was followed by time-lapse microscopy and further analysed via immunocytochemistry.

2240

L. Horvath[1], D. Bodmer[2], V. Radojevic[2], A. Monge Naldi[1]

Activin signaling disruption in the cochlea does not influence hearing in adult mice

ORL, University Hospital, Zürich[1], Basel University Hospital, Basel[2]

Introduction:
Activin, a member of the TGF-β superfamily, was found to play an important role in the development, repair and apoptosis of different tissues and organs. Interestingly, activin is highly expressed in the central nervous system (CNS) whereas its production is elevated after acute brain injury, during inflammation or ischemic stress and it has crucial roles in neuronal development. Accordingly, activin signaling is involved in the development of the cochlea. Activin binds to its receptors (ActRI or ActRII) and induces a signaling pathway resulting in gene expression. The absence of activin receptors and therefore disrupted activin signaling results in embryonic lethality. A study reported a case of fibrodysplasia ossificans progressiva (FOP) with an unusual mutation in the ActRI gene leading to sensineural hearing loss. This draws attention to the role of activin and its receptors in the developed cochlea. To date, only the expression of ActRII is known in the mammalian cochlea.

Methods:
Mammalian cochlea was analyzed for expression of Activin A and ActRIB. Transgenic mice with postnatal dominant negative ActRIB expression causing disruption of activin signaling in vivo were used for assessing cochlear morphology and hearing ability through auditory brainstem response (ABR) threshold.

Results:
Activin A and ActRIB are expressed within the inner ear. Non-functioning ActRIB did not affect the ABR thresholds and did not alter the microanatomy of the cochlea.

Conclusion:
ActRIB inoperability with subsequent disruption of activin signaling does not alter the microanatomy of the cochlea nor do dnActRIB transgenic mice show different hearing thresholds than comparable wild-type mice. We conclude that activin signaling is not necessary for hearing in adult mice under physiological conditions but may be important during and after damaging events in the inner ear.

2241

H. Takizawa[1], Y. Saito[1], L. Kovtonyuk[1], K. Fritsch[1], M. Manz[1]

Lipopolysaccharide impairs hematopoietic stem cell function via direct activation of Toll-like receptor 4 pathway

Division of Hematology, University Hospital Zürich, Rämistrasse 100, CH-8091 Zürich[1]

Introduction:
Systemic bacterial infection triggers inflammatory responses and increases demand of hematopoietic cell production to replenish mature cells that fight and are consumed during the infection. The danger signals need to be translated to hematopoieisis by either indirect or direct sensing mechanism in which early hematopoietic cells in bone marrow (BM) express cytokine receptor to respond to soluble factors or pathogen recognition receptors that directly sense pathogen associated molecules. While mature hematopoietic cell reactions are well studied in this process, little is known about the effect of systemic infection on lifelong selfrenewing hematopoietic stem cells (HSCs). Here we examine the change in cellular function of HSCs upon systemic challenge of lipopolysaccharide (LPS), a gram negative bacterial component recognized by Toll-like receptor 4, and the underlying molecular and cellular mechanism.

Methods:
To dissect if systemic LPS injections activate TLR4 on HSCs directly or indirectly, we reconstituted wild-type (WT) recipients with WT and Toll-like receptor 4 deficient (*Tlr4-/-*) cells in a 1:1 ratio (thereafter called mixed BM chimera), and examined a relative contribution of two genotype cells in peripheral blood lineage repopulation over months following repetitive systemic LPS challenges. To test functionality of long term selfrenewing HSCs, BM cells were isolated from the chimeric mice and serially transplanted into another recipient under lethal irradiation. To identify the downstream signals active in HSC, mixed BM chimera experiments were performed with cells deficient for TLR4 signal related molecules or under in vivo treatment of small inhibitors against them. Finally, to further characterize the cellular and molecular outcome of TLR4 activation in HSC, proliferation of HSC and DNA damage in HSC upon LPS were evaluated by in vivo BrdU retention and immunocytochemistry with anti-gH2AX, a surrogate marker for DNA double strand break, respectively.

Results:
Mixed BM chimera experiments showed that in LPS treated animals *Tlr4-/-* cells outcompeted WT cells, while PBS treated controls remained at a 1:1 chimerism as expected. The same result was observed in serial transplantation and when *Tlr4-/-* primary recipient were used, demonstrating that direct TLR4 activation on HSCs limits their competitive repopulating ability. *In vivo* proliferation assay showed LPS induced proliferation of dormant HSC through both direct and indirect mechanism. *Trif-/-* HSCs, similarly as *Tlr4-/-* HSCs, retained a competitive repopulating advantage over WT cells upon LPS stimulation, while this was not the case for *Myd88-/-* HSCs. *In vivo* pharmacological inhibition of reactive oxygen species (ROS) and p38 rescued HSC from the LPS-induced dysfunction. LPS stimulation caused more DNA damages in HSCs.

Conclusion:
These data demonstrate that LPS directly activates TLR4 signals in BM HSC and causes their functional impairment possibly through increasing divisional history and DNA damage. Our findings indicate that inflammatory environment induced by systemic bacterial infection might foster accumulation of ablative genetic events in HSCs that leads to full malignant transformation and leukemia development.

2242

D. Vital[1], M. Roessle[2], RD. Laske[1], GF. Huber[1]

Prognostic markers of salivary gland carcinomas

Dept. of Otorhinolaryngology, Head & Neck Surgery, University Hospital Zurich, Zurich[1], Inst. of Surgical Pathology, University Hospital Zurich, Zurich[2]

Introduction:
There are few reports suggesting that cancer/testis antigens might be of use in the differential diagnosis of salivary gland carcinomas. However, their prognostic value so far is unknown. Aim of this study was to analyze the diagnostic and prognostic implications of these tumor antigens in malignant salivary gland neoplasms.

Methods:
Demographic and outcome data of patients with malignant salivary gland neoplasms were collected. Tissue microarrays of normal salivary gland tissue, benign and malignant salivary gland neoplasms were analyzed and correlated statistically with outcome data like recurrence free, disease specific and overall survival.

Results:
Cancer testis antigens may enable a discrimination of malignant salivary gland neoplasms from benign diseases and normal tissue. Distinct tumor antigens are of prognostic implication regarding local recurrence, development of distant metastasis and survival.

Conclusion:
Beside diagnostic purposes, cancer testis antigens are of potential prognostic importance in patients with salivary gland carcinomas. Further research has to verify whether they play a potential role in future patient tailored medicine according to predicted patterns of aggressiveness.

2243

N. Echeverry[1], G. Ziltener[1], R. Stahel[1], E. Felley-Bosco[1]

Characterizing sensitivity to dual PI3K/mTOR inhibitors in Mesothelioma

University Hospital Zürich, Clinic and Policlinic for Oncology, Zürich [1]

Introduction:
Malignant pleural mesothelioma (MPM) is cancer with poor prognosis arising from the mesothelial cells lining the pleura. Its development is associated with the exposure to asbestos fibers. The disease is mostly diagnosed at advanced stages. Current first line treatment is cisplatin combined with pemetrexed and there is no other alternative when the treatment fails.
Upregulation of the PI3K/mTOR pathway activation in MPM tumors is correlated with bad prognosis. MPM cell lines show high sensitivity to PI3K/mTOR inhibitors and the absence of the tumor suppressor NF2, which is the most abundantly mutated gene in MPM, increases sensitivity to rapamycin. Therefore, in our study we aimed to investigate the therapeutic potential of two new generation dual PI3K/mTOR inhibitors NVP-BEZ235 and GDC0980 in MPM, with a special emphasis on the predictive value of the tumor suppressor genes PTEN and NF2.

Methods:
Cell growth inhibitory effect of NVP-BEZ235 and GDC0980 on 19 MPM cell lines (MTT Assay)
Selection of sensitive and resistant cell lines and investigation of possible molecular mechanisms of resistance and sensitivity

Results:
The drug response was normally distributed allowing the identification of resistant and sensitive lines. The IG50 range was wider for NVP-BEZ235 compared to GDC0980. The resistant lines, which were consistent for both drugs, showed higher mTOR activity remaining after treatment. Furthermore, basal S6 phosphorylation was significantly higher in the sensitive cell lines underlining their dependency on this pathway.

Conclusion:
Altogether, these data indicate that it will be possible to find predictive markers and identify possible resistance mechanisms, such as autophagy which is focus of our current research.

2244

M. Frick[1], V. Jacomella[1], S. Roth[1], B. Amann -Vesti[1], N. Ulmer[1], M. Husmann[1]

Pulse wave velocities in peripheral arterial disease derived from carotid-femoral and brachial assessments

Klinik für Angiologie, Universitätsspital Zürich[1]

Introduction:
Elevated pulse wave velocity (PWV) is a marker for arterial stiffness and cardiovascular risk. Peripheral arterial disease (PAD) is associated through its extensive atherosclerotic burden with both increased arterial stiffness and cardiovascular events. Recently, different novel non-invasive assessment devices that measure carotid-femoral or brachial PWV have become commercially available. We compared PWV derived from carotid-femoral (cfPWV) or brachial (bPWV) assessments in patients with PAD.

Methods:
Measurement of pulse wave velocities with the two different non-invasive methods was performed as part of standard of care assessment in outpatients with PAD. Pulse wave velocities were assessed as bPWV by Mobil-O-Graph (ABPM by IEM; Stolberg, Germany), which is a brachial cuff-based method and as cfPWV by Vicorder (SMT medical, Würzburg, Germany*),* an oscillometric technique for carotid and femoral pulse wave assessment. Differences between the two methods were compared by Mann Whitney U test and Bland Altmann analysis. Spearman rank correlation was performed to test for age dependency.

Results:
In 67 Patients (35.8% female, mean age 69, range 39-91 years) bPWV (mean 10.5 ± 2.4 m/s) was significantly higher than cfPWV (mean 9.2 ± 2.1 m/s). Brachial PWV showed a significant correlation with increasing age (r=0.935, p=<0.0001) whereas cfPWV did not (r=0.311, p=0.116). Bland Altmann anaylsis were used to compare the bPWV against cfPWV: Mean -1.04,2 SD 4.31, -2 SD -6.38.

Conclusion:
The gold standard assessment (cfPWV) differs from brachial PWV and lacks a correlation with age in patients with peripheral arterial disease. Extensive aorto-peripheral atherosclerotic burden may in part explain these findings questioning the gold standard assessment in PAD and needs further evaluation.

2245

J. Mata Pavia[1], S. Sanchez Majos[2], E. Charbon[3], M. Wolf[2]

Measurement and modeling of microlenses for sensitivity enhancement of novel near-infrared imager.

KFSP Molecular Imaging Network, University Hospital Zurich[1], KFSP Tumor Oxygenation, University Hospital Zurich[2], TU Delft[3]

Introduction:
Monitoring oxygenation is of great importance in many clinical fields. E.g. brain lesions are the most severe complication of preterm infants, often leading to long term cognitive and motor impairment. Currently diagnosis is based on ultrasound imaging. Ultrasound is able to detect hemorrhage immediately, but ischemia or hypoxia, which usually leads to more serious impairment, can only be detected once tissue is structurally altered after several days and permanent damage has occurred. Although other methods such as MRI and PET can better detect most brain lesions in preterm infants, transporting these critically ill patients could lead to severe complications. Cancer treatment is another important field where monitoring the oxygenation is critical. Tumor hypoxia is associated with adverse prognosis and tumor progression. In addition, hypoxia often substantially reduces effectiveness of therapy in particular for radio- and chemotherapy.
NIRI measures the hemoglobin concentration and oxygenation in tissue, being therefore a promising method for detecting hypoxia, ischemia and hemorrhage. NIRI systems are compact and affordable, which makes them suitable for bedside application. However due to their poor spatial resolution so far, they were not fit for clinical measurements. We have recently developed a new NIRI system based on a novel single-photon imager that demonstrated that 3D millimetric resolution is possible. The aim of our project is to develop this system for measurements on preterm infants and tumor patients.

Methods:
Our NIRI system is based on large arrays of single-photon avalanche diodes (SPADs) pixels. These detectors allow measuring the arrival time of photons with picosecond resolution while offering a high light sensitivity (single photon detection). SPAD imagers typically have a relatively low fill factor, i.e. a low proportion of the pixel's surface is light sensitive, due to in-pixel circuitry. For the application in patients a high photon detection efficiency is of critical importance, because this increases the signal to noise ratio, which leads to a higher image resolution and lower acquisition time.
The amount of photons detected by the imager can be increased by placing microlenses on the SPADs to concentrate the light in the pixel's light sensitive area. We present a new software that simulates the microlenses' performance under different optical systems and light conditions, and a new non-destructive contact-less method to estimate the height of the microlenses, which is a critical parameter in the microlenses' performance.

Results:
The new simulation software was completed and applied to simulate the microlenses' performance under different conditions. The simulation results where compared with measurements on existing sensors with microlenses showing a very good agreement. Based on the simulations a gain factor in light intensity of 3.1 is achievable for our NIRI system. The optimal microlens design was calculated with the simulator and a new microlens array was fabricated on our SPAD imager to improve its light sensitivity.

Conclusion:

The newly designed microlenses increase the photon detection efficiency by a 3.1 factor in our NIRI system, reducing the acquisition time by the same factor. Measurements in patients will take substantially shorter time due to the microlenses, diminishing the impact of movement artifacts and environmental factors.

2246

RD. Laske[1], I. Scholz[2], C. Meerwein[1], D. Vital[1], M. Rössle[2], GF. Huber[1]

Is perineural invasion really a predictive factor?

Dept. of Otorhinolaryngology, Head & Neck Surgery, University Hospital Zurich, Zurich[1], Inst. of Surgical Pathology, University Hospital Zurich, Zurich[2]

Introduction:
Perineural invasion (PNI) describes a malignant tumor's affinity for neural tissue. In histopathology sections, PNI presents as tumor cells infiltrating or expanding alongside peripheral nerves. Tumor cells may even be found encircling nerves distant from the histological tumor border. As an under-recognized route of metastatic spread it is associated with a higher rate of local and regional recurrence and its presence has a major impact on the decision on postoperative adjuvant radiotherapy.
The primary treatment of squamous cell carcinomas of the oral cavity is surgical resection combined with selective neck dissection or sentinel lymph node biopsy if no regional spread is suspected. Surgery is followed by adjuvant radiochemotherapy only if histology shows incomplete resection, positive lymph node status of the neck, extracapsular tumorgrowth, soft tissue metastasis or, as mentioned, PNI.
Histologically, different patterns of tumor cells interacting with neural tissue count as PNI. A review of the literature showed 5 distinct parameters, which alone or combined with each other are referred to as PNI. These parameters are: 1) tumor cells encircling at least 30% of a nerve (cross section), 2) invasion of the epineurium of the nerve, 3) invasion of the perineurium of the nerve, 4) invasion of the endoneurium of the nerve, and, 5) presence of tumor cells attached to neural tissue distant from the tumor front.
The aim of this study is to investigate whether subgroups of PNI based on these 5 parameters show different recurrence rates and to identify the parameters, which particularly increase the risk of recurrence and therefore justify a more aggressive treatment.

Methods:
Patients with oral carcinoma, who underwent tumor resection between 2000 and 2008, and, whose histopathology report showed PNI, were identified and their charts were reviewed retrospectively. Their histopathology sections were re-analyzed by a single pathologist and the pattern of PNI was assessed according the five parameters mentioned above.
The clinical course of disease in the five-year follow-up period was reviewed. Comparison to data of a control group with no PNI is in process.

Results:
A total of 17 patients with oral squamous cell carcinoma who underwent primary surgery between 2000 and 2008 and whose histopathology report mentioned PNI were identified. 12 (70.6%) patients had progressed disease (Stage III-IV) and 5 (29.4%) patients had local disease (Stage I-II) at the time of surgery. 3 patients were lost in follow-up. Overall, local recurrence was observed in 6 (35.3%) patients and regional recurrence in 4 (23.5%) patients. 10 patients (58.8%) died within the 5 year follow up period. PNI pattern 1) was found in 12 (70.6%), pattern 2) in 12 (70.6%), pattern 3) in 7 (41.2%), pattern 4) in 2 (11.8%) and pattern 5) in 2 (11.8%) patients.
From the 7 patients without recurrence, parameter 1) and 2) was present in 5 patients, and either parameter 1) or 2) was found in all of them. Parameter 3) was positive in 2 cases. There were no cases with parameter 4).
From the 7 patients with recurrence, histopathology of 4 patients showed parameter 3) and histopathology of 3 patients showed parameter 4).

Conclusion:
Invasion of perineurium, endoneurium or tumor cells identified along nerve tissue distant from the microscopic tumor front seem to form a more aggressive subcategory of PNI. Further analysis is in progress. We recommend that subcategories of PNI be mentioned specifically in histopathology reports.

2247

J. Kresoja-Rakic[1], G. Ziltener[1], R. Stahel[1], E. Felley-Bosco[1]

Characterization of the mechanisms regulating calretinin expression in malignant pleural mesothelioma

Laboratory of Molecular Oncology, Clinic of Oncology, University Hospital Zurich[1]

Introduction:
Malignant pleural mesothelioma (MPM) is an aggressive form of cancer arising from mesothelial tissue lining pleural cavity. MPM development is mainly related to the previous chronic asbestos exposure. Current treatment approach consists of surgery, radiotherapy and chemotherapy and a vast majority of patients have median survival time around 12 months.
Calretinin (CR) is a highly conserved Ca^{2+} protein that belongs to the EF-hand family protein and physiologically expressed in the subset of the neurons, adipose tissue, Leydig and Sertoli cells. Like other members of the EF-hand family, CR has potentially two roles, Ca^{2+}-buffering or Ca^{2+}-sensor protein. CR is also expressed in MPM and it is used as a diagnostic marker for epithelioid and mixed (biphasic) mesothelioma whereas it is absent in the sarcomatoid type. CR is also a prognostic marker since patients having high CR-expressing tumors have a better overall survival. However, the role of CR is not clear since silencing of CR decreases mesothelioma cell growth *in vitro.*

Methods:
The aim of the study is to better characterize the regulation of CR gene expression on the transcriptional and post-transcriptional level. To investigate transcriptional regulation of CR, we used promoter-reporter luciferase assay and cloned several genomic sequences surrounding +1 (800bp upstream and 160bp downstream) in the pGL3-B vector. Sequence activity was tested across the panel of mesothelioma cell lines expressing different levels of the CR in order to define cis-regulatory elements.

Results:
The use of constructs containing different lenght of the promoter region allowed us to identify a minimal region responsible for calretinin expression.

Conclusion:
The definition of minimal region responsible for calretinin expression is now allowing us to characterize cis-regulatory elements and trans-acting element that have role in driving calretinin expression.

2248

I. Opitz[1], O. Lauk[1], M. Meerang[1], M. Friess[1], G. Wuilleret[1], C. Bommeli[1], A. Jetter[3], D. Günther[4], R. Stahel[2], W. Weder[1]

Intracavitary Cisplatin-Fibrin Chemotherapy after Resection for Malignant Pleural Mesothelioma Patients (INFLuenCe-Meso) – preliminary results

Division of Thoracic Surgery, University Hospital Zürich, Zürich[1], Laboratory of Molecular Oncology, University Hospital Zürich, Zürich [2], Department of Clinical Pharmacology and Toxicology, University Hospital Zurich, Zurich[3], Department of Chemistry and Applied Biosciences and Laboratory of Inorganic Chemistry, ETH Zurich, Zurich[4]

Introduction:
Local mesothelioma recurrence remains a challenge even after multimodal therapy. Intracavitary chemotherapy is a promising approach to improve local tumor control. In preclinical studies we observed improved pharmacokinetic characteristics when cisplatin was loaded to a fibrin carrier and applied to the chest wall after surgery while effectiveness remained the same compared to cisplatin applied as a solution. We will present the first results of a phase I –dose-escalation-clinical study.

Methods:
Since 11/2012, six patients were included in the study. Cisplatin-fibrin was applied after pleurectomy/decortication (P/D) to the chest wall in a concentration of 11 and 22 mg/m^2 body surface area (BSA) (n=3 each dose level). Blood samples were taken at several time points after the application (2, 6, 10, 24, 48 and 120 hours) to assess serum cisplatin levels and to test toxicity in the early phase until 14 days postoperatively. The concentration of total platinum was quantified by means of inductively coupled plasma sector field mass spectrometric detection. Adverse events were graded according to the CTCAE.

Results:
Between November 2012 and December 2013 six patients (3x epitheloid, 3x biphasic) in stage II, III and stage IV were included and received P/D plus cisplatin-fibrin in a concentration of 11 and 22 mg/m^2 BSA. The peak serum cisplatin concentration was observed at 2 hours after the application of cisplatin-fibrin (0.21 ug/g for the dose level of 11 mg/m^{2}BSA and 0.47ug/g for the dose level of 22 mg/m^{2}BSA). Serum cisplatin levels continued to decrease and showed the median concentration of 0.07 ug/g and 0.14 ug/g (for the dose level of 11 and 22 mg/m^{2}BSA, respectively) at 120 hours after the application. No dose-limiting toxicity was observed at both dose levels.

Conclusion:
Our preliminary results show, that cisplatin-fibrin application to the chest wall and the lung surface after P/D is safe on a dose level of 11 and 22 mg/m^2 BSA. As no treatment related toxicities was observed we escalate the dosage to 33 mg/m^2 BSA.

2249

A. Zhakupova[1], M. Krols[2], S. Janssens[2], A. Von Eckardstein[1], T. Hornemann[1]

REGULATION OF THE MAMMALIAN SERINE PALMITOYLTRANSFERASE

Institute of Clinical Chemistry, University Hospital Zürich[1], Department for Molecular Biomedical Research, VIB, Ghent, Belgium[2]

Introduction:
Serine Palmitoyltransferase (SPT) typically catalyzes the condensation of palmitoyl-CoA and L-serine, the first step in *de novo* sphingolipid synthesis. Studies in yeast demonstrated that SPT activity is tightly regulated by a metabolic feedback loop, mediated by Orm1 and Orm2 proteins. At high cellular sphingolipid levels Orm proteins bind to SPT and inhibit its activity. Low sphingolipid levels, in contrast, lead to phosphorylation of Orm proteins, which results in their dissociation from SPT and activation of the enzyme. However, the role of the ORM proteins in regulating SPT activity in mammalian cells is not yet understood. In contrast to yeast, mammalian cells express three Orm isoforms (ORMDL1-3) and phosphorylation sites found in yeast are not conserved in the mammalian orthologs. We were therefore interested to see if a similar metabolic feedback inhibition also exists in mammalian cells.

Methods:
HEK293 cells were treated with increasing amounts of membrane permeable C6-ceramide (C6Cer) in FBS-deficient medium for 24 hours. In the reverse approach cells were treated with increasing concentrations of myriocin, which is a specific inhibitor of SPT. SPT activity was measured using isotope-labeled substrates. Lipids were then extracted and analyzed using LC-MS.

Results:
An inverse correlation between the amount of the de-novo formed sphingolipids and the intracellular ceramide levels was observed. At low concentrations (up to 0.5 nM) myriocin-mediated inhibition of SPT was compensated by a metabolic activation of the enzyme, whereas at higher myriocin concentrations (above 0.5 nM) the inhibition could not be compensated and resulted in a reduced de-novo formation of sphingolipids. The role of the individual ORMDL isoforms in regulating SPT activity was further tested in HEK293 cells overexpressing ORMDL1-3. Reduced *de novo* sphingolipid synthesis and cell viability were observed in ORMDL1 but not in ORMDL2 and 3 overexpressing cells. However, MEF cells in which ORMDL3 expression was abolished, showed an increased SPT activity, whereas enzyme activity was decreased in cells which overexpressed an ORMDL3-GFP construct.

Conclusion:
Increasing levels of C6 Ceramide seems to inhibit SPT activity. And the role of the individual ORMDL isoforms in regulating SPT activity might be redundant and possibly depends on the cellular or metabolic context.

2250

N. Samartzis[1], I. Ihnenfeld[1], A. Noske[2], EP. Samartzis[1], D. Fink[1], P. Imesch[1]

Tissue microarray analysis of steroid receptors including GPER in adenomyosis

Department of Gynecology, University Hospital Zurich[1], Department of Surgical Pathology, University Hospital Zurich[2]

Introduction:
Adenomyosis, also referred to as endometriosis genitalis interna, is a common but poorly understand disease. The disease is defined by the presence of endometrial glands and stroma within the myometrium and is often associated with chronic and cycle-dependent lower abdominal pain and bleeding disorders. The prevalence in women consulting for gynecological routine examination is given to approximately 20 %, with an age-dependent peak at the age of 40-49 years. The pathogenesis of adenomyosis has not yet been clarified. Both an increased uterine contractility, as well as an increased infiltrative potential of endometrial cells, have been discussed as a cause for his disease. An impact of regulation of the disease by steroid hormones is obvious in a clinical context. The aim of our study was to analyse the immunohistochemical expression of the novel G protein-coupled estrogen receptors (GPER) and the classical estrogen receptors (ER)-alpha and -beta, as well as the progesterone receptors (PR) in adenomyosis and the endometrium of the same patients, compared to a control group without adenomyosis.

Methods:
We analysed the immunohistochemical expression of ectopic and eutopic endometrium in 74 patients with adenomyosis using tissue micro arrarray. Tissue samples were chosen in different phases of the menstruation cycle (29 in proliferative and 20 in secretory phase, as well as 25 in postmenopause). We compared the results to a control group of 48 patients without adenomyosis (16 in proliferation and 11 in the secretory phase, as well as 21 in postmenopause) and to clinical parameters.

Results:
Both the classical hormone receptors ER- alpha, ER -beta and PR, as well as the newly identified GPER receptor are expressed in adenomyosis. The expression patterns are different in adenomyosis compared to the controls, suggesting a hormonal dependence of the disease.

Conclusion:
A better comprehension of adenomyosis is needed to develop new strategies of hormonal therapy and to reduce the significant rate of hysterectomies caused by this disease. In particular specific GPER inhibitors may be evaluated in future as a possible treatment modality.

2251

M. Riwanto[1], S. Kapoor[1], D. Rodriguez[1], I. Edenhofer[1], S. Segerer[2], R.P. Wüthrich[2]

Glycolytic inhibition with 2-deoxyglucose retards disease progression in Han:SPRD rats with polycystic kidney disease (PKD)

Institute of Physiology, University Zürich and Clinic for Nephrology, University Hospital Zürich[1], Clinic for Nephrology, University Hospital, Zürich, Switzerland[2]

Introduction:
Autosomal dominant polycystic kidney disease (ADPKD) is a common genetic disorder characterized by the development of multiple bilateral renal cysts. The Han:SPRD rat is a PKD model with a phenotype that closely resembles human ADPKD. Using microarray analysis and real-time RT-PCR for renal gene expression in Han:SPRD (Cy/+) and wild-type (+/+) rats, we identified altered glucose metabolism in the Han:SPRD rat model, i.e. upregulation of genes involved in aerobic glycolysis (*Hk1, Hk2, Ldha*) and downregulation of genes involved in gluconeogenesis (*G6pc, Lbp1*), indicating a 'Warburg effect'. We hypothesized that reversing this process by a glycolytic inhibitor might halt the disease progression.

Methods:
Thus, we examined the effect of 2-deoxyglucose (2-DG) treatment, a glycolytic inhibitor, on renal function loss and cyst progression in Han:SPRD rats. Five-week-old male heterozygous cystic (Cy/+) and wild-type (+/+) rats were administered 2-DG (500 mg/kg/day) via subcutaneous injection for 5 weeks. The renal function was monitored throughout the treatment phase. Rats were sacrificed thereafter and kidneys were harvested for histomorphometric analyses.

Results:
Cy/+ rats treated with 2-DG showed significantly reduced kidney weights and 2-kidney/total body weight ratios and decreased renal cyst indices, as compared to vehicle-treated Cy/+ rats (27%, 20% and 18% reduction, respectively). Treatment of Cy/+ rats with 2-DG also resulted in significantly higher clearances for creatinine, BUN and uric acid, and lower urinary albumin excretion as compared to vehicle treatment. Interestingly, administration of 2-DG led to a sustained 2-fold increase of the urine volume output, suggesting renal resistance to vasopressin. Western blot analysis of kidney tissues harvested from Cy/+ rats showed an increased phosphorylation of AMPK, a negative regulator of mTOR, following 2-DG treatment. Moreover, in cultured tubular epithelial cells from Cy/+ rats, 2-DG dose-dependently inhibited cell growth, reduced lactate and ATP production, and increased phosphorylation of AMPK.

Conclusion:
Taken together, our results show that the cystic kidneys of Han:SPRD rats display enhanced aerobic glycolysis which may play an important role in the pathogenesis of PKD. The inhibition of glycolysis with 2-DG markedly delayed the loss of renal function and retarded cyst development in Han:SPRD rats with PKD. Targeting the glycolytic pathway may therefore present a novel therapeutic strategy to control cyst growth in polycystic kidney disease.

2252

RK. Clemens[1], TK. Kreindel[3], AI. Alomari[2]

Imaging Characterization of Central Conducting Lymphatic Anomalies

Clinic for Angiology, University Hospital Zürich, Switzerland[1], Division of Interventional Radiology, Boston Children`s Hospital, MA, USA [2], Dept. of Radiology, Hopital Italiano de Buenos Aires, Argentinia[3]

Introduction:
The central conducting lymphatic channels receive lymph return from the body and GI tract. Dysfunction leads to reflux and chylous leakage disorders. The purpose of this study is to report the imaging characterization of central conducting lymphatic anomalies.

Methods:
The medical records and imaging studies in patients with central conducting lymphatic anomalies were reviewed. Imaging was reviewed concerning the malformations' anatomical location, distribution, size, morphology, margins, density (CT)/signal intensity (MRI) and post-contrast enhancement pattern. Special attention was given to lymphatic abnormalities along the course of the thoracic duct and in the perivascular space.

Results:
There were 41 patients (m=26, f =15) with age range of 5 months to 52 years (mean=12.7 years). MR imaging was available for 32 patients and CT scans in 30. Clinical presentation varied depending on the anatomical involvement, including chylous pleural effusion (n=20), chylous ascites (n=17) and pericardial effusion (n=4). Abdominal involvement was found in 32 patients. Thoracic involvement was found in 32 patients, including lung involvement (n=14). One patient with lung involvement died of pulmonary failure. 32 patients had an involvement of both thoracic and pelviabdominal regions and only 9 patients had a single region involved. Bone (n=11) and skin involvement (n=19) was also common. In addition to the chyle collections, typical imaging features include perivascular and peribronchial soft tissue thickening with loss of perivascular fat rim.

Conclusion:
Central conducting lymphatic anomalies are characterized by chylous leak from dysfunctional channels which are localized in the perivascular and peribronchial spaces. Combined clinical and imaging features may obviate the need for biopsy to establish the diagnosis.

2253

RK. Clemens[1], C. Stamoulis[2], BR. Amann - Vesti[1], AI. Alomari[2]

Sclerotherapy in Venous malformations: Risk of Intraprocedural Complications

Clinic for Angiology, University Hospital Zürich, Switzerland[1], Division of Interventional Radiology, Boston Children`s Hospital, MA, USA [2]

Introduction:
To assess the sclerosant, dosage and age related risk of complications of sclerotherapy for venous malformations in children and adults.

Methods:
Review of medical records conducted for sclerotherapy of venous malformations over the past 8 years at Boston Children´s Hospital with documentation of intraprocedural complications. Correlation between complications and sclerosant was assessed using a logistic regression model with complication as the outcome to assess their potential combinatorial effects on complications.

Results:
166 patients (age 0.7 to 39 years) were treated with 327 procedures. Mean age was 12.6 years. 59% of the patients were female. Sodium tetradecyl sulfate 3% (292 procedures), dehydrated ethanol (80), N-Butyl Cyanoacrylate (50) or bleomycin (21) were used. Minor complications occurred in 16 procedures (4.9%) including blistering/ ulceration of involved skin (n=8). There were no major complications such as nerve injury. No correlation between complications and sclerosants ($p>0.5$ for all) or for age at procedure ($p=0.67$) nor area treated ($p=0.1$) was found.

Conclusion:
Sclerotherapy for venous malformations with STS as the main sclerosing agent is a safe procedure even with the use of combinations of agents without major complications. Minor complications, such as blistering are expected and are not related to age, dose or sclerosant. Symptoms of venous malformations are well controllable with sclerotherapy.

2254

RK. Clemens[1], C. Stamoulis[2], BR. Amann - Vesti[1], AI. Alomari[2]

Ethiodol in Sclerotherapy of Venous Malformations

Clinic for Angiology, University Hospital Zürich, Switzerland[1], Division of Interventional Radiology, Boston Children`s Hospital, MA, USA [2]

Introduction:
Our porpose was to investigate the safety of ethiodized oil contrast in sclerotherapy of venous malformations in children and adults.

Methods:
A review of medical records was conducted for sclerotherapy of venous malformations over the past 8 years and intraprocedural complications documented by using the SIR classification system. The correlation between complications and dose was assessed using a logistic regression model with complication as the outcome. The model also included terms for age at procedure and area treated, to assess their potential combinatorial effects on complications.

Results:
115 patients (age 1 to 35 years) had 202 scleortherapy procedures in combination with one or more of the following sclerosing agents: STS 3%, dehydrated ethanol, glue or bleomycin. The mean age at procedure was 11.8 and the median 11 years. Dosage varied between 0.2 ml to 20 ml. There was no statistically significant correlation between use/dose and complications (p=0.64) and no significant effects of age at procedure and area treated. Ethiodol dose was only correlated with age at procedure (p=0.04) and area treated (p=0.0003). Only minor complications (16) occurred.

Conclusion:
The minor complications including skin blistering and hemoglobinuria are known side effects of sclerotherapy and are not specific to Ethiodol. The results of this study suggest that ethiodized oil contrast may be safely used in children and adults with venous malformations that are treated with sclerotherapy. The dosage was found to be correlated with area treated and age at procedure.

2255

MY. Emmert[1], P. Wolint[1], S. Winklhofer[3], H. Alkadhi[3], V. Falk[2], SP. Hoerstrup[1]

Intramyocardial transplantation and in vivo tracking of human stem cell based three dimensional microtissues in the porcine heart

Swiss Centre for Regenerative Medicine University of Zurich, Zurich, Switzerland[1], Clinic for Cardiovascular Surgery, University Hospital of Zurich, Zurich, Switzerland[2], Institute of Diagnostic Radiology, University Hospital Zurich, Zurich, Switzerland[3]

Introduction:
The overall low retention-rate of applied single cell suspensions limits the efficacy of current stem cell therapy concepts. Taking advantage of threedimensional (3D) cellular self-assembly prior to transplantation may be beneficial. We investigate the principal feasibility of intramyocardial transplantation of in-vitro generated stem-cell based 3D-microtissues (3D-MTs) in a porcine model.

Methods:
3D-MTs were generated from iron-oxide (MPIO) labeled human adipose-tissue derived mesenchymal stem cells (ATMSCs) using a modified hanging-drop method. Nine pigs comprising seven healthy ones and two with chronic MI underwent intramyocardial transplantation of $16x10^3$ 3D-MTs (1250cells/MT; accounting for $2x10^7$ single ATMSCs) into the anterior-wall (n=7)/ the MI border-zone (n=2) using a 3D NOGA mapping-guided, transcatheter approach. Follow-up (FU) was performed for up to 6weeks and in-vivo cell-tracking was done using serial Magnetic Resonance Imaging (MRI), followed by PCR and immunohistochemistry.

Results:
Intramyocardial transplantation of human ATMSC based 3D-MTs was successful in eight animals while one pig (without MI) died during the NOGA-mapping due to sudden cardiac-arrest. During FU, no arrhythmogenic or neurological events occurred. Serial MRI displayed intramyocardial presence of the 3D-MTs by detection MPIOs during FU. Intramyocardial retention of 3D-MTs was confirmed by PCR-analysis and was further verified on histology and immunohistochemistry. 3D-MTs were viable, integrated and showed intact micro-architecture.

Conclusion:
We demonstrate the feasibility and safety of intramyocardial transplantation of in-vitro generated human stem-cell based 3D-MTs. Multimodal cell-tracking strategies comprising imaging and in-vitro tools allow for in-vivo monitoring and post-mortem analysis of 3D-MTs. 3D cellular self-assembly may represent a promising application-format for stem-cell based therapies.

2256

MY. Emmert[1], P. Wolint[1], J. Pavicevic[2], E. Caliskan[2], V. Falk[2], SP. Hoerstrup[1]

Image guided evaluation of cellular retention and survival after intramyocardial transcatheter based mesenchymal stem cell transplantation into the infarcted pig heart

Swiss Centre for Regenerative Medicine University of Zurich, Zurich, Switzerland[1], Clinic for Cardiovascular Surgery, University Hospital of Zurich, Zurich, Switzerland[2]

Introduction:
Cardiac cell therapy represents as a promising concept for the failing heart. However, while several delivery methods exist, the overall low retention and survival within the heart remains a major issue and numerous studies suggest a high washout particularly in the early phase after transplantation. We investigate the efficacy of transcatheter-guided, intramyocardial transplantation of mesenchymal stem cells (MSCs) in a translational porcine myocardial infarction model with particular regards to retention and survival.

Methods:
Allogenic porcine MSCs were characterized and labelled with iron-oxide micro-particles (MPIOs). Next, eight pigs (30-35kg) with chronic MI underwent 3D NOGA mapping-guided, transcatheter intramyocardial transplantation of $1.5x10^7$ MSCs into the anterior-septal wall of the MI border-zone. Thereafter in-vivo cell-tracking was performed using MRI, before the hearts were harvested at different time-points (1, 3, 6, 12 and 24hours) post transplantation for post-mortem assessment. According to the 3D NOGA injection-map, tissue-samples were taken to undergo a combined MACS/FACS cell-separation approach and immunohistochemistry (IHC) to determine cell retention and survival.

Results:
Transplantation was successful in all animals and MRI displayed the transplanted MPIO-labelled MSCs in the anterior-septal wall (corresponding to the injection sites). At all time-points, viable MSCs could be isolated from the heart and combined MACS/FACS separation (purity up to 98%) revealed up to 11.4% of the injected MSCs (mean: 5.2±4.1%) in the respective samples. IHC further verified intramyocardial presence via positive staining for MSC-specific markers and anti-FITC targeting the MPIOs. The cells appeared to be integrated and could be detected in clusters or in the interstitial areas.

Conclusion:
This study provides important insights into the early efficacy of transcatheter guided intramyocardial MSC transplantation in a translational animal model. Although the overall retention appears to be relatively low, these data confirm intramyocardial cell survival in the early phase after transplantation. Further optimization of delivery strategies and cell application formats is mandatory to improve intramyocardial retention and survival in future cell therapy concepts.

2257

Y. Boege[1], M. Malehmir[1], F. Böhm[1], L. Frick[1], J. Friemel[1], J. Mertens[4], R. Maire[1], M. Vucur[5], B. Müllhaupt[4], R. Boger[3], H. Schulze-Bergkamen[3], T. Lüdde[5], H. Moch[1], M. Heikenwalder*[2], A. Weber*[1]

An apoptosis-driven pathway to hepatocarcinogenesis in mice and men

Institut für Klinische Pathologie, Universitätsspital Zürich[1], Helmholtz Zentrum, Munich, Germany[2], NCT Heidelberg[3], Gastroenterology and Hepatology, University Hospital Zurich, Switzerland[4], Department of Medicine III, University Hospital RWTH Aachen, Aachen[5]

Introduction:
Chronic liver diseases (CLD) like chronic viral (HCV/HBV) infection, nutritive-toxic and metabolic disorders (alcohol abuse, non-fatty liver disease), autoimmune or chronic cholestatic disorders (AIH, PBC, PSC) are characterized by a constant loss of hepatocytes. Increased hepatocytes apoptosis is a hallmark in liver tissues of these patients. Recently, we have shown that mice with hepatocyte-specific deletion of the anti-apoptotic factor Mcl-1 (Mcl-$1^{\Delta hep}$ mice) reveal increased hepatocyte apoptosis, constant liver regeneration and spontaneous development of hepatocellular carcinoma (HCC) with an incidence of about 50% at 1 year. Thus, Mcl-$1^{\Delta hep}$ mice closely recapitulate human CLD.

Methods:
To better understand apoptosis- and proliferation-driven tumorigenesis on a molecular and cellular level, we analyzed Mcl-$1^{\Delta hep}$ mice and intercrossings thereof as well as mice of a second spontaneous HCC mouse model (TAK$1^{\Delta hep}$ mice) and intercrossings thereof, for gene expression, apoptosis and proliferation as well as DNA damage and compared the findings to human liver tissues of patients suffering from CLD and HCC of various etiologies.

Results:
Remarkably, those Mcl-$1^{\Delta hep}$ mice which eventually developed liver tumors at 12 months had displayed significantly higher serum transaminase levels early in life compared to those Mcl-$1^{\Delta hep}$ mice without tumor. In addition, gene expression studies, protein analysis and immunohistochemistry showed the activation of DNA repair pathways, indicating replicative stress and DNA damage in the hyper-apoptotic and hyper-proliferative environment of Mcl-$1^{\Delta hep}$ mice. The findings from the Mcl-$1^{\Delta hep}$ were also found in TAK$1^{\Delta hep}$ mice, and in different patient cohorts with CLD (HBV, HCV, NASH). The amount of hepatocyte death and replicative stress correlated with liver tumor development.

Conclusion:
Our data indicates that liver tumor development is determined by the (accumulated) amount of liver damage, going along with DNA damage in mice and men. These findings suggest that a vicious circle of chronic liver damage, apoptotic hepatocyte death and consecutive regenerative proliferation may be considered as the decisive event generally underlying human CLD-related HCC development, irrespective of the underlying etiology.

2258

M. Emmert[1], B. Weber[1], P. Wolint[1], PE. Dijkman[1], V. Falk[2], SP. Hoerstrup[1]

Marrow stromal cell based transcatheter aortic valve implantation – experiences in a preclinical animal model

Swiss Centre for Regenerative Medicine University of Zurich, Zurich, Switzerland[1], Clinic for Cardiovascular Surgery, University Hospital of Zurich, Zurich, Switzerland[2]

Introduction:
Transcatheter aortic-valve implantation (TAVI) has rapidly evolved as an effective treatment alternative for aortic-valve disease. The currently utilized bio-prostheses are prone functional degeneration. Autologous, stem cell based, tissue-engineered heart-valves (TEHV) with self-repair capacity have been repeatedly proposed to overcome these limitations. However, so far, successful TEHV implantation has been primarily reported for the low-pressure system in the pulmonary-position. We summarize our initial experience on marrow stromal cell based transcatheter aortic-valve implantation in an adult sheep model.

Methods:
Tri-leaflet TEHV generated from biodegradable synthetic-scaffolds were integrated into self-expanding Nitinol stents, seeded with autologous marrow-stromal cells. Thereafter, in a series of animal experiments, TEHV were transapically delivered into the descending aorta (n=3) and the orthotopic aortic-valve position of adult sheep (n=16) using different delivery systems including a generic system and the anatomically-orienting JenaValve transapical TAVI System (JenaValve, Munich/Germany). Follow up was up to two weeks. Delivery, positioning and functionality were assessed by angiography and echocardiography before the TEHV underwent post-mortem gross examination and histological assessment. Computed tomography analysis was used to assess stent positioning.

Results:
Transcatheter implantation of TEHV into the descending aorta (n=3) and into the orthotopic aortic-valve position (n=16) was successful in all animals with a duration from cell-harvest to TEHV implantation of approximately two hours. Fluoroscopy and echocardiography confirmed sufficient positioning at the intended delivery site. All TEHV tolerated the loading-pressure of the systemic-circulation and no acute ruptures or tears occurred. Animals displayed intact and mobile leaflets with an adequate functionality (mean trans-valvular gradient <10mmHg in all animals). Importantly, TEHV orthotopically implanted (n=16) entirely excluded the native aortic leaflets and did not compromise the coronary arteries. Histology and ECM displayed a high cellularity indicative for an early cellular-remodelling and in-growth. Paravalvular leakage occurred in selected animals and was primarily related to the leaflet-design.

Conclusion:
We demonstrate transcatheter based TEHV implantation into the aorta within a one-step intervention. Our data indicate the principal feasibility to combine the concept of TEHV and transcatheter delivery representing a key step towards clinical translation. Long-term functionality proven, a marrow stromal cell based TEHV approach may represent a next generation heart-valve concept.

2259

RM. Fakin[1], HJ. Klein[1], P. Giovanoli[1], M. Calcagni[1]

To suture or not to suture? Outcome assessment after epineural coaptation of digital nerves with different testing modalities

Division of Plastic Surgery and Hand Surgery, University Hospital Zurich / Switzerland[1]

Introduction:
The epineural coaptation of digital nerves after finger injury is common standardized surgical treatment. However the indication of this procedure was recently being questioned. Poor functional recovery and the lack of consensus about prognostic factors are cited as main causes.

Methods:
We assessed the clinical outcome after digital nerve repair in zone I and II in patients treated in 2006-2011 in our clinic. Sensory testing was conducted with a standard two point discrimination disk, with the pressure specified device (PSSD) and the grating test. Contralateral uninjured digit serves as control group. Moreover other modalities (warm/cold, pressure threshold) were tested. Patient epidemiology and surgical factors were also analyzed.

Results:
93 digital nerves were evaluated with a mean follow-up of 3.5 years. 2 neuromas (2.1%) and one CRPS Type 2 were observed. Sharp-blunt discrimination was preserved in 68% and cold-warm discrimination in 79% of patients. In 41% a cold intolerance was reported. The mean 2-point discrimination was 10.6 mm (vs. 4.4 mm) and 20.8 g/mm2 (vs. 5.2 g/mm2) as assessed by PSSD. The estimated probability of sharp-blunt discrimination was 0.66 for the injured side (vs. 0.97), for cold-warm discrimination was 0.85 (vs. 0.96). The mean grating score was 2.2 (vs. 1.4). Differences were encountered comparing the different testing modalities. The patients treated by experienced surgeons achieved a better score in the sensory tests.

Conclusion:
The epineural coaptation remains the therapy of choice after digital nerve injury. None of our patients recovered normal sensation, however the excellent protective sensation contributed to their high satisfaction. Surgery could prevent the development of CRPS or of painful neuromas in 98% of cases. The single most important factor affecting outcome appears to be surgeon`s experience. Hence epineural coaptation of peripheral nerves should be performed and should be concentrated in specialized units.

2260

R. Schweizer[2], P. Kamat[3], HJ. Klein[1], P. Kaenel[3], S. Salemi[4], M. Calcagni[1], P. Giovanoli[1], D. Eberli[4], A. Andres[3], JA. Plock[1]

Adipose-derived mesenchymal stem cells may promote breast cancer growth and metastatic spread

Division of Plastic Surgery and Hand Surgery, University Hospital Zurich / Switzerland[1], Department of Plastic Surgery, University of Pittsburgh, UPMC / USA[2], Department of Clinical Research, University of Bern, Bern / Switzerland[3], Center for Clinical Research, University Hospital Zurich / Switzerland[4]

Introduction:
Stem-cell enriched fat grafting has recently been proposed for reconstructive purposes on the breast level. This novel approach however has raised concerns about safety of stem cell-based therapies, especially in the post-cancer scenario. The aim of the present study was to investigate the interactions between human adipose-derived mesenchymal stem cells (ASCs) and human breast cancer cells (MCF-7- and MDA cell line), while focusing on the tumor microenvironment, tumor growth and metastatic spread.

Methods:
Human ASCs ($CD34^{-}CD73^{+}CD90^{+}CD105^{+}$) and MDA or MCF-7 breast cancer cell lines were used in this study. In vitro co-culture systems and assays were utilized for assessment of cytokine analysis and cell viability. An in-vivo breast cancer model in nu/nu mice was used for assessment of cancer progression and metastasis. Different proportional ratios of ASCs and MDA/MCF-7 cells were investigated. Tumor and metastatic tissue samples were analyzed with multiplex assays for oncogene expression, growth factors and metastatic phenotype markers.

Results:
In vivo, metastatic spread (40% vs. 0% in controls) and mean tumor size (408±527mg vs. 38±99mg in controls, $p<0.01$) were both significantly increased in MDA tumor bearing animals receiving higher ASC aliquots. In vitro, these results were paralleled by up-regulation of RANTES, eotaxin and TNF-a expression. ASC treatment induced phenotypic switching in MCF-7 tumors, with coincident expression of HER2 oncogene, follistatin and osteopontin. In vivo tumor growth was significantly ($p<0.05$) promoted. Also metastatic spread was observed in 20% in comparison to 0% in cancer controls without ASC influence.

Conclusion:
Our results suggest that human ASCs used in post mastectomy reconstruction or aesthetic breast augmentation may actually promote breast cancer. This may not necessarily preclude ASC use, but emphasizes due consideration of a dose dependent effect of such therapies and careful patient selection.

2261

I. Alecu[1], TW. Mühlbradt[2], C. Arenz[2], A. Penno[3], C. Thiele[3], A. Von Eckardstein[1], T. Hornemann[1]

Trafficking and Metabolism of 1-Deoxysphingolipids and Their Implications in Pathophysiological Changes

Institute of Clinical Chemistry, University Hospital Zürich[1], Institut für Chemie, Humboldt-Universität zu Berlin[2], Life and Medical Science Institute, University of Bonn[3]

Introduction:
Sphingolipids (SLs) are a highly diverse class of lipids with important roles in plasma membrane biology and as lipid-signaling molecules. Serine palmitoyltransferase (SPT) catalyzes the first step in the *de novo* synthesis of SLs, normally forming sphinganine (SA) from the condensation of serine and palmitoyl-CoA. Under certain conditions SPT can also use alanine or glycine in this condensation reaction, which then forms a class of atypical 1-deoxysphingolipids (1-deoxySLs). Due to the missing C1 hydroxyl group, the 1-deoxySLs are not metabolized to complex SLs nor degraded by the canonical catabolic pathway. Nothing is known about the metabolism and transport of 1-deoxySLs. They may accumulate intracellularly and impair cell function by affecting sorting and transport processes or membrane permeability. Pathologically elevated 1-deoxySLs are neurotoxic and cause hereditary sensory and autonomic neuropathy type 1 (HSAN1). There is a very high level of clinical similarity between HSAN1 and diabetic sensory polyneuropathy (DSN). Our group has found high levels of 1-deoxySLs in the plasma of type 2 diabetic patients, indicating that 1-deoxySLs may also be involved in the pathology of DSN.

Methods:
We analyzed the intracellular trafficking and metabolism of 1-deoxySLs using Nile red (NR) labeled deoxySA. We also developed a new method for tracking the SLs in cells using click chemistry, which does not change the size and polarity of the natural SL molecules. The only change made to the click (alkyne)-deoxySA and SA molecules is the insertion of a triple bond between the last two carbons. Click chemistry refers to a new class of chemical reactions in which triazoles are formed from an aizde and an alkyne group in the presence of a copper catalyst (in our case, the alkyne-deoxySA and SA were reacted with an azide-derived fluorophore). In a parallel approach we analyzed the intracellular distribution of exogenously added fluorescent and click-deoxySA with isotope labeled (d3)-deoxySA and endogenously formed deoxySA after subcellular fractionation. The SL profile of each fraction was analyzed by LC-MS, which also allowed us to detect downstream metabolites of the labeled lipids.

Results:
We found that NR-deoxySA is not metabolized and concentrates in the nucleus of the cells. The NR-deoxySA was not seen in any other cellular structures even after prolonged incubation. The intracellular localization of NR-deoxySA was further confirmed by cellular fractionation which showed that over 60% of it partitioned to the nuclear and mitochondrial fractions, whereas endogenously produced or externally added isotope labeled d3-deoxySA was primarily found in the microsomal fraction. We also observed that in contrast to the NR-deoxySA, d3-deoxySA was metabolized to the downstream metabolites d3-deoxy-ceramide and d3-deoxy-sphingosine. As the presence of the NR fluorophore interfered with the cellular distribution and metabolism of deoxySA, we developed an alternative approach using click chemistry. We found that click-deoxySA, like d3-deoxySA, was metabolized to downstream metabolites like click-deoxysphingosine, albeit at a slower rate than the d3-deoxySA was

converted. Furthermore, the click-deoxySA localized around the nucleus, its distribution not changing even after 24 hours, unlike that of the click-SA.

Conclusion:
The addition of an NR group interferes with the intracellular localization and metabolism of deoxySA. However, alkyne-deoxySA is metabolized and accumulates around the nucleus, its distribution remaining unchanged with time. These findings could help to elucidate the patho-mechanism of neuropathies like HSAN1 and DSN.

2262

H. Sievert[1], N. Pällmann[1], K. Miller[2], I. Hermans-Borgmeyer[2], S. Venz[3], A. Sendoel[6], M. Preukschas[1], M. Schweizer[2], S. Böttcher[7], T. Streicher[4], M. Manz[7], M. Balabanov[7], J. Hauber[5], K. Duncan[2], N. Parrinello[7], S. Balabanov[7]

A novel mouse model for inhibition of DOHH mediated hypusine modification reveals crucial function for embryonic development, proliferation and oncogenic transformation

Department of Hematology and Oncology, University Hospital Eppendorf, Eppendorf, Germany[1], Center for Molecular Neurobiology (ZMNH), Hamburg, Germany[2], Department of Medical Biochemistry and Molecularbiology, Ernst-Moritz-Arndt Univeristy, Greifswald[3], Department for Clinical Chemistry, University Hospital of Cologne, Germany[4], Heinrich Pette Institute - Leibniz Institute for Experimental Virology, Hamburg, Germany[5], Insitute of Molecular Life Science, University of Zurich, Zurich, Switzerland[6], Division of Hematology, University Hospital Zurich[7]

Introduction:
The highly conserved and unique posttranslational hypusine modification of a single cellular protein, the eukaryotic initiation factor 5A (eIF5A), represents an essential signaling mechanism in control of proliferation of eukaryotic cells. Hypusine modification occurs in two isoforms of human and rodent eIF5A. The eIF5A-1 isoform is expressed at high levels in all tissues, while the eIF5A-2 isoform is detectable only in some embryonic tissues, adult testis, central nervous system, and cancer tissue. Hypusine formation in eIF5A has been proposed to promote various cellular processes that potentially regulate proliferation, most notably mRNA translation and nucleocytoplasmic transport of RNA or other cargoes. Hypusine modification has also been implicated in numerous pathological conditions, including malignant transformation, diabetes, and HIV infection.

Methods:
We established a new conditional mouse model for selective inhibition of the hypsine modification.

Results:
Using a novel conditional knockout mouse model and a *Caenorhabditis elegans* knockout model, we found an evolutionarily conserved role for the DOHH-mediated second step of hypusine synthesis in early embryonic development. At the cellular level we observed reduced proliferation and induction of senescence in 3T3 *Dohh*$^{-/-}$ cells as well as reduced capability for malignant transformation. Furthermore, by mass spectrometry we observed that deletion of DOHH results in an unexpected complete loss of hypusine modification. Our results provide new biological insight into the physiological roles of the second step of the hypusination of eIF5A. Moreover, the conditional mouse model presented here provides a powerful tool to manipulate hypusine modification in a temporal and spatial manner, both to analyze how this unique modification normally functions in vivo, as well as how it contributes to different pathological conditions.

Conclusion:
In conclusion, we have demonstrated that DOHH is crucial for early embryonic development of mice and *C. elegans.* We provide evidence that DOHH acts as a key regulator of both normal and malignant mammalian cell proliferation. Our studies suggest that the inhibition of the final step of hypusine modification results in reduced efficiency of protein synthesis and

establish this enzymatic reaction as essential for the cellular function of eIF5A and for the viability of mammalian cells.

2263

JA. Plock[1], J. Schnider[2], HJ. Klein[1], W. Zhang[2], W. Tsuji[2], K. Marra[2], P. Giovanoli[1], V. Gorantla[2]

Immunomodulation with Adipose and Bone Marrow Derived Mesenchymal Stem Cells in Vascularized Composite Allotransplantation

Division of Plastic Surgery and Hand Surgery, University Hospital Zurich / Switzerland[1], Department of Plastic Surgery, University of Pittsburgh, UPMC / USA[2]

Introduction:
Reconstructive transplantation has become a clinical reality over the past decade. Life-long immunosuppression is mandated to sustain graft acceptance with coincident adverse effects. Cellular therapies incorporating bone marrow or adipose tissue derived mesenchymal stem cells (BM-MSC/ASCs) have shown promise as immunomodulatory strategies in autoimmune disease, experimental models of solid organ and vascularized composite allotransplantation (VCA).

Methods:
Lewis (LEW) rat recipients received fully mismatched Brown-Norway (BN) limb transplants in this study. BM-MSCs or ASCs were isolated and cultured. Specific mesenchymal markers [$CD29^+CD73^+CD90^+CD45^-$] were used to characterize MSCs. BM-MSCs or ASCs were tested for suppressive function in mixed lymphocyte reaction (MLR) assays incorporating BN (donor) lymphocyte stimulation of LEW responders. In addition, stimulated peripheral blood mononuclear cells (PBMCs) were co-cultured with BM-MSCs or ASCs.

Results:
Both BM-MSCs and ASCs exhibited immunosuppressive function. However, ASCs demonstrated superior efficacy. In *in vivo* experiments, rats were treated one day after the transplantation with ASCs or BM-MSCs (10^6 cells/animals, all cells <P3). Immunosuppression with tacrolimus was withdrawn at POD 21. While all animals revealed peripheral multilineage chimerism at 4 weeks and upregulation of regulatory T cells (T reg; CD4CD25FoxP3), these effects were transient and not detectable at later timepoints. Notably >50% of the animals treated with ASCs or BM-MSCs showed long-term acceptance of the transplanted hindlimb with survival >120 days. These findings were correlated to microchimerism in the marrow, spleen and inconsistently in lymphnodes.

Conclusion:
In summary, our results confirm that ASCs and BM-MSCs have immunomodulatory effects that may be of benefit in reducing the intensity, frequency or duration of immunosuppression in VCA. The high cell yields of ASCs combined with the insights supporting the superior immunomodulatory potential of ASCs versus BM-MSCs truly advocate adipose-based cellular therapies. It still remains to be defined if paracrine effects as an important function of ASCs/MSCs are also involved in tolerogenic or immunomodulatory effects in transplantation.

2264

M. Balabanov[1], N. Pällmann[2], M. Preukschas[2], D. Steinemann[3], W. Hofmann[3], A.. Gompf[4], T. Streichert[5], T. Braunschweig[6], M. Copland[7], K. Rudolph[8], C. Bokemeyer[2], S. Koschmieder[10], A. Schuppert[9], S. Balabanov[1], T. Brümmendorf[10]

A "telomere-associated secretory phenotype" (TASP) cooperates with BCR-ABL to drive malignant proliferation of leukemic cells

Division of Hematology, University Hospital Zürich, Zürich[1], Department of Hematology and Oncology, University Hospital Eppendorf, Eppendorf, Germany[2], Institute of Cell and Molecular Pathology, Hannover Medical School, Hannover[3], Institute of Molecular Medicine and Max-Planck-Research Group on Stem Cell Aging, Ulm[4], Institute of Clinical Chemistry, University Hospital Cologne, Cologne[5], Department of Pathology, University Hospital of the RWTH Aachen, Aachen[6], Paul O'Gorman Leukaemia Research Centre, College of Medical, Veterinary and Life Sciences, Institute of Cancer Sciences, University of Glasgow, Glasgow[7], Leibniz Institute of Age Research - Fritz-Lipmann Institute (FLI), Jena[8], Aachen Institute for Advanced Study in Computational Engineering Science (AICES), RWTH Aachen University, Aachen[9], Department of Hematology and Oncology, University Hospital of the RWTH Aachen, Aachen[10]

Introduction:
Telomere biology is frequently associated with disease evolution in human cancer and dysfunctional telomeres have been demonstrated to contribute to genetic instability. In BCR-ABL positive chronic myeloid leukemia (CML), accelerated telomere shortening has been shown to correlate with disease evolution, risk score and response to treatment. However, the causal role of telomeres in the progression of CML remains elusive.

Methods:
To study the impact of telomeres in BCR-ABL-driven proliferation, we established a primary CML-like cell culture model based on hematopoietic cells of the telomerase knockout mouse with different telomere length.

Results:
note, we could demonstrate that proliferation of CML-like bone marrow cells strongly depends on telomere maintenance. CML-like cells of telomerase knockout mice with critically short telomeres (CML-iG4) are growth retarded and proliferation is terminally stalled by a robust senescent cell cycle arrest. In sharp contrast, CML-like cells with pre-shortened, but not critically short telomere lengths (CML-G2) grew most rapidly and were found to express a specific "telomere-associated secretory phenotype" (TASP), comprising secretion of chemokines, interleukins and other growth factors, thereby potentiating oncogene-driven growth. Moreover, conditioned supernatant of CML-G2 cells markedly enhanced proliferation of CML-WT and pre-senescent CML-iG4 cells. Strikingly, a similar inflammatory mRNA expression pattern was found with disease progression from chronic phase to accelerated phase in CML patients.

Conclusion:
These findings demonstrate that telomere-induced senescence needs to be bypassed by leukemic cells in order to progress to blast crisis and provide a novel mechanism by which telomere shortening may contribute to disease progression in CML.

2265

R. Meletta[1], A. Müller[1], L. Mu[2], A. Chiotellis[1], N. Borel[3], Z. Rancic[4], P.A. Kaufmann[5], S.M. Ametamey[1], R. Schibli[1], S.D. Krämer[1]

Evaluation of radiolabeled inhibitors of the immune co-stimulatory molecule CD80 for vulnerable atherosclerotic plaque imaging

Center for Radiopharmaceutical Science of ETH, PSI and USZ, ETH Zurich, Zurich[1], Center for Radiopharmaceutical Science of ETH, PSI and USZ, USZ Zurich, Zurich[2], Institute of Veterinary Pathology, Vetsuisse Faculty, University of Zurich, Zurich[3], Clinic for Cardiovascular Surgery, University Hospital Zurich, Zurich[4], Cardiac Imaging, University Hospital, Zurich[5]

Introduction:
The immune system is a key factor in the development of vulnerable atherosclerotic plaques. We have identified the co-stimulatory molecule CD80 as a candidate marker for plaque vulnerability. Here, we present further target evaluation in surgically removed human vulnerable and stable carotid plaques and the characterization of two structurally related low molecular weight CD80 inhibitors as candidate tracers for CD80 imaging by Positron Emission Tomography (PET).

Methods:
CD80 expression and localization in human carotid plaques was investigated by RT-PCR and IHC. Two CD80 ligands were labeled with carbon-11 and fluorine-18, respectively. Radiotracer binding was examined in carotid plaques and CD80-positive tissue by in vitro autoradiography. Their affinity to recombinant CD80 and plasma protein binding were assessed by equilibrium dialysis, and logD by the shake flask method. Blood cell partitioning was determined in vitro. In vivo pharmacokinetics was evaluated by PET using wild type mice; formation of radiometabolites was tested by chromatographic methods.

Results:
Relative CD80 mRNA and protein expression were higher in human vulnerable than stable plaques. Both radiotracers bound with nanomolar affinity to human CD80 and showed specific binding in CD80-rich regions in vulnerable plaques. Tracer lipophilicity was moderate with logD 0.1 and 0.9, respectively. Plasma protein binding was >95%, blood cell binding <12%. PET with mice revealed a short blood half-life of 2-3 min with negligible distribution into tissue. No radiometabolites were detected.

Conclusion:
Target evaluation identified CD80 as a promising indicator for plaque vulnerability. Two low molecular weight molecules labeled with PET isotopes specifically bound to human CD80 and accumulated in vulnerable plaques in vitro. Further in vivo studies and the evaluation of an adequate rodent model are in process.

2266

A. Woloszyk[1], J. Buschmann[2], T. Mitsiadis[1]

Dental pulp stem cells enhance the vascularization of 3D silk scaffold constructs for tissue engineering purposes

Institute for Oral Biology, University of Zurich, Zurich[1], Plastic and Hand Surgery, University Hospital Zurich[2]

Introduction:
Successful tissue engineering depends on rapid blood vessel formation towards the transplanted tissue as insufficient oxygen and nutrient transport leads inevitably to necrosis. The basis of tissue engineered transplants is the combination of preferably autologous multipotential stem cells with a suitable biocompatible and biodegradable material. The aim of the current study was to evaluate the angiogenic potential of human dental pulp stem cells (hDPSCs), which can be easily isolated from extracted wisdom teeth and possess a multilineage differentiation capacity, similar to bone marrow stem cells. Silk fibroin scaffolds have been chosen as the cell carrying material due to its good biocompatibility and mechanical properties, which are particularly suitable for bone tissue engineering purposes.

Methods:
hDPSCs were isolated from wisdom teeth with written informed consent of the patients. CD34+/CD117+ cells were seeded on silk fibroin scaffolds (5 mm Ø, 2 mm height) and incubated for 24 hours in vitro before performing the chorioallantoic membrane (CAM) assay for 6 days. Vessel formation was analyzed qualitatively by H&E staining and immunohistochemistry using vimentin and von Willebrand factor (vWF) antibodies on 5 µm paraffin sections. Empty scaffolds were used as a control.

Results:
Prelimiary results showed that the cell-free scaffold remained empty inside, while the dental pulp stem cells seemed to proliferate well filling up the pores of the scaffold. Vessel-like structures were visible in H&E stainings inside the hDPSC-seeded scaffolds. Both, empty and cell-seeded scaffolds were surrounded by a membrane, most probably the result of a foreign body reaction of the chicken embryo. The mesenchymal-derived cell marker vimentin was only expressed in the center of hDPSC-seeded scaffolds, but not in chicken-derived tissue. The endothelial cell marker vWF was found to be expressed within tissue of human origin, suggesting that some of the seeded hDPSCs have differentiated to endothelial cells, contributing to the formation of new blood vessels.

Conclusion:
The study has shown that hDPSCs are able to survive, to proliferate and to differentiate in a 3D construct of the above mentioned dimensions cultured on the CAM of fertilized chicken eggs. Furthermore, they have the potential to contribute to new blood vessel formation, which is crucial for long term survival of the implanted tissue making this system an interesting tool for clinic applications. Apart from being applied in tissue engineering approaches, also the treatment of wounds, myocardial infarction and stroke could profit from these findings.

2267

L. Jaatinen[2], S. Salemi[1], S. Miettinen[3], J. Hyttinen[2], D. Eberli[1]

Neuronal differentiation of adipose-derived stem cells by electric current and copper for bladder engineering

Laboratory for Urologic Tissue Engineering and Stem Cell Therapy, Department of Urology, University Hospital Zurich, Switzerland. [1], Department Electrical Engineering and Communication Technology, Tampere University of Technology and BioMediTech, Tampere, Finland[2], Adult Stem Cells, Institute of Biomedical Technology, University of Tampere, Tampere, Finland[3]

Introduction:
Engineering of contractile bladder tissue is still limited by several factors. One reason is the lack of innervation of the newly formed tissue. Neurons differentiated from stem cells have a great potential to support autonomic neuronal regeneration in engineered bladder tissues and are considered as a potential solution to overcome this shortcoming. For fast clinical translation we investigated a growth factor-free method for the differentiation of readily available human adipose derived stem cells (hADSCs) toward neuron-like cells using defined protocols of electric current and copper concentrations.

Methods:
Human ADSCs were isolated and characterized by morphological analysis, immunocytology and FACS using lineage-specific markers. ADSCs were stimulated for one hour with electricity and/or copper. Briefly, in the Cu + 1 mA and Cu + 1.5 mA groups, the copper was released gradually via electrolysis for one hour using a current of 1 mA or 1.5 mA, respectively. After the stimulation, the cells were collected and seeded on chamber slides (immunohistochemistry) or cell culture flasks (real-time PCR and western blotting) and cultured for 4, 7, or 14 days.

Results:
We analyzed the morphological changes and the mRNA and protein expression levels in the stimulated cells and showed that the combination of current and copper induces stem cell differentiation toward the neuronal lineage with elongation of the cells and the upregulation of neuron-specific proteins such as Beta- III tubulin and MAP2. The stimulation of ADSCs with copper and current significantly increased the mRNA expression of beta-tubulin isotype III already at day 4 compared to the untreated control. Increase was greatest when the ADSCs were stimulated with 1 mA current and a gradual copper release via electrolysis (Cu + 1 mA). The MAP-2 mRNA levels showed a significant increase at day 4, being highest at day 14 when cells were stimulated with 1 mA current and exposed to a gradual copper release (Cu + 1 mA).

Conclusion:
The induction of the neuronal differentiation of hADSCs by electric field and copper offers a novel approach for growth factor free stem cell differentiation to neuron-like cells used for bladder tissue engineering.

2268

SN. Schweizer[1], TC. Tiberi[2], RE. Rushing[2], WH. Welzl[3], WM. Wojtal[1], ST. Suter[1]

The absence of TNF exacerbates spontaneous neuroinflammation in MOG-specific TCR-transgenic (2D2) mice

University Hospital Zurich, Clinic for Immunology and Section of Neuroimmunology and MS Research[1], Neuropathology, University Hospital Zürich[2], Institute of Anatomy, University of Zürich[3]

Introduction:
A fraction of mice carrying the MOG-specific T cell receptor (TCR) 2D2 spontaneously develop autoimmune encephalomyelitis accompanied by demyelination of the central nervous system (CNS). These symptoms resemble the ones seen in human multiple sclerosis (MS). A greater fraction of 2D2 mice, however, develop peripheral neuropathy, likely caused by the reported cross-reaction of the 2D2 TCR with a neurofilament M (NF-M) peptide. Several cytokines play distinct roles during MS as well as experimental autoimmune encephalomyelitis (EAE), a commonly used animal model of MS. One of these cytokines, TNF, has been shown to have pro-inflammatory as well as protective activities during neuroinflammation, however, the mechanisms and regulation of its dual role are incompletely understood.
In this study, we crossed TNF-deficient (TNFko) and 2D2 mice to further investigate the role of TNF in the context of spontaneous neuroinflammation. Beginning at the age of 3 months, approximately half of the 2D2-TNFko mice spontaneously developed clinical signs of neurological impairment, and analysis of the sciatic nerves revealed severe peripheral neuropathy in the hind limbs. Furthermore, we found increased numbers of activated T cells in the secondary lymphoid organs. Interestingly, 2D2-TNFko mice rarely developed signs of typical EAE. Still, they had moderate infiltrates of CD4 and CD8 T cells in the CNS. It remains to be determined whether the lack of TNF leads to immune-deregulation and therefore to tissue-specific autoimmunity or to impaired tissue repair in the presence of a low level autoimmune attack.

2269

YC. Yakkala[1], KD. Kingston[1], SY. Saito[1], ST. Sparwasser[2], TH. Takizawa[1], MM. Manz[1]

Flt3 expression in Hematopoietic Stem Cells

University Hospital Zurich, Division of Hematology, Zurich[1], Twincore, Institute of infection immunology, Hannover, Germany[2]

Introduction:
FMS like tyrosine kinase 3 (Flt3) is a class III membrane bound tyrosine kinase receptor involving in cell survival and differentiation, originally described as a surface receptor expressed on murine hematopoietic stem cells (HSCs) and progenitors in bone marrow (BM). Later reports in contrast, have shown that surface expression of Flt3 is absent on HSCs in steady state, and marks the loss of self-renewal potential and lineage commitment. This project aims to conclusively establish if Flt3 expression is initiated as early as in HSC.

Methods:
By using BAC transgenic technology, a reporter-depleter transgenic (TG) mouse model was generated, in which the cells that express Flt3 co-express green fluorescent protein (GFP) and diphtheria toxin (DT) receptor. DT was administered to specifically ablate the Flt3+ cells, and the BM of mice were flow cytometrically analyzed at different time points post treatment, to check the depletion of phenotypic HSC. In order to know if functional HSC were indeed depleted, total BM from PBS or DT treated TG was transplanted competitively with wild type (WT) BM cells into lethally irradiated recipients. Peripheral blood (PB) of the transplants was monitored to check the competitive contribution of donor to mature hematopoietic repopulation. To examine if DT mediated depletion leads to creation of free space in BM and thus facilitates HSC engraftment, WT HSC and progenitor enriched BM fraction was transplanted into TG recipients with or without DT treatment, followed by monthly peripheral blood analysis.

Results:
Flow cytometric analysis showed that GFP expression is correlated with Flt3 expression in steady state BM, and DT administration efficiently depleted all the GFP expressing cells within 24 hours, with a significant decrease in phenotypic HSC compartment. Compared to PBS treated control BM, the hematopoietic contribution of DT treated donor cells in all blood lineages was significantly reduced, indicating the depletion of functional HSC upon DT administration. Monthly PB analysis of PBS treated recipient in prior to transplantation showed only 1% engraftment of donor cells at any given time, whereas DT pretreatment resulted in 8% donor contribution that is sustained over 5 months, functionally validating the Flt3 expression in HSC compartment.

Conclusion:
By employing efficient and sensitive DTR mediated cell targeting, we herein show that at least part of normal murine HSCs initiate Flt3 expression.

2270

Fabian Wolpert[1], Isabel Tritschler[1], Alexander Steinle[2], Michael Weller[1] and Günter Eisele[1]

A disintegrin and metalloproteinases (ADAM) 10 and 17 modulate the immunogenicity of glioblastoma stem cells

[1] Department of Neurology, University Hospital Zurich, Frauenklinikstrasse 26, 8091 Zurich, Switzerland
[2] Institute for Molecular Medicine, Goethe University Frankfurt am Main, Theodor-Stern-Kai 7, 60590 Frankfurt am Main, Germany

Introduction:
Glioblastoma stem cells (GSC) have been identified as a putative target for immunotherapy of glioblastoma. However, an immune inhibitory phenotype of GSC might counteract immunotherapeutic approaches. A disintegrin and metalloproteinases (ADAM) are involved in the maintenance of the malignant phenotype of glioblastomas. Notably, ADAM proteases 10 and 17 might impair the immune recognition of glioma cells via the activating immunoreceptor NKG2D by cleavage of its ligands from the cell surface.

Methods:
Expression of NKG2D ligands (NKG2DL), ADAM10 and 17 was assessed by RT-PCR and cell surface levels by flow cytometry in LNT-229 cells and 4 well characterized GSC lines. Cells were treated with ADAM specific inhibitors (GI254023X = ADAM10; GW280264X = ADAM10 and 17) following flow cytometry for NKG2DL. Furthermore, we performed ADAM10, ADAM17 or combined gene silencing following flow cytometry for NKG2DL. Soluble ULBP2 was assessed by ELISA from conditioned media of GI254023X or GW280264X treated cells or controls. The modulation of GSC immunogenicity upon ADAM inhibition was assessed employing a flow cytometry based NK cell lysis assay and Interferon-γ ELISA of conditioned media of NK cell and GSC co cultures.

Results:
Here, we show that ADAM10 and ADAM17 are expressed on the cell surface by the use of a panel of GSC lines. The cell surface expression of NKG2D ligands (NKG2DL), is enhanced upon gene silencing of ADAM10 and ADAM17 or ADAM10 and ADAM17 specific inhibitors. Soluble ULBP2 in GSC culture supernatants is reduced upon blocking of ADAM10 and ADAM 17 underscoring the view that these proteases cleave ULBP2 from the surface of GSC. The impairment of ADAM 10 and ADAM17 leads to enhanced immune recognition of GSC by natural killer cells and enhanced secretion of interferon-γ by these immune effector cells.

Conclusions:
ADAM10 and ADAM17 constitute suitable targets to boost an immune response against GSC.

Conference Location

University Hospital Zurich
Grosser Hörsaal Ost
Rämistrasse 100
8091 Zürich

Contact Address

Prof. Dr. med. Gregor Zünd
Direktor Forschung und Lehre
Managing Director ZKF
UniversitätsSpital Zürich
gregor.zuend@usz.ch
phone: +41 (0) 44 634 55 00
fax: +41 (0) 44 634 55 03
Secretary office: +41 (0) 44 634 55 01